



Keele
University

This work is protected by copyright and other intellectual property rights and duplication or sale of all or part is not permitted, except that material may be duplicated by you for research, private study, criticism/review or educational purposes. Electronic or print copies are for your own personal, non-commercial use and shall not be passed to any other individual. No quotation may be published without proper acknowledgement. For any other use, or to quote extensively from the work, permission must be obtained from the copyright holder/s.



Three-Dimensional Structured Hybrid Scaffolds for Enhanced Bone formation

By

Yanny Marliana Baba Ismail

School of Postgraduate Medicine

Institute for Science and Technology in Medicine

Keele University

Thesis submitted to Keele University in fulfillment requirements for the degree of
Doctor of Philosophy (Biomedical Engineering)

JULY 2016

SUBMISSION OF THESIS FOR A RESEARCH DEGREE**Part I. DECLARATION by the candidate for a research degree. To be bound in the thesis**

Degree for which thesis being submitted

Title of thesis Three-dimensional Structured Hybrid Scaffolds for Enhanced Bone formation

This thesis contains confidential information and is subject to the protocol set down for the submission and examination of such a thesis.**NO [please delete as appropriate; if YES the box in Part II should be completed]**Date of submission Original registration date 19th September 2012
(Date of submission must comply with Regulation 2D)

Name of candidate YANNY MARLIANA BINTI BABA ISMAIL

Research Institute INSTITUTE FOR SCIENCE AND TECHNOLOGY IN MEDICINE

Name of Lead Supervisor PROFESSOR ALICIA J EL HAJ

I certify that:

- (a) The thesis being submitted for examination is my own account of my own research
- (b) My research has been conducted ethically. Where relevant a letter from the approving body confirming that ethical approval has been given has been bound in the thesis as an Annex
- (c) The data and results presented are the genuine data and results actually obtained by me during the conduct of the research
- (d) Where I have drawn on the work, ideas and results of others this has been appropriately acknowledged in the thesis
- (e) Where any collaboration has taken place with one or more other researchers, I have included within an 'Acknowledgments' section in the thesis a clear statement of their contributions, in line with the relevant statement in the Code of Practice (see Note overleaf).
- (f) The greater portion of the work described in the thesis has been undertaken subsequent to my registration for the higher degree for which I am submitting for examination
- (g) Where part of the work described in the thesis has previously been incorporated in another thesis submitted by me for a higher degree (if any), this has been identified and acknowledged in the thesis
- (h) The thesis submitted is within the required word limit as specified in the Regulations

Total words in submitted thesis (including text and footnotes, but excluding references and appendices)

Signature of candidate Date

Note

Extract from Code of Practice: If the research degree is set within a broader programme of work involving a group of investigators – particularly if this programme of work predates the candidate's registration – the candidate should provide an explicit statement (in an 'Acknowledgments' section) of the respective roles of the candidate and these other individuals in relevant aspects of the work reported in the thesis. For example, it should make clear, where relevant, the candidate's role in designing the study, developing data collection instruments, collecting primary data, analysing such data, and formulating conclusions from the analysis. Others involved in these aspects of the research should be named, and their contributions relative to that of the candidate should be specified (*this does not apply to the ordinary supervision, only if the supervisor or supervisory team has had greater than usual involvement*).

Abstract

The most common clinical treatments for large bone deficiencies resulting from trauma, disease or infection are autograft, allograft or bone graft substitutes (BGS). However, these treatments still have limitations for clinical applications. Thus, this project aims to fabricate an optimal scaffold design for enhanced bone formation. Human bone is not solely hydroxyapatite (HA) but consists of multi-ionic substitutions in the HA lattice. Here, we have developed multi-substituted HA (SiCHA) nanopowders as bone substitute materials. SiCHA-2 was found to closely mirror the composition of the bone mineral content associated with the most enhanced proliferation and osteogenic activity.

An innovative coating materials assembly was then established using SiCHA-2 nanopowders in combination with hyaluronan and collagen type I by the Polyelectrolyte Multilayers (PEMs) technique. Increasing the number of deposition cycles resulted in linear increases of surface properties and cell activities up to 5-bilayers. One common problem in scaffold-based tissue engineering (TE) is the rapid formation of tissue on the outer edge of the scaffolds whereas inner regions of the scaffold undergo necrosis. In this study, we incorporated aligned channels on the structure of three-dimensional (3D) scaffolds by Rapid Prototyping (RP) technique using Poly (lactic acid) (PLA) followed by PEMs. We investigated the fate of human mesenchymal stem cells (hMSCs) on these scaffolds in a rotary bioreactor compared to static conditions using osteogenic and proliferation media. We demonstrate that the combination of appropriate substrates with aligned channels, biochemical cues from the osteogenic media and better mass transport provided by rotary bioreactor enhances bone formation.

In order to create pre-vascularized 3DP hybrid scaffolds, proof of concept work introduces the co-culture model of human umbilical vein endothelial cells (HUVECs) and hMSCs into the best scaffold design. Co-culture shows enhanced expression of both pro-angiogenic markers, which is an early indication of an ability supporting vessel formation *in vitro*.

Keywords: Multi-substituted hydroxyapatite, Polyelectrolyte Multilayers coating, Rapid Prototyping, Three-Dimensional scaffolds, Rotary bioreactor, Human Mesenchymal Stem Cells, Osteoarthritis, Tissue engineering.

Publications and Presentations

Yanny M. Baba Ismail, Oana Bretcanu, Kenneth W. Dalgarno, Alicia J. El Haj, 2014. Synthesis and *in vitro* biocompatibility of multi-substituted hydroxyapatite for bone tissue engineering applications. *European Cells and Materials*, 8 (4): 4.

Yvonne Reinwald, Pierre O. Bagnaninchi, Ying Yang, Yanny M. Baba Ismail, Alicia J. El Haj, 2016. Online monitoring of mechanical properties of three-dimensional tissue engineered constructs for quality assessment. *Proc. SPIE 9710, Optical Elastography and Tissue Biomechanics III*, 971007.

Yanny M. Baba Ismail, Oana Bretcanu, Kenneth W. Dalgarno, Alicia J. El Haj, 2014. Physico-chemical properties and *in vitro* biological assessment of multi-substituted hydroxyapatite powders. *Tissue Engineering & Regenerative Medicine International Society*, Genova, Italy, June 2014 (Poster).

Yanny M. Baba Ismail, Oana Bretcanu, Kenneth W. Dalgarno, Alicia J. El Haj, 2014. Synthesis and *in vitro* biocompatibility of multi-substituted hydroxyapatite for bone tissue engineering applications. *Tissue and Cell Engineering Society*, Newcastle-upon-tyne, United Kingdom, July 2014 (Oral).

Yanny M. Baba Ismail, Oana Bretcanu, Kenneth W. Dalgarno, Alicia J. El Haj, 2014. Synthesis and *in vitro* biocompatibility of carbonated hydroxyapatite for bone tissue engineering applications. *European Society of Biomaterials*, Liverpool, United Kingdom, August 2014 (Poster).

Yanny M. Baba Ismail, Oana Bretcanu, Kenneth W. Dalgarno, Alicia J. El Haj, 2014. Nanoscale multi-substituted hydroxyapatite particles for bone tissue engineering applications. *European Materials Research Society*, Warsaw, Poland, September 2014 (Oral).

Yanny M. Baba Ismail, Oana Bretcanu, Kenneth W. Dalgarno, Alicia J. El Haj, 2014. Nanoscale multi-substituted hydroxyapatite particles for bone tissue engineering applications. *Malaysian Tissue Engineering and Regenerative Medicine Scientific Meeting*, Kuala Lumpur, Malaysia, September 2014 (Poster).

Yvonne Reinwald, Pierre O. Bagnaninchi, Ying Yang, Yanny M. Baba Ismail, Alicia J. El Haj, 2016. Online monitoring of mechanical properties of three-dimensional tissue engineered constructs for quality assessment. *SPIE Optical Elastography and Tissue Biomechanics III*, San Francisco, California, United States, February 2016 (Oral).

YM Baba Ismail, Y Reinwald, O Bretcanu, K Dalgarno, AJ El Haj, 2016. Designs of three-dimensional printed scaffolds promote formation of vascularized engineered bone. *Tissue Engineering & Regenerative Medicine International Society*, Uppsala, Sweden, June 2016 (Oral).

Table of Contents

Abstract.....	i
Publications and presentations.....	iii
Table of Contents.....	v
List of Abbreviations.....	xiii
List of Figures.....	xiv
List of Tables.....	xviii
Acknowledgement.....	xx
Chapter 1: Introduction.....	1
1.1. Clinical needs for bone regeneration.....	2
1.2. Bone anatomy	3
1.3. Natural bone formation and remodelling pathways.....	7
1.3.1. Bone formation	7
1.3.2. Bone remodelling.....	9
1.3.3. The role of vascularization in bone development.....	12
1.4. Bone repair and regeneration	13
1.4.1. Bone defects.....	13
1.4.2. Bone graft	14
1.5. Bone Tissue Engineering	18
1.6. Development of scaffolds for bone tissue engineering applications	18
1.6.1. Biomaterials used as bone tissue engineering scaffolds	22
1.6.1.1. Bioactive ceramics.....	23
1.6.1.2. Biodegradable Polymers.....	26
1.6.1.3. Composites.....	29
1.6.2. Fabrication techniques	29
1.6.2.1. Conventional fabrication technique.....	30
1.6.2.2. Rapid Prototyping technology	33
1.6.3. Surface modification.....	37
1.7. Cells for Bone Tissue Engineering.....	40
1.8. Mesenchymal stem cells.....	41
1.8.1. The discovery of mesenchymal stem cells	41
1.8.2. <i>In vitro</i> characteristics of mesenchymal stem cells	43

1.8.3. Mesenchymal stem cells for tissue repair	43
1.9. Approaches to accelerate osteogenesis	45
1.10. Characterization	50
1.10.1. Physico-chemical Characterization.....	50
1.10.1.1. X-Ray Diffraction analysis.....	50
1.10.1.2. Fourier Transform Infra-Red Spectroscopy.....	51
1.10.1.3. X-Ray Photoelectron Spectroscopy.....	53
1.10.1.4. Carbon, Hydrogen, Nitrogen Analysis.....	54
1.10.1.5. Inductively Couple Plasma Optical Emission Spectroscopy.....	54
1.10.1.6. X-Ray Fluorescence.....	56
1.10.1.7. Atomic Force Microscopy.....	57
1.10.1.8. Electron Microscopy.....	58
1.10.2. Biocompatibility Assessments.....	58
1.10.2.1. Histochemical staining.....	61
1.10.2.2. Immunohistochemical staining.....	61
1.10.2.3. Micro-computed tomography.....	61
1.11. Thesis Aims and Objectives	62
1.12 Research hypotheses.....	63
Chapter 2: Materials and Methods.....	64
2.1. Introduction	65
2.2. Synthesis of multi-substituted HA by nanoemulsion method	68
2.2.1. Optimization of carbonate and silicon ions contents.....	68
2.2.2. Physico-chemical characterization	73
2.2.2.1. X-Ray Diffraction	73
2.2.2.2. Fourier Transform Infra-Red Spectroscopy.....	73
2.2.2.3. Carbon, Hydrogen, Nitrogen Analysis.....	73

2.2.2.4. Inductively Coupled Plasma-Optical Emission Spectroscopy Measurement	74
2.2.2.5. X-Ray Fluorescence Analysis	74
2.2.3. As-calcined multi-substituted HA	75
2.2.4. Physico-chemical characterization	76
2.2.4.1. X-Ray Spectroscopy	76
2.2.4.2. XRD Analysis	76
2.2.4.3. FTIR Spectroscopy	76
2.2.4.4. CHN Analysis	76
2.2.4.5. ICP-OES Measurement.....	77
2.2.4.6. XRF Analysis.....	77
2.2.4.7. Transmission Electron Microscopy	77
2.2.5. Cell Characterization	78
2.2.5.1. Multi-lineage Differentiation of hMSCs.....	78
2.2.5.2. Histological Staining.....	80
2.2.5.3. Immunostaining of hMSCs surface markers.....	81
2.2.5.4. Flow cytometry	82
2.2.6. <i>In vitro</i> biocompatibility assessment	83
2.2.6.1. Sample Preparation	83
2.2.6.2. Cell culture and seeding.....	83
2.2.6.3. Cell viability.....	84
2.2.6.4. Cells activity and proliferation.....	84
2.2.6.5. Cells metabolism.....	85
2.2.6.6. Statistical analysis for different powders group.....	85
2.3. Polyelectrolyte multilayer assemblies using two-dimensional Poly (lactic acid) films to enhance cell-material interaction.....	86
2.3.1. Fabrication of PLA films	86
2.3.2. Surface modification of PLA films.....	86
2.3.3. Construction of multilayered PLA films	87
2.3.4. Physical and chemical characterization	88
2.3.4.1. X-Ray Photoelectron Spectroscopy Analysis	88
2.3.4.2. Atomic Force Microscopy Analysis	89
2.3.4.3. Transmission Electron Microscopy Analysis	89

2.3.4.4. Semi-quantitative analysis of Calcium and Collagen distribution.....	89
2.3.5. <i>In vitro</i> biocompatibility tests	89
2.3.5.1. Samples Preparation.....	90
2.3.5.2. Cell seeding.....	90
2.3.5.3. Statistical analysis for different number of multilayers PLA films	90
2.3.6. Fabrication of three-dimensional scaffolds.....	91
2.3.6.1. Three-dimensional printing of Poly (lactic acid) scaffolds.....	91
2.3.7. Fabrication of 3DP hybrid scaffolds.....	93
2.3.7.1. Surface modification of 3DP PLA scaffolds.....	93
2.3.7.2. Scaffold assemblies with newly developed coating materials	93
2.3.8. <i>In vitro</i> study on the 3DP hybrid scaffolds	94
2.3.8.1. Seeding efficiency on 3DP scaffolds	94
2.3.8.2. Static versus rotary bioreactor cultivation	95
2.3.8.3. Alkaline phosphatase staining.....	96
2.3.8.4. Lactate dehydrogenase Assay	96
2.3.8.5. Micro-computed tomography analysis.....	97
2.3.8.6. Statistical analysis	97
2.4. Promoting pre-vascularization of the scaffolds.....	98
2.4.1. Scaffolds fabrication	98
2.4.2. Sample preparation	98
2.4.3. Cell culture.....	98
2.4.4. Labelling with fluorescent dyes.....	99
2.4.5. Seeding of 4C scaffolds	100
2.4.6. Imaging	102
2.4.6.1. RUNX- 2 staining	102
2.4.6.2. CD31 staining	103
2.4.7. Enzyme linked immunosorbent assay for platelet derived growth factor-BB and vascular endothelial growth factor	103
2.4.8. Statistical analysis.....	104

Chapter 3: Production of multi-substituted Hydroxyapatite nanopowders for Bone Tissue Engineering.....	105
3.1. Introduction	106
3.2. Results	108
3.2.1. Optimization of carbonate and silicon ions contents	108
3.2.1.1. XRD Analysis	108
3.2.1.2. FTIR Analysis	111
3.2.1.3. Quantification of carbonate and silicon substituted apatite structure	113
3.2.2. Development of the as-synthesized multi-substituted HA (SiCHA)	114
3.2.2.1. XRD Analysis	114
3.2.2.2. FTIR Analysis	116
3.2.2.3. CHN analysis	117
3.2.2.4. ICP-OES Measurement.....	117
3.2.2.5. XRF Analysis.....	118
3.2.3. Development of multi-substituted HA as biomedical materials.....	119
3.2.3.1. XPS analysis	119
3.2.3.2. XRD analysis	120
3.2.3.3. FTIR analysis	122
3.2.3.4. TEM analysis	127
3.2.3.5. CHN analysis	128
3.2.3.6. Elemental analyses.....	129
3.2.4. <i>In vitro</i> biological assessments	130
3.2.4.1. Cell viability.....	130
3.2.4.2. Cell proliferation and osteogenic activity	132
3.2.4.3. Cell metabolic activity	135
3.3. Discussion.....	138
3.3.1. Preparation of as-synthesized multi-substituted HA powders.....	138
3.3.2. Development of multi-substituted HA powders as biomedical materials	145
3.3.3. <i>In vitro</i> biocompatibility assessments of the optimum as-calcined powders.....	149
3.4. Conclusion.....	152

Chapter 4: Development of novel coating materials assembly on Poly (lactic acid) (PLA) films to enhance cell-material interaction.....153

4.1. Introduction	154
4.2. Results	156
4.2.1. Investigation of the novel coating materials on PLA films	156
4.2.2. Optimization on the number of deposition cycles	158
4.2.2.1. Atomic Force Microscopy analysis.....	158
4.2.2.2. Transmission electron microscopy analysis.....	161
4.2.2.3. X-Ray Photoelectron Spectroscopy analysis	162
4.2.2.4. Histochemical characterization of calcium and collagen deposition	165
4.2.3. <i>In vitro</i> biocompatibility test.....	167
4.2.3.1. Cell viability.....	167
4.2.3.2. Cell proliferation and differentiation	169
4.2.3.3. Cell metabolic activity	173
4.3. Discussion.....	175
4.3.1. The effect of coupling agent in PEMs assembly	175
4.3.2. The effect of different number of bilayers on surface properties	177
4.3.3. <i>In vitro</i> hMSCs growth and osteogenic differentiation	179
4.4. Conclusion.....	184

Chapter 5: How does structural and functional design of three-dimensional printed scaffolds affect stem cells fate?186

5.1. Introduction	187
5.2. Results	190
5.2.1. Scaffold designs for bone TE.....	190
5.2.2. Seeding efficiency on three-dimensional scaffolds	192

5.2.3.	Optimization on the rotational speed of the rotary bioreactor	194
5.2.4.	Determining the fate of cellular scaffolds in several culture conditions	195
5.2.4.1.	Cell seeding and cell viability	196
5.2.4.2.	Cell proliferation on different scaffold designs	202
5.2.4.3.	Total protein production.....	210
5.2.4.4.	Measuring the percentage of cytotoxicity	216
5.2.4.5.	Cell phenotypic expression	225
5.2.4.6.	Early osteogenic differentiation.....	230
5.2.4.7.	Micro-computed tomography analysis.....	238
5.3.	Discussion.....	249
5.3.1.	The effect of seeding efficiency on establishing a 3D culture.....	249
5.3.2.	The impact of rotating speed on cell survival	252
5.3.3.	The fate of hMSCs cultured on several structural and functional designs of 3DP hybrid scaffolds under different culture conditions	254
5.4.	Conclusion.....	263
Chapter 6: Does the crosstalk between human mesenchymal stem cells and human umbilical vein endothelial cells promote pre-vascularization of bone constructs?.....264		
6.1.	Introduction	265
6.2.	Results	270
6.2.1.	Imaging labelled cells on the 3DP hybrid scaffolds	270
6.2.2.	Immunocytochemistry staining.....	273
6.2.3.	Quantification of secretion of pro-angiogenic growth factors.....	277
6.3.	Discussion.....	280
6.4.	Conclusion.....	285

Chapter 7: General discussion, Concluding Remarks and Future Work.....	286
7.1. General Discussion	287
7.2. Concluding Remarks	301
7.3. Future Work.....	302
References.....	305
Appendix.....	338

List of Abbreviations

3DP	Three-dimensional printing
AFM	Atomic Force Microscopy
ALP	Alkaline Phosphatase
AR	Alizarin Red
BE	Binding Energy
BL	Bilayers
CaCO ₃	Calcium carbonate or Calcite
CaO	Calcium oxide
CAD	Computer-aided design
CHA	Carbonated Hydroxyapatite
CHN	Carbon, Hydrogen, Nitrogen
CLSM	Confocal Laser Scanning Microscopy
DNA	Deoxyribonucleic acid
ECM	Extracellular Matrix
EM	Endothelial Media
FITC	Fluorescein isothiocyanate
FDM	Fused Deposition Modelling
FTIR	Fourier Transform Infra-Red
HA	Hydroxyapatite
hMSC	Human Bone Marrow-derived Mesenchymal Stem Cell
HUVEC	Human Umbilical Vein Endothelial Cell
ICP-OES	Inductively Couple Plasma-Optical Emission Spectroscopy
LBL	Layer-by-layer
LDH	Lactate dehydrogenase
MTT	3-(4, 5-dimethylthiazol-2-yl)-2, 5-diphenyltetrazolium bromide
OM	Osteogenic Media
PDGF	Platelet-Derived Growth Factor
PEMs	Polyelectrolyte Multilayers
PLA	Poly (lactic acid)
PLGA	Poly (lactic-co-glycolic acid)
PI	Propidium Iodide
PM	Proliferation Media
RP	Rapid Prototyping
RWV	Rotating Wall Vessel
SEM	Scanning Electron Microscope
SiHA	Silicon Hydroxyapatite
SiCHA	Multi-substituted Hydroxyapatite
SR	Sirius Red
TEM	Transmission Electron Microscope
XRD	X-Ray Diffraction
XRF	X-Ray Fluorescence
XPS	X-Ray Photoelectron Spectroscopy
VEGF	Vascular Endothelial Growth Factor

List of Figures

Chapter 1

1.1	Hierarchical structural units of bones on different scales.	6
1.2	Bone remodelling.	9
1.3	Phases of bone remodeling.	11
1.4	Schematic description of diffusion and transport processes in vascularized tissues <i>in vivo</i> .	12
1.5	Common treatment for bone trauma and diseases.	14
1.6	The <i>in vitro</i> tissue engineering approach.	18
1.7	Representative HA scaffolds.	24
1.8	Schematic diagrams of different RP techniques categorized by the processing method.	34
1.9	3D scaffold systems of various porosity and pore geometry fabricated by FDM.	36
1.10	The mesengenic process.	42
1.11	Rotary bioreactor.	47

Chapter 2

2.1	Flowchart of the process for the synthesis of CHA powders by nanoemulsion method.	70
2.2	Flowchart of the process for the synthesis of SiHA powders by nanoemulsion method.	71
2.3	Flowchart of the process for the synthesis of SiCHA powders by nanoemulsion method.	72
2.4	CAD drawing for (a) 2- and (b) 4 channel scaffolds designed in this study.	92
2.5	Printing steps at different layers in the construction of the 3D scaffolds.	93
2.6	Illustration, summarising the seeding protocols for the co-culture of HUVECs/hMSCs 4C scaffolds.	101

Chapter 3

3.1	XRD pattern of the CHA as-synthesized powders with different carbonate contents.	109
3.2	XRD pattern of the SiHA as-synthesized powders with different silicon contents.	109
3.3	FTIR spectra of CHA as-synthesized powders.	112
3.4	FTIR spectra of SiHA as-synthesized powders.	112
3.5	XRD spectra of the SiCHA as-synthesized powders.	115
3.6	FTIR spectra of the SiCHA as-synthesised powders.	116
3.7	XPS analysis of the as-calcined powders.	119
3.8	XRD analysis of the calcined powders at 500-700°C.	120
3.9	FTIR spectra of CHA and SiHA as-calcined powders.	123
3.10	FTIR spectra of SiCHA-1 and SiCHA-2 as-calcined powders.	125
3.11	TEM images of the investigated powders calcined at 500°C.	127
3.12	CLSM of the positive controls.	131
3.13	CLSM images of CHA, SiHA, SiCHA-1 and SiCHA-2 powders	131

	cultured in osteogenic media for different time periods.	
3.14	Effect of CHA, SiHA, SiCHA-1 and SiCHA-2 as-calcined powders on (a) cell proliferation indicated by the amount of DNA and (b) the ALP activity were measured after day 7, 14 and 21 of treatment.	134
3.15	Effect of carbonate or/and silicon-substituted HA as-calcined powders on (a) the total protein production and (b) cell metabolic activity determined by alamar blue.	137
 Chapter 4		
4.1	Surface topography of the PLA films was assessed using SEM analysis. Images demonstrated different PLA surfaces.	157
4.2	AFM images showing topography of (a) 0-BL; (b) 1-BL; (c) 3-BL; (d) 5-BL and (e) 10-BL PLA films.	160
4.3	TEM images of (a) 1-BL; (b) 3-BL; (c) 5-BL and (d) 10-BL.	161
4.4	XPS scan spectra of control PLA films, (a) before (0-BL) and (b) after (0-BL*) aminolysis.	163
4.5	XPS scan spectra of coated PLA films deposited with (a) 1-BL, (b) 3-BL, (c) 5-BL and (d) 10-BL, respectively.	163
4.6	Light microscopy imaging of Alizarin Red (AR) and Sirius Red (SR) Staining on 0-, 1-, 3-, 5- and 10-BL films.	166
4.7	CLSM images of control and coated PLA films.	168
4.8	Cell proliferation of hMSCs indicated by the DNA contents after 7 and 14 days cultured on control PLA (0-BL) and PLA films deposited with different number of coating layers of 1-, 3-, 5- and 10-BL, respectively.	171
4.9	The ALP activity of hMSCs seeded on control PLA (0-BL) and PLA films deposited with different number of coating layers of 1-, 3-, 5- and 10-BL, respectively.	171
4.10	The levels of total protein released by hMSCs cultured on control PLA (0-BL) and PLA films deposited with different number of coating layers of 1-, 3-, 5- and 10-BL, respectively.	174
4.11	Metabolic activity of hMSCs seeded on control and coated PLA films at 7 and 14 days of culture.	174
 Chapter 5		
5.1	Examples of three-dimensional drawing for 2- and 4-channel scaffolds.	191
5.2	Cell distribution on different scaffold designs seeded with one-sided and two-sided seeding method.	193
5.3	Cell viability on different structural designs of 3DP hybrid scaffolds at 20 and 40 rpm, respectively.	194
5.4	CLSM of hMSCs seeded on all four scaffold designs cultured under static condition OM and PM after 1 day (for 3DP hybrid scaffolds) and 3 days (for HA scaffolds).	196
5.5	CLSM images of hMSCs seeded on HA scaffolds cultured either under static or dynamic conditions in OM and PM for different time periods of 7, 14 and 21 days.	197
5.6	CLSM images of hMSCs seeded on 2C scaffolds cultured either under static or dynamic conditions in OM and PM for different time periods of	198

	7, 14 and 21 days.	
5.7	CLSM images of hMSCs seeded on 4C scaffolds cultured either under static or dynamic conditions in OM and PM for different time periods of 7, 14 and 21 days.	199
5.8	CLSM images of hMSCs seeded on mesh scaffolds cultured either under static or dynamic conditions in OM and PM for different time periods of 7, 14 and 21 days.	200
5.9	Comparison of cell viability for different scaffold designs after 21 days cultured under static and dynamic conditions in OM and PM.	201
5.10	The amount of DNA of hMSCs growing on (a) HA; (b) 2C; (c) 4C and (d) mesh scaffolds under different culture conditions.	207
5.11	Comparison of the DNA amounts released by hMSCs after 21 days cultured on HA, 2C, 4C and mesh scaffolds in different culture conditions.	209
5.12	The levels of total protein produced by hMSCs cultured on (a) HA; (b) 2C; (c) 4C and (d) mesh scaffolds under different culture conditions	214
5.13	Comparison of the levels of total protein produced by hMSCs after 21 days cultured on HA, 2C, 4C and mesh scaffolds in different culture conditions.	216
5.14	The percentages of LDH activity of hMSCs cultured on (a) HA; (b) 2C; (c) 4C and (d) mesh scaffolds under different culture conditions.	222
5.15	The percentages of LDH activity on HA, 2C, 4C and mesh scaffolds in different culture conditions after 21 days.	224
5.16	ALP staining for all scaffold designs at day 0.	225
5.17	ALP staining of the HA scaffolds after 7, 14 and 21 days under static and dynamic conditions in both OM and PM.	225
5.18	ALP staining of the 2C scaffolds after 7, 14 and 21 days under static and dynamic conditions in both OM and PM.	226
5.19	ALP staining of the 4C scaffolds after 7, 14 and 21 days under static and dynamic conditions in both OM and PM.	227
5.20	ALP staining of the mesh scaffolds after 7, 14 and 21 days under static and dynamic conditions in both OM and PM.	228
5.21	ALP staining for different scaffold designs after 21 days cultured under static and dynamic conditions in OM and PM.	229
5.22	The levels of ALP activity of hMSCs growing on (a) HA; (b) 2C; (c) 4C and (d) mesh scaffolds under different culture conditions.	235
5.23	The comparison of the levels of ALP activity of hMSCs after 21 days cultured on HA, 2C, 4C and mesh scaffolds in different culture conditions.	237
5.24	Density maps of HA cellular scaffolds in different culture conditions after 7, 14 and 21 days obtained from Micro-CT analysis.	240
5.25	Density maps of 2C cellular scaffolds in different culture conditions after 7, 14 and 21 days obtained from Micro-CT analysis.	241
5.26	Density maps of 4C cellular scaffolds in different culture conditions after 7, 14 and 21 days obtained from Micro-CT analysis.	242
5.27	Density maps of mesh cellular scaffolds in different culture conditions after 7, 14 and 21 days obtained from Micro-CT analysis.	243
5.28	Density maps of HA, 2C, 4C and mesh scaffolds after 21 days in different culture conditions.	244

Chapter 6		
6.1	Illustration depicting the mechanism involved in the crosstalk between HUVECs and hMSCs co-culture system.	268
6.2	CLSM images showing the fluorescent labelling of the hMSCs (labelled blue) and HUVECs (labelled red) on 4C scaffolds on different samples after day 3 and 10 post hMSCs addition.	271
6.3	Cell morphology of the co-culture system in the channel of the 4C scaffolds after 3 and 10 days post-hMSCs addition.	272
6.4	Immunostaining of the RUNX-2 expression on the surface of the scaffolds after 3 and 10 days post-hMSCs addition and their relative fluorescence intensity, respectively.	274
6.5	Immunostaining of the CD31 expression in the channel of the scaffolds after 3 and 10 days post-hMSCs addition and their relative fluorescence intensity, respectively.	276
6.6	The level of (a) PDGF-BB and (b) VEGF produced by hMSCs alone, HUVECs alone and co-culture model after day 3 HUVECs seeding only, day 6 and 10 post-hMSCs additions.	279
Appendix		
A1	hMSCs adhere to the tissue culture plastic.	341
A2	Multi-lineage differentiation of hMSCs after 21 days in culture.	342
A3	hMSC staining for CD markers.	343
A4	Quantification of hMSC CD markers.	344
A5	X-ray Micro-CT of different structural designs of dry scaffolds (before seeding).	345

List of Tables

Chapter 1

1.1	The comparative composition of human bone, enamel and synthetic hydroxyapatite (HA) ceramics.	4
1.2	Mechanical properties of cortical and cancellous bones.	5
1.3	Bone cell types and their respective functions.	7
1.4	Definitions of osteoinductive, osteoconductive and osseointegration.	23
1.5	Advantages and disadvantages of conventional scaffold fabrication techniques.	32
1.6	The merits and demerits of RP technique for different processing methods.	35
1.7	Examples of PEMs used in Tissue Engineering Applications.	38
1.8	Basic desired characteristics for ideal bone scaffolds.	39
1.9	Osteogenic supplements and their respective functions.	45
1.10	Comparisons of bioreactor system in BTE applications.	49
1.11	Typical vibration bands of multi-substituted hydroxyapatite (SiCHA).	52
1.12	Basic principle, depth analysed, spatial resolution and analytical sensitivity of XPS analysis.	53
1.13	Standard categories of biocompatibility evaluation of biomaterials.	60

Chapter 2

2.1	Summary of the raw material used in nanoemulsion method and their functions.	68
2.2	Different carbonate (x) and silicon (y) molar contents of the powders.	75
2.3	Relevant proliferation and differentiation media compositions used in this study.	79
2.4	Elements of interest and their binding energies on PLA films.	88

Chapter 3

3.1	Lattice parameters and crystallite sizes of CHA and SiHA as-synthesized powders.	110
3.2	Percentage of carbonate, Ca/P+Si and Si/P ratios of the as-synthesized CHA and SiHA powders.	113
3.3	Lattice parameters and crystallite sizes of SiCHA and SiHA as-synthesized powders.	115
3.4	Percentage of carbonate (wt% CO ₃) of SiCHA as-synthesized powders.	117
3.5	Ca, P and Si concentrations of the SiCHA as-synthesized powders.	117
3.6	Calculated Si, measured Si and Si/P ratio of SiCHA as-synthesized.	118
3.7	Lattice parameters and crystallite sizes of CHA, SiHA, SiCHA-1 and SiCHA-2 nanopowders calcined at 500-700°C.	121
3.8	Results of FTIR analysis of as-calcined powders at 500-700°C.	126
3.9	CHN analysis of the investigated powders at 500-700°C.	128
3.10	ICP-OES and XRF elemental analyses of the investigated powders at 500-700°C.	129

Chapter 4

4.1	Surface roughness of PLA films measured on the control PLA (0-BL) and coated PLA with 1-, 3-, 5- and 10-BL, respectively.	158
4.2	Atomic percentage (at%) of the control PLA (0-BL) and coated PLA with 1-, 3-, 5- and 10-BL, respectively.	164

Chapter 5

5.1	Summary of the basic properties of HA, 2C, 4C and mesh scaffold.	191
5.2	Percentages of cell attachment onto the scaffolds with different cell volume suspensions on different scaffold designs.	192
5.3	Total volume of the dry scaffolds (before seeding) obtained from Micro-CT analysis.	245
5.4	The total volumes and percentages of mineralization of the cellular scaffolds under different culture conditions after 21 days.	246
5.5	Summary of the overall performances for HA, 2C, 4C and mesh scaffolds under different culture conditions.	248

Acknowledgement

I would like to take this golden opportunity to express my special heartiest gratitude and thankfulness to my main supervisor, Professor Alicia El Haj, for her constant guidance, support and patience throughout the years that had made this thesis a reality. Alicia has successfully pushed me beyond my comfort zone, which had helped me to be an independent researcher. I am particularly thankful to Alicia for all the opportunities to travel and present my work at seminar and conference locally and abroad, thus enabling me to meet and expand my network with renowned experts all around the world. That broadens my knowledge and wisdom too. Thank you, Alicia.

I also wish to express my warmest and sincere thanks to both my co-supervisors in Newcastle University, Professor Kenny Dalgarno and Dr Oana Bretcanu. Thank you for helping me so much from the first moment I arrived in Newcastle till I finished the 15 months collaboration work there. Kenny's positive vibes, calm and patience always boosted my motivation to work and succeed, in particular when I felt down. Oana has been a great help and kind supervisor - Thank you. I am also very thankful to my academic advisor, Professor Sally Roberts from Robert Jones and Agnes Hunt Orthopaedic Hospital, for her support and advice throughout the years.

I would also like to thank Alicia for giving me two amazing post-docs, Dr Ian Wimpenny and Dr Yvonne Reinwald. They are my guardian angels that were always by my side through the ups and downs during my PhD's life. Ian is a fantastic teacher who was the first person that taught me about cell culture when I started with zero knowledge. And as for Yvonne the rotary bioreactor's queen, thank you for the time and patience in training me on the bioreactor. I am very thankful and appreciate both, Ian and Yvonne for their effort in proof reading of this thesis.

I would like to thank Dr Ana Marina Ferreira Duarte for her help with the coating technique. Thank you for your suggestions and guidance. Marina's drive has inspired me to develop the innovative coating materials assembly established in this work.

A massive thank you to all El Haj research group in particular to my triplet, Michael Rotherham and Joshua Price. Thank you for all the help in the lab and support during writing this thesis. I would like to acknowledge the Dalgarno research group back in Newcastle University as well for all the help and making my stay in Newcastle

unforgettable. A special thanks goes to Dr Paul Roach for his generous supports in helping me with the CAD drawing and for the mock-viva.

I am highly indebted to Universiti Sains Malaysia (USM) for giving me the support and opportunity to enhance my knowledge and research ability under the Academic Staff Training Scheme and to Ministry of Higher Education Malaysia (MOHE) for the scholarship provided. Their support had enabled me to achieve my dreams thus far. I am also very grateful to be part of Arthritis Research UK (ARUK) family. Thank you to all ARUK-TEC team from Keele, Cambridge, York, Aberdeen and Newcastle for the activities and interchange of expertise. I also wish to extend my gratitude to my previous supervisors back in Malaysia, Professor Ahmad Fauzi and Associate Professor Ahmad Azmin, for their support and encouragement for me to pursue my study. Fauzi has been a great motivator to me since I was an undergraduate student till now- Thank you so much.

To my fellow PhD colleagues and postdocs at Guy Hilton, a genuine thank you for all your help with literally every aspect of my research and for making my every day work so enjoyable. A heartfelt thank you goes to Anthony Deegan, Sandhya Moise, Faiza Musa, Tugce Ipek and Mohammed, for lending me your shoulders to cry on and cheer me up. To my 81 BG'girls- Wani, Laily, Sheila and Sufea, thank you for the amazing time we had especially for the baking in the middle of the night, hopefully our dream to own a café will come true. To those whom I have not mentioned your names but had directly or indirectly assisted me, thank you ever so much to all of you for the assistance and support.

Last but most importantly from the deepest of my heart, special words of heartiest appreciation and syukur belongs to my beloved dad and mum, Hj Baba Ismail Eusoff Ahmad and Hjh Latipah Othman, my loving sisters, Yanty Azliana and Norhayu and my caring brother, Yazry Helmy for their never ending love, blessings, continuous prayers and valuable support for me to be where I am now. TERIMA KASIH SEMUA. Last but never the least, my loving hugs and kisses to my little nephew and nieces, Yusry, Tasnim and Auni, who bring the sunshine of happiness to my family and me. I love you all.

YANNY MARLIANA BABA ISMAIL

1st June 2016

Chapter 1

Introduction

1.1. Clinical needs for bone regeneration

Bone defects resulting from trauma, disease or infection can dramatically alter one's body equilibrium and quality of life (Salgado et al. 2004). It is considered as one of the major public health problems, which would result in huge socioeconomic implications (Rupani et al. 2012). For younger people who generally have higher regenerative capacity, most of fractures will possibly heal without the need of any intervention (Stevens 2008). However, as the individual and society grows older (65 years plus population), they are exposed to higher risk of bone-related health problems such as osteoarthritis or osteoporosis (Hing 2004; Lemaire et al. 2004). Osteoarthritis (OA) is not only a wear and tear disease leading to loss of cartilage, but rather, an abnormal remodelling of joint tissues driven by a host of inflammatory mediators within the affected joint (Loeser et al. 2012; Berenbaum 2013). Based on statistical study conducted by Arthritis Research United Kingdom (ARUK) in 2013, approximately 8 million people in the UK are affected by osteoarthritis in which more severe cases were seen in woman aged in the late 40s onwards. On the other hand, osteoporosis, typically as a result of hormonal changes and oxidative stress related to aging, is a condition that weakens bones, thus making them fragile and more likely to break (Hing 2004; Lemaire et al. 2004). The reduction of bone mass from osteoporosis is mainly due to a decrease in the number of osteoblasts rather than their functioning capacity, which could be due to reduce osteoblastogenesis or increased apoptosis (Jilka et al. 1996). According to the National Health Service (NHS) records, more than 300 000 people received hospital treatment for fragility fractures every year as a result of osteoporosis, thus resulting in NHS to spend a massive amount of money. For instance, hip fractures alone cost the UK an estimated £5 million per day- that is approximately £2 billion pounds per year.

Historically, bone defects are treated by autograft or allograft. Transplanting autologous bone (i.e. bone from patient) has been considered as gold standard in clinic as it integrates reliably with the host bone and avoid the immune- and disease-related complications (Stevens 2008). Allograft, on the other hand, is bone donated from another member of the same species. However, the drawbacks with this treatment such as short supply, high cost, donor site morbidity as associated with the harvest and potential risk of disease transmission have driven increasing needs and use of bone graft substitute (BGS) materials (Lord et al. 1988; Siber et al. 2003). Although several advances have been made for BGS to address these drawbacks, each of the current BGS has still their own limitations. To date, no adequate bone implant has been developed to meet the clinical needs, hence, bone deficiencies remains unresolved. The search of new bone regeneration strategies is therefore a key priority fuelled by the debilitating pain associated with bone damage, and the increasing medical and socioeconomic challenge of the aging population. In this context, bone tissue engineering (BTE) appears to be a promising approach to overcome the limitations of current bone grafts (Salgado et al. 2004; Rupani et al. 2012).

1.2. Bone anatomy

Bone is a dynamic and a highly vascularized tissue, which undergoes remodelling (continuously broken down and rebuilt), throughout the lifetime of an individual (Rodan 1992; Sommerfeldt & Rubin 2001). Bone tissue is comprised of two core components; (i) the mineralized inorganic phase consisting mainly of carbonated hydroxyapatite, and (ii) non-mineralized organic phase, which is predominantly the collagen type I. The comparative composition of human bone, enamel and synthetic hydroxyapatite (HA) ceramics are shown in Table 1.1 (LeGeros 1991; Landi et al. 2003; Pietak et al. 2007; Sprio et al. 2008; Landi et al. 2010).

Table 1.1: The comparative composition of human bone, enamel and synthetic hydroxyapatite (HA) ceramics (LeGeros 1991; Landi et al. 2003; Pietak et al. 2007; Sprio et al. 2008; Landi et al. 2010).

Constituents (wt%)	Bone	Enamel	HA
Calcium	24.5	36.0	30.9
Phosphorus	11.5	17.7	18.5
Sodium	0.7	0.50	tr
Potassium	0.03	0.08	tr
Magnesium	0.55	0.44	tr
Carbonate	2-8*	3.20	tr
Silicon	0.03-0.5**	0.04	-
Fluoride	0.02	0.01	-
Chloride	0.10	0.30	-
Total inorganic	65.0	97.0	100
Total organic	35.0	1.0	

*Carbonate content varies depending on the age of the individual and bone site; ** Silicon content in bone mineral density depends on the levels of silicon dietary intake, age and sex of the individual and bone site; tr = trace elements.

Typically, bone consists of approximately 65% mineralized inorganic phase and 35% non-mineralized organic matrix (Weiner & Wagner 1998; Best et al. 2008; Hannink & Arts 2011). Collagen is known to provide the bone with tensile strength and flexibility, whereas mineralization increases the stiffness and the compressive strength of the bone at the expense of its energy-storing capacity (Rupani et al. 2012). Besides the collagenous matrix, over 200 different types of non-collagenous matrix proteins such as glycoproteins, proteoglycans and sialoprotein were also found in the bone extracellular matrix (ECM). These organic proteins contribute to the abundance of signals in the immediate ECM milieu (Stevens 2008). In addition, these organic proteins also form physically or chemically cross-linked networks, which regulates the expression of osteoblast phenotype and supports osteogenesis both *in vitro* and *in vivo* (Zhao et al. 2014). Therefore, these ECM-like biomacromolecules such as hyaluronic acid and collagen type I have been incorporated into the production of 3D scaffolds for bone regeneration with the aim to closely mimic the bone structure (Zhang et al. 2005; Hoyer et al. 2012; Yu et al. 2012).

The development of macroscopically diverse bony structures *in vivo* is greatly influenced by distinct loading conditions. Adult skeleton is made up of more than 206 different bones, ranging from the long bones found in limbs, short bones in the wrist and ankle, flat bones in the sternum and skull as well as the irregular bones such as pelvis and vertebrae. The human skeleton consists of 80% cortical bone (compact) and 20% spongy cancellous bone (porous) (Sikavitsas et al. 2001; Salgado et al. 2004). Cortical bone is the denser bone, consisting of parallel cylindrical units with 5-10% porosity (Buckwalter et al. 1995). Cortical bone is primarily found in the shaft of long bones (e.g. femur, tibia, fibula) and forms the outer shell around the cancellous bone at the end of joints and the vertebrae (Hill 1998; Sikavitsas et al. 2001). In contrast, the cancellous bone acquires sponge-like honeycomb morphology, comprising of branching bars, plates, and rods of various sizes called trabeculae (Buckwalter et al. 1995; Sikavitsas et al. 2001). The mechanical properties of cancellous bone are greatly dependent on its porosity and the way it is structured. Its porosity ranges from 50 to 90%, making its ultimate compressive strength and modulus of elasticity 10 times inferior compared to the cortical bone as shown in Table 1.2 (Velasco et al. 2015). Besides that, the pores also perform other physiological functions and contain the marrow. Cancellous bone is normally found at the end of the long bones in vertebrate and in flat bones like the pelvis (Buckwalter et al. 1995; Hill 1998; Sikavitsas et al. 2001).

Table 1.2: Mechanical properties of cortical and cancellous bones (Velasco et al. 2015).

Property	Cortical	Cancellous
Compressive strength (MPa)	130-230	2-12
Tensile strength (MPa)	50-150	10-100
Strain to failure	1-3	5-7
Young Modulus (GPa)	7-30	0.02-0.5

Bone performs several primary functions in the maintenance of body systems. These include (1) protection of vital internal organs, (2) assists in locomotion by providing support and site of muscle attachment, (3) ensuring that the skeleton has sufficient load-bearing capacity, (4) generation of red and white blood cells for oxygenation and immunological protection of other tissues and (5) serving as mineral reservoir of calcium, phosphate, and other important ions (Rodan 1992; Sommerfeldt & Rubin 2001; Sikavitsas et al. 2001). Fig. 1.1 shows the different level of structural units in typical human bones.

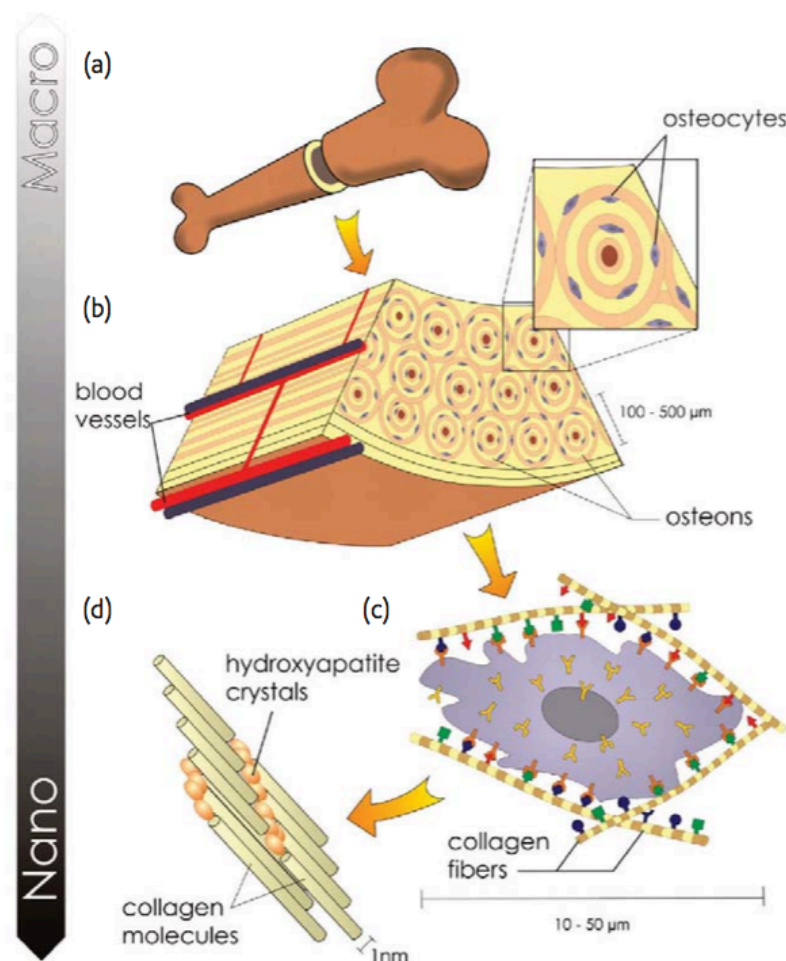


Fig. 1.1: Hierarchical structural units of bones on different scales. The strong calcified outer compact layer (a), contains many osteons (b), The resident cells are coated in a forest of cell membrane receptors that respond to specific binding sites (c) and the explicit nanoarchitecture of the surrounding extracellular matrix (d) (Stevens & George 2005). Re-printed with permission from Science.

The formation, maintenance and resorption of bone tissue results from the interaction of three major cell types: osteoblasts, osteocytes and osteoclasts. The morphological characteristics and functions of these cells are listed in Table 1.3 (Salgado et al. 2004; Young et al. 2006; Jayakumar & Di Silvio 2010).

Table 1.3: Bone cell types and their respective functions (Noble & Reeve 2000; Knothe Tate et al. 2004; Salgado et al. 2004; Young et al. 2006; Jayakumar & Di Silvio 2010).

Cell type	Morphological characteristics	Function
Osteoblasts	Mononuclear cells around 15-30 μm in size with a spherical nucleus and abundant basophilic cytoplasm comprising rough endoplasmic reticulum, golgi apparatus, and mitochondria, along with active cytoskeletal proteins	Responsible for the production and mineralization of the bony matrix (collagen type I and non-collagenous proteins)
Osteocytes	Most abundant cells in bone, stellate shaped, possess fewer organelles than the osteoblasts, present in the lacunae within the mineralized matrix	Mechanosensor cells of bone and actively involved in bone turnover (regulators of osteoblasts and osteoclasts)
Osteoclasts	Polarized cells, multi-nucleated cells	Responsible for bone resorption during remodelling, the repair of microdamage and the adaptation to mechanical loading

1.3. Natural bone formation and remodelling pathways

1.3.1. Bone formation

The development of bone tissue can be classified into two distinct process, endochondral or intramembranous ossification, depending on the type of bone that is being developed. Both of the ossification processes occur in close proximity to vascular ingrowth. The distinction between endochondral and intramembranous formation rests on whether cartilage serves as the precursor for the bone (endochondral ossification) or whether the bone is formed by simpler method, without the intervention of a cartilage precursor

(intramembranous ossification). Endochondral ossification developed the bones of the extremities and those parts of the axial skeleton that bears weight, for example, the vertebrae. On the other hand, the flat bones of the skull and various facial bones were developed by intramembranous ossification during embryonic development (Kanczler & Oreffo 2008).

In endochondral ossification, the coupling of chondrogenesis and osteogenesis to control the rate of bone ossification is regulated on the level of vascularization of the growth plate (Gerber & Ferrara 2000). Indeed, vascular endothelial growth factor (VEGF) isoforms play an important role in organizing metaphyseal and epiphyseal vascularization, cartilage formation and ossification during endochondral bone growth (Maes et al. 2002). Besides VEGF, Indian Hedgehog (Ihh) and parathyroid hormone-related protein (PTHrP) are also the essential components in endochondral ossification. Ihh is one of the proteins in the mammalian hedgehog family, which involved in chondrocyte differentiation, proliferation and maturation especially during endochondral ossification. It regulates its effect by feedback control of PTHrP, which acts as endocrine, autocrine, paracrine and intracrine hormone. PTHrP regulates endochondral bone development by maintaining the endochondral growth plate at a constant width (Lai & Mitchell 2005).

In contrast, intramembranous ossification is characterized by infiltration of capillaries into the mesenchymal zone, as well as the advent and differentiation of mesenchymal cells into mature osteoblasts. Bone matrix is then constitutively deposited by osteoblasts leading to the formation of bone spicules. These bone spicules will then grow and develop by combining with other spicules, subsequently forming trabeculae. While the trabeculae increase in size and number, they form interconnected woven bone, which ultimately is replaced by more organized, stronger, lamellar bone (Marks & Hermey 1996).

1.3.2. Bone remodelling

Back in 1892, Wolff proposed the idea that bone remodelling is controlled by mechanical as well as metabolic factors (Frost 1994). During our daily life, bone is exposed to several kinds of loading such as tension, compression, bending, shear, torsion and a combination of these loads which has been found to regulate its metabolism and growth (Palmoski et al. 1979).

Calcium-containing inorganic mineral is a bone building block and in order to mobilize calcium, tissue has to be broken down essentially (Rodan 1992). To provide structural support, bone is continuously being remodelled in response to the applied stresses (Manolagas 2000). For a normal healthy bone, the breakdown and formation of bones should be almost at the same rate so as to avoid bone loss and other serious conditions such as osteoporosis, Paget's disease, and metastatic disease. Besides these diseases, bones are also prone to injuries, defects, and tumours. Fig. 1.2 shows the states of (a) normal bone remodelling and (b) defective resorption (Kini & Nandeesh 2012).

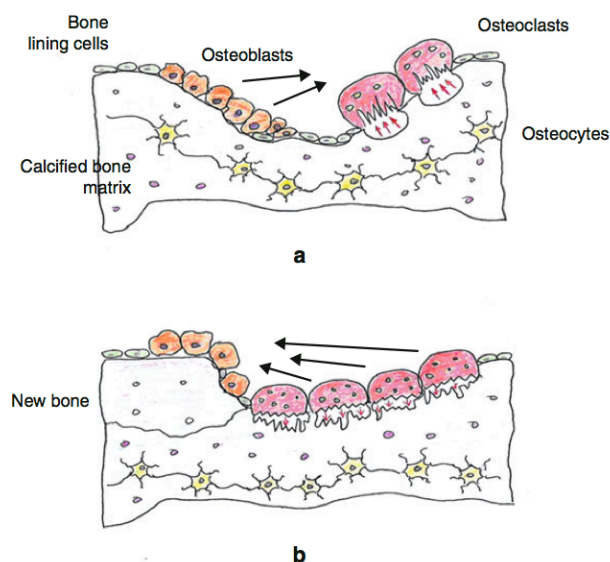


Fig. 1.2: Bone remodelling. This figure shows the states of (a) normal bone remodelling and (b) defective resorption (Kini & Nandeesh 2012). Re-printed with permission from Springer, License Number: 3786041281497.

Bone remodelling involves the coupling process of bone formation and resorption and they consists of six phases as described below (Fig. 1.3) (Rucci 2008; Kini & Nandeesh 2012).

1. Quiescence phase, where the lining cells are inactive osteoblasts. Quiescence is the resting state of the bone surface.
2. Activation stage. Osteoclasts then gather on the bone surface, in small pits known as Howship's lacunae at the second phase.
3. Resorption is the third phase, whereby these osteoclasts remove old bone tissues by removing the mineral matrix and breaking down the organic collagen fibres.
4. Reversal phase. The resorption of osteoclasts ends and osteoblasts now replaced osteoclasts at phase four.
5. The formation of new bone begins at phase five where the osteoblasts lay down new bone by firstly creating a matrix of collagen known as osteoid. The osteoblasts then mineralize osteoid to form new bone.
6. The final phase of bone remodelling is called mineralization. The process begins 30 days after deposition of the osteoid and ends at 90 days in cancellous bone, while ending in 130 days in cortical bone. The bone returns to its resting state at phase six. At the end of bone remodelling, the amount of bone formation should be equal to bone resorbed.

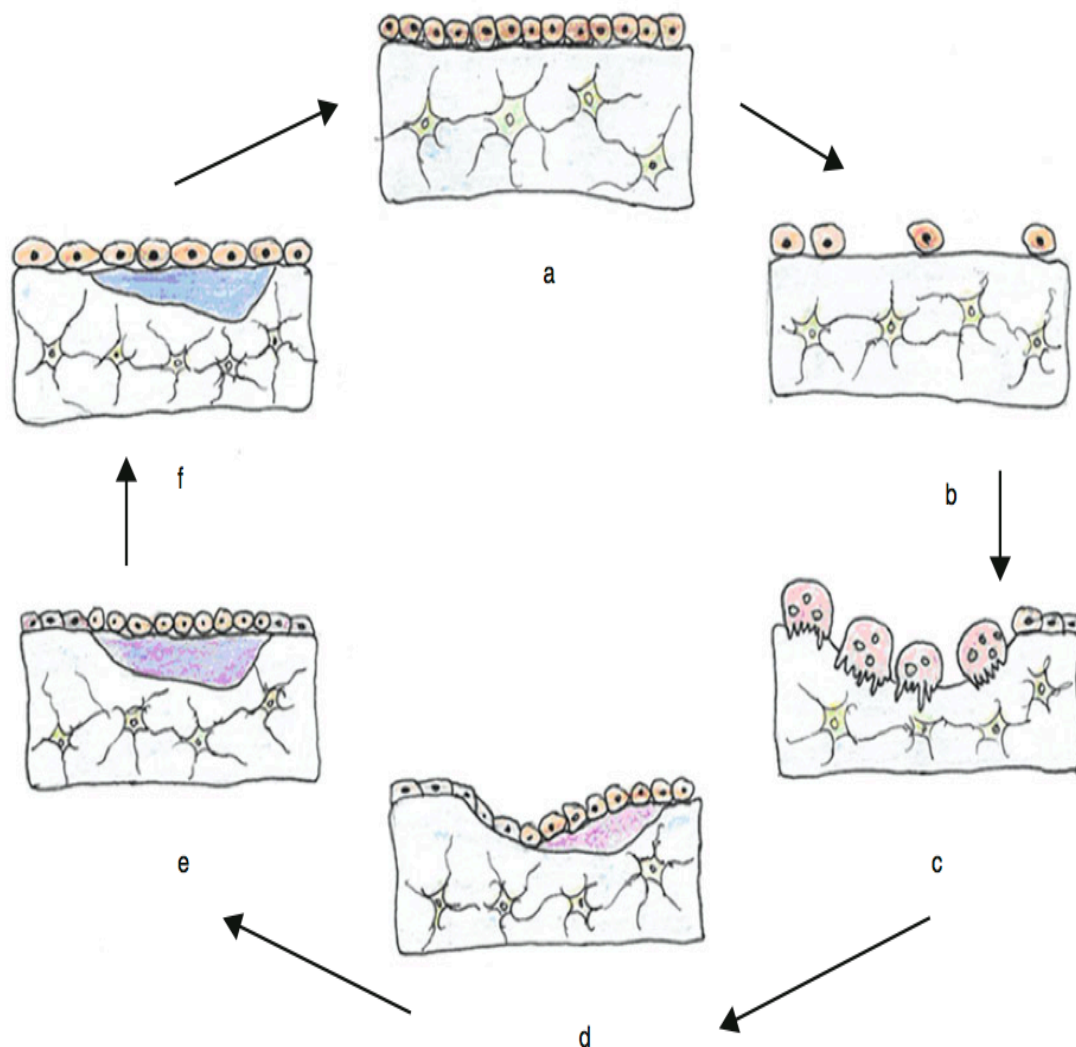


Fig. 1.3: Phases of bone remodelling: (a) quiescent phase where flat bone lining cells are seen lining the endosteal membrane, (b) showing activation stage characterized by cell retraction with resultant membrane resorption, (c) resorption phase where these osteoclasts remove old bone tissue by removing the mineral matrix and breaking down the organic collagen fibres, (d) reversal phase where the resorption of osteoclasts ends and replaced by osteoblasts with underlying new osteoid matrix, (e) formation phase where the osteoblasts lay down new bone by firstly creating a matrix of collagen known as osteoid, (f) mineralization phase where formation of bone structure unit with progression to quiescent phase (Kini & Nandeesh 2012). Re-printed with permission from Springer, License Number: 3786041281497.

1.3.3. The role of vascularization in bone development

Bone is a complex tissue interpenetrated with a highly vascularized network in the human body (Salgado et al. 2004; Duttonhoefer et al. 2013). Most tissues in the body are supplied with nutrients and oxygen through blood vessels with a maximum distance of 200 μm from the adjacent capillary network (Rouwkema et al. 2008; McFadden et al. 2013). The maximum distance between these capillaries is correlated with the diffusion limit of oxygen (Fig. 1.4). However, only limited soft tissues like skin and cornea, where the cells can be supplied with nutrients and oxygen via diffusion from the blood system over longer distance (Novosel et al. 2011). As bony tissue is highly dense, the nutrients cannot be diffuse over long distance and they therefore demand a highly efficient vascular supply (Hing 2004). Even within dense cortical bone tissue, the organization of vascular canals ensures that the blood vessels are no more than 300 μm away from the cells (Buckwalter et al. 1995).

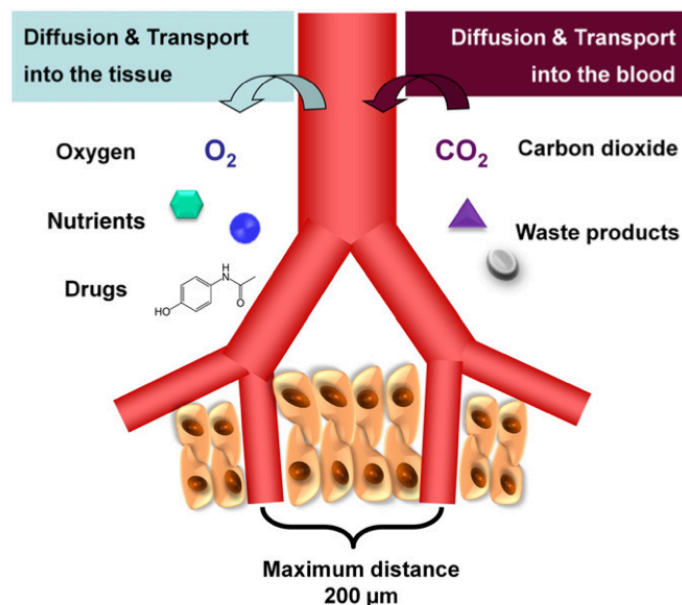


Fig. 1.4: Schematic description of diffusion and transport processes in vascularized tissues in vivo. The surrounding tissue is supplied with oxygen, nutrient and drugs via the vasculature. Waste products and CO₂ are cart away from the tissue into the blood vessel (Novosel et al. 2011). Re-printed with permission from Elsevier, License Number: 3781960701104.

1.4. Bone repair and regeneration

1.4.1. Bone defects

Bone has the intrinsic regenerative capacity as part of the repair process in response to injury, as well as through the skeletal development or continuous remodelling throughout an adult life (Einhorn 1998). Unlike in other tissues, bone injuries or fractures would heal without leaving any scar. In fact, the regenerated bone is largely restored and it is indistinguishable from the adjacent uninjured bone (Einhorn 1998). However, there are cases of impaired fracture healing where, for instance, up to 13% of fractures in the tibia are being associated with delayed union or non-union fracture (Audigé et al. 2005). According to the US Food and Drugs Administration (FDA), a non-union is defined as a fractured bone that has not completely recovered within 9 months of injury and that has not shown progression towards healing over 3 following months on serial radiographs (Somford et al. 2013). It is a serious complication and may be caused through fracture movement, insufficient blood supply or infection. On the other hand, delayed union fracture is one that requires more time than usual to heal; in other words it shows healing progression over time (Gómez-Barrena et al. 2015). In orthopaedic and maxillofacial surgery bone regeneration is required in large quantity beyond the normal potential of self-healing such as for skeletal reconstruction of large bone defects resulted from trauma, infection, tumour resection and skeletal abnormalities. There are also cases in which the regenerative process is compromised, including avascular necrosis and osteoporosis. Thus, bone repair has been the ultimate goal of surgery from ancient times to the present (Dimitriou et al. 2011).

1.4.2. Bone graft

Though bone possesses good capacity of regeneration, in some cases like in repairing large bone defects, an aid is usually required to facilitate bone healing (Gómez-Barrena et al. 2015). There are a number of different methods for treat bone ailments as demonstrated schematically in Fig. 1.5 with the pros and cons of each technique are also listed (Rupani et al. 2012).

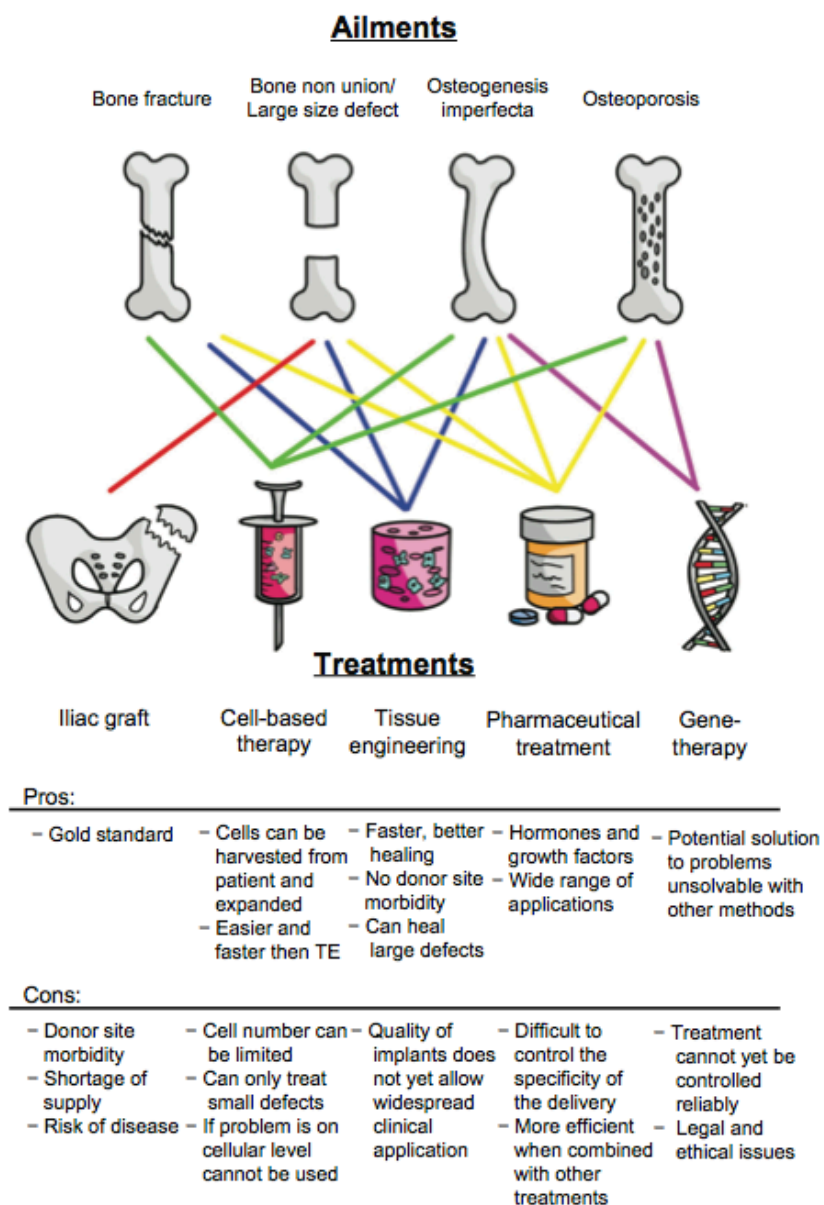


Fig. 1.5: Common treatment for bone trauma and diseases (Rupani et al. 2012). Re-printed with permission from Dove Medical Press, License Number: 3786011188175.

Standard approaches routinely used in clinical practice in order to stimulate bone regeneration include the use of several different bone-grafting methods, such as autograft, allograft and bone graft substitutes, BGS (Green et al. 1992; Giannoudis et al. 2005; Giannoudis & Einhorn 2009). Typically, bone graft source can be adopted from another part of the patient's body (autograft) or from another individual tissue obtained from a bone bank (allograft) (Meeder & Eggers 1994; LeGeros et al. 2006). Bone autograft is considered as the gold standard in clinic as it is the safest and most effective grafting procedure (Gómez-Barrena et al. 2015). However, harvesting (e.g. from the iliac crest) requires an additional surgical procedure, frequent with consequences of pain and complications (Dimitriou et al. 2011). The next solution is allograft, which were 10 times more commonly used than autograft as reported by Albert et al. (2006). In all orthopaedic procedures, allografts were used in 10.7%-12.7% as against 0.9%-1.3% of autografts (Albert et al. 2006). Nevertheless, shortage of supply and prone to potential disease transmission has become a major concern in the application of allograft procedure to treat bone defects (Hing 2005; Kanczler & Oreffo 2008).

A range of synthetic grafts or implant made of various materials like metals and its alloys, ceramics, polymers and composites have also received well-deserved attention, but there are associated limitations to their applications (Salgado et al. 2004). For instance, metals and their alloys are widely been used for orthopaedic load bearing and joint replacement applications, as it is known to have superior mechanical properties like high impact strength, tough, ductile and high resistance to wear. However, these metals and alloys have low biocompatibility, may corrode over long time usage and exhibit poor overall integration with the tissue at the implantation site (Yaszemski et al. 1994).

Bioceramic materials are good alternative to metallic implants as they offer unique characteristics such as good biocompatibility, corrosion resistance, and the ability to be bioresorbed; but the brittle nature and very low tensile strength of ceramics can hinder its application for load bearing sites (Yaszemski et al. 1994). Calcium phosphate ceramics (CaPs) are one of the most promising groups of synthetic bone substitutes. Hydroxyapatite (HA) and tricalcium phosphate (TCP), or intrinsic combinations of the two, are the most extensively used CaPs. This is due to their similarity in composition and bone-like properties such as, bioresorbability, bioactivity, and osteoconductivity (Bonfield 2006).

Adaptation of aforementioned materials, which have already been used in prior applications in human, proved that they are safe and non-toxic. However, the most critical concern of using synthetic materials is related to its bonding ability as they often integrate poorly with the host tissue and fail over time. This is most probably due to wear and fatigue or adverse body response (Hollister 2005).

Synthetic materials alone are not able to replace all of the bone functions naturally. The lack of vascularisation of the synthetic materials usually leads to non-unions, which will cause more pain, longer healing time and increase in cost due to the need for a secondary operation. Hence, it is clearly seen that adequate bone replacement is yet to be found as the need for bone regeneration is alarming. To address these problems, tissue engineering (TE) seems as a possible solution to embarked (Salgado et al. 2004).

1.5. Bone Tissue Engineering

TE is an interdisciplinary field of research that applies the principles of engineering and life sciences toward the development of biological substitutes that restore, maintain and improve tissue function (Langer & Vacanti 1993). Contrary to classic materials approach used in BGS, TE is based on the understanding of tissue formation and regeneration, and aims to promote new functional tissue instead of just implant new spare (Salgado et al. 2004).

Basically, TE can be divided into cell-based therapies and scaffold-based therapies. Cell-based therapies involved the direct injection of cell suspension (autologous or allogenic origin) or the transplantation of cell-sheets into the injured or defect tissue (Hutmacher & Cool 2007). However, since many cell types are anchorage-dependent, this approach could lead to cell death due to the absence of a matrix for cells to adhere onto (Gomes 2004). In addition, this approach is limited to small bone defects (Rupani et al. 2012). To engineer tissues of predetermined shapes, cell-based therapies have serious limitations (Song et al. 2008). Therefore, scaffold-based TE, which involves growing specific cell types in 3D scaffolds, has become increasingly actively investigated (Hutmacher & Cool 2007; Song et al. 2008). Scaffold-based TE concept was firstly introduced in the middle of 1980s when Dr Joseph Vacanti of the Children's Hospital approached Dr Robert Langer of MIT with an idea to design scaffolds for cell delivery as opposed to seeding cells onto or mixing cells into naturally occurring matrices with physical and chemical properties that are difficult to manipulate (Vacanti 2006). In scaffold-based TE, there are three main pillars: cells, scaffolds and the culture environment (bioreactor) as shown Fig. 1.6 (Vacanti et al. 2001; Quarto et al. 2001; Warnke et al. 2006).

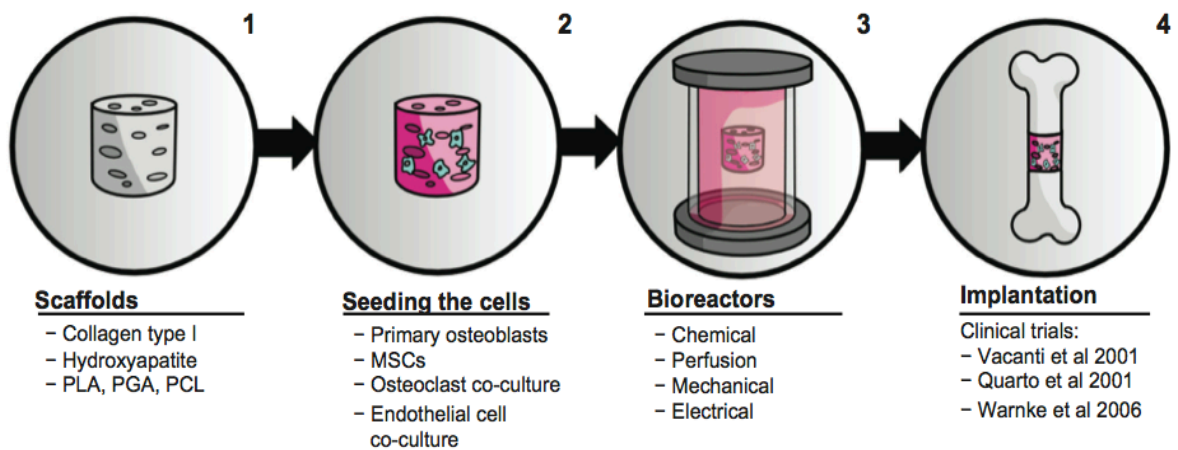


Fig. 1.6: The in vitro tissue engineering approach: (1) A biomaterial scaffold, which can be a flat sheet to mimic skin, a bundle of fibres to replace tendons or a three-dimensional cylinder to be implanted into bone. (2) Seeding the scaffold with cells (i.e. primary cells or cell lines). (3) Culturing the cell-seeded scaffolds in a bioreactor, simulating at least one aspect of the in vivo environment. (4) The final step is implantation of the scaffolds, if possible, ex vivo monitoring of the behaviour of the scaffold (Rupani et al. 2012). Reprinted with permission from Dove Medical Press, License Number: 3786011188175.

TE offers several advantages over current therapies; (1) reducing the number of operations needed (after implantation) – resulting in shorter recovery time; (2) avoiding the risk of immunological responses (hyperacute and delayed); (3) minimizing viral infections; and (4) providing cost-effective treatment for long term usage (Lanza et al. 2000; Stock & Vacanti 2001; Rezwan et al. 2006). In this multidisciplinary research field, no organ or tissue is excluded, *i.e.* skin, liver, heart, blood vessels, bone, bone marrow, and cartilage, are included as reported by Stock & Vacanti (2001).

1.6. Development of scaffolds for bone tissue engineering applications

Scaffolds are defined as three-dimensional (3D) structure biomaterials serve as a support for cells to proliferate and maintain their differentiated function, and its architecture defines the ultimate shape of the new tissue form (Hutmacher 2000; Dhandayuthapani et al. 2011). It is then logical to say that 3D scaffold is an essential component in bone

regeneration and repair (Salgado et al. 2004; Swetha et al. 2010). Scaffolds play an important role not only in guiding cells growth but also the synthesis of ECM and other biological molecules, as well as facilitate the formation of functional tissues and organs (Song et al. 2008). Scaffolds can be used either as permanent or temporary template to restore organ functionality (Yarlagadda 2005). To meet the requirement for tissue repair, scaffold should meet certain criteria, which might vary slightly between types of tissues (Jones 2006). Nevertheless, the following properties have been identified as essential scaffold criteria for BTE applications:

- (a) Scaffolds should be biocompatible, which suggests that they should be well integrated in the host's tissue without inducing any adverse response (Salgado et al. 2004; Rezwan et al. 2006). Scaffold should also be osteoconductive in order to guide the formation of new bone tissue along their surfaces (Freed & Vunjak-Novakovic 1998; Leong et al. 2003; Hannink & Arts 2011).
- (b) Scaffolds can either be biodegradable or non-biodegradable depending on its intended application, i.e. as temporary or permanent scaffolds, respectively (Hutmacher 2000). A temporary scaffold allowed tissues/cells to adhere, proliferate, and differentiate to form healthy tissues and help tissue recovers to the original shape and strength. Subsequently, the temporary structure would then degrade over time with regeneration of the tissues. In the case of young patients, these types of scaffolds are useful since the growth rates of tissues are still higher. However, temporary scaffold fail to meet the requirement for most cases of the older patient due to poor mechanical strength, mismatch between the growth rates of tissues and the degradation rate of the scaffold. Thus, there is a need for a stronger scaffold which can be either permanent or have a very low degradation rate. Permanent scaffold should retain their shape and strength through

regeneration/repair process (Chen et al. 2002). For temporary scaffolds, the degradation rate of the scaffolds must be tuned approximately with the rate of tissue regeneration under the culture conditions of interest. The degradation product must also be non-immunogenic and non-toxic (Chen et al. 2001; Dhandayuthapani et al. 2011).

- (c) Scaffolds should be osteoinductive by itself in order to promote bone tissue regeneration in large bone defects. Natural osteoinduction in combination with a biodegradable scaffold may not be enough to facilitate bone healing (Albrektsson & Johansson 2001).
- (d) Surface properties both chemical and topographical of a scaffold, are primarily important to regulate cell activities, provide sufficient surface for adhesion, differentiation, proliferation and thus promote tissue growth (Temenoff & Mikos 2000; He et al. 2003). The surface roughness can enhance cell adhesion and migration, and it could also affect the cytocompatibility of the osteoblastic cells (Oh et al. 2006; Schwartz et al. 2008).
- (e) Scaffolds should possess sufficient amount of porosity (40-90% depends on the nature of biomaterials used) to allow cell ingrowth as well as flow transport of nutrients and metabolic waste throughout the entire scaffold (Hutmacher 2000). To allow cell attachment, the scaffold must have a large surface area, which can be achieved by having highly interconnected porous structure (Mikos & Temenoff 2000). Scaffolds fabricated from highly biodegradable biomaterials should not have high porosities (>90%), since rapid depletion of the biomaterial will compromise the mechanical and structural integrity before the formation of new bone. In contrast, scaffolds fabricated using low degradation rate biomaterials and robust mechanical properties can be highly porous, because the higher pore surface area

interacting with the host tissue can increase the degradation rate due to macrophages via oxidation and/or hydrolysis (Karageorgiou & Kaplan 2005).

- (f) The pore size of a scaffold should be large enough to allow cell penetration (Mikos & Temenoff 2000). It is well recommended that for BTE application, the pore size should be in the range of 200-900 μm (Burg et al. 2000). However, Holy et al. (2000) believed that bone reconstruction can only be achieved by having a 3D scaffold with large macroporous interconnected structure with pore size ranging from 1.2-2.0 mm (Holy et al. 2000). This larger pore was reported to favor in direct osteogenesis, since they could facilitate cell, tissue and blood vessels ingrowth as well as provides high oxygenation (Salgado et al. 2004; Karageorgiou & Kaplan 2005).
- (g) Scaffolds should demonstrate adequate mechanical strength so that they do not collapse during handling and during the patient's daily activities (Mikos & Temenoff 2000; Salgado et al. 2004; Rezwan et al. 2006). *In vitro*, the scaffolds should have sufficient strength to withstand the mechanical stimuli applied when cultured in the 3D environment (Leong et al. 2003). *In vivo*, and because bone is always under continuous stress, the mechanical properties of the implanted scaffold should ideally match the natural bone intended to be replaced, so that an early mobilization of the injured site can be made possible (Salgado et al. 2004).
- (h) Biomaterials used should also be reproducible and processable into 3D scaffolds with various shapes and sizes (Leong et al. 2003; Hutmacher 2000). The fabrication process should be controllable and cost-effective (Hutmacher et al. 2004).
- (i) As the scaffolds will be in direct contact with the biological environment, they should be easily sterilizable to prevent infection (Rezwan et al. 2006).

(j) Substrate stiffness is also important because it affects the strains acting on a cell while being attached to a scaffold. It has a huge influence on cell migration, proliferation and apoptosis (Pelham & Wang 1997; Wang et al. 2000). However, it is difficult to define a general guideline for a suitable scaffold stiffness that optimally stimulates tissue regeneration. According to literature, scaffold stiffness should probably exhibit the stiffness of a developing skeletal tissue, which might be lower than the stiffness of mature tissue (Breuls et al. 2008). A study on MSC cultured on collagen coated polyacrylamide hydrogels with varying stiffness has shown that on soft gels (0.1-1.0 kPa), MSC differentiated into neurogenic, stiffer gels enabled myogenic development and very stiff gels (25-40 kPa), which mimic the bone properties resulted in osteogenic differentiation of MSC (Engler et al. 2006).

1.6.1. Biomaterials used as bone tissue engineering scaffolds

Given the demanding clinical need, it is not surprising the market for biomaterial-based treatments in the orthopaedics is evolving at a rapid rate. While materials intended for the implantation in the classical approach were in the past designed to be bioinert, materials scientists have now shifted toward the used of bioactive materials. These bioactive materials are supposed to integrate with the host's tissue and regenerate tissue (Langer & Vacanti 1993; Hench & Polak 2002). For bone TE applications, these bioactive materials should preferably be both osteoinductive, osteoconductive and osseointegrative (Stevens 2008). The term of osteoinductive, osteoconductive and osseointegrative are repeatedly used in many orthopaedic papers, but not always correctly defined. Thus, the suggested definitions of these terms are shown in Table 1.4 (Albrektsson & Johansson 2001; Stevens 2008).

Table 1.4: Definitions of osteoinductive, osteoconductive and osseointegration (Albrektsson & Johansson 2001; Stevens 2008).

Terms	Definitions
Osteoinductive	Capable to stimulate the differentiation of progenitor cells down towards osteoblastic lineage.
Osteoconductive	Permits bone growth on its surface and support the ingrowth of surrounding bone.
Osseointegrative	Ability to integrate into surrounding bone which formed a direct contact between host bones and implant.

The selection of the most appropriate material for the fabrication of a scaffold is very important, as its properties will influence the properties of the scaffold to a great extent. A number of materials such as metals, ceramics and polymers have been proposed but most metals and ceramics are non-biodegradable, which leaves the researcher's choice to limited small number of ceramics and biodegradable polymers (Salgado et al. 2004).

1.6.1.1. Bioactive ceramics

Bioactive ceramic materials having similar in composition to the inorganic mineral phase of bone, such as hydroxyapatite (HA) and tricalcium phosphate (TCP) are of clinical interest (Best et al. 2008; Stevens 2008). The rationale of using these calcium phosphate (CaP) based materials is from the fact that CaP is the major component of biological apatite and that it shows promises of biocompatibility, osteoconductivity and biodegradability. Representative of porous HA scaffolds with fully interconnected pores are shown in Fig. 1.7 (Oh et al. 2006).

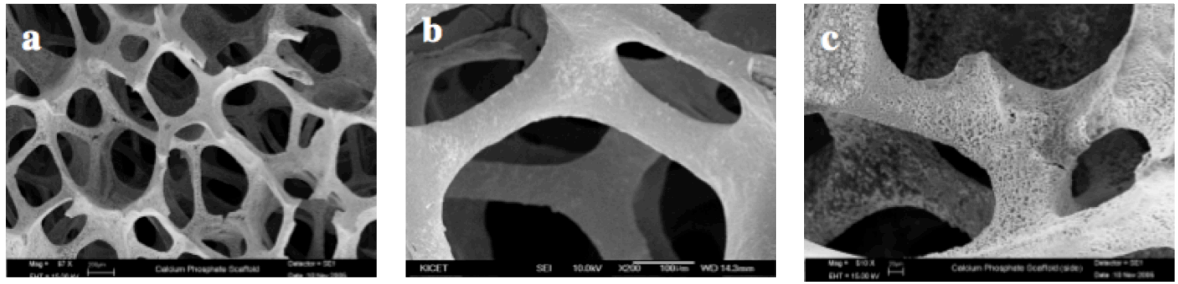


Fig. 1.7: Representative HA scaffolds showing (a) bulk architecture, (b) micro-crystalline surface and (c) nano-crystalline surface (Oh et al. 2006). Re-printed with permission from Science Publication.

Synthetic HA has been used as coatings on metallic implants, fillers in polymer matrices and scaffolds for maxillofacial reconstruction, treatment of bone defects, total joint replacement and revision surgery for the last 20-30 years (Best et al. 2008). However, previous studies have reported that pure HA shows negligible resorption even years after implantation (Yuan et al. 1999; Sepulveda et al. 2002; Mastrogiacomo et al. 2006). Besides, it was found that the biological apatites differ chemically from stoichiometric HA in that they contain a number of additional trace elements substituted into the HA lattice (Gibson & Bonfield 2002; Boanini et al. 2010; David et al. 2013).

Back in 1960s, Raquel LeGeros first started the work on the characterization of carbonate substituted HA (CHA) for biomedical application. Since then, synthetic CHA has been extensively studied, as carbonate is the most abundant substitution in bone mineral (2-8 wt%), the amount depends on bone age, site, animal species and individual. Thus, biological apatite is more accurately described as carbonated HA (CHA) rather than HA alone (Merry et al. 1998; Tadic et al. 2002; Landi et al. 2003; Best et al. 2008). There are three types of carbonate substitution; (i) the substitution of carbonate for hydroxyl ions (A-type), (ii) carbonate substitution for phosphate site (B-type) or (iii) both hydroxyl and phosphate groups substituted by carbonate (AB-type) (LeGeros et al. 1969; Landi et al. 2010; Shepherd et al. 2012). Previous studies have shown that the presence of B-carbonate

in the apatite lattice cause a decrease in crystallinity and increase in solubility in both *in vitro* and *in vivo* tests (Landi et al. 2003; Porter et al. 2005; Murugan & Ramakrishna 2006). The increase in solubility has considerably enhanced the bioactivity of CHA. This has been shown by greater bone apposition found around dense CHA compared to pure HA (Porter et al. 2005). A study conducted by Spence et al. (2009) discovered that greater increase in calcium ion concentration occurred when human osteoblasts cells were cultured on sintered AB-type CHA compared to HA. They also found increased in collagen synthesis, which indicated that human osteoblasts cells on AB-type CHA have produced more ECM proteins than when cultured on HA *in vitro* (Spence et al. 2009).

Among the biological trace elements, the important role of silicon (Si) for normal bone and cartilage growth and development has also been studied (Carlisle 1970; Schwarz & Milne 1972; Carlisle 1979). Similar to carbonate content in the bone, silicon content also varies depending on bone age and site (Landi et al. 2010). The level of Si in human bone mineral density (BMD) is also linked to the dietary intake of Si (Pietak et al. 2007). In the early 1970s, a report by Carlisle (1970) showed that Si deficiency resulted in abnormal bone formation. This was confirmed by Schwarz & Milne (1972) who identified Si as a cross-linking agent in connective tissue and its importance to vascular health. Increasing evidences in the role of Si in bone and cartilage development has been reported where Si influences cartilage synthesis and the integrity of the ECM as well as the biomineralization process (Landi et al. 2010). It was also reported in the literature that Si has a dose-dependent effect on the differentiation, proliferation and collagen synthesis of osteoblast, with a direct influence on the remodelling process and osteoclast development as well as the resorption activities (Pietak et al. 2007). All these results show that rapid bone remodelling and enhanced quality of the bone around the implant are due to the increased in the dissolution rate of the substituted HA compared to pure HA (Klein et al. 1983;

Daculsi et al. 1989). The increased reactivity with the existing bone drives to a higher stability of the implanted region. This is because a strong mechanical bond is formed between the implant and the host's tissue. As a result, the time required for the rehabilitation of patient is reduced once this bond is formed. For all the aforementioned reasons, the development of synthetic HA powders with fully complete and controlled level of ionic substitutions in the HA lattice seem as promising candidate for an ideal scaffold bone materials, in order to approach to the “gold standard”, mimicking the composition of the natural human bone mineralized matrix (Sprio et al. 2008).

1.6.1.2. Biodegradable Polymers

There are two types of biodegradable polymers, i.e. natural and synthetic polymers (Chen et al. 2002; Rezwan et al. 2006). Natural polymers, such as collagen, hyaluronic acid and chitosan, are other potential candidates for bone substitute materials which would provide essential biological informational guidance to the cells, supporting cell attachment and promote chemotactic responses (Stevens 2008). Collagen type I is the major component of ECM which is responsible for cellular adhesion and proliferation (Kim et al. 2010; Zhao et al. 2014). Collagen occurs in many places throughout our body. For instance, it is found in bone (Type I), cartilage (Type II), blood vessel walls (Type III), cell basement membrane (Type IV) and cell surfaces (Type V). Collagen type I is a popular choice of material in making scaffold for bone regeneration since it offers excellent biocompatibility, easily degrade and resorb by the body. It also promotes cell attachment, but its mechanical properties alone however, are far less than that of the native bone (Wahl & Czernuszka 2006; Jones et al. 2010).

On the other hand, hyaluronic acid is the major non-collagenous component presents in ECM and of the synovial fluid (Zhang et al. 2005; Zhao et al. 2014). Therefore, numerous

natural ECM components, in particular hyaluronic acid and collagen, have been incorporated into 3D scaffolds for bone regeneration (Datta et al. 2005; B. Yu et al. 2012). Hyaluronic acid and collagen type I have been used as coating materials on PLLA films to enhance cell-material interaction. Zhao et al. (2014) forecasted that these coating materials may improve the bioactivity of ECM-based films, which might be a potential application for BTE applications (Zhao et al. 2014).

Chitosan is another example of natural polymer that has been used widely for biomedical applications, such as hemodialysis membranes, drug delivery systems, orthopedic and dental coating materials as well as artificial skin (Chen et al. 2002; Thein-Han & Misra 2009). The ability of chitosan to support cell attachment and proliferation is attributed to the presence of amino acid sequences in the chitosan structure (Croisier & Jérôme 2013). However, poor control of enzymatic degradation and lack of mechanical properties are two major objections to the use of natural polymers. In addition, concerns about the availability of the materials in large quantity required for clinical application has motivated the researchers towards the production of synthetic biodegradable polymers (Karageorgiou & Kaplan 2005; Rezwani et al. 2006).

The most often utilized biodegradable synthetic polymers for 3D scaffolds in BTE are saturated poly- α -hydroxyl esters such as poly (lactic acid) (PLA), poly (glycolic acid) (PLGA), as well as poly (lactic-co-glycolide) (PLGA) copolymers (Athanasios et al. 1996; El-Amin et al. 2003; Li et al. 2010). These polymers have been approved by the US Food and Drug Administration for certain human clinical use, such as surgical sutures and some implantable devices (Chen et al. 2001). The chemical properties of these polymers allow hydrolytic degradation through de-esterification. The degradation by-products of these polymers can be removed through natural pathway as lactic and glycolic acids by the body.

PGA can be broken down by hydrolysis, non-specific esterases and carboxypeptidases, while PLA can be eliminated by the tricarboxylic acid cycle (Chen et al. 2002; Rezwan et al. 2006). The degradation rate, physical and mechanical properties of these polymers can be easily tailored over a wide range by using various molecular weights and copolymers. However, these polymers undergo bulk erosion process, where a massive release of the acidic by-products could cause inflammatory reaction *in vivo*. Consequently, this can cause the scaffold to fail prematurely (Bergsma et al. 1993; Martin et al. 1996; Hutmacher 2000).

Another drawback of these synthetic polymers is related to its hydrophobicity and lack of physiological activity (Kim et al. 2006; Jahno et al. 2007). It has been shown that PLA does not provide a favorable surface for cell attachment and proliferation due to lack of specific cell recognition signals (Ravichandran et al. 2012). Modification of the outermost part of the material is seen to be sufficient as to tailor its biocompatibility, while the bulk properties of the materials are maintained (Tzoneva et al. 2008). The rationale underlying this concept is that when the scaffold is implanted *in vivo*; the surface become in contact with the biological environment before the bulk. Recent studies have proposed various strategies such as coating, plasma treatment and entrapment in an attempt to influence cell adhesion, proliferation and differentiation as in contact with PLA-based scaffolds (Zhao et al. 2014).

Polycaprolactone (PCL) is also a biodegradable synthetic polymer that has been used as scaffolds for TE applications. It is a semicrystalline polymer and an important member of aliphatic polyester family (Rezwan et al. 2006). PCL has similar biocompatibility to PLA and PGA, but much slower degradation rate. This makes PCL less attractive for scaffold-based TE, but it become an appropriate candidate as long-term drug delivery carrier (Liu et al. 2007).

1.6.1.3. Composites

Composite or hybrid materials are generated via the combination of functional polymers with inorganic nanostructured compounds. Inorganic-organic composites aiming to closely mirror the composite nature of real bone, which combine the toughness of a polymer phase with the compressive strength of a ceramic phase has been shown to improve both the degradation and mechanical properties of the composite scaffolds (Stevens 2008). For instance, tissue-engineered HA-Collagen nanocomposite systems are developing rapidly and showing promise (Wahl & Czernuszka 2006; Jones et al. 2010). Comparing ceramic scaffolds and ceramic composite scaffolds, it was shown that HA-Collagen composite has better osteoinductive capacity compared to single HA or TCP (Wang et al. 2004). Several synthetic approaches have been developed to create the inorganic-organic polymer composites including blending, sol-gel and emulsion polymerization. The main challenge in making composite materials is to re-create the same degree of nanoscale order in the organization of the organic and inorganic components found *in vivo*. However, mechanical properties of such composites is still low compared to the native bone (Stevens 2008).

1.6.2. Fabrication techniques

Cells and tissues in the body are organized into 3D architecture. In order to engineer these functional tissue and organs, scaffold should be fabricated to closely mimic the composition and architecture of the intended implant (Subia et al. 2010). A successful scaffold should have a balance between temporary mechanical function with morphological properties (pore architecture, size and interconnectivity) in order to aid biological delivery and tissue regeneration (Hollister 2005; Hutmacher & Cool 2007). However, there is often a tradeoff between a denser scaffold offering better mechanical function and a more porous scaffold providing better biological delivery (Hollister 2005).

For this reason, several fabrication techniques have been developed, but only the main techniques are mentioned here. In general, scaffold fabrication can be divided into conventional and rapid prototyping (RP) techniques (Hutmacher et al. 2004). A brief description on the concept of these fabrication techniques will be discussed in the following section.

1.6.2.1. Conventional fabrication techniques

This technique includes solvent casting, particulate leaching, gas foaming, phase separation and freeze-drying (Hutmacher 2000; Chen et al. 2002; Rezwan et al. 2006; Salgado et al. 2004; Subia et al. 2010). Table 1.5 summarizes the advantages and disadvantages of conventional scaffold fabrication techniques.

Solvent casting

Solvent casting technique is based on the evaporation of some solvent in order to form scaffolds by one or two routes (Subia et al. 2010). This can be achieved by dipping the mold into polymeric solution and providing ample time to draw off the solution; as a result a layer of polymeric membrane is formed. Alternatively, a polymeric solution can be poured into the mold and allow sufficient time for the solvent to be evaporated, which will then create a layer of polymeric membrane on the mold (Mikos et al. 2004).

Porogen leaching

This technique involves the casting of a mixture of polymer solution and porogen in a mold, drying the mixture and leaching out the porogen with water to create the pores (Hutmacher 2000; Chen et al. 2002). The porogen materials used are usually water-soluble particulates such as salts and carbohydrates (Subia et al. 2010). The pore size can be easily controlled by manipulating the amount of porogen added as well as the size and shape of the porogen (Plikk et al. 2009).

Gas forming

The gas foaming technique uses high-pressure carbon dioxide (CO₂) gas for the fabrication of highly porous scaffolds (Chen et al. 2002; Subia et al. 2010). The process involves saturating highly porous biodegradable polymer (e.g. PLGA) with CO₂ at high pressure (800 psi). This high level of CO₂ is then return to ambient level in order to rapidly decrease the solubility of the gas in the polymer, resulting in nucleation and growth of gas bubbles, or cells with pore sizes ranging from 100-500 μm in the polymer (Sachlos & Czernuszka 2003).

Phase separation

A biodegradable synthetic polymer is dissolved in phenol or naphthalene, followed by dispersion of biologically active molecule (i.e. alkaline phosphatase) in these solutions. By lowering the temperature a liquid-liquid phase is separated and quenched to form a two-phase solid. The solvent is then removed by extraction, evaporation and sublimation to give a porous scaffold with bioactive molecules incorporated in the structure (Sachlos & Czernuszka 2003; Subia et al. 2010).

Table 1.5: Advantages and disadvantages of conventional scaffold fabrication techniques.

Fabrication Technique	Advantages	Disadvantages	References
Solvent casting/ particulate leaching	<ul style="list-style-type: none"> Control over porosity, pore size and crystallinity 	<ul style="list-style-type: none"> Use of organic solvent Irregular shaped pores and insufficient interconnectivity 	Mikos et al. 1996; Hutmacher 2000; Rezwan et al. 2006
Porogen leaching	<ul style="list-style-type: none"> Control over porosity and pore geometry 	<ul style="list-style-type: none"> Limited pore size and pore interconnectivity 	Plikk et al. 1999; Chen et al. 2002; Subia et al. 2010
Gas foaming	<ul style="list-style-type: none"> Free from organic solvent Control over porosity and pore size 	<ul style="list-style-type: none"> Limited mechanical property Inadequate pore interconnectivity 	Mooney et al. 2006; Sachlos & Czernuszka 2003; Subia et al. 2010
Phase separation	<ul style="list-style-type: none"> Easily combine with other fabrication technology 	<ul style="list-style-type: none"> Difficult to control precisely scaffold morphology 	Lo et al. 1995; Sachlos & Czernuszka 2003; Mikos et al. 2004; Subia et al. 2010

1.6.2.2. Rapid Prototyping technology

Rapid prototyping (RP) is also called solid free-form fabrication (SFF). Unlike conventional machining which involves constant removal of materials, RP is able to build scaffolds by selectively adding materials, layer by layer, as specified using a computer added design (CAD) software, which is then expressed as a series of cross section (Woodfield et al. 2009). Corresponding to each cross section, the RP machine deposits a layer of material starting from the bottom and moving up a layer at a time to construct the 3D scaffolds. This is the principal advantage of RP technique compared to other fabrication techniques. A section of bone defect from the patient can be imaged using Magnetic Resonance Imaging (MRI) or X-Ray computed tomography (CT scan), subsequently converting the acquired image to the file format for RP manufacturing (usually in stereolithography or .STL format) and finally a customized 3D scaffolds for that individual patient can be printed (Bagaria et al. 2011). RP technologies can be categorized based on the processing method, and these include fused deposition modeling (FDM), 3D Plotter, 3D Printing, selective laser sintering and stereolithography (Hutmacher et al. 2004; Hollister 2005). Fig. 1.8 demonstrates the schematic of different RP systems categorized by the processing method (Hollister 2005). The merits and demerits of the RP techniques with different processing methods are summarized in Table 1.6. In the following section, we only focus on the fused deposition modelling method as this technique was used to fabricate the scaffolds in this study.

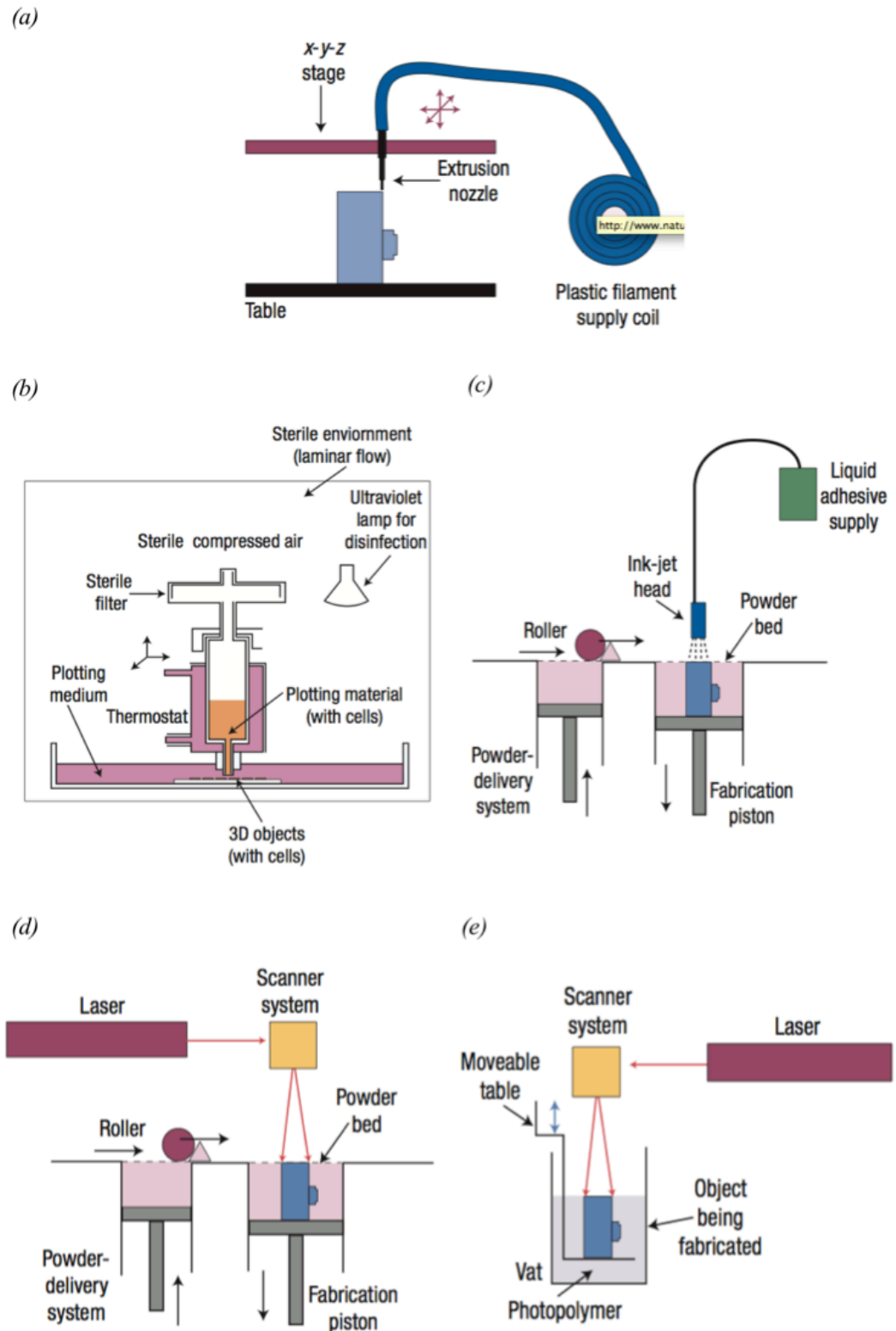


Fig. 1.8: Schematic diagrams of different RP techniques categorized by the processing method; (a) Fused Deposition Modelling, (b) 3D Plotter, (c) 3D Inkjet Printing, (d) Selective Laser Sintering and (e) Stereolithography (Hollister 2005). Re-printed with permission from Nature Publishing Group, License Number: 3786030665261.

Table 1.6: The merits and demerits of RP technique for different processing methods.

Processing methods	Merits	Demerits	References
Fused Deposition Modelling (FDM)	<ul style="list-style-type: none"> Free from organic solvent 	<ul style="list-style-type: none"> Limited range of polymer can be used due to processing parameters and temperatures 	Leong et al. 2003; Salgado et al. 2004
3D Plotter	<ul style="list-style-type: none"> Possibility of operating at physiological condition 	<ul style="list-style-type: none"> Limited resolution 	Landers & Mullhaupt 2000; Hutmacher et al. 2008
3D Printing	<ul style="list-style-type: none"> High flexibility in the choice of material 	<ul style="list-style-type: none"> Require post-processing to remove binder and enhance mechanical properties 	Lam et al. 2002; Leukers et al. 2005
Selective Laser Sintering (SLS)	<ul style="list-style-type: none"> Wide range of materials 	<ul style="list-style-type: none"> Printed model suffer from shrinkage/ deformation due to thermal heating from the laser and subsequent cooling 	Wang et al. 2007; Gross et al. 2014
Stereolithography (SLA)	<ul style="list-style-type: none"> Higher accuracy over SLS method 	<ul style="list-style-type: none"> Require the use of resin (majority of resin are brittle and shrink upon polymerization) 	Hull 1990; Gross et al. 2014

Fused Filament Fabrication

Fused filament fabrication is also known as fused deposition method, FDM (Fig.1.8 a), which was developed by Scott Crump in 1992. In this technique, a moving nozzle is used to extrude a fiber of polymeric material from which the physical model is built layer-by-layer onto a platform. The base of the platform is lowered and next layer is deposited. The platform moves in the z direction while the nozzle head moves in x and y direction (Hutmacher 2000; Salgado et al. 2004). This technique has been used to produce various 3D PCL or PCL-HA scaffolds with honeycomb-like morphologies and different degree of porosity by Hutmacher (2000) (Fig. 1.9.) *In vitro* study have shown that human fibroblast and periosteal cells can proliferate, differentiate and produce a cellular tissue throughout the 3D PCL scaffolds over 3-4 weeks of culture (Hutmacher et al. 2001; Zein et al. 2002). The potential application of these FDM fabricated scaffolds were further investigated *in vivo* by Hutmacher's group, where they found that osteoid formation could be obtained when these scaffolds were previously cultured with periosteal cells under osteogenic conditions were further implanted *in vivo* in a subcutaneous model (Schantz et al. 2002).

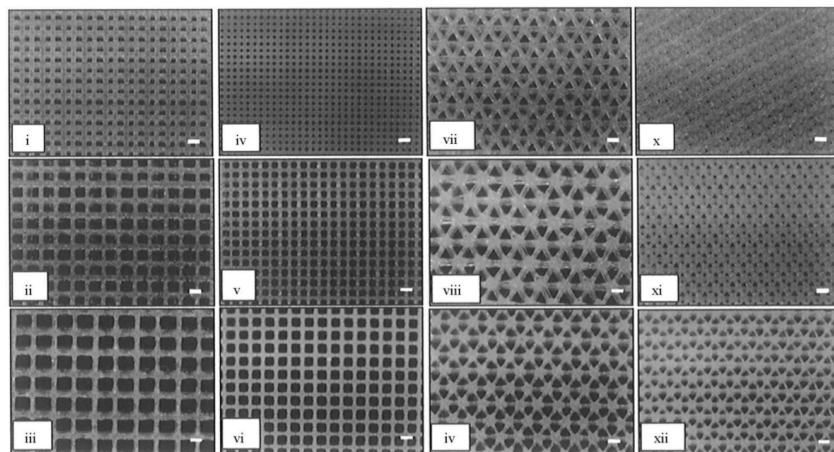


Fig. 1.9: 3D scaffold systems of various porosity and pore geometry fabricated by FDM. Magnification X 7.5, scale bar represents 1mm. (i)-(iii) lay-down pattern: 0/90°; nozzle tip: 0.016"; porosity: 50, 68, 75%; (iv)-(vi) 0/90°; 0.010"; 50, 68, 75%; (vii)-(viii) 0/60/120°; 0.016"; 68, 75%; (ix) 0/60/120°; 0.010"; 80%; (x)-(xii) 0/60/120°; 0.010"; 50, 68, 75% (Hutmacher 2000).

1.6.3. Surface modification

Despite the advance in RP techniques, the application of the fabricated scaffolds for bone regeneration is still limited due to the nature of the biomaterial used. Most of the synthetic polymer used in RP technique, PLA for example, is known to be hydrophobic (Zhao et al. 2014). PLA is also poor in cytocompatibility, which resulted in the inefficiency of the scaffolds in providing a friendly interface with the living cells. Once implanted in the body, it is the surface of a biomaterial that first become into contact with the biological environment; hence, the early response of cells to the biomaterial critically dependent, among others, on the surface of the biomaterial. Many different strategies have been developed as to improve the biocompatibility of PLA, such as, grafting polymerization, ozone oxidization, plasma modification and coating natural polymers (Zhu et al. 2003).

Naturally, the biological world is made up of well organize self-assembly of biomacromolecules. This has inspired the researchers to engineer the scaffold via macromolecules self-assembly (Kim & Bruening, 2003; Huang et al. 2012). Layer-by-layer (LbL) is electrostatic self-assembly (ESA) seems to be a novel and promising technique in order to modify the polymer surface in a controlled manner (Hammond 2011; Ni et al. 2011). LbL is also known as Polyelectrolyte Multilayers (PEMs) assembly. This technique involves the alternate deposition of negative and positive charged polyelectrolytes as to build up a thin layer of extracellular (ECM) environment on the surface. Before PEMs assembly, the surface is initially chemically modified with reactive group such as $-OH$, $-NH_2$ and $-COOH$ to permit binding with biomolecules (Okada & Ikada, 1991; Yamauchi et al. 1991; Suh et al. 1998). With the advancement in surface modification, many natural ECM-like macromolecules, such as hyaluronic acid and collagen type I, have been incorporated into 3D scaffolds for bone regeneration. Table 1.5 summarize the example of PEMs assembly used in tissue engineering applications.

Table 1.7: Examples of PEMs used in Tissue Engineering Applications.

Research Objective	Polyelectrolytes used	Cell type	Significant finding	Reference
To enhance osteogenic induction	HA / Collagen type I	hMSCs	HA/ Collagen type I nanocomposite multilayers improved cell adhesion and proliferation and enhanced osteogenic induction of hMSCs	Kim et al. (2010)
To modify PLA surface toward improving its cytocompatibility	PSS/ Chitosan	HUVECs	Better cell attachment, activity and proliferation of PLA coated with 3- and 5-bilayers of PSS/ Chitosan compared to control PLA.	Zhu et al. (2003)
To enhance the cell-material interaction	Hyaluronic acid/ Collagen type I	Osteoblasts	The present of collagen I has greatly improved the cytocompatibility of the PLLA films in terms of cell viability, proliferation and ALP expression	(Zhao et al. 2014)
To improve biocompatibility of PLLA scaffolds	Collagen type I/ bFGF	Chondrocytes	Incorporation of bFGF in the collagen layer enhanced cell growth.	Ma et al. (2005)

*HA= hydroxyapatite, PLA= polylactic acid, PSS= poly (styrene sulfonate, sodium salt), bFGF= basic fibroblasts growth factor, ALP= alkaline phosphatase.

In summary, the development of scaffolds for BTE applications has not reached the final conclusion on the optimal design requirements, biomaterials and fabrication technique to produce an ideal bone scaffold. The inherent conflicts in the nature of an ideal bone scaffold for bone regeneration ensure that this issue will remain debated, particularly among researchers and clinicians. The variety of conclusion may be due to complexity of the process of bone regeneration, which is multivariable and multiobjective (Karageorgiou & Kaplan 2005; Velasco et al. 2015). In this study, a scaffold is considered as an ideal bone scaffolds for bone regeneration when they meet the basic desired characteristics as summarized in Table 1.8.

Table 1.8: Basic desired characteristics for ideal bone scaffolds.

Characteristic	Description	References
Composition	65-70% inorganic mineralized matrix (mainly carbonated HA), 30% organic non-mineralized matrix (predominantly collagen type I) and the remaining portion is organic proteins and water	Stevens 2008; Rupani et al. 2012; Velasco et al. 2015
Porosity	Depends on the nature of biomaterial: -Highly degradable biomaterials: <90% -Low degradation rate biomaterials: 40-90%	Hutmacher 2000; Karageorgiou & Kaplan 2005; Velasco et al. 2015
Pore size	-Minimum pore size to promote osteogenesis: 200-900 μm ; -Larger pore size could favor direct osteogenesis and support angiogenesis: 1.2- 2.0 mm	Mikos & Temenoff 2000; Holy et al. 2000; Salgado et al. 2004
Mechanical properties	<i>-In vitro</i> : Sufficient to withstand mechanical stimuli induced by the 3D culture environment (i.e. bioreactor) and maintain the spaces required for cell in-growth and matrix production <i>-In vivo</i> : Match the mechanical properties of bone to be implanted (refer Table 1.2)	Leong et al. 2003; Salgado et al. 2004
Degradation/resorption rates (for temporary scaffolds)	Depends on the nature of biomaterials: -PLLA (2-5 years) -PLGA (2-6 months) -PCL (2-3 years) -TCP (6-24 months) -Si-CaP (6-12 weeks)	Rezwan et al. 2006; Hing et al. 2007; Velasco et al. 2015

1.7. Cells for Bone Tissue Engineering

One of the major issues in BTE is sources of cells. An ideal cell sources should be easily expandable to higher passage, have consistent osteogenic potential, non-immunogenic and non-tumorigenic (Heath 2000). The cell used for BTE can either be from cell lines or primary osteoblastic cells. The selection of cells is depending on the stage of optimization that the researcher is aims to investigate. For instance, primary human mesenchymal stem cells (hMSCs) or osteoblasts is typically used for *in vitro* study that is closer to clinical application as these cells could be the final type of cell source used in the tissue engineered product being developed. Likewise, for early stage of *in vitro* study of cell-biomaterial interactions, several osteoblast-like cell lines has been utilized, as they are easy to grow and the results can be compared (Rupani et al. 2012). Immortalized cell lines, such as MG63, SaOS-2 and U-2OS are osteosarcoma cells derived from malignant bone tumors. These cells are popular choice for the study of osteoblast models as they share some osteoblastic features. However, their chromosomal alterations lead to abnormal molecular and cellular functions, hence, they do not fully represent the behavior of natural human osteoblasts (Pautke et al. 2004). In this context, stem cell biology appears to be the most valid and more promising solution (Salgado et al. 2004).

Stem cells are undifferentiated cells with high proliferation capability, self-renewal ability, multi-lineage differentiation and regenerative capacity (Morrison et al. 1997). Nevertheless, stem cells have diverse degrees of differentiation potential. In general, stem cells can be divided into two main groups: embryonic stem cells (ES) and adult stem cells (ASC). ES cells reside in the Inner Cell Mass (ICM) and are considered to be pluripotent. These cells have almost unlimited *in vitro* growth potential, accessibility and ease of genetic manipulation. However, the use of ES cells in biomedical applications are hindered

due to ethical constraints and issues regarding their immunogenicity and tumorigenicity (Jukes et al. 2010). On the other hand, ASCs also known as multipotent stem cells are the cells that reside in the fully differentiated or adult tissues, which are normally found in the bone marrow, periosteum, muscle, fat, brain and skin (Salgado et al. 2004; Rupani et al. 2012). Among the cell sources, bone marrow-derived MSCs typically known as Mesenchymal Stem Cells (MSCs) have received a special attention in BTE field (Petrankova et al. 1963; Friedenstein et al. 1968). A brief description on MSCs is described in the following section.

1.8. Mesenchymal stem cells

1.8.1. The discovery of mesenchymal stem cells

The discovery of non-hematopoietic stem cells in bone marrow was first proposed by a German pathology Cohnheim about 140 years ago. His work suggested that bone marrow might be the source of fibroblast that deposits collagen fibres as part of normal process of wound healing (Prockop 1997). Following this, Friedenstein and colleagues (1976) revealed that bone marrow contains cells that can differentiate into other mesenchymal cells, as well as fibroblast (Friedenstein et al. 1976). They placed the whole bone marrow in plastic culture dishes and removed the non-adherent cells after 4 hours in order to discard the hematopoietic cells. They found that the adherent cells appeared to be heterogeneous, but the most tightly adherent cells were spindle shaped and formed foci of two or four cells, which remained inactive for 2-4 days and subsequently began to proliferate rapidly. After several passages, these cells appeared to be more homogenous fibroblast-like shaped. They also reported that the cells could be potentially differentiated into colonies that resembled small deposits of bone or cartilage. In the early days, these cells are usually referred as marrow stromal cells as they appear to rise from the complex array of supporting structures found in the marrow (Ashton et al. 1980; Castro-Malaspina

et al. 1980; Bab et al. 1986). Friedenstein's works were further extended by other groups throughout the 1980s (Chamberlain et al. 2007).

In the meantime, the name of Mesenchymal Stem Cells has today was given back in early 1990s by Caplan (Caplan 1991). This is because when these cells were placed in the adequate culture conditions, they could be differentiated into cells with mesenchymal origin (i.e. bone, cartilage, fat, muscle, skin tendon) through what was called "The Mesengenic Process" as shown in Fig. 1.10 (Caplan 1994; DiMarino et al. 2013). In saying this, the concept of non-hematopoietic stem cell in bone marrow still did not resonate worldwide until additional similar work was published by Pittenger et al. (1999), which demonstrated similar observations to the earlier work reported by Friedenstein and colleagues (1976).

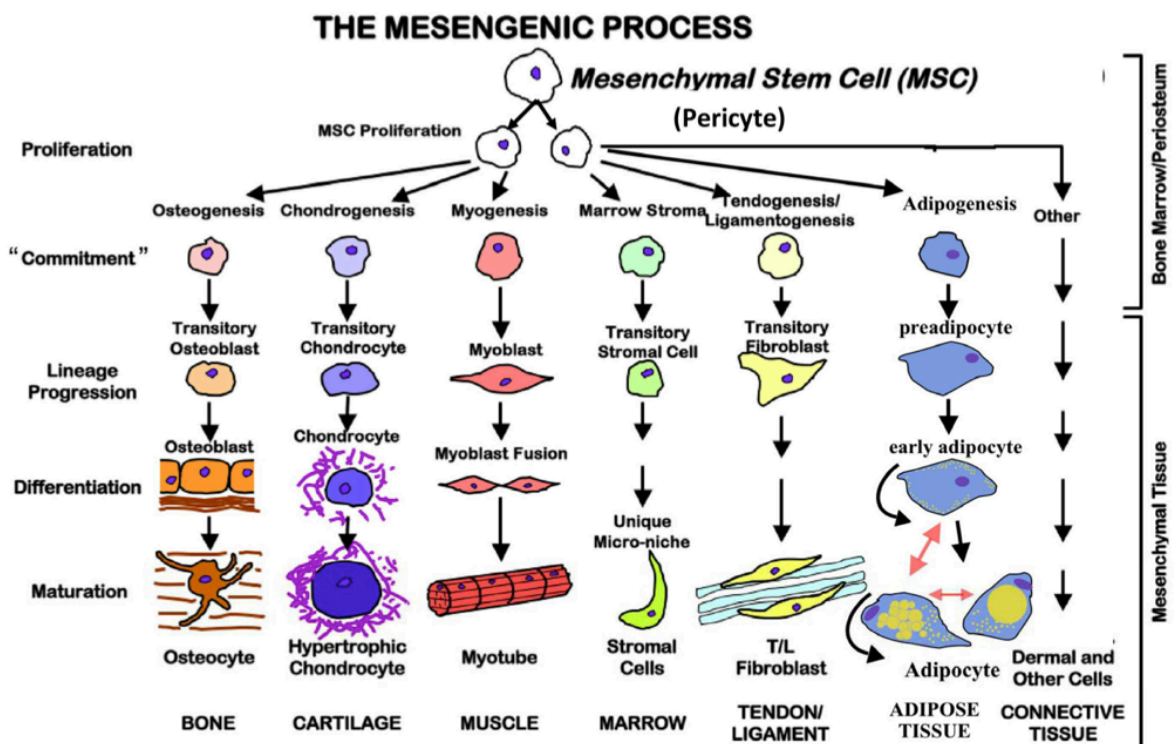


Fig. 1.10: The mesengenic process. Mesenchymal stem cells are multipotent and possess the ability to proliferate and commit to different cell types based on the environmental conditions. They also may be redirected from one lineage to another (DiMarino et al. 2013). Re-printed with permission from PubMed Central.

1.8.2. *In vitro* characteristics of mesenchymal stem cells

Given the various sources and techniques from which MSCs can be isolated, in 2006 the International Society of Cellular Therapy (ISCT) proposed minimal criteria for the cell characterizations (Dominici et al. 2006). First, MSCs must adhere to tissue culture plastic (TCP) under standard culture conditions. Second, MSCs must positively express CD105, CD73 and CD90 and lack of CD45, CD34, CD14 or CD11b, CD19 and HLA-DR surface molecules (Pittenger et al. 1999; Boxall & Jones 2012). Finally, histological staining should also positively demonstrate that the cells are capable to differentiate into osteogenic, chondrogenic and adipogenic (Dominici et al. 2006; Chamberlain et al. 2007; Phinney & Prockop 2007; DiMarino et al. 2013).

1.8.3. Mesenchymal stem cells for tissue repair

The fact that MSCs can be differentiated towards multilineage cell types *in vitro*, relatively easily expanded in culture and being non-immunogenic make MSCs as promising source of stem cells for tissue repair and gene therapy (Chamberlain et al. 2007).

In 2013, there are 344 registered clinical trials in different clinical trial phase intended to evaluate the potential of MSCs-based cell therapy worldwide (Wei et al. 2013). In clinical settings, MSCs underwent clinical trials for various applications, such as orthopaedic injuries, cardiovascular diseases and liver diseases (Kim & Cho 2013). MSCs have attracted interest for clinical application due to their therapeutic properties. They are believed to be responsible for growth, wound healing, and replacing cells that are lost through daily wear and tear and pathological conditions. As a result of these excellent functions, MSCs have been shown to be effective in the treatment of tissue injuries and degenerative diseases (Wei et al. 2013). The ability of MSCs to differentiate into osteoblasts, tenocytes and chondrocytes has attracted attention for their use in orthopaedic

settings. Some clinical trials using allogenic bone marrow-MSCs therapy for cartilage defects, osteogenesis imperfecta (OI), and hematopoietic stem cell transplantation (HSCT) have shown great improvements in the outcome (Horwitz et al. 1999; Horwitz et al. 2002; Wakitani et al. 2004; Le Blanc et al. 2005; Baron et al. 2010).

Cultured MSCs have been clinically applied to treat several conditions including osteogenesis imperfecta (OI), which is a genetic disorder in which osteoblasts produce defective collagen type I, the primary structural protein in bone. These leads to by deformities, multiple fractures, and retarded bone growth, resulting in shortened stature. A study conducted by Horwitz et al. (1999) used allogenic bone marrow transplantation (BMT) to treat children with OI. After 3 months, there was new dense bone formation, an increase in total body bone mineral content, an increase in growth velocity and reduced frequency of bone fracture in the child patients. This study shows that allogenic bone marrow transplantation can lead to bone engraftment in children with OI, which then give rise to osteoblast whose presence correlates with an improvement in bone structure and function (Horwitz et al. 1999). However, with increasing time post-transplantation, growth rates slowed and finally reached a plateau while bone mineral content continuously increase. In 2002, the same author hypothesized that additional therapy using isolated hMSCs without marrow ablative therapy would safely boost responses. They infused culture-expanded hMSCs into children who had previously undergone conventional BMT and found that the hMSCs can engraft after transplantation, differentiate to osteoblasts as well as skin fibroblasts, extending the clinical benefits attributable to the engraftment of functional mesenchymal precursors (Horwitz et al. 2002).

1.9. Approaches to accelerate osteogenesis

Osteogenesis is a process of bone formation, which can be accelerated by using biomolecules, novel scaffold design and culture technique (Rupani et al. 2012). The presence of biomolecules in the culture media acts as the chemical cues, which would greatly influence the proliferation and differentiation of serially passaged bone marrow cells. Two widely used basic culture media for these cells are α -Minimum Essential Medium Eagle, alpha-modification (α -MEM) and Dulbecco's Modified Eagle's Medium (DMEM) with serum and osteogenic supplements. The basic culture media favors in the expansion of cells to achieve higher cell numbers before the cells are ready to be used in cell- or scaffold-based therapies. Conversely, different nutrient-containing media affect the expression of the osteoblastic phenotype (Coelho & Fernandes 2000). The presence of dexamethasone, β -glycerolphosphate and ascorbic acid is responsible to stimulate osteogenic differentiation of the hMSCs (Birmingham et al. 2012; Langenbach & Handschel 2013). Table 1.9 summarized the osteogenic supplements and their respective functions.

Table 1.9: Osteogenic supplements and their respective functions.

Osteogenic supplements	Functions
Dexamethasone	Enhances cell proliferation and differentiation by inducing the master osteogenic transcription factor RUNX-2 expression. (Gaur et al. 2005; Hamidouche et al. 2008).
β -glycerolphosphate	Serves as a phosphate source needed to produce hydroxyapatite mineral, which is the inorganic mineralized component of bone (Foster et al. 2006; Fatherazi et al. 2009; Tada et al. 2011).
Ascorbic acid	Aids in production of collagenous ECM of bone, associated with higher ALP activity and capability to form mineralized matrix (Choi et al. 2008; Vater et al. 2011).

Osteoblastic cells are sensitive to the changes in physiological changes such as the oxygen level, temperature, pH, solute concentration and osmolarity (Sorkin et al. 2004). Previous studies have shown the importance of oxygen in bone formation and osteoblastic cells. Most of the studies reported on the process of matrix maturation and mineralization has been investigated in cell cultured under regular culture conditions, which is 20% oxygen (Nicolaije et al. 2012). Oxygen levels in the bone marrow and the surrounding bone tissue however, have been measured and modeled to be approximately between 1 and 10% (Chow et al. 2001; Harrison et al. 2002). Oxygen tension can heavily affect the cell-cell interaction (Park et al. 2002). For instance, osteoblastic cells cultured under hypoxic conditions (under 2% oxygen tension) might influence cell metabolism, reduce in mineralization and collagen production (Nicolaije et al. 2012).

Various innovative scaffolds are being designed to facilitate nutrient transfer and oxygen supply from the media to the cell-seeded scaffolds in order to enhance osteogenesis. A common problem encountered in using scaffold-based therapies is the rapid formation of tissues on the outer edge of the scaffold whilst the tissues in the center undergo necrosis. To address this problem, recent studies have incorporated aligned channels into the general structure of the scaffold to achieve this goal (Rose et al. 2004; Silva et al. 2006). The idea behind this approach is to improve the nutrient and cell transfer to the core of the scaffold when cultured *in vitro* and *in vivo* (Ma & Zhang 2001; Gabriel et al. 2002; Hollister et al. 2002; Lin et al. 2003).

In addition, several bioreactors have been developed to improve mass transfer into larger tissue constructs (El Haj & Cartmell 2010). Bioreactors are defined as an automated devices that develop biological and/or biochemical process under closely monitored as well as strictly controlled environmental and operating conditions (Martin et al. 2004).

Bioreactors permit the defined and reproducible control over many environmental conditions required for cell culture, including nutrient supply, oxygen, medium flow rate, pH, temperature and waste removal (Antoni et al. 2015). Different bioreactors have been designed based on dynamic flow, perfusion, mechanical stimulation and magnetic force (Martin et al. 2004; El Haj & Cartmell 2010; Rauh et al. 2011; Yeatts & Fisher 2011). In the following section, rotary bioreactor that was used in this study is described. The comparisons of bioreactor system are summarized in Table 1.9.

Rotary Cell Culture System (RCCS) Bioreactors

Rotary cell culture system (RCCS) bioreactor was designed by National Aeronautics and Space Administration (NASA) in the early 1990s to study the growth of 3D cell tissue of mammals in microgravity. Fig. 1.11 demonstrates the RCCS developed by Synthecon (Houston, Texas, United States).

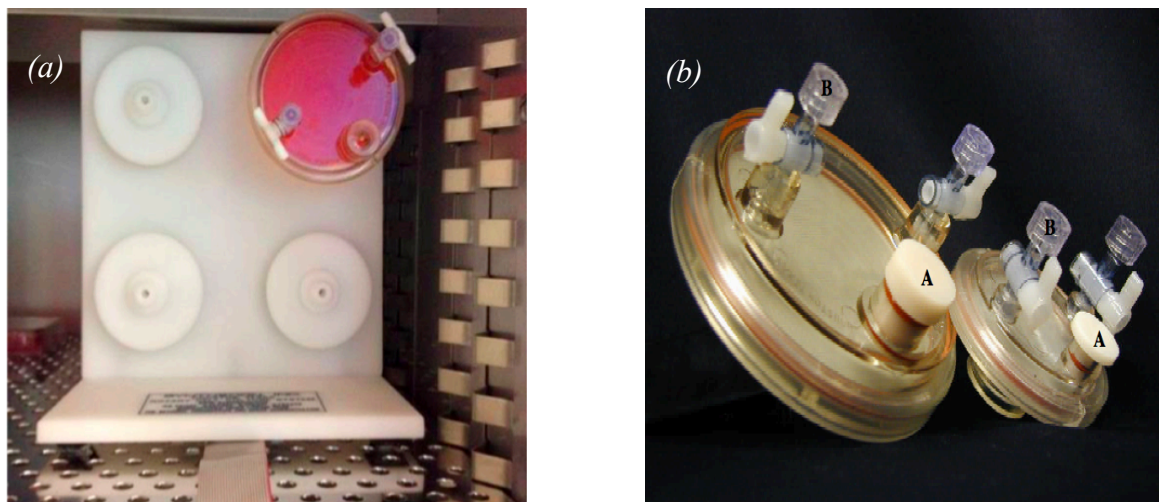


Fig. 1.11: Rotary bioreactor; (a) RCCS with disposable vessel on four stations motor base (b) and different vessel sizes i.e. 50 mL (big vessel) and 10mL (small vessel) (Antoni et al. 2015 and Synthecon official website. Re-printed with permission from MDPI.

This rotary bioreactor (Fig. 1.11 a) has two basic design principles: (1) solid body rotation and (2) a silicone rubber membrane for oxygenation. The chamber which is filled with culture media that rotates horizontally is the solid body rotation, while, the silicone membrane in the centre of the chamber (labelled as A in Fig. 1.11 b) allows oxygen to diffuse through (El Haj & Cartmell 2010).

Uniquely, this bioreactor can be used for both anchorage-dependent and suspension cells. In this bioreactor, scaffolds are allowed to freely move in the media in the vessel. The station motor base rotates the vessel at a constant angular speed as shown in Fig. 1.11 (a). The vessel wall is rotated at a speed which can balance the downward gravitational force and the upward hydrodynamic drag force acting on each scaffold. This constant rotation permits maximum fluid flow throughout the scaffolds, which helps in the supply of nutrient and waste of removal. In addition, gas exchange can also be authorized using this bioreactor through the gas exchange membrane. Typical rotational speed for the RCCS lies between 15 to 30 rpm depending on the scaffold use (Plunkett & O'Brien 2011).

Besides bone TE, this bioreactor has also been used in other regenerative studies such as cartilage TE, human ovarian surface epithelial (OSE) cells and cardiogenic bioprocess (Li et al. 2008; Lawrenson et al. 2009; Consolo et al. 2012).

Table 1.10: Comparisons of bioreactor system in BTE applications (Martin et al. 2004; El Haj & Cartmell 2010; Rauh et al. 2011; Yeatts & Fisher 2011; Plunkett & O'Brien 2011; Henstock et al. 2013).

Bioreactor system	Advantages	Disadvantages
Spinner flask	Reproducible and easy to use	Turbulent flow increase shear stress; leading to cell necrosis Mass transfer is not good enough, resulting in cell death in the center of the scaffolds
Rotating vessel	Minimize shear force and turbulence associated with stirred bioreactor Enhances mass transport throughout the scaffolds	Centrifugal force also cause scaffold to frequently collide with the wall-induce cell damage
Perfusion	Enhanced nutrient and waste transport	Operate under specific cell culture and sterile conditions
Compression	Enhanced osteogenesis compared to perfusion system Improved cell ingrowth and ECM synthesis	Any force-producing mechanism that invades the bioreactor (i.e. piston, compression system) may cause infection Scaffolds must be strong to transmit the force to the cells; resulting in long degradation times.
Hydrostatic	Provide physiological pressure ranges similar to those predicted to be sensed by osteocytes <i>in vivo</i> Fine computer control of both the magnitude and frequency of force can be applied	Evaporation of medium during mechanical stimulation

1.10. Characterization

Characterization of scaffold-based tissue engineering can be divided into two primary parts; the assessment of the physico-chemical properties of the fabricated scaffold and the cell responses *in vitro* as in direct contact to the scaffold materials. Both parts of the characterizations can further be subdivided to another two categories, the qualitative and quantitative analyses. Briefly, qualitative analysis is based on visual observation, while quantitative analysis allow the reporting summary results in numerical terms to be given with a specified degree of confidence.

1.10.1. Physico-chemical Characterization

1.10.1.1. *X-Ray Diffraction analysis*

The characterization of the crystal structure of a system is made possible through X-Ray Diffraction (XRD) and it is considered as one of the most determinative tool in characterization of crystalline materials (Brundle et al. 1992). Typically, XRD is used to obtain qualitative and quantitative phase analysis, crystallography, and crystal structure of the material.

XRD can also be used to study the variations in chemical composition of a known substance involve in the substitution of atoms, generally of somewhat different size; in specific in a crystal structure. As a result of this substitution, the unit cell dimensions and the interplanar spacing are slightly altered as compared to the standard reference diffraction pattern (i.e. for HA, a -axis= 9.418 Å; c -axis= 6.884 Å). By measuring this small shift in the position of lines in the powder pattern of substance for the known structure, modification in chemical composition may be often accurately detected (Dana 1977).

When x-ray is directed onto a crystalline material, the plane of the atoms within the crystal would diffract the x-rays. When the diffraction angle corresponding to a given line on a powder photograph has been determined, the interplanar spacing of the family of atomic planes can be calculated using Bragg's law (Eq. 1.1):

$$n\lambda = 2d \sin\theta \quad \dots \text{Equation 1.1}$$

where, n = integer; λ = wavelength of Copper K-alpha radiation (Cu K α , λ = 1.5406 Å); d = distance between crystal planes; and θ = half of diffraction angle.

In this study, the diffraction peak at about 25.8° and 32.9° corresponding to the (002) and (300) Miller plane family of HA, were chosen to calculate the distance between crystal planes along the crystallographic of c - and a -axes, respectively. Plane (002) was chosen to calculate the crystallite size because it is the strongest peak without any overlapping in the HA pattern (Kee et al. 2013; Bang et al. 2011). The crystallite size of the powders was calculated based on Scherrer equation (Equation 1.2):

$$d = \frac{K\lambda}{\beta \cos\theta} \quad \dots \text{Equation 1.2}$$

where, d = crystallite size; K = a shape factor equal to 0.9; λ = wavelength of Copper K-alpha radiation (Cu K α , λ = 1.5406 Å); β = full width at half maximum (FWHM) and θ = half of diffraction angle. In this study, the lattice parameter and crystallite size were calculated automatically using Reitveld refinement software.

1.10.1.2. Fourier Transform Infra-Red Spectroscopy

Fourier transform infra-red (FTIR) spectroscopy is one of the most common methods to characterize biomaterial surfaces. The principle involved in FTIR spectroscopy is IR

radiation is adsorbed and excites molecular vibration. This bond vibration of molecular species can then reveal information on specific chemistries and orientation of structures (Ratner et al. 2013). FTIR result can be represented either in transmittance or absorbance spectrum. This would indicate at which wavelength the IR was transmitted/ absorbed by the sample and therefore allow the interpretation of the functional group presents in the sample, and thus confirms the phase of the materials (Ślósarczyk et al. 2005). Table 1.11 represent the typical vibration bands of multi-substituted hydroxyapatite (SiCHA) nanopowders, which is the main interest in this study.

Table 1.11: Typical vibration bands of multi-substituted hydroxyapatite (SiCHA) nanopowders.

Vibration bands	Wavelength (cm ⁻¹)	References
OH ⁻	1600-1700, 3200-3700	Kim et al. 2003; Murugan & Ramakrishna 2006; Lafon et al. 2008;
PO ₄ ³⁻	565-601, 963, 1036, 1095	Lafon et al. 2008; Fathi et al. 2008; Kee et al. 2013
CO ₃ ²⁻ (A-type)	877-880, 1500, 1540-1545	Krajewski et al. 2005; Murugan & Ramakrishna 2006;
CO ₃ ²⁻ (B-type)	870-875, 1410-1430, 1450-1470	Landi et al. 2003, Ślósarczyk et al. 2010; Baba Ismail & Mohd Noor 2011; Bang et al. 2014
SiO ₄ ⁴⁻	490-505, 890-895, 947	Sprio et al. 2008; Marchat et al. 2013

In this study, the produced powders were analysed using Perkin Elmer FTIR Spectroscopy with Spectrum 100 software. This instrument has limitation in terms of the detected wavelength, where the minimum wavelength is 650cm⁻¹. Any wavelength falls under this wavelength could not be detected. Therefore, some of the PO₄³⁻ and SiO₄⁴⁻ vibration bands are not shown on the IR spectra.

1.10.1.3. X-Ray Photoelectron Spectroscopy

X-Ray Photoelectron Spectroscopy (XPS) is an exceptionally sensitive tool to investigate the chemical elements constituting the outermost layer of a surface approximately up to 200 Å (Shin et al. 2006). The basic principle, depth analysed, spatial resolution and analytical sensitivity of XPS analysis is shown in Table 1.12.

Table 1.12: Basic principle, depth analysed, spatial resolution and analytical sensitivity of XPS analysis (Ratner et al. 2013).

Basic principle	X-ray induces the emission of electrons of characteristics energy
Depth analyzed	10-200 Å
Spatial resolution	10-150 µm
Analytical sensitivity	0.1 atom%

XPS is a quantitative technique where the number of atoms recorded for a given transition is directly proportional to the number of atoms detected on the surface (Fairley 2009). In XPS, x-rays are focused upon a specimen and the interaction of the x-rays with the atoms in the specimen causes the emission of core level (inner shell) electrons. XPS then measured the energy of these electrons, which provide information about the nature and environment of the atoms or atoms from which they originate. The basic energy balance describing this process is given by the following relationship (Equation 1.3):

$$BE = h\nu - KE \quad \dots \text{Equation 1.3}$$

where, BE is the energy binding the electron to an atom (the desired value), KE is the kinetic energy of the emitted electron (the measured value given by XPS) and $h\nu$ is the energy of the x-rays (a known value) (Ratner et al. 2013).

An example of a powerful application of XPS in making biomaterials for medical purpose is to determine the chemical compositions on a surface of the materials. This has become critically important, as any changes in the surface structural and composition will indirectly influence their cytocompatibility and thus affect the sequence steps that lead to bone bonding (Botelho et al. 2002).

1.10.1.4. Carbon, Hydrogen, Nitrogen Analysis

Carbon, Hydrogen, Nitrogen (CHN) analysis is used to estimate the percentage compositions of carbon, hydrogen and nitrogen presence particularly in newly synthesised organic compounds. In this technique, the sample is encased in a tin cup, subsequently dropped vertically into an oxygen-rich chamber and combusted at high temperature in a stream of oxygen. The instrument then measures the carbon, hydrogen and nitrogen in a single analysis.

A typical application of CHN in the making of bioceramics (i.e. carbonated hydroxyapatite, CHA) is the quantification of carbonate content incorporated in the structure (Murugan & Ramakrishna 2006; Lee et al. 2007; Ana et al. 2010). Similarly, in this work only the percentage of carbon was calculated from the CHN analysis obtained, as this is the main element of interest. To ensure the measurement is accurate and consistent for every batch of powders, the instrument was firstly calibrated using Acetanilide Organic Analytical Standard before any analysis was performed. The confidence limits for the analysis is <0.3% for solids.

1.10.1.5. Inductively Couple Plasma Optical Emission Spectroscopy

In mid-1960s, the inductively couple plasma (ICP) was developed for optical emission spectroscopy (OES) at Iowa State University in United States and at Albright & Wilson Ltd. in United Kingdom. The first ICP/OES instrument was commercialized in 1974.

ICP/OES is a powerful tool in determining trace elements in a numerous of sample types. It has been widely used in agricultural and food, geological, environment and water as well as in biological and clinical studies. In theory, this technique is based on the spontaneous emissions of photon from atoms and ions that had been excited in a radio frequency (RF) discharge. ICP/OES instrument require the sample to be either in liquid or gas forms. In the case of solid samples, simple preparation is required where sample needs to undergo acid digestion to convert the sample into liquid form. The sample solution is transformed to an aerosol and directed into the central channel of the plasma. ICP sustains a temperature of approximately 10 000K (9726.85°C) at its core to allow the aerosol to vaporize rapidly. The elements of interest to be identified or chemically term as analyte elements are liberated as free atoms in the gaseous state. Foster collisional excitation within the plasma imparts additional energy to the atoms, and hence promotes them to the excited states. Appropriate energy is often available to convert the atoms to ions and in which afterwards these ions are promoted to excited states. Both atoms and ions in the excited states may then relax to the ground state via the emission of photons. These emitted photons have characteristics energies that are determined by the quantized energy level structure for the specific atoms or ions. The wavelength of the emitted photons identified the origin of the anlyte elements (Hou & Jones, 2000).

In making biomaterial for bone substitutes application for example, ICP-OES is normally used to precisely quantify the elements present in the chemical compositions of the samples (Kim et al. 2003; Landi et al. 2003; Ibrahim et al. 2011). During each experiment, a diluted nitric acid (1M HNO₃) and de-ionized water were used as blank and control, respectively. Details on the sample preparation for ICP-OES used in this study is described in Chapter 2 (section 2.2.2.4).

1.10.1.6. X-Ray Fluorescence

X-Ray Fluorescence (XRF) is fast, accurate and non-destructive for quantitative analysis of elemental composition in wide ranges of materials (Brundle et al. 1992). XRF is a bulk analysis technique with the depth of sample analysed varying from less than 1 mm to 1 cm depending on the energy of the emitted x-ray and the sample composition. The elements commonly detected range from beryllium to uranium. Lighter elements from boron to fluorine may also be detected. Basically, the sample is irradiated by an intense x-ray beam, which causes the emission of fluorescent x-rays. The emitted x-rays can either be detected using energy dispersive system or wavelength dispersive system to identify the elements present in the sample. The concentrations of the elements are then determined by the intensity of the x-rays. The precision and reproducibility of XRF analysis is very high. Very accurate results are possible to achieve when good standard specimens are available (Brouwer 2010).

In this study, XRF analysis was used to measure the Ca/P and Si/P ratios of the prepared powders. The sample for XRF was prepared by making glass beads. This requires that the sample powder to be mixed with flux (lithium tetraborate and lithium metaborate) to get a glassy phase. The ratio of flux to sample is 10:1. The flux and sample were accurately weighed and placed into a 95% platinum-5% gold fusion crucible. The crucible was then placed in the furnace using platinum-tipped tongs at a temperature of 1100°C, and left to fuse according to the type of material being fused. The fusing machine was control automatically. Prior to XRF analysis, a calibration was firstly run using calcium phosphate programme developed by the supplier. The 2910a sample (54.48% CaO, 41.25% P₂O₅, 0.21% SiO₂, 0.043% Na, 0.011% Mg, 0.094% Al, 0.078% Sr, 0.011% Fe and 0.01% Zr) was used as check standards for the analysis, which were run pre, and post sample analyses to ensure the accuracy of the results obtained.

1.10.1.7. Atomic Force Microscopy

Atomic force microscopy (AFM) has been beneficial to investigate materials performance, processes, physical and surface properties at nanometer scale. The measurement of surface topography is an example of typical application of AFM in materials characterization (Hoskins et al. 2012). AFM technique has been used to determine the surface roughness of the coated samples either in 2D or 3D samples (Zhang et al. 2005; Kim et al. 2010; Zhao et al. 2014).

In AFM, a sharp probe or tip (3-6 μm tall pyramid with 15-40 nm end radius) is used to scan the sample. This tip is situated at the apex of a flexible cantilever that is often in V-shaped, usually made of silicon. When certain voltage is applied, AFM utilizes a piezoelectric scanner that moves the sample in 3 dimensions. The tip is then brought close to the sample and raster-scanned over the surface causes the cantilever to be deflected due to probe-sample interaction. A line-by-line image is generated as a result of this deflection. The cantilever vertically bends upwards or downwards as a result of repulsion or attraction interactions between the tip and sample surface, respectively (Leite et al. 2007).

In this study, AFM analysis was used to qualitatively and quantitatively measure the surface roughness of different numbers of bilayers coating on 2D PLA films. AFM is a sensitive technique to detect the changes in surface roughness, however it still has its own limitation. The AFM tip (normal tip), spring constant, scan rates and amplitude available are limited. Details on the AFM parameters used in this study are described in Chapter 2 (section 2.3.4.2).

1.10.1.8. *Electron microscopy*

For the resolution of detailed materials characterization, two powerful instruments based on electron microscopy are used: the Scanning Electron Microscope (SEM) and the Transmission Electron Microscope (TEM) (Rosenberg & Weis 1983).

In SEM, three types of principle images could be produced: secondary electron images, backscattered images and elemental X-ray maps. In general, the working voltage of SEM is between 2 to 50 kV. Conventionally, the secondary and backscattered electrons are separated according to their energies. Secondary electron is considered when the energy of emitted electron is <50 kV, while when the energy is >50 kV, it is referred as backscattered electrons. SEM is only used to characterize the surface morphology and both resolution and crystallographic information are limited. With this, TEM has become an attractive alternative over SEM (Voutou et al. 2008).

TEM is a technique where an electron beam interacts and passes through the specimen instead of scanning only the top surface of the material (Voutou et al. 2008). Both SEM and TEM are widely been use in the assessment of nanoparticles in particular in characterizing the morphology, size, shape and distribution of the particles ranging from micron to nano-scale materials (Zhou et al. 2008; Baba Ismail & Mohd Noor 2011; Shepherd et al. 2012). In scaffold fabrications, SEM is typically use to observe the pore morphology and chemical composition of the surface with the aid of Energy Dispersive X-Ray analysis (Qing-Qing et al. 1999; Lee et al. 2005).

1.10.2. Biocompatibility Assessments

In the past years, biocompatibility assessment had a change of paradigm and is now divided into two principal areas. The first principle is assessing the “biosafety”, which involves the exclusion of any cytotoxic effects of the biomaterial to the surrounding

biological environment. The second area is focussed on the “biofunctionality” of the material, i.e. encourage cell proliferation and differentiation of cells towards osteoblastic lineage, which will always be the golden goal in scaffold-based TE (Kirkpatrick et al. 1998). International Standard of Organization (ISO 10993-5) has drawn guidelines for biological evaluation of materials for medical devices, which includes both qualitative and quantitative analysis. Basically, there are four main evaluations that should be carried out; (1) assessment of cell damage by morphological means, (2) measurement of cell damage, (3) measurement of cell growth and (4) measurement of specific aspects of cellular metabolism. There are three categories of tests, which include extract, direct and indirect tests. The choice of test is depend on the nature of the materials to be evaluated, the potential site of use and the nature of the use. In extracting condition, attempt should be made to stimulate or exaggerate the clinical use conditions so as to determine the potential toxicological hazard without causing significant changes in the test sample. This includes fusion, melting or any alteration of the chemical structure, unless this is expected during application. Direct contact test is the commonly use to assess the biocompatibility of the cells seeded directly on the materials. Various sizes, shape physical states of materials can be tested by direct contact even in basal culture medium. While, indirect contact test is stricter in terms of the culture media used, where, it requires condition growth media. In this study, ISO 10993-5 was adapted only as a basic guideline for the *in vitro* biocompatibility study and was modified for lab scale study as shown in Table 1.13.

Table 1.13: Categories and common staining/ biochemical assays used for in vitro biocompatibility evaluation of biomaterials.

Assessment Objective	Common staining/ biochemical assays used	Results Interpretation	References
Cell viability	-Live/ Dead Staining	Green fluorescent (given by Calcein-AM) indicates the live cells while, dead cells represented by Propidium Iodide or Ethidium homodimer	Araujo et al. 2010; Jones et al. 2010
Cell proliferation	-Picogreen assay -Bradford Total Protein assay	The amount of DNA and total protein roughly indicates the cell number presents	Bradford 1976; Datta et al. 2005; Prosecká et al. 2012
Cell metabolic activity	-Alamar Blue assay -MTT assay	The level of fluorescent indicates the intracellular enzyme activity	Zhu et al. 2003; Rodrigues et al. 2013
Cell differentiation towards osteoblastic lineage	- ALP activity assay	ALP is known to be associated with bone metabolism and early differentiation of cells towards osteoblastic lineage	Chen et al. 2008; Zhao et al. 2014

**MTT*= 3-(4, 5-dimethylthiazol-2-y-l)-2, 5-diphenyltetrazoliumbromide, *ALP*= alkaline phosphatase

1.10.2.1. *Histochemical staining*

Some of the histochemical stain can provide both qualitative and quantitative analysis. For instance, Alizarin Red solution is commonly used to stain calcium formation, where positive stain will result in red matrix precipitate. The precipitates can be dissolved with cetylpyridinium chloride to yield a purple solution, which then can be quantified using colorimetric analysis (Yu et al. 2004; Song et al. 2008).

1.10.2.2. *Immunohistochemical staining*

Immunohistochemistry (IHC), or immunocytochemistry is a qualitative method for localizing specific antigens in tissue or cells that is based on antigen-antibody recognition. The interactions of antigen-antibody can be seen via a coloured histochemical reaction that is visible by light or fluorescent microscopy (Taylor et al. 2006). IHC has been used for the identification of osteogenic expression using numerous specific osteogenic markers such as ALP, runt-related transcription factor 2 (RUNX-2), osteopontin (OPN) and osteocalcin (OCN). To identify if the microvascular networks formed throughout the scaffolds were of human cell origin, human specific CD31 antibody is commonly used (Pirraco et al. 2014).

1.10.2.3. *Micro-computed tomography*

Micro-computed tomography (Micro-CT) has been established as gold standard for the assessment of the 3D structure of bone and scaffolds designed for bone TE (Cartmell et al. 2004). The density and geometry of the 3D construct can be determined by quantifying the attenuated X-rays. By using Micro-CT analysis, it is possible to distinguish between the investigated scaffolds and if any mineralized matrix produced by the cells during culture (Jones et al. 2010). This can be achieved by analysing the samples at different threshold, where low threshold is usually chosen for the scaffolds and the higher threshold is applied for the analysis of mineralization (Henstock et al. 2013; Reinwald et al. 2015).

1.11. Thesis Aims and Objectives

Numerous 3D scaffolds have been fabricated as reported in the literature, but none of them is able to take over the role of the current clinical gold standard, which is the autograft. To date, the existence developed bone scaffolds still have not met the actual practical needs. To address this problem, more advance materials and fabrication technique should be implemented. Therefore, the overall aim of this project is to fabricate a three-dimensional (3D) hybrid scaffold to enhance bone formation *in vitro* for BTE applications.

The specific aims of this research are to:

1. Produce multi-substituted hydroxyapatite nanopowders as bone substitute materials
2. Develop an innovative coating materials assembly using Polyelectrolyte Multilayers (PEMs) technique
3. Fabricate different structural and functional designs of 3DP hybrid scaffolds using Fused Filament Fabrication technique
4. Investigate the influences of different structural and functional designs of 3DP hybrid scaffolds on hMSCs fate in static and dynamic conditions
5. Introduction of co-culture system of HUVECs and hMSCs as to promotes pre-vascularized hybrid scaffolds

1.12. Research hypotheses

In order to achieve the research aims, five major hypotheses have been considered in this study as described below:

1. Simultaneous substitutions of carbonate and silicon ions into HA lattice in fully controlled amount enhance osteogenic behaviour.
2. Coating materials assembly consists of osteoconductive (multi-substituted HA) and osteoinductive materials (Collagen type I) closely resemble the bone composition.
3. The novel designs of the 3DP hybrid scaffolds promote better bone formation than the commercial HA scaffolds.
4. Scaffolds cultured under dynamic flow and the use of osteogenic media enhance bone formation *in vitro* compared to those cultured under static condition and in proliferation media.
5. The crosstalk between HUVECs and hMSCs enhance both osteogenesis and angiogenesis of the pre-vascularized bone scaffolds.

Chapter 2

Materials and Methods

2.1. Introduction

In general, this chapter is divided into four main sections. The first part of the chapter describes the wet chemical method used to synthesize the multi-substituted hydroxyapatite (SiCHA) nanopowders, followed by the physico-chemical characterizations, i.e., X-Ray Diffraction (XRD), Fourier Transform Infra-Red (FTIR), Carbon-Hydrogen-Nitrogen (CHN) analysis and Inductively Coupled Plasma-Optical Emission Spectroscopy (ICP-OES) technique.

Prior to *in vitro* cytotoxicity assessment, the cells used were firstly characterized. Human bone marrow-derived mesenchymal stem cells purchased from Lonza (United States) were used for all experimental work. The cells donor and passage (P3) number were kept constant throughout the experiment. The *in vitro* cytotoxicity tests were performed on four different groups of the optimum multi-substituted HA powders. This test includes the investigations on the cell viability obtained by Live/Dead staining, cell proliferation given by PicoGreen and total protein production. Cell metabolic activity was assessed by Alamar Blue assay and the early indication of osteogenic differentiation from ALP activity.

In this study, polyelectrolytes multilayers (PEMs) coating was used to fabricate hybrid 3D scaffolds. The 3DP scaffolds were initially fabricated by 3D printed (3DP) technique via Fused Deposition Modelling method using a synthetic polymer, Poly (lactic acid) (PLA). Three different structural designs were fabricated i.e., the mesh, two- and four channel scaffolds. Before fabricating hybrid 3DP scaffolds, the number (n) of coating layers of the PEMs method was firstly optimized. Among different n -layers of the coating materials assembly, coating surface that could provide the best growth environment for the hMSCs, i.e. produces the highest level of total proteins, DNA concentration and early osteogenic activity, was chosen as the optimum n -layers. The term “hybrid” is referring to the

combination of more than two different materials used to fabricate the 2D films/ 3DP scaffolds. For instances, the assemblies of PEMs established in this work consists of newly developed SiCHA powders dispersed in two different electrolytes, namely the hyaluronan and collagen type I which acts as the polyanions and polycations, respectively. EDC/NHS was then introduced to crosslink these layers before proceeding to the next layer. The number of coating layers was optimized based on the atomic composition of the deposited powders (XPS), surface roughness (AFM), particle scattering (TEM) and semi-quantification of Calcium and Collagen distribution on the coated surface of the PLA films (Alizarin Red and Sirius Red, respectively).

The 3DP PLA scaffolds were then coated in a similar manner of the PLA hybrid films fabrication using the optimum number of layers. These scaffolds were then tested in different culture conditions and medium. Rotary Cell Culture System (RCCS, Synthecon Inc., Cellon, Strassen, Luxembourg) was used to study the effect of dynamic condition in stimulating rapid osteogenesis as compared to the static culture condition. Different culture medium was used to investigate the effect of supplements on the cell activity in particular when the samples were exposed to dynamic condition. Hydroxyapatite (HA) scaffolds purchased from Ceramisys (Sheffield, United Kingdom) was used as the experimental control.

The scaffolds were tested *in vitro* to investigate the cells survival and capability to differentiate into osteoblastic lineage. The early osteogenic differentiation of hMCSs cultured on different structural designs of the hybrid scaffolds was qualitatively quantified using ALP staining. Micro-computed tomography (Micro-CT) analysis was an important tool in determining the best structural design and functional 3DP hybrid scaffolds.

The final section of this chapter described the procedure used to promote the pre-vascularization of the scaffolds. In this study, human umbilical vein endothelial cells (HUVEC) and hMSCs were used as the coculture system. Both cells were fluorescently labelled as to ease the imaging and quantification of relative fluorescence intensity. RUNX-2 and CD31 expression were used to define the early osteogenesis and vasculogenesis. The level of pro-angiogenic markers, namely, Platelet Derived Growth Factor (PDGF-BB) and Vascular Endothelial Growth Factor (VEGF) were quantified using the enzyme linked immunosorbent assay (ELISA).

2.2. Synthesis of multi-substituted HA by nanoemulsion method

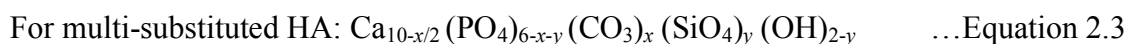
2.2.1. Optimization of carbonate and silicon ions contents

The synthesis of multi-substituted HA (SiCHA) powders was performed based on a nanoemulsion method at ambient temperature described elsewhere (Zhou et al. 2008). Acetone was used as organic solvent to create the nanoemulsion phase. An acetone solution of calcium nitrate tetrahydrate was added dropwise into the di-ammonium hydrogen phosphate, ammonium hydrogen carbonate and silicon tetra acetate in aqueous solution. Before making the SiCHA powders, pure carbonate substituted HA (CHA) and silicon substituted HA (SiHA) were synthesized to optimize the composition of carbonate- and silicon substituted into the apatite structure. The best compositions of the pure CHA and SiHA powders were chosen to closely mimic the composition of carbonate and silicon in bone mineral as shown in Table 1.1 (section 1.2); these powders then act as the control. Table 2.1 listed all the reagents used in the nanoemulsion method and their functions.

Table 2.1: Summary of the raw material used in nanoemulsion method and their functions.

Chemical Name	Chemical Formula	Molecular weight (g/mol)	Function	Source	Purity
Calcium nitrate tetrahydrate	$\text{Ca}(\text{NO}_3)_2 \cdot 4\text{H}_2\text{O}$	236.15	Calcium Source	Sigma	≥ 99.0
Di-ammonium hydrogen phosphate	$(\text{NH}_4)_2\text{HPO}_4$	132.00	Phosphate Source	Sigma	≥ 98.0
Ammonium hydrogen carbonate	NH_4HCO_3	79.06	Carbonate Source	Sigma	≥ 99.0
Silicon tetra acetate	$\text{Si}(\text{CH}_3\text{COO})_4$	264.27	Silicon Source	Sigma	≥ 98.0
Acetone	$\text{C}_3\text{H}_6\text{O}$	58.08	Solvent for making nanoemulsion		100
Sodium hydroxide	NaOH	40.00	pH adjustment	Sigma	≥ 99.0

The amounts of CO_3 and SiO_4^{4-} substituted into the apatite structure were calculated based from the stoichiometry empirical formula as shown in Equations 2.1-2.3:



Provided no carbonation in A site occurred.

The flowcharts (Fig. 2.1-2.3) demonstrate the process involved in the synthesis of CHA, SiHA and SiCHA hydroxyapatite powders, respectively. In brief, $\text{Ca}(\text{NO}_3)_2 \cdot 4\text{H}_2\text{O}$ solution which was prepared in acetone was added dropwise using a dropping funnel into the mixture of the $(\text{NH}_4)_2\text{HPO}_4$ containing either NH_4HCO_3 , $\text{Si}(\text{CH}_3\text{COO})_4$, or both carbonate and silicon sources. The addition of calcium solution caused a drastic change in the colour of the mixture from crystal transparent to milky and wax-like in appearance. The mixture was stirred for 30 minutes at 450 rpm using a magnetic stirrer. Subsequently, the mixture was filtered using a Whatmann vacuum filtration set. About 1000 mL of dH_2O was used in each washing stage. The filtration cake formed after filtration was washed three times with dH_2O to clean from potential by-product or impurities, e.g. ammonia. Finally, the filtered cake was dried at 90°C for overnight in an oven (Carbolite, United Kingdom). The dried filtered cake was ground with an agate mortar; $90 \mu\text{m}$ particles were extracted using a sieve. The synthesized powders were then characterized physically and chemically using various techniques, i.e. XRD, FTIR, CHN and ICP-OES. The term “as-synthesized powders” refers to the powders produced by the nanoemulsion method in this study.

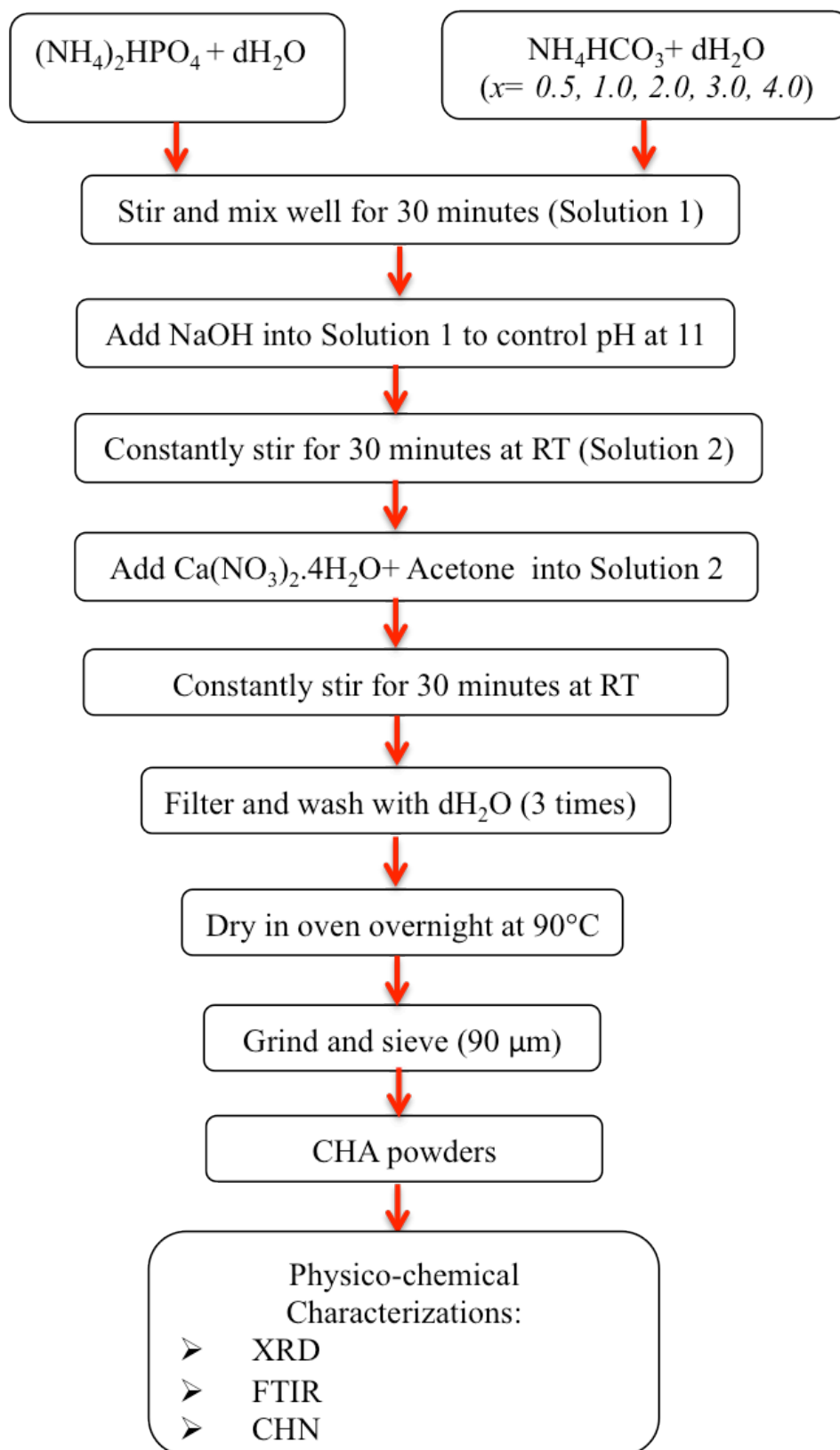


Fig. 2.1: Flowchart of the process for the synthesis of CHA powders by nanoemulsion method.

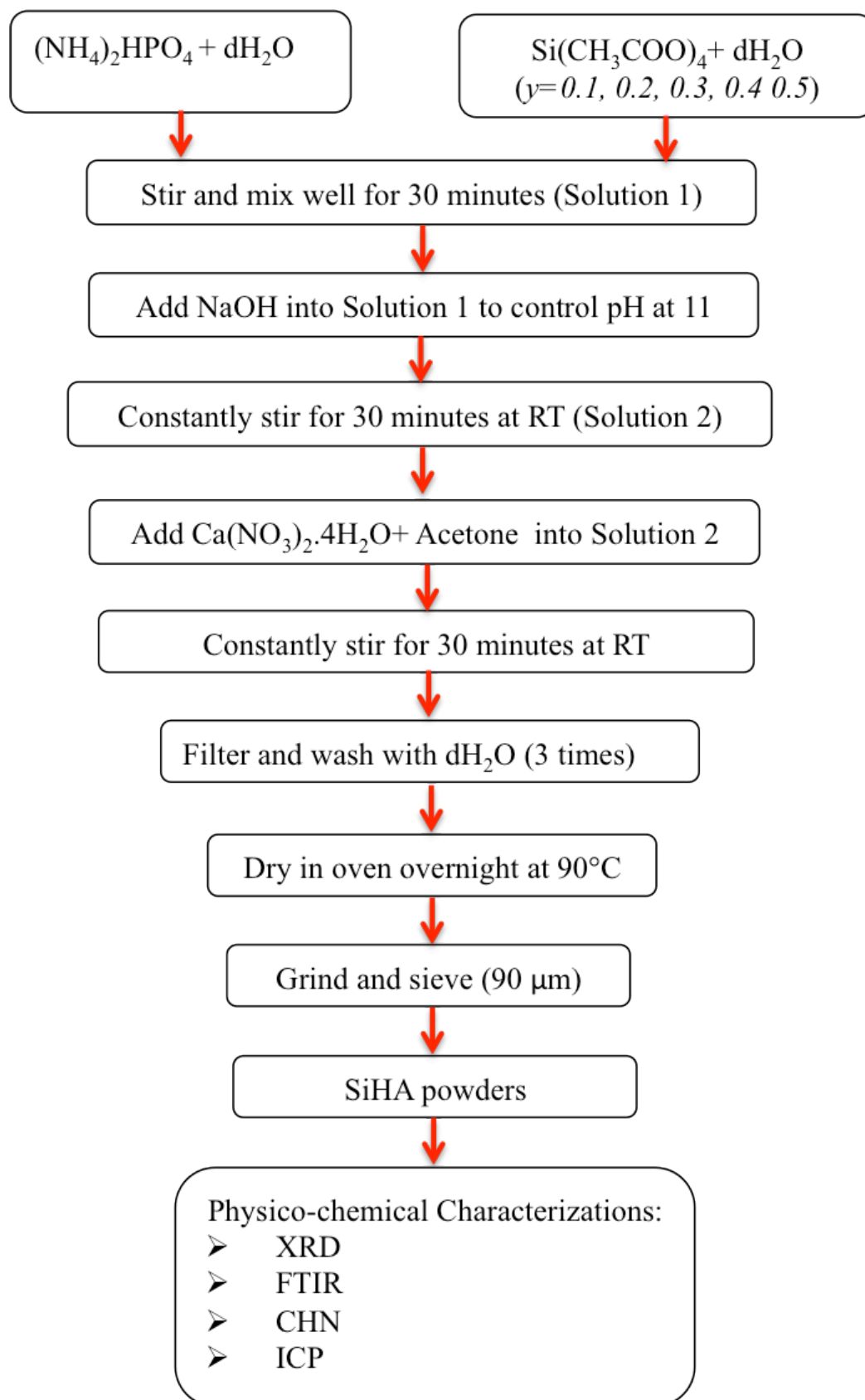


Fig. 2.2: Flowchart of the process for the synthesis of SiHA powders by nanoemulsion method.

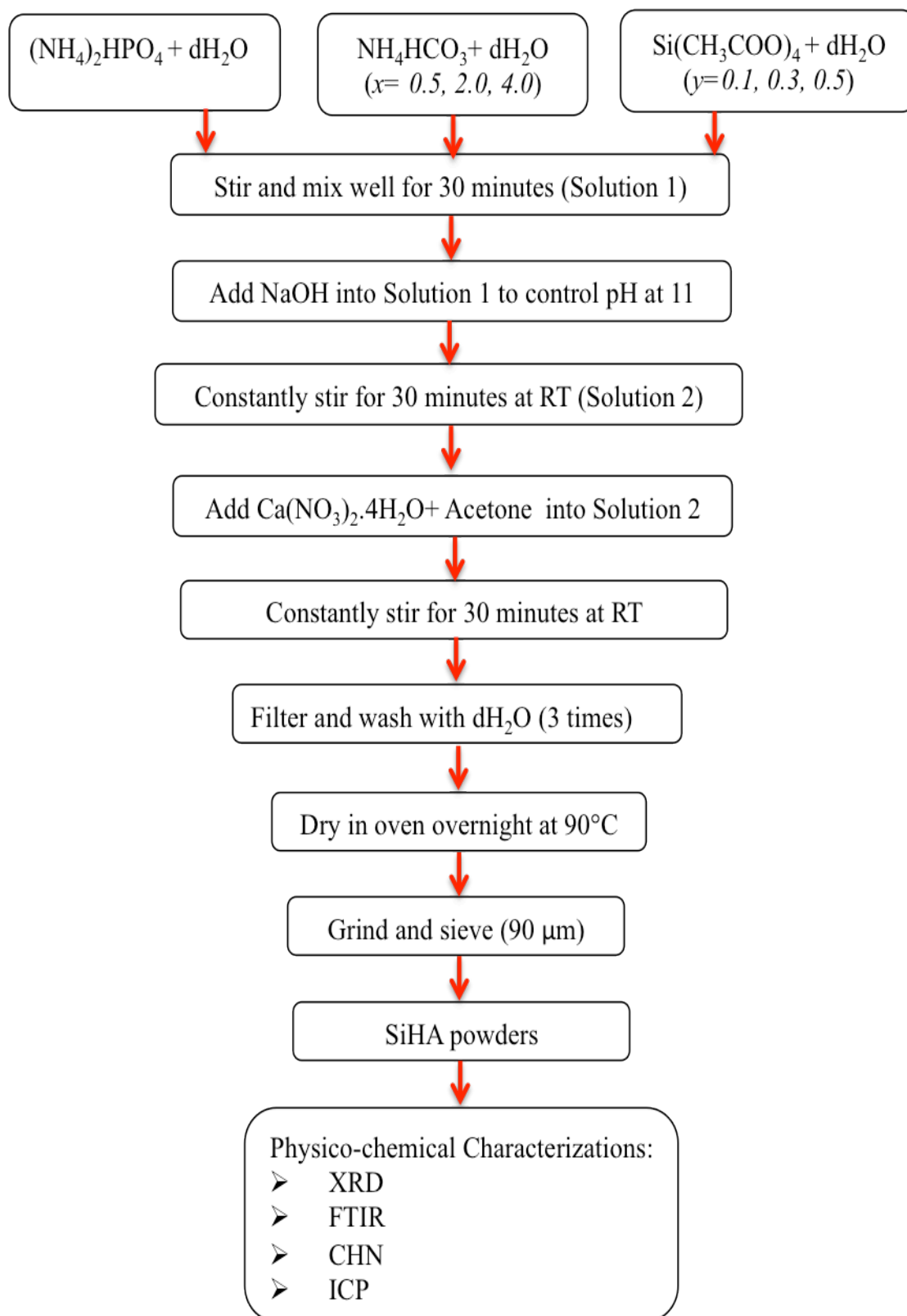


Fig. 2.3: Flowchart of the process for the synthesis of SiCHA powders by nanoemulsion method.

2.2.2. Physico-chemical characterization

2.2.2.1. *X-Ray Diffraction*

X-Ray Diffraction (XRD) was used to obtain qualitative and quantitative purity of the phases, crystallography, and structure of the materials of as-synthesized powders. HA standard pattern with ICDD file number of 09-0432 was used as the reference pattern. XRD was carried out using a Bruker D8 XRD with a copper anode (Cu K_{α} , $\lambda = 1.5406 \text{ \AA}$) as X-Ray source. X-ray data for the prepared powders were collected using PANalytical X'Pert Pro diffractometer with the X'Celerator area detector. All samples were mounted on a silicon low background substrate using a drop of isopropanol. The range of x-ray scan was fixed from $2\theta = 10^{\circ}$ to 90° with scan step size = 0.01. Data analyses were done using X'Pert HighScore Plus software. Lattice parameters and crystallite size were calculated based on Rietveld refinement.

2.2.2.2. *Fourier Transform Infra-Red Spectroscopy*

The as-synthesized powders were characterized using Fourier Transform Infra-Red (FTIR) Spectroscopy by transmittance mode (Perkin Elmer 100, Perkin Elmer, United Kingdom) to determine the mechanism of carbonate and silicon substitutions within the HA structure. The wavenumber range was 4000 to 650 cm^{-1} ; with a resolution of Spectrum 100 Software. Each sample was scanned four times. The detected bands were compared to the typical vibration bands of SiCHA as shown in Table 1.11 (section 1.10.1.2).

2.2.2.3. *Carbon, Hydrogen, Nitrogen Analysis*

The carbonate content (wt%) of the as-synthesized powders were measured using Carbon, Hydrogen, Nitrogen (CHN) analysis. CHN was performed by Carlo Erba 1180 Elemental Analyser controlled with CE Eager 200 Software, run in accordance to the manufacturer's instruction and weighed using a certified Mettler MX5 Microbalance. In this

characterization method, samples used was in the form of powders of about 1.5-2.0 mg. The powders were combusted at high temperatures in a stream of oxygen, and the products of the combustion for carbon, hydrogen and nitrogen were measured by the instrument in a single analysis. The sample, encased in a tin cup, was dropped vertically into an oxygen-rich chamber and was combusted into its elemental oxides at high temperatures of 925°C. In this particular study, the carbonate in the apatite powder will easily decompose into CO₂ gas as exposed at high temperature. This resultant gas was then transferred to a gas chromatographic column for separation. Thermal conductivity detector (TCD) then detected and quantified these resultant gases. In order to estimate the amount of carbonate present in the sample, the wt% of carbon obtain was multiplied by a factor of five (Krajewski et al. 2005).

2.2.2.4. *Inductively Coupled Plasma-Optical Emission Spectroscopy Measurement*

The concentrations of Ca, P and Si in the as-synthesized apatite powders were determined by inductively coupled plasma with optical emission spectroscopy (ICP-OES) using Perkin Elmer Optimal 4300DV instrument. About 0.01 g of the as-synthesized powders was digested in 1M HNO₃ (2.5 mL of HNO₃, 1.5 mL of H₂O₂, and 0.3 mL of HCl) in a 100 mL Erlenmeyer flask (Vázquez et al. 2005).

2.2.2.5. *X-Ray Fluorescence Analysis*

X-Ray Fluorescence (XRF) is an emission spectroscopic technique, which identify the elements present in the sample. XRF is a simple, non-destructive technique for qualitative and quantitative analyses of elemental composition in wide range of materials (Brundle et al. 1992). The sample preparation and analysis of the as-synthesized powders were performed at Glass Technology Service (GTS) in Sheffield. The elemental compositions in the powders were quantified using a Rigaku RIX-3000 wavelength dispersive XRF

spectrometer. The 2910a sample (54.48% CaO, 41.25% P₂O₅, 0.21% SiO₂, 0.043% Na, 0.011% Mg, 0.094% Al, 0.078% Sr, 0.011% Fe and 0.01% Zr) was used as check standards for the analysis, which were run pre- and post-sample analyses to ensure the accuracy of the results obtained. The results obtained were then used to quantify the percentage of silicon that successfully incorporated into the apatite structure and the ratio of Si/P of the multi-substituted HA (SiCHA) before and after calcination was performed.

2.2.3. As-calcined multi-substituted HA

Three different groups of powders with optimize carbonate (x) and silicon (y) molar contents were synthesized in this work: CHA, SiHA and multi-substituted HA (SiCHA-1 and SiCHA-2), as shown in Table 2.2.

Table 2.2: Different carbonate (x) and silicon (y) molar contents of the powders.

Sample codes	x (molar content)	y (molar content)
CHA	2.0	-
SiHA	-	0.3
SiCHA-1	2.0	0.5
SiCHA-2	2.0	0.3

Calcination was then performed on the as-synthesized powders at 500, 600 and 700°C with a heating rate of 10°C /min and at least one hour soaking time in ambient atmosphere. The term “as-calcined powders” refers to the powders after heat treatment (calcination).

2.2.4. Physico-chemical characterization

2.2.4.1. *X-Ray Photoelectron Spectroscopy*

X-Ray Spectroscopy (XPS) is an extremely sensitive technique used to quantify the surface chemistry of the sample at the atomic level. In this study, XPS was used to study the effect of calcination temperature on the surface atomic chemistry of the calcined powders. This technique required a simple sample preparation where, the powders were formed into a compacted layer (>10 nm thickness) immobilised onto the foil which could then be mounted on carbon tape for analysis using Theta Probe instrument (Thermo Scientific, United States). The XPS spectrometer employed a monochromatic Al K α X-Ray source. Samples were dried completely under ambient conditions before analysis was performed. The XPS analysis was carried out by NEXUS (Newcastle University, United Kingdom). CasaXPS Processing Software was used to analyse the XPS spectrum obtained.

2.2.4.2. *XRD Analysis*

XRD was used to determine the crystallinity of powders after calcination, using the same method as described for the as-synthesized powders (section 2.2.2.1.).

2.2.4.3. *FTIR Spectroscopy*

FTIR spectroscopy was used to identify any changes in the mechanisms of carbonate and silicon ions substitution within the HA structure after calcination. The same method as describe for the as-synthesized powders (section 2.2.2.2.) was used.

2.2.4.4. *CHN Analysis*

The percentages of carbonate incorporated in the calcined powders were determined using CHN analysis using the same method for the as-synthesized powders (section 2.2.2.3.).

2.2.4.5. ICP-OES Measurement

The same technique as describe in section 2.2.2.4. was used to quantify the amount of Si presents in the calcined powders.

2.2.4.6. XRF Analysis

The Ca/ P ratio of the calcined powders was determined using the using the same method as described for the as-synthesized powders (section 2.2.2.5.).

2.2.4.7. Transmission Electron Microscopy

Philip CM100 Transmission Electron Microscope (TEM) was used to examine the morphology of the as-calcined powders in terms of their particle size and shape. Prior imaging the samples, 0.1 mg of powders were suspended in pure water and sonicated for ten minutes to allow the powders to be well dispersed. A drop of the suspension was then carefully placed onto a copper grid (diameter= 3.05 μm , mesh= 400) and allowed to dry. Samples were imaged at a magnification of 130 kX at HV= 100.0kV.

2.2.5. Cell Characterization

Human bone marrow-derived mesenchymal stem cells (hMSCs) used were obtained from Lonza (United States). The cells used were obtained from a 24 years old male donor. hMSCs were characterized upon isolation by evaluating their multi-lineage differentiation (section 2.2.5.1.-2.2.5.2.) and the expression of key cell CD surface markers, which were quantified qualitatively using immunostaining (section 2.2.5.3) and quantitatively by flow cytometry (section 2.2.5.4.). The same batch of cells was used for the characterization of hMSCs (section 2.2.5.1.- 2.2.5.4.).

2.2.5.1. *Multi-lineage Differentiation of hMSCs*

The ability of hMSCs to adhere to the tissue culture plastic and undergo differentiation into osteocytes, chondrocytes and adipocytes was investigated by histological staining for Osteogenic (Alizarin Red; section 2.2.5.2.1.), Chondrogenic (Alcian Blue; section 2.2.5.2.2.) and Adipogenic (Oil Red O; section 2.2.5.2.3) lineages. Cells were seeded at a density of 2.5×10^3 cells/cm² ($n=3$) and cultured in the relevant differentiation media as shown in Table 2.3. Cells cultured in proliferation media acted as the experimental controls. Cells were cultured for 21 days. Media was changed every three days. For histological staining, cells were fixed after 21 days. In order to characterize the osteogenic and chondrogenic samples, cells were fixed with 95% methanol (Fisher Scientific, United Kingdom) for 15 minutes. While, for adipogenic samples, cells were fixed in 4% formalin (Sigma-Aldrich, United Kingdom).

Table 2.3: Relevant proliferation and differentiation media compositions used in this study.

Reagent	Quantity
Proliferation media	
4.5g/L Dulbecco's Modified Eagle Medium, DMEM (Lonza, United Kingdom)	500 mL
L-glutamine (Lonza, United Kingdom)	1% v/v
Penicilin-Streptomycin (Lonza, United Kingdom)	1% v/v
Fetal Bovine Serum (Biosera labtech, United Kingdom)	10% v/v
Osteogenic media	
4.5g/L Dulbecco's Modified Eagle Medium, DMEM (Lonza, United Kingdom)	500 mL
L-glutamine (Lonza, United Kingdom)	1% v/v
Penicilin-Streptomycin (Lonza, United Kingdom)	1% v/v
Fetal Bovine Serum (Biosera labtech, United Kingdom)	10% v/v
Dexamethasone (Sigma-Aldrich, United Kingdom)	0.1 μ M
Ascorbic Acid (Analar, United Kingdom)	50 μ M
β -Glycerophosphate (Sigma-Aldrich, United Kingdom)	50 mM
Chondrogenic media	
DMEM-F12 (Lonza, United Kingdom)	500 mL
L-glutamine (Lonza, United Kingdom)	1% v/v
Penicilin-Streptomycin (Lonza, United Kingdom)	1% v/v
Fetal Bovine Serum (Biosera labtech, United Kingdom)	1% v/v
Insulin Transferin, ITS (Sigma-Aldrich, United Kingdom)	1% v/v
Dexamethasone (Sigma-Aldrich, United Kingdom)	0.1 μ M
Ascorbic Acid (Analar, United Kingdom)	50 μ M
L-proline (Sigma-Aldrich, United Kingdom)	40 μ g/mL
Sodium pyruvate (Sigma-Aldrich, United Kingdom)	1% v/v
Transforming growth factor- beta 3, TGF- β 3 (Peprotech, United Kingdom)	10 ng/mL
Adipogenic media	
4.5g/L Dulbecco's Modified Eagle Medium, DMEM (Lonza, United Kingdom)	500 mL
L-glutamine (Lonza, United Kingdom)	1% v/v
Penicilin-Streptomycin (Lonza, United Kingdom)	1% v/v
Fetal Bovine Serum (Biosera labtech, United Kingdom)	10% v/v
3-Isobutyl-1-methylanthine, IBMX (Sigma-Aldrich, United Kingdom)	0.5mM
Dexamethasone (Sigma-Aldrich, United Kingdom)	0.5 μ M
Insulin (Sigma-Aldrich, United Kingdom)	10 μ g/mL
Indomethacin (Sigma-Aldrich, United Kingdom)	100 μ M

2.2.5.2. *Histological Staining*

2.2.5.2.1. *Alizarin Red*

The osteogenic differentiation of hMSCs was confirmed by Alizarin Red (Sigma-Aldrich, United Kingdom) staining. Prior to staining, Alizarin Red solution was prepared at 1% in dH₂O and syringe filtered using a 2 µm filter. The pH of the solution was kept at pH 4. Samples were washed in Phosphate Buffer Saline, PBS (Sigma-Aldrich, United Kingdom) and stained with Alizarin Red solution for 5 minutes at room temperature. The stain was removed and washed three times in dH₂O. Calcium depositions were stained red (positive) and imaged using a bright field microscope AMG-EVOS X1 CORE at magnification of 10X. Results are demonstrated in the Appendix (Fig. A2).

2.2.5.2.2. *Alcian Blue*

Alcian Blue stain (Sigma-Aldrich, United Kingdom) was used as to characterize the chondrogenic differentiation. The stain was prepared at pH 1.5 using 3% acetic acid made using dH₂O and syringe filtered (2 µm filter). Samples were washed in PBS and stained with Alcian Blue solution for overnight at room temperature. The stain was removed and samples were washed three times in dH₂O. Blue staining of matrix indicated a positive result for the presence of GAGs secreted by chondrocytes. Samples were imaged using a bright field microscope AMG-EVOS X1 CORE at magnification of 10X. Results are shown in the Appendix (Fig. A2).

2.2.5.2.3. *Oil Red O*

Adipogenic differentiation was characterised using Oil Red O (Sigma-Aldrich, United Kingdom) prepared in 60% Isopropanol (IPA) and syringe filtered using 2 µm filter. After fixation, formalin was completely removed and the cells were washed twice with dH₂O followed by 60% IPA for five minutes at room temperature. The prepared staining solution was then added into the well and allowed to stain for 15 minutes at room temperature.

Upon removal of the staining solution, samples were washed three times in dH₂O. Lipid formation as a result of differentiated hMSCs into adipocytes appeared as small red droplets. Samples were imaged using a bright field microscope AMG-EVOS X1 CORE at magnification of 10X. Results are presented in the Appendix (Fig. A2).

2.2.5.3. *Immunostaining of hMSCs surface markers*

hMSCs at passage two (P2) were seeded at a density approximately 5000/cm² and cultured in standard basal media until 80-90% confluency prior to immunophenotyping. Once the cells reached about 80-90% confluency, the cells were washed with PBS and fixed with ice cold 90% methanol for 10 minutes. The cells were washed once again with PBS. In order to block non-specific antibody binding, 2% Bovine Serum Albumin, BSA (Fisher Scientific, United States) in PBS was added to each well and allowed to stand for 1 hour at room temperature. After 1 hour had elapsed each well was washed twice with PBS and cells were characterized using human MSCs characterization kit, which contained anti-human mouse anti-CD73, anti-CD90, and anti-CD105 (BD Bioscience, United Kingdom). IgG1 and IgG2a were used as the assorted isotypes and negative controls consisted of CD14, CD20, CD34 and CD45 (Immunotools, Germany). The fluorophores associated for each isotype is in red. The following CD markers and isotype controls were used at the described concentrations in 2% BSA/PBS; CD73 (1:20), CD90 (1:200) and CD105 (1:50), CD14 (1:50), CD19 (1:50), CD34 (1:100), CD31 (1:50), CD45 (1:200), CD105 (1:50). Isotype control antibodies include IgG1 (1:50) and IgG2a (1:50). Propidium iodide staining to detect dead cells was not included. Cells were then incubated at 4°C on a shaker overnight. Cells were washed with PBS, counterstained with DAPI and washed again in PBS. A UV fluorescent microscope (Nikon Eclipse Ti-ST, Japan) was used to image the cells once the staining was completed. Results are demonstrated in the Appendix (Fig. A3).

2.2.5.4. *Flow cytometry*

The cell CD surface markers were evaluated using Fluorescence-Activated Cell Sorting (FACS; FACS can flow cytometer (Becton Dickinson, UK)). hMSCs at passage two (P2) were expanded to 80-90% confluence, trypsinised, and re-suspended at a cell density of 1×10^6 cells/mL in PBS supplemented with 10% Human IgG (Flebogamma, United Kingdom). Cells were incubated for 1 hour at 4°C, then centrifuged at 400 g to form a cell pellet; the supernatant was discarded. Cells were then re-suspended in 2% BSA/ PBS solution resulting in a cell density of 1×10^6 /mL and dispensed at a at a cell density of 1.68×10^4 cells per 5 mL in Falcon tube. The directly conjugated antibody or the respective isotype control (same as those used in immunostaining) was then re-suspended in 2% BSA/PBS and added to cells for 30 minutes at 4°C with gentle agitation. Cells were centrifuged twice at 400 g for 5 minutes before being re-suspended in a final volume of 200 μ L of 2% BSA/PBS to be analysed.

Fluorescein isothiocyanate (FITC) fluorescence was detected using FL-1 channel, while, FL-2 channel was used to detect R-phycoerythrin (R-PE). FITC has the maximum absorbance and maximum emission at 565 nm and 578 nm, respectively. R-PE has maximum absorbance at 490 and 565 nm and maximum emission at 578 nm. Excitation was achieved at 488 nm with an Argon laser. Data gated to exclude dead cells and select the required cell population on the basis of forward scatter versus side profiles. Mean fluorescence intensity (MFI) and percentage positive cells were measured. Data were collected and displayed in dot plot and histogram format using CellQuestPro software (Becton Dickinson, United Kingdom). Results are demonstrated in the Appendix (Fig. A4).

2.2.6. *In vitro* biocompatibility assessment

International Organization for Standardization (ISO) 10993-5: Biological Evaluation of Medical Devices, Part 5: Tests for Cytotoxicity, was adapted and used as guideline in this study. This test involved the study on the cell viability, proliferation, metabolic activity and early osteogenic differentiation of hMSCs in direct contact with the investigated samples.

2.2.6.1. *Sample Preparation*

As all samples tested were in powder form, aliquots of 0.05 g of the calcined powders were sterilized in 1.0 mL of 70% industrial methylated spirit (IMS) for three hours followed by rinsing twice with PBS.

2.2.6.2. *Cell culture and seeding*

Human bone marrow derived-mesenchymal stem cells (hMSCs) obtained from a 24-year old male (Lonza, United States) were expanded until passage two when the required cell number was obtained. Cells were cultured in the proliferation media (PM) with composition as shown in Table 2.3 followed by, incubation at humidified environment at 37°C with 5% CO₂. hMSCs at passage 3 were seeded at 5x10⁴ into 24 well plates. Cells were allowed to adhere for three hours before 0.05 g of the powders were added into the well. Osteogenic media (OM) was used after the addition of powders and culture media was replenished every three days for 21 days. In all cases, tissue culture plastic alone cultured in OM acts as the positive control. At 7, 14 and 21 days, cells were rinsed with PBS, trypsinized, washed again with PBS and finally samples were lysed in 1mL of dH₂O followed by being frozen at -80°C.

2.2.6.3. Cell viability

The cell viability was observed using Confocal Laser Scanning Microscope (CLSM) Olympus Fluoview FV 1200 with Fluoview Version 4.1 software (Olympus, UK). The viability of the cells was assessed at 7, 14 and 21 days using the Live/Dead Assay Kit (Invitrogen, United Kingdom) according to the manufacturer's instructions. Calcein-AM ester was used to fluorescently label viable cells (green); the nucleus of dead cells is labelled with Propidium Iodide (red). Briefly, cell culture media was removed from samples. They were washed with PBS then immersed in a PBS staining solution containing 10 μ M Calcein-AM and 1 μ M Propidium Iodide and incubated at 37°C for 20 minutes in the dark. The samples were then washed once with 1.0 mL of PBS and immediately imaged using CLSM.

2.2.6.4. Cells activity and proliferation

The Quant-iT™ Picogreen® dsDNA assay kit (Invitrogen, United Kingdom) was used according to the manufacturer's instruction. The Picogreen solution was prepared as 1: 200 dilutions in 1 X Tris-EDTA (TE) buffer. Ranges of DNA dilutions (0-2 μ g/mL) were used to construct a standard curve. 100 μ L of cell lysate or DNA standard was placed each well of a 96 well plate, followed by 100 μ L of Picogreen reagent to each well. This was placed in the dark for 5 minutes before reading the fluorescence at 485/535 nm (excitation/emission) using Synergy II BioTek plate reader.

Alkaline phosphatase (ALP) activity was obtained from a 4-Methylumbelliferyl phosphate, 4-MUP (Sigma-Aldrich, United Kingdom) reaction. Ranges of 4-Methylumbelliferone, 4-MU (Sigma-Aldrich, Switzerland) dilutions (0-2 μ g/mL) were used to construct a standard curve. 50 μ L of the cell lysate from each sample or standard of 4-MU and 50 μ L of 4-MUP was then added into the relevant well of 96 well plate to this followed by incubation at

37°C for 90 minutes. To terminate the reaction, 100 µL of 1 X TE was added and the reading of the fluorescence was taken at 360/440 nm (excitation/emission) using Synergy II BioTek plate reader.

2.2.6.5. *Cells metabolism*

The levels of total protein were quantified using Bradford reagent (Sigma-Aldrich, United Kingdom). Ranges of protein standard solutions (0-2 mg/ mL) were prepared by dissolving Bovine Serum Albumin, BSA (Sigma-Aldrich, United Kingdom) in distilled water. For total protein assay, 50 µL samples or standards were placed in each well of 96 well plates, followed by addition of 50 µL of Bradford reagent. Samples were incubated for 5 minutes at room temperature before reading the absorbance level at 595 nm using Synergy II BioTek plate reader.

Alamar Blue (Sigma-Aldrich, United Kingdom) reduction was measured after every time-points to determine the cell metabolic activity. The cells were washed with PBS and stained with Alamar Blue reagent, which was prepared as 1: 10 dilution of stock (prepared by the manufacturer) in DMEM. The samples were incubated at 37°C for three hours in dark environment. Subsequently, 100 µL of the supernatant was transferred into a 96 well culture plates and fluorescence readings were taken at 530/590 nm (excitation/emission) using Synergy II BioTek plate reader.

2.2.6.6. *Statistical analysis for different powders group*

Quantitative data were presented as means ± standard deviation (SD). Data were initially tested for normality using the Kolmogorov-Smirnov test, with Dallal-Wilkinson-Lillie for corrected P value (recommended for small *n* data analysis). To determine any differences between powders group at each time point, a two-way ANOVA with multiple comparisons Tukey test was performed. Statistical significance was considered for $p \leq 0.05$ (*), $p \leq 0.01$

(**), $p \leq 0.001$ (***) and $p \leq 0.0001$ (****). For biochemical assays, tests were performed on $n=3$ in duplicate. All statistical analyses were performed using GraphPad Prism 7 software. No statistical test was performed on the confocal analysis, $n=1$ was used for imaging.

2.3. Polyelectrolyte multilayer assemblies using two-dimensional Poly (lactic acid) films to enhance cell-material interaction.

These sections described the construction of multilayer depositions on two-dimensional (2D) poly (lactic acid) (PLA) films using the innovative coating materials assembly established in this study. The numbers of bilayers depositions were then optimized by the physical and chemical characterizations followed by *in vitro* biocompatibility assessment using hMSCs.

2.3.1. Fabrication of PLA films

PLA resin was dissolved in 1, 4 Dioxane (Sigma-Aldrich, United Kingdom) (30 mg/mL) with magnetic stirrer at 70°C for three hours to obtain a homogenously dissolved solution. The viscous translucent solution was carefully poured to cast into a glass petri dish as to prevent any formation of bubbles. The glass culture dish was then covered with parafilm (small pores were created in the film to permit slow evaporation of the solvent) and left in the fume cupboard overnight providing a PLA film of 5 μm thickness. The film was removed from the petri dish and cut into 1 mm X 1 mm squares.

2.3.2. Surface modification of PLA films

The surface of the PLA films were modified by introducing amino functional groups through aminolysis, which has been described by previously Liu et al. (2010). Briefly, the PLA films were immersed in 0.1 M sodium hydroxide, NaOH (Sigma-Aldrich, United Kingdom) for 20 minutes and then rinsed in distilled water for 5 minutes. The films were

washed in 1:1 v/v of ethanol/water solution for 30 minutes and washed in distilled water for 5 minutes. Films were subsequently immersed in the solutions of 3 mg/mL of 1-ethyl-3-(3-dimethylaminopropyl) carbodiimide hydrochloride, EDC (ThermoFisher Scientific, United Kingdom) and 5 mg/mL of N-hydroxysulfosuccinimide sodium salt, NHS (Sigma-Aldrich, United Kingdom). Afterwards, the PLA films were transferred into a mixture of EDC/NHS solution (3 and 5 mg/mL respectively, pH 6.0) solution under constant shaking. The films were then washed with excess distilled water. Finally, the films were immersed in 10 mg/mL Poly (ethylene imine) solution, PEI (Sigma-Aldrich, United Kingdom) at pH 7.4 and stirred for 3 hours at 40°C followed by washing thoroughly in large amounts of distilled water for 15 minutes before left to dry for overnight.

2.3.3. Construction of multilayered PLA films

The multilayered PLA films were fabricated by Polyelectrolytes Multilayers (PEMs) technique modified from the process used by (Zhao et al. 2014). Prior to the layer-by-layer (LBL) assembly, the coating solutions were firstly prepared. 0.5 g of the optimum SiCHA powders were dispersed in 1.0 mg/mL hyaluronic acid (Lifecore Biomedical, United States) solution with the pH of the solution adjusted to pH 5.0, which served as the polyanions solution. The polycations solution was prepared by dispersing 1.0 g of the optimum SiCHA powders in 2.0 mg/mL Collagen type I (high concentration rat tails) (BD Bioscience, United Kingdom) and was kept constant at pH 5.0. In this study, we introduced a coupling agent to cross-link the LBL assembly in order to improve the chemical bonding between the polyanions and polycations. The coupling agent consists of 3 mg/mL EDC mixed with 5 mg/mL NHS solutions at pH 5.0. All solutions were adjusted to pH 5.0 using either 0.1 M HCl (Sigma-Aldrich, United Kingdom) or 1 M NaOH (Sigma-Aldrich, United Kingdom).

In brief, the aminolyzed PLA films that have a positive charged surface were firstly immersed into the polyanions solution for 15 minutes followed by rinsing in the ultrapure water (pH 5.0). After washing, the films were subsequently immersed into the polycations solution for 15 minutes. The films were then washed again in fresh ultrapure water (pH 5.0) to remove any unbound materials and prevent contamination of the polyelectrolytes solution. EDC/NHS solution was then introduced at the final step of each multilayer coating followed by washing in ultrapure water. These coating steps were repeated for three, five and ten multilayers as to optimize the number of coating layers. The coated films were then dried at room temperature for overnight.

2.3.4. Physical and chemical characterization

2.3.4.1. X-Ray Photoelectron Spectroscopy Analysis

The XPS analysis was carried out by NEXUS (Newcastle University, United Kingdom). XPS analysis is important tool to detect the elements present before and after coating. The films were analyzed using K-Alpha Instrument (Thermo Scientific, United States). This technique employed a monochromatic Al K α X-Ray source. Samples were dried completely under ambient conditions before analysis was performed. The relative atomic concentrations were determined using the built-in CASAXPS software. The elements of interest and their binding energies (BE) are listed in Table 2.4. At least 3 samples of each film were used for XPS analysis.

Table 2.4: Elements of interest and their binding energies on PLA films (Botelho et al. 2002; Li et al. 2008; Kim et al. 2010; Zhao et al. 2014).

Elements of interest	Binding Energy (BE, eV)
C1s	288.9
O1s	533.0
N1s	400.0
Ca2p	349.0
P2p	135.0
Si2p	101.0

2.3.4.2. Atomic Force Microscopy Analysis

The surface topography of the PLA films before and after coating with different number of multilayers was observed using atomic force microscopy (AFM) in the tapping mode using BioScope Catalyst AFM (Bruker, Germany) with ScanAsyst Adaptive Mode. The PLA films were imaged using an RTESPA tip of spring constant 4 N/m, 896 scans/lines, 0.32 Hz scan rates, and 1.102 V amplitude (Hoskins et al. 2012). The scan area was 1 mm X 1 mm squares. At least 3 samples were imaged to calculate the surface roughness for both whole and localized areas of the films. The term whole area refers to the entire scan area of 1mm²; localized areas means several spot areas of 1 nm² on the entire scan area.

2.3.4.3. Transmission Electron Microscopy Analysis

The uniformity of the SiCHA nanopowders distribution on the PLA films coated with different number of multilayers were observed using Transmission Electron Microscope (TEM, Philip CM100). Three samples with scan area 1 mm X 1 mm were used for TEM analysis ($n= 3$).

2.3.4.4. Semi-quantitative analysis of Calcium and Collagen distribution

The distribution of the coating materials on the PLA films were further characterized specific to the SiCHA nanopowders and Collagen type I. Alizarin Red (AR) was used to stain the Calcium deposition while Collagen type I was stained using Sirius Red (SR) solutions. Samples ($n=3$) were imaged using a bright field microscope AMG-EVOS x1 CORE with a magnification of 4X.

2.3.5. In vitro biocompatibility tests

Cytotoxicity test was performed on the PLA films coated with different number of multilayers. A protocol similar to that explained in section 2.2.6. was used in this study.

The cell donor (24 year old male) and passage number (P3) were kept constant throughout the experimental study.

2.3.5.1. Samples Preparation

Samples with an area of 1 mm X 1 mm squares were used for the *in vitro* biocompatibility test on different *n*-layers of the coating materials assembly deposited on the 2D PLA films. The bare (uncoated) and coated PLA films were sterilized for three times for 90 seconds in the Ultra Violet (UV) chamber before cell seeding.

2.3.5.2. Cell seeding

After cell counting, 0.5×10^5 of hMSCs (P3) were directly seeded on the surface of the PLA films and incubated for 3 hours at 37°C with 5% CO₂ and humidified atmosphere to allow cell attachment. Afterwards, 1.5 mL of complete proliferation media (PM) was added to each sample in wells of 24 well plates. Samples were cultured for 14 days. hMSCs on tissue culture plastic acted as the experimental control in comparison to the bare PLA, 1-, 3-, 5-, and 10 multilayers samples. Media was changed every three days.

2.3.5.3. Statistical analysis for different number of multilayers PLA films

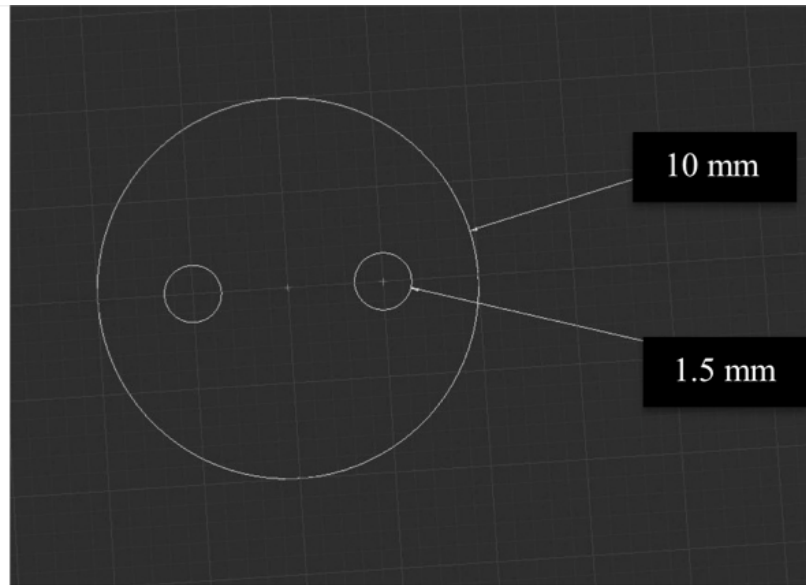
Quantitative data were presented as means \pm standard deviation (SD). Data were initially tested for normality using the Kolmogorov-Smirnov test, with Dallal-Wilkinson-Lillie for corrected P value (recommended for small *n* data analysis). A two-way ANOVA with multiple comparisons Tukey test were performed to optimize the number of multilayer depositions on the 2D PLA films. Statistical significance was considered for $p \leq 0.05$ (*), $p \leq 0.01$ (**), $p \leq 0.001$ (***) and $p \leq 0.0001$ (****). All statistical analyses were performed using GraphPad Prism 7 software. For biochemical assays, tests were performed on $n=3$ in duplicates.

2.3.6. Fabrication of three-dimensional scaffolds

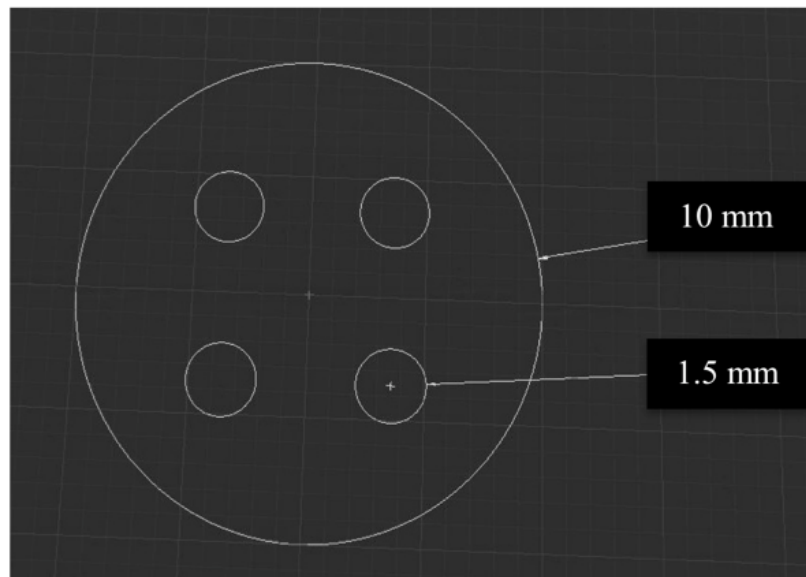
These sections demonstrated the fabrication of three-dimensional (3D) scaffolds by Rapid Prototyping (RP) technique. Different channel designs were incorporated in the scaffolds fabrication. The fabricated scaffold is referred as 3DP scaffolds in this study.

2.3.6.1. *Three-dimensional printing of Poly (lactic acid) scaffolds*

RP technique was used to engineer three different structural designs of the scaffolds namely four (4C), two channels (2C) and mesh scaffolds. The 3D scaffolds were fabricated via Fused Deposition Modelling method using Poly (lactic acid) resin (Product code: 4032 D) purchased from NatureWorks® LLC (United States). Scaffolds were printed using Ultimaker 2 from Ultimaker (United Kingdom). Prior printing, the scaffolds were firstly designed using Autodesk Inventor Professional 2014. The computer-aided design (CAD) drawings for 2- and 4 channel scaffolds are illustrated in Fig. 2.4. This is followed by optimization of the printing parameters (i.e. fill density, print speed and temperature) using the Cura software provided by Ultimaker. The scaffolds were then printed at the optimized speed of 40% (at 210°C) for the first four layers from bottom, slightly slower speed for the middle layers (5-14 layer from bottom), which was 25% (at 200°C) and finally the last five layers were printed at 40% (at 210°C). The fill density was kept constant for each layer at 75%. Fig. 2.5 (a-d) shows the printing steps at different layers in the construction of the 3D scaffolds.



(a)



(b)

Fig. 2.4: CAD drawings for (a) 2- and (b) 4 channel scaffolds designed in this study. The outer diameter of the scaffolds = 10 mm; channel diameter= 1.5mm and the thickness of the scaffolds= 2 mm.

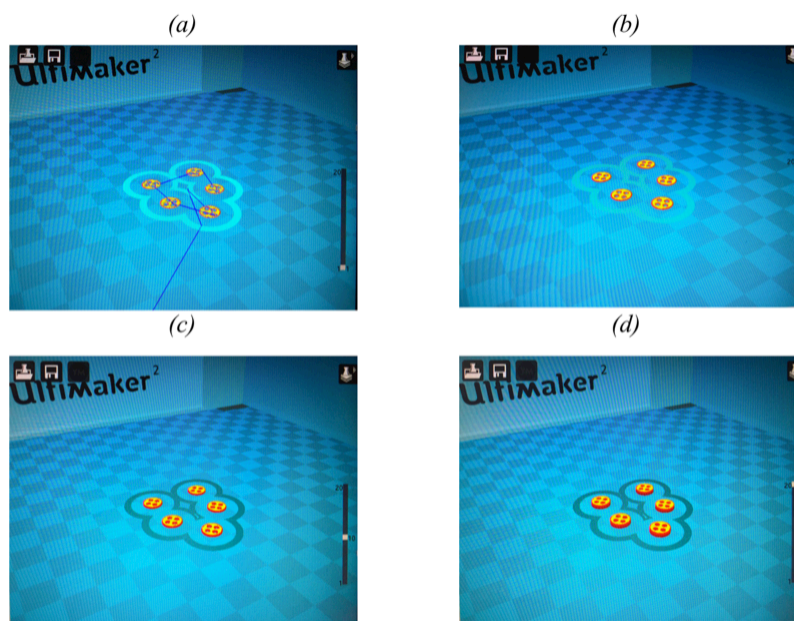


Fig. 2.5: Printing steps at different layers in the construction of the 3D scaffolds;
(a) First layer; (b) Fifth layer; (c) Tenth layer and (d) Final layer.

2.3.7. Fabrication of 3DP hybrid scaffolds

The fabricated scaffolds were then surface modified by a chemically route. In order to create the 3DP hybrid scaffolds, the printed scaffolds were deposited with the innovative coating materials assembly, which was established in this study.

2.3.7.1. *Surface modification of 3DP PLA scaffolds*

Similar steps described in section 2.3.2. were used to modify the surface charge of the 3DP PLA scaffolds.

2.3.7.2. *Scaffold assemblies with newly developed coating materials*

The 3DP PLA scaffolds were coated with 5 bilayers (5-BL) of the newly developed coating materials assembly of SiCHA nanopowders in hyaluronan and collagen type I. Mixture of EDC/NHS was used to crosslink the polyelectrolytes layers. Details on the coating procedure were described in section 2.3.3.

2.3.8. *In vitro* study on the 3DP hybrid scaffolds

The characterized hMSCs were used to study the effect of different structural and functional designs of the 3DP hybrid scaffolds on the cells fate *in vitro*, which can be divided into two main studies; (1) a bioreactor system was used to investigate the impact of dynamic flow on the cell behaviour compared to the static culture condition and (2) different culture medium was used to identify the effect of biochemical cues that could enhanced the bone formation.

2.3.8.1. *Seeding efficiency on 3DP scaffolds*

Coated hybrid scaffolds were firstly sterilized for three times in the UV Chamber for 90 seconds each cycle followed by pre-wetting in PM for three hours before cell seeding. Commercial hydroxyapatite (HA) scaffolds were used as control samples and scaffolds required longer soaking in PM (72 hours) as recommended by the manufacturer (Ceramisis, Sheffield, United Kingdom). Pre-wetting is a crucial step to improve the seeding efficiency by promoting a formation of thin layer of proteins which are required for cell adhesion to the scaffolds.

Scaffold seeding was carried out in 24 well plates coated and uncoated well plates. The coated well plate used was a 24 well plate coated with 1% w/v Pluronic F-127 (Sigma-Aldrich, United States), to prevent the cell from attached to the well plate. As control, the uncoated well plate (ordinary 24 well culture plate) was used. After cell counting, 1×10^5 cells were seeded onto each scaffold in the wells. To choose the right seeding method, cells were seeded by two ways i.e. (1) seeded the total amount of cells only one side; (2) seeded half of the amount on one side, incubate for 3 hours and repeat these steps on the other side before topping up with proliferation media. The cell volume suspensions were also optimized using two different volume suspensions namely, 20 and 40 μL . The cellular

scaffolds were then cultured for 6 hours at 37°C and 5% CO₂ in humidified atmosphere. Seeding efficiency was then calculated using the following formulation.

$$\text{Cell seeding efficiency (\%)} = \frac{n_i - n_f}{n_i} * 100$$

where, n_i is the cell number seeded and n_f is the cell number adhered to the scaffolds after 6 hours incubation at 37°C and 5% CO₂ in humidified atmosphere, respectively. The cell distributions throughout the scaffolds were indicated using MTT stain and live/dead staining.

2.3.8.2. Static versus rotary bioreactor cultivation

Optimized seeding conditions (small cell volume suspension $\leq 20 \mu\text{L}$, seeded in two-sided method in a coated well plate) were then applied in the following study. Briefly, after incubation overnight, the cellular scaffolds were then divided into two groups namely static and dynamic cultivation. A rotary bioreactor (Synthecon Inc., Cellon, Strassen, Luxembourg) was used to culture the cellular scaffolds in dynamic condition. The speed of the rotating bioreactor was firstly tested at two different speeds (20 and 40 rpm) and the speed that could allow the scaffolds to maintain in the free-fall condition throughout the cultivation period was chosen as the best speed (20 rpm) and used to study the effect of culture conditions on different scaffold designs. Two test groups were then established: half of the scaffolds were transferred to fresh 24 well plates and incubated statically after adding up 1.5 mL media to each well; the other half of the cellular scaffolds were directly transferred to the rotary bioreactor chambers containing 60 mL complete medium (either osteogenic or proliferation media). Both of the tested groups were then divided into two more groups of different culture medium used: (1) Osteogenic media (OM); and (2) Proliferation media (PM). Both media were prepared with the same compositions

described in Table 2.3. In order to identify the best structural design and functional 3DP hybrid scaffolds, *in vitro* assessments including cell viability, proliferation, metabolic activity and early osteogenic differentiation were performed following similar procedure as described in section 2.2.6.

2.3.8.3. Alkaline phosphatase staining

The pre-cursor of early bone mineralization was stained using alkaline phosphatase (ALP) detection kit purchased from Merck Milipore (United Kingdom). Scaffolds were transferred to fresh 24 well plates and rinsed once with PBS. Scaffolds were fixed in 4% Paraformaldehyde (Sigma-Aldrich, United Kingdom) for 90 seconds followed by washing in TBST solution (20 mM Tris-HCl, pH 7.40, 0.15 M NaCl, 0.05% Tween-20). The working solution was freshly prepared according to the manufacturer's instruction with 2:1:1 ratios of Fast Red Violet solution: Naphthol AS-BI phosphate solution: ddH₂O. To each well, 500 µL of the working solution was added and left in dark condition at room temperature for 30 minutes. Afterward, the scaffolds were carefully rinsed twice with distilled water. The stained scaffolds were imaged under dissection microscope (Leica, United Kingdom).

2.3.8.4. Lactate dehydrogenase Assay

Lactate dehydrogenase (LDH) assay is a reliable colorimetric assay to quantify the LDH release into the media from damaged cells as a biomarker for cellular cytotoxicity. LDH assay kit (Thermo Fisher, United Kingdom) was used according to the manufacturer's instruction. At every time-point, 50 µL of media from either the well or rotary chamber were transferred into a 96 well plate followed by incubation for 45 minutes at 37°C with 5% CO₂. Afterward, 50 µL of reaction mixture was added into the relevant well. Samples were incubated for 30 minutes in the dark at room temperature. Finally, 50 µL of stop solution was added to each well followed by mixing with gentle tapping. Absorbance

readings were taken at 530/590 nm (excitation/emission). LDH activity and percentage of cytotoxicity (%cytotoxicity) of each sample was calculated using the following equations:

$$\text{LDH Activity} = \text{Abs. value (490 nm)} - \text{Abs. value (680 nm)} \quad \dots \text{Equation 2.4}$$

$$\% \text{ Cytotoxicity} = \left(\frac{\text{Compound-treated LDH activity} - \text{Spontaneous LDH activity}}{\text{Maximum LDH activity} - \text{Spontaneous LDH activity}} \right) * 100 \dots \text{Equation 2.5}$$

2.3.8.5. *Micro-computed tomography analysis*

At every time-point, media was aspirated from the wells/chambers and scaffolds were rinsed with 1.0 mL PBS. Scaffolds were then fixed in 1.0 mL of 10% formalin (Sigma-Aldrich, United Kingdom) and kept at 4°C for overnight. X-ray micro-computed tomography, Micro-CT (microCT40 Scanco Medical GmbH, Switzerland) with beam energy of 55 kVp, beam intensity of 145 μ A, 200 ms integration time, and spatial resolution of 10 μ m was used to observe any sign of early formation of bone mineralization on the cellular scaffolds. Scaffolds were scanned and analyzed at threshold 40, 42, 55 and 120 for bare PLA 3DP scaffolds, coated scaffolds, cell-seeded scaffolds and bone mineralization, respectively. For control, acellular scaffolds were also scanned at the same thresholds. The total volume (TV) value was obtained at threshold 55, while bone volume (BV) value was generated at higher threshold of 120. The estimated percentage of bone mineralization (% BV/TV) was obtained by normalizing the values of BV at thresholds 120 over TV at threshold 55.

2.3.8.6. *Statistical analysis*

Quantitative data were presented as means \pm standard deviation (SD). A Kolmogorov-Smirnov test, with Dallal-Wilkinson-Lillie for corrected P value was performed to determine the normal distribution of the data (recommended for small n data analysis). A three-way ANOVA with multiple comparisons Tukey test was used to determine the

effects of culture conditions (static and dynamic) and culture medium (OM and PM) in the cell responses on different structural scaffold designs over time. A two-way ANOVA with multiple comparisons Tukey test was performed to define the best scaffold design after 21 days under different culture conditions and culture medium. Statistical significance was considered for $p \leq 0.05$ (*), $p \leq 0.01$ (**), $p \leq 0.001$ (***) and $p \leq 0.0001$ (****). For biochemical assays, tests were performed on $n=3$ in duplicates. All statistical analyses were performed using GraphPad Prism 7 software. No statistical analyses were performed for the confocal microscopy analysis ($n=1$), ALP staining ($n=3$), μ CT analysis ($n=3$).

2.4. Promoting pre-vascularization of the scaffolds

2.4.1. Scaffolds fabrication

Four channel (4C) scaffolds were used as this design demonstrated the highest percentage of mineralization among the three scaffold designs tested as demonstrated in Chapter 5. The surface modified 3DP scaffolds was coated using the similar PEMs technique described in section 2.3.3.

2.4.2. Sample preparation

The hybrid scaffolds were sterilized three times in the UV Chamber for 90 seconds at each cycle followed by pre-wetting in PM for three hours incubation prior to cell seeding. Samples were kept at 4°C during incubation.

2.4.3. Cell culture

Human umbilical vein endothelial cells, HUVECs (Life Technologies, United Kingdom) at passage three (P3) were cultured in complete Endothelial Media (EM) consists of Medium-200 with Low Serum Growth Supplement (LSGS) containing 2% v/v FBS, 1 μ g/mL hydrocortisone, 10 ng/mL human epidermal growth factor, 3 ng/mL basic fibroblast growth factor and 10 μ g/mL heparin. Both Medium-200 and LSGS kits were purchased

from Thermo-Fisher Scientific (United Kingdom). hMSCs (Lonza, United States) at same passage number (P3) was expanded in proliferation media. Both cell types were cultured in standard cell culture flasks incubated at 37°C with 5% CO₂ and 95% relative humidity for about 10 days till 80-90% confluent levels were achieved. Both HUVECs and hMSCs were expanded up to passage three (P3) and used for the study at passage four (P4).

2.4.4. Labelling with fluorescent dyes

Red fluorescent dye, PKH26 (Paul Karl Horan 26, Sigma-Aldrich, United Kingdom) was used to label the HUVECs, while hMSCs were labelled using the Cell Tracker Blue CMAC (7-amino-4-chloromethylcoumarin, Molecular Probes, Life Technologies, United States). The fluorescent dyes were used to allow morphological observations within the scaffolds as they clearly distinct the two cell types used in the co-culture particularly. Labelling was carried out according to the manufacturer's instructions with 4 µL/mL PKH26 (red dye) in Dilute C. Briefly, after cell counting, 2.0×10^6 cells were resuspended in complete media. The cell pellet obtained was then washed with serum-free media and resuspended in complete media; these steps were repeated for three times. After pelleting, 1.0 mL of Dilute C was added directly to the cell suspension and mixed well, subsequently 4 µL of red dye was then added to the cell solutions followed by incubation at 37°C for 10 minutes. To ensure the cells were properly labelled, the unbound dye was blocked using 1% BSA followed by incubation at room temperature for one minute. Cell solution was resuspended and subsequently washed three times with complete EM. To ease HUVECs proliferation, 1344 µL Matrigel from BD Bioscience (United States) was then added to the cell solution. This was then divided into two groups with each aliquot containing 1.2×10^6 and 0.6×10^6 cells for the HUVECs control and co-culture samples, respectively.

Similar procedure was used to label the hMSCs with CMAC (blue dye). The concentration of the blue dye used was 4 $\mu\text{L}/\text{mL}$ blue dye in serum-free media. For hMSCs, the cell solution was incubated at 37°C for 30 minutes after the blue dye was added. The cell solution was washed with PM three times. Finally, 2.0 mL of fresh OM was added into the cell solution and the total amount was divided into two groups with each aliquot containing 1.2×10^6 and 0.6×10^6 cells for the hMSCs control and co-culture samples, respectively.

2.4.5. Seeding of 4C scaffolds

For co-culture samples, 1:1 of HUVECs:hMSCs cell ratio was used based on the previous studies reported by Rouwkema et al. (2006) and Gershovich et al. (2013). The culture medium of 1:1 of endothelial media (EM) to osteogenic media (OM) was reported to support the proliferation of both cells (Rouwkema et al. 2006). The channels on the 4C scaffolds were directly seeded with 6.25×10^3 of HUVECs in 1.75 μL Matrigel per channel. Scaffolds were then incubated for 30 minutes at 37°C to enhance gelation of Matrigel. The scaffolds were then turned onto the opposing side, and the process repeated. The cellular scaffolds were cultured for 3 days in complete EM at 37°C with 5% CO_2 and 95% relative humidity prior to the addition of hMSCs (McFadden et al. 2013). Each side of the scaffold was seeded with 2.5×10^4 labelled hMSCs. Each side was subjected to 3 hours incubation to allow the hMSCs to adhere to the surface, followed by repeating the seeding procedure on the other side. The HUVECs-hMSCs seeded scaffolds were then cultured in 1:1 of EM:OM mixture. Figure 2.6 shows the seeding protocols for the co-culture. Control scaffolds were seeded with a single cell type, either HUVECs or hMSCs alone. Same seeding protocols were used. For ECs controls, 5×10^4 of labelled HUVECs were seeded in the channels and cultured in EM. While 5×10^4 of labelled hMSCs were seeded on the surface of the scaffolds and cultured in OM acting as the hMSCs control samples. Medium was refreshed every 3 days.

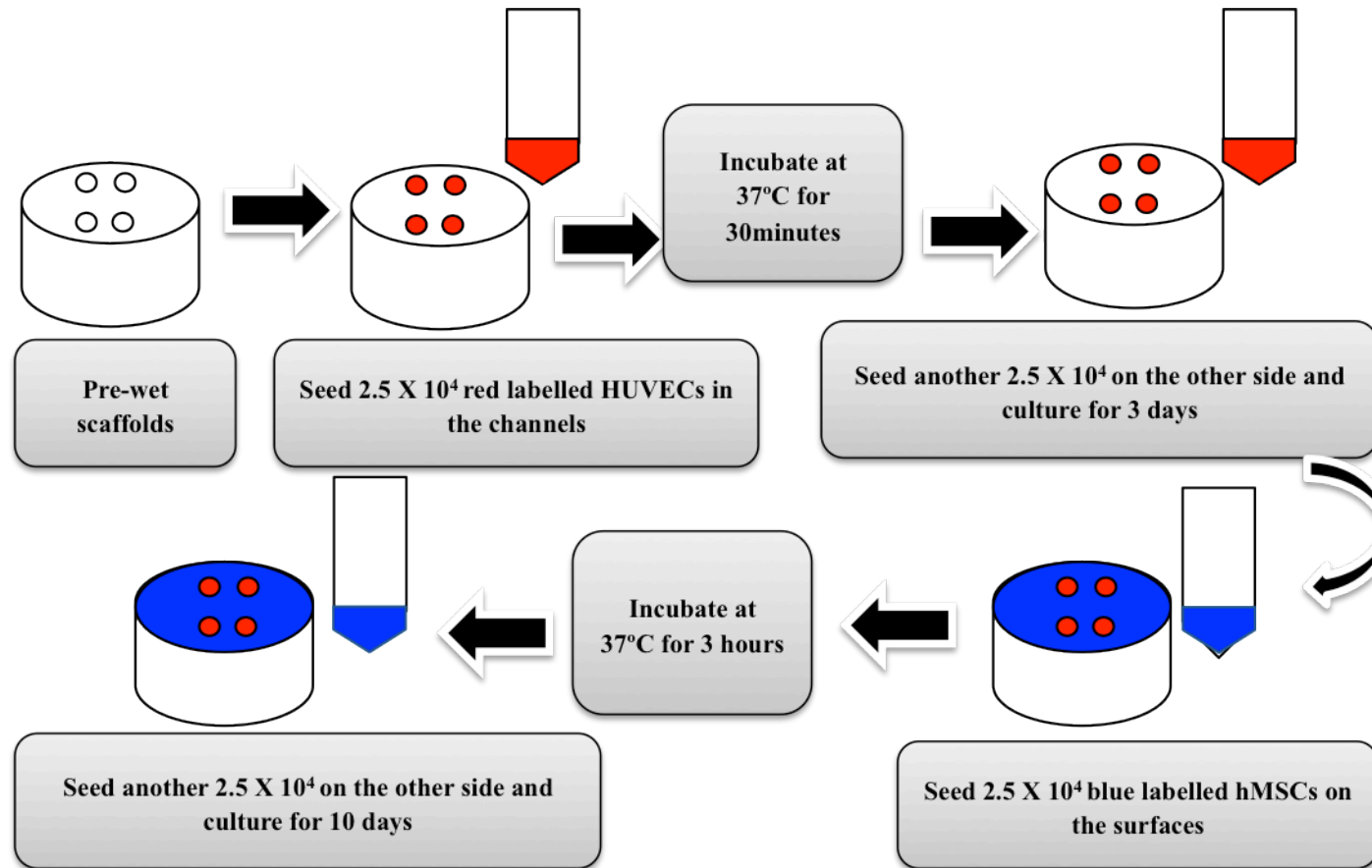


Figure 2.6: Illustration, summarising the seeding protocols for the co-culture of HUVECs/hMSCs on 4C scaffolds.

2.4.6. Imaging

Cell seeded scaffolds were imaged in 3D using a CLSM to identify the distribution of each cell type and to observe any vessel formation. Cultures were terminated after 3 and 10 days. At each time-point, the samples were washed once in PBS and fixed with 4% Paraformaldehyde, PFA (Sigma-Aldrich, United Kingdom). Samples were then imaged using a CLSM to observe cell migration across the scaffolds. Samples were kept at 4°C overnight prior to immunocytochemical staining of RUNX-2 and CD31 expressions. Quantification of the fluorescence signals was conducted on the 3D reconstruction of the confocal series using IMARIS (Bitplane, CH). Contour surfaces were generated in Surpass mode and the intensity sum was used to calculate the relative intensity of the fluorescence signals. Surpass mode was used to create the contour surfaces by segmenting the image based on colour and intensity. The contour surface allows the extraction of a 3D object by manually drawing the object contours on 2D slices focusing on specific details, i.e. by selecting the red fluorescent on the image. The IMARIS software will then automatically calculate the intensity of the specific dye selected.

2.4.6.1. *RUNX- 2 staining*

In this study, RUNX-2 was used to determine the early osteogenic makers. Fixed samples were washed twice in PBS. The cells were permeabilized in 0.1% Triton-X 100 (Sigma-Aldrich, United Kingdom) in PBS for 10 minutes followed by washing twice in PBS. Samples were blocked using 1% BSA for 1 hour at room temperature. Again, samples were washed twice in PBS. Primary antibody of Goat anti Human RUNX-2 (R&D System, United Kingdom) of 2 µg/mL diluted 1:1000 in 0.1% BSA, 0.1% Tween-20 in PBS was added to the samples and incubated at 4°C overnight. Samples were washed twice in PBS. Scaffolds were incubated in secondary antibody donkey- anti-goat Alexa Fluor 488 (R&D System, United Kingdom) diluted 1:200 in 0.1% BSA, 0.1% Tween-20 in PBS for 1 hour.

Finally, samples were washed twice in PBS and fresh PBS was then added to each well to prevent the samples from drying.

2.4.6.2. CD31 staining

Fixed samples were washed twice in PBS. Samples were incubated for 30 minutes in 10% FBS in PBS to prevent non-specific background staining. All PBS was removed and samples were then incubated for 1 hour with CD31 monoclonal mouse-anti-human primary antibody (DAKO, United Kingdom) diluted 1:20 in PBS. Samples were washed twice in PBS followed by incubation in goat-anti-mouse secondary antibody Alexa Fluor 488 (R&D System, United Kingdom) diluted 1:200 in PBS. Finally, samples were washed with PBS and imaged using a CLSM.

2.4.7. Enzyme linked immunosorbent assay for platelet derived growth factor-BB and vascular endothelial growth factor

The levels of platelet derived growth factor-BB (PDGF-BB) and vascular endothelial growth factor (VEGF) were quantified using enzyme linked immunosorbent assay (ELISA) kits purchased from R&D Systems (United Kingdom). The cell culture media of HUVECs alone, hMSCs alone and co-culture of HUVECs/hMSCs were collected at day 3 and 10 of culture. The culture medium (without cells) of EM, OM and mix media of EM:OM were used as the experimental control for both immunoassays. Assays were performed according to the technical datasheet provided by the manufacturer and the absorbance of each sample was read at 450 nm. Assays were performed in duplicates for three samples ($n=6$) and the mean \pm SD.

2.4.8. Statistical analysis

Quantitative data were presented as means \pm standard deviation (SD). Data were initially tested for normality using the Kolmogorov-Smirnov test, with Dallal-Wilkinson-Lillie for corrected P value (recommended for small n data analysis). To compare the level of PDGF and VEGF expressions secreted by the co-culture and their monoculture systems at each time point, a two-way ANOVA with multiple comparisons Tukey test was performed. Statistical significance was considered for $p \leq 0.05$ (*), $p \leq 0.01$ (**), $p \leq 0.001$ (***) and $p \leq 0.0001$ (****). Tests were performed on $n=3$ in duplicates. All statistical analyses were performed using GraphPad Prism 7 software. No statistical tests were performed on the immunocytochemical staining and relative fluorescent intensity, $n=3$ were used for each sample for every time-point.

Chapter 3

Production of multi-substituted Hydroxyapatite nanopowders for Bone Tissue Engineering Applications

3.1. Introduction

Hydroxyapatite (HA) is among the most widely used bone replacement materials due to its strong affinity with the mineral component of bones; it possesses good bioactivity, osteoconductivity and biocompatibility with the human bone tissue (Sprio et al. 2008; David et al. 2013). Although, stoichiometric Hydroxyapatite (HA) - $\text{Ca}_{10}(\text{PO}_4)_6(\text{OH})_2$ has been a widely used model for the apatite present in the bone tissues for many years, the chemical composition of biological apatites differs from the stoichiometric HA (Landi et al. 2010). The biological apatites are uniquely similar in that they all comprise carbonate in varying amounts of 2-8wt%, preferentially substituting the phosphate site (B-type) compared with hydroxyl (A-type) ions in the apatite lattice. The composition of carbonate depends on bone age, site, sex and health of the individual (Driessens et al. 1983; Gibson & Bonfield 2001; Landi et al. 2010; Boyer et al. 2013). Among other trace elements present in natural bone, silicon (Si) plays an important role in stimulating bone growth and development (Hing et al. 2006; Landi et al. 2010).

The development of multi-substituted HA powders with a fully controlled level of ionic substitutions into the HA lattice and high similarity to bone mineral, is of great interest to achieve the “gold standard” represented by the natural bone. For this reason, researchers have now focussed on the production of multi-substituted HA for instance, silicon carbonated hydroxyapatites (SiCHA). The adequate solubility of CHA and the benefits of soluble silicon could be combined in order to improve the bioactivity of the apatite bioceramics (Boyer et al. 2013). Thus, SiCHA has great potential as a biomedical material for promising approach toward achieving the “gold standard”.

Several studies on the development of multi-substituted HA powders has been reported in the literature. However, limited studies have investigated the effect of ionic substitutions in

the HA lattice on the cell responses. Many research groups focus on the different synthesis techniques used to produce the powders, various physico-chemical characterizations and some solubility tests in simulated body fluid (SBF) to predict the ability to form apatite layer *in vitro* (Sprio et al. 2008; Zhou et al. 2008; Bianco et al. 2009; Boanini et al. 2010; Marchat et al. 2013). A number of studies on human osteoclast differentiation and resorption on CHA and SiHA has also been reported in the literature. For instance, the osteoclastogenesis on CHA was significantly enhanced compared to HA and β -tricalcium phosphate (Nakamura et al. 2013). On sintered ceramics, no significant differences were found in the osteoclast numbers on HA and SiHA after 21 days *in vitro*, but actin ring sealing zone morphology on SiHA resembled that commonly found on bone or CHA (Friederichs et al. 2015). These findings highlighted the benefits of CHA and SiHA in stimulating better cell responses compared to HA alone. As the production of multi-substituted HA is aimed for BTE, it is extremely important to understand the cell behaviour in particular osteogenic cells as they become in contact with the powders. For this reason, Landi et al. (2010) has looked at the human osteoblasts behaviour on as-synthesized CHA and different compositions of SiCHA powders. The aim of the work presented in this chapter was to develop multi-substituted hydroxyapatite (SiCHA) powders with controlled amounts of carbonate (2-8 wt%) and silicon (0.03-0.5 wt%) substituted into the apatite structure to closely mimic the range of compositions observed within bone mineral as demonstrated in Table 1.1 (Sprio et al. 2008; Landi et al. 2010). Different compositions of as-synthesized powders as a mean to optimize the level of ionic substitutions, followed by the calcination process to obtain pure SiCHA powders were investigated. In order to meet the main aim in developing biomedical materials, the produced powders were tested *in vitro* with human bone marrow-derived mesenchymal stem cells (hMSCs).

3.2. Results

3.2.1. Optimization of carbonate and silicon ions contents

3.2.1.1. XRD Analysis

The as-synthesized powders were found to be nanocrystalline as evidenced from broad diffraction peaks. The XRD pattern of the pure hydroxyapatite (HA) reported in International Centre of Diffraction Database (ICDD) with file number of 09-0432 was used as the reference pattern as the patterns are similar with only a slight shift of the peaks position due to the ion substitutions. The amount of carbonate substituted into the HA lattice is less than 10%, and so is unlikely to affect the structural pattern of HA.

Samples containing 0.5, 1.0 and 2.0CHA demonstrated that only a single phase HA pattern was present. No secondary phases such as CaCO_3 or CaO were found, as shown in Fig. 3.1. The peak of (112) at $2\theta = 32^\circ$, which usually appears in pure HA, was not detected in the XRD pattern of any samples. There were eight main peaks detected; $2\theta = 26^\circ$ which was indexed to (002), $2\theta = 32-34^\circ$, which represent three overlapped peaks of (211), (300) and (202), $2\theta = 39.8^\circ$ indexed to (310), $2\theta = 49.4^\circ$ for (222), $2\theta = 50$ and 53° indexed to (213) and (004), respectively. The presence of CaCO_3 was detected at $2\theta = 29.4, 35.9$ and 43.2 for 3.0 and 4.0CHA with high carbonate contents.

For SiHA as-synthesized powders, the only diffraction peak detected was closely related to HA characterized patterns (ICDD: 09-0432) as shown in Fig. 3.2. The incorporation of Si ions into the HA lattice had no significant effect on its crystallographic structure or crystallinity.

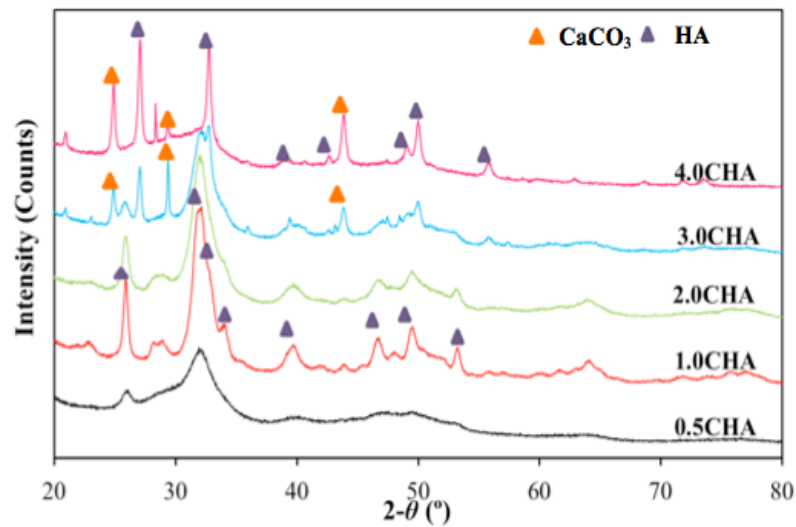


Fig. 3.1: XRD pattern of the CHA as-synthesized powders with different carbonate contents. At low carbonate contents (0.5-2.0CHA), only pure single HA phase detected. As the carbonate content increased, secondary phase of calcium carbonate (CaCO_3) was found besides the HA phase.

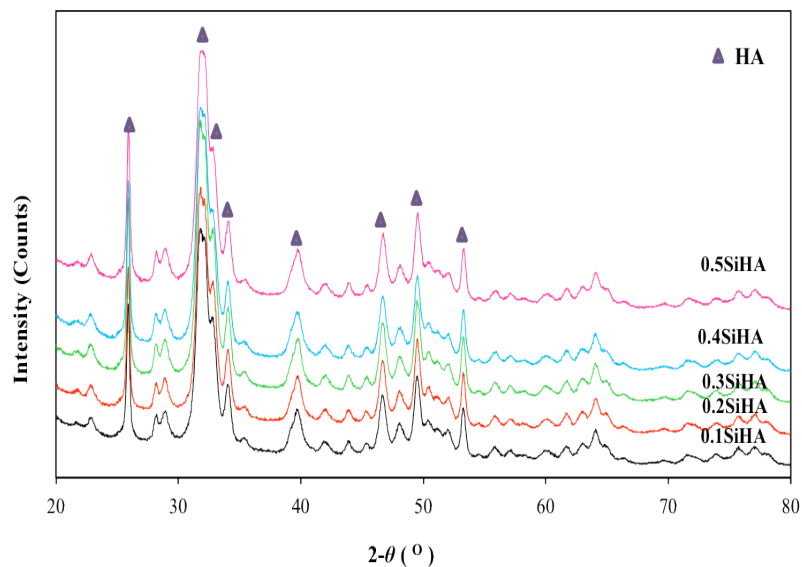


Fig. 3.2: XRD pattern of the SiHA as-synthesized powders with different silicon contents. Only pure single phase of HA was revealed. The diffraction patterns getting marginally broader as more silicon enter the apatite structure.

It is widely accepted that the ionic substitutions in the HA lattice cause changes of lattice parameters. However, in this study, the effect of carbonate (CO_3^{2-}) and silicon (Si) substitutions into the HA structure were less apparent on the XRD spectra. The lattice parameters (a - and c - axis) and crystallite sizes of CHA and SiHA as-synthesized powders were refined by Rietveld and the values obtained are presented in Table 3.1.

Table 3.1: Lattice parameters and crystallite sizes of CHA and SiHA as-synthesized powders.

Samples	Lattice parameters (Å)		Crystallite size (nm)
	$a \pm 0.003$	$c \pm 0.003$	
0.5CHA	9.415	6.891	19.86
1.0CHA	9.411	6.895	18.25
2.0CHA	9.409	6.902	16.95
3.0CHA	9.406	6.907	16.21
4.0CHA	9.401	6.909	15.87
0.1SiHA	9.420	6.889	20.29
0.2SiHA	9.425	6.893	22.09
0.3SiHA	9.437	6.906	22.82
0.4SiHA	9.439	6.912	23.59
0.5SiHA	9.442	6.915	24.93

From the refinement analysis, it is clearly seen that the substitution of CO_3^{2-} and Si into the HA structure resulted in distinct effects on the lattice parameters and crystallite size. A contraction in a -axis and expansion in c -axis was observed when CO_3^{2-} substituted PO_4^{3-} in the apatite structure. The crystallite size of CHA nanopowders gradually decreased with increasing CO_3^{2-} content. In contrast, Si-substituted HA structure caused increases in both a - and c -axes as well as the crystallite size of SiHA nanopowders.

3.2.1.2. FTIR Analysis

The FTIR analysis of the CHA powders in Fig. 3.3 clearly demonstrated typical peaks of B-Type CHA with the bands originating from stretching vibrations of CO_3^{2-} ions at 870-875, 1410-1430, and 1450-1470 cm^{-1} . These data confirmed that the as-synthesized CHA powders were B-Type CHA. The bands at about 550-570 (ν_4), and 960-966 cm^{-1} (ν_1), which correspond to the phosphate group as reported by Krajewski et al. (2002); Blakeslee et al. (2006); and Kovaleva et al. (2008) were also detected. The broad bands around 1600-1700 cm^{-1} and 3200-3600 cm^{-1} are attributed to the presence of adsorbed and occluded water. This is also reported by Liu et al. (2003) and Wang et al. (2006). However, the CaCO_3 phase as detected in XRD was not detected in the FTIR spectra. No calcite band was observed at 712 cm^{-1} due to the small amount present (Krajewski et al. 2002). Fig. 3.4 illustrated the FTIR spectra of the as-synthesized SiHA powders. All of the spectra represent the characteristic transmittance bands correspond to HA with an additional band of Si in SiHA band detected at about 880-895 and 947 cm^{-1} . The triple intense bands at 963, 1036 and 1090 cm^{-1} corresponds to the stretching vibration modes of phosphate were also detected. IR spectra of the SiHA powders revealed the broad band at about 1600-1700 cm^{-1} corresponds to the adsorbed water on the surface (Tang et al. 2005).

Higher silicon content substituted the apatite structure resulted in significantly narrower phosphate group (the triplet bands). There was also a missing band of one of the hydroxyl groups at 3500-3700 cm^{-1} , which is in agreement with the work reported by Tang et al. (2005).

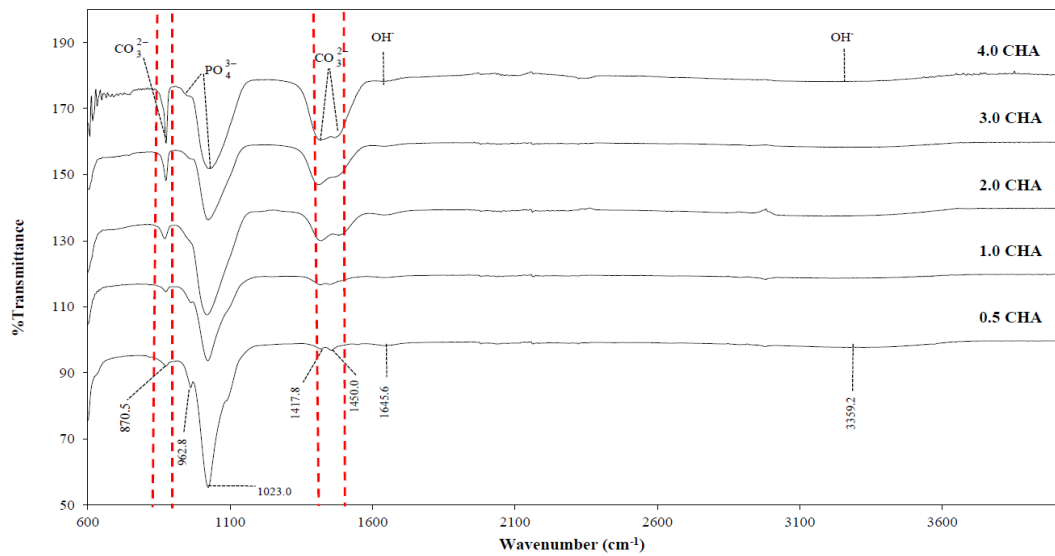


Fig. 3.3: FTIR spectra of CHA as-synthesized powders. The typical peaks of B-type CHA were detected at 870-875, 1410-1430, and 1450-1470 cm^{-1} . Calcium carbonate peak at 712 cm^{-1} was not appeared in the spectra. This confirmed that the as-synthesized powders are pure B-type CHA.

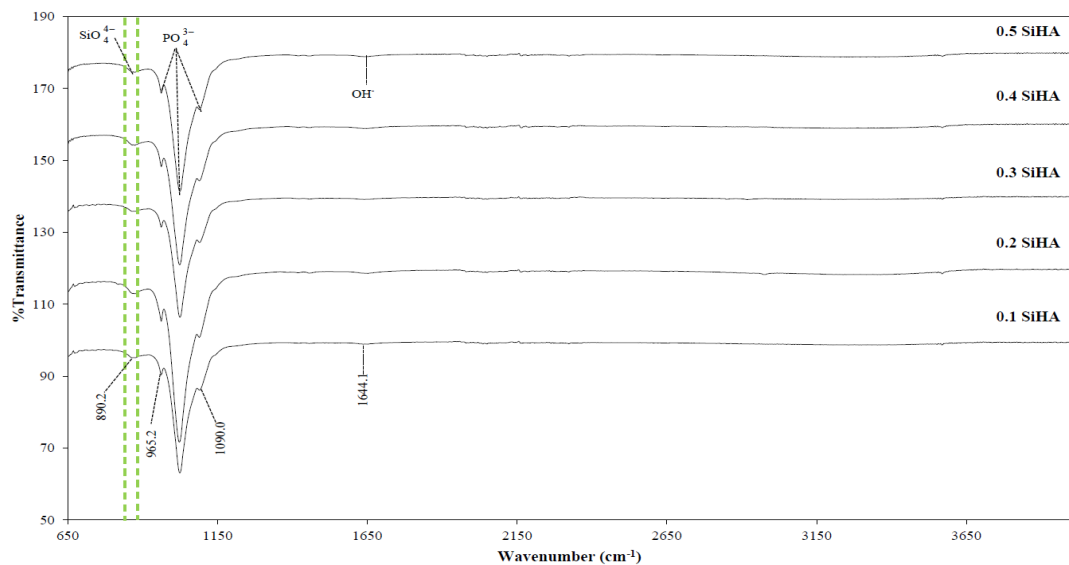


Fig. 3.4: FTIR spectra of SiHA as-synthesized powders. The spectra of the as-synthesized SiHA powders showed at various Si contents showed the present of Si in SiHA structure with the band detected at 880-895 and 947 cm^{-1} .

3.2.1.3. *Quantification of carbonate and silicon substituted apatite structure*

The percentage of carbonate present in the apatite structure increased with increasing carbonate molar content. It is observed that, for 0.5CHA and 1.0CHA, the percentages of carbonate detected were relatively low, which were less than 5wt%. While, 3.0CHA and 4.0CHA have extremely high carbonate contents. 2.0CHA shows the optimum composition of carbonate, which falls in the range of carbonate presents in the natural bone as represented in Table 3.2. All as-synthesized SiHA powders revealed negligible amount of carbonate incorporated in the apatite structure.

The Ca/P+Si ratio for every sample of as-synthesized SiHA powders was determined from the ICP-OES measurements. Results demonstrated a higher value compared to the nominal Ca/P of the standard HA (1.67). The work by Sprio et al. (2008) suggested that the ratio of initial Si/P ratio is required to be equal to 0.05 for the simultaneous occupation of the phosphate site by carbonate and silicate ions to occur (Table 3.1).

Table 3.2: Percentage of carbonate, Ca/P+Si and Si/P ratios of the as-synthesized CHA and SiHA powders.

Samples	% CO ₃	Ca/P+Si	Si/P
0.5CHA	3.48	-	-
1.0CHA	4.08	-	-
2.0CHA	7.40	-	-
3.0CHA	12.93	-	-
4.0CHA	18.25	-	-
0.1SiHA	0.07	1.70	0.03
0.2SiHA	0.05	1.72	0.04
0.3SiHA	0.04	1.73	0.05
0.4SiHA	0.05	1.73	0.06
0.5SiHA	0.04	1.75	0.08

3.2.2. Development of the as-synthesized multi-substituted HA (SiCHA)

3.2.2.1. XRD Analysis

Figure 3.5 indicates the XRD spectra of SiCHA as-synthesized powders containing different molar content of carbonate and silicon substituted HA lattice. The addition of a small amount of silicon ($y= 0.1-0.5$ mol) has no significant different on the HA lattice (ICDD:09-0432).

From the XRD spectra, it is also revealed that at high carbonate content ($x=4.0$) in any of the combinations assessed (4.0:0.1SiCHA and 4.0:0.5SiCHA), there are additional peaks of calcite detected besides the HA peaks. On the other hand, at low carbonate content ($x=0.5$ and 2.0) the SiCHA as-synthesized powders in particular exhibits the XRD spectrum of an amorphous and purely single phase of carbonated hydroxyapatite with corresponds to the HA standard pattern. No secondary phase of other calcium phosphate or silicate was found. It was also observed that the addition of carbonate and silicon simultaneously has a great effect on the crystallinity of the powders. At highest carbonate and silicon content, 4.0:0.5SiCHA for instance, the crystallinity of the powders was substantially decreased.

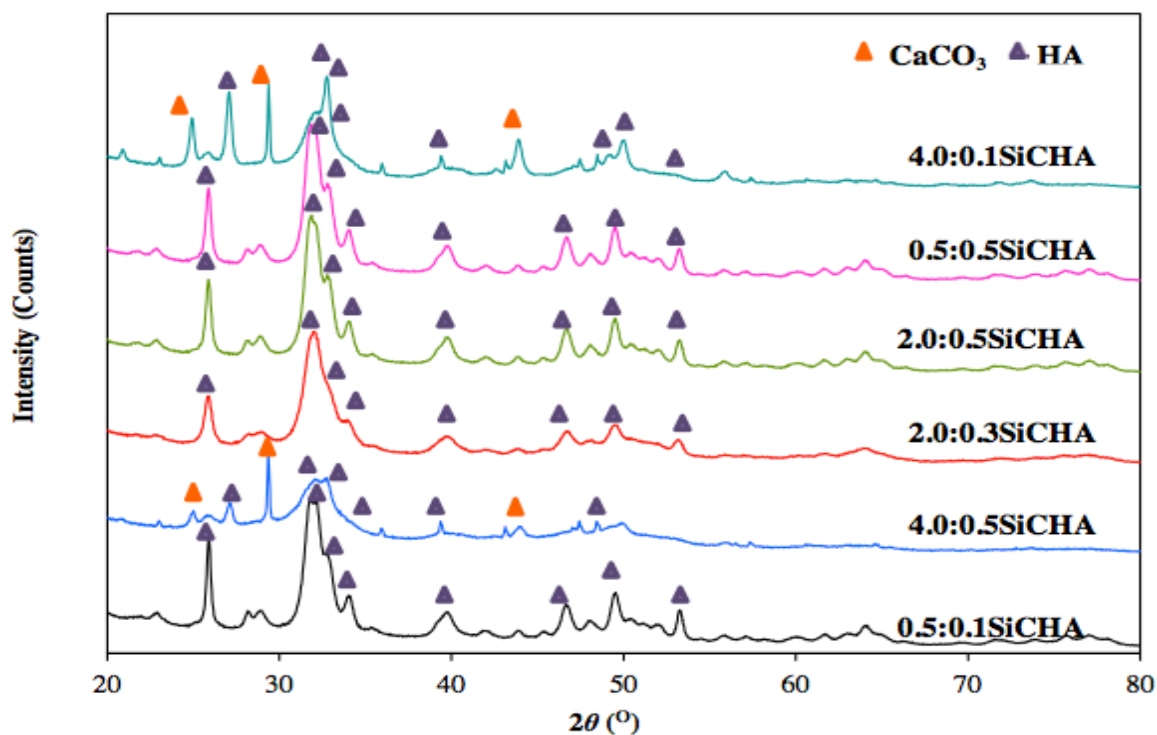


Fig. 3.5: XRD spectra of the SiCHA as-synthesized powders. The diffraction spectra indicating the present of secondary phase at higher carbonate substitution ($x = 4.0$). Simultaneous substitution of silicon and low carbonate ions ($x \leq 2.0$) into the apatite structure resulted in a single phase HA.

Regardless of the degree of carbonate and silicon substitutions into the HA structure, all SiCHA as-synthesized powders showed that the simultaneous substitutions of these ions resulted in a contraction of a -axis and expansion in the c -axis. The crystallite size of SiCHA as-synthesized powders falls in between the crystallite sizes of SiHA and CHA as-synthesized powders demonstrated earlier in section 3.2.1.1.

Table 3.3: Lattice parameters and crystallite sizes for as-synthesized SiCHA nanopowders.

Samples	Lattice parameters (Å)		Crystallite size (nm)
	$a \pm 0.003$	$c \pm 0.003$	
4.0:0.1SiCHA	9.401	6.970	16.95
0.5:0.5SiCHA	9.425	6.982	21.38
2.0:0.5SiCHA	9.412	6.897	18.79
2.0:0.3SiCHA	9.407	6.899	17.02
4.0:0.5SiCHA	9.402	6.972	22.18
0.5:0.1SiCHA	9.405	6.890	19.91

3.2.2.2. FTIR Analysis

The IR spectra of the investigated SiCHA as-synthesized powders show the typical bands at 963, 1036 and 1090 cm^{-1} , which corresponds to the stretching vibration modes of phosphate (Fig. 3.6). The presence of silicon can only be detected at 880-895 cm^{-1} (Sprio et al. 2008) on sample 0.5:0.5SiCHA as-synthesized powders. All the other samples can be considered mainly B-type CHA, as carbonate is the domain substitution. The carbonate ions in the B position were detected at about 870-875, 1414-1430 and 1450-1470 cm^{-1} .

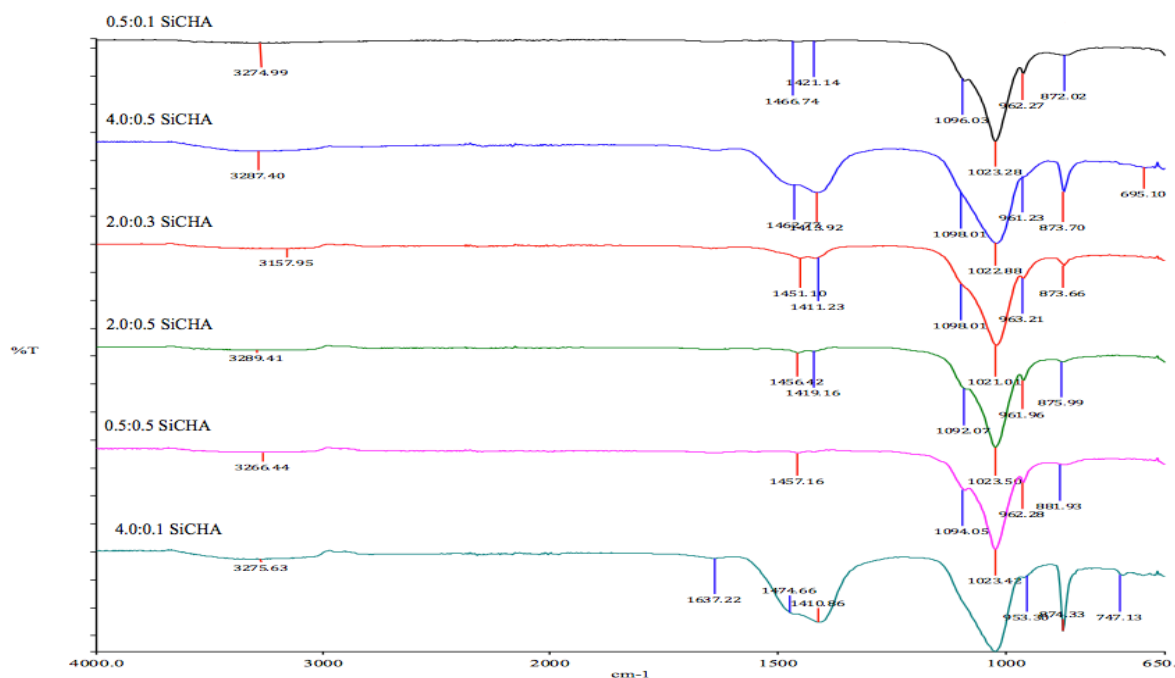


Fig. 3.6: FTIR spectra of the SiCHA as-synthesized powders. IR spectra showing the typical bands of B-type CHA at 870-875, 1414-1430 and 1450-1470 cm^{-1} besides the bands of phosphate and hydroxyl. Silicon band at 880-895 cm^{-1} can only be detected in 0.5:0.5 SiCHA as-synthesized powders.

3.2.2.3. CHN Analysis

It is observed that all SiCHA as-synthesized powders have lower wt% CO₃ compared to the pure CHA (Table 3.4). For instances, sample 0.5:0.1SiCHA, the percentage of carbonate was <2wt%. While, at higher carbonate content for instance 4.0:0.1 and 4.0:0.5SiCHA, the percentage of carbonate were far beyond the required value. Thus, 2.0:0.3 and 2.0:0.5SiCHA seem to possess the physiological relevant amounts of carbonate required because they falls between the ranges of carbonate present in the bone mineral.

Table 3.4: Percentage of carbonate (wt% CO₃) of SiCHA as-synthesized powders.

Sample code	Average wt%CO ₃	Standard deviation
0.5:0.1SiCHA	1.35	0.14
4.0:0.5SiCHA	12.65	0.07
2.0:0.3SiCHA	5.20	0.21
2.0:0.5SiCHA	3.85	0.14
4.0:0.1SiCHA	16.28	0.18
0.5:0.5SiCHA	2.15	0.49

3.2.2.4. ICP-OES Measurement

ICP-OES is a chemical analysis, which was performed on SiCHA as-synthesized powders to confirm the presence of silicon ions, as they were not visible in the FTIR spectra. The results suggested that the amount of silicon decreased as carbonate molar content increased as shown in Table 3.5.

Table 3.5: Ca, P and Si concentrations of the SiCHA as-synthesized powders.

Sample code	Ca (ppm)	P (ppm)	Si (ppm)	Si/P
0.5:0.1SiCHA	652.03	332.41	5.57	0.02
4.0:0.5SiCHA	524.30	260.50	2.69	0.01
2.0:0.3SiCHA	528.00	314.80	12.59	0.04
2.0:0.5SiCHA	587.00	284.50	14.23	0.05
4.0:0.1SiCHA	529.0	253.60	3.050	0.01
0.5:0.5SiCHA	455.50	216.40	17.32	0.08

3.2.2.5. XRF Analysis

XRF analysis was performed in order to further confirm the presence of silicon ions and quantify the amount of silicon incorporated in the multi-substituted HA as-synthesized powders. The calculated and measured Si shown in Table 3.6 represent the amount of Si calculated based on the stoichiometry empirical formula described earlier compared to the amount of Si obtained from the XRF analysis.

Table 3.6: Calculated Si, measured Si and Si/P ratio of SiCHA as-synthesized.

Sample code	0.5:0.1 SiCHA	4.0:0.5 SiCHA	2.0:0.3 SiCHA	2.0:0.5 SiCHA	4.0:0.1 SiCHA	0.5:0.5 SiCHA
Calculated Si (wt%)	0.28	3.81	0.86	1.99	0.36	1.35
Measured Si (wt%)	0.08	0.77	0.68	0.85	0.14	0.51

Higher carbonate content resulted in lower Si-substituted into the apatite structure and *vice versa*. This result highlights the evidence on the competitive substitution of carbonate and silicon ions to substitute the same position in the crystallographic structure of the phosphate sites.

3.2.3. Development of multi-substituted HA as biomedical materials

3.2.3.1. XPS analysis

The XPS spectra indicated that the carbonate and silicon ions were successfully substituted into the HA lattice. This was confirmed by the presence of the carbon and silicon peaks binding energies (BE) of 209 and 101 eV, respectively (Li et al. 2007; Zhao et al. 2014). The typical BE of HA elemental composition were also detected at 533 eV (O_{1s}), 349 eV (Ca_{2p}), and 135 eV (P_{2p}) as demonstrated in Fig. 3.7 (Kim et al. 2010). Qualitatively, the XPS spectra of the calcined powders were not affected by increasing temperature from 500 to 700°C; with all peaks traced at similar binding energies.

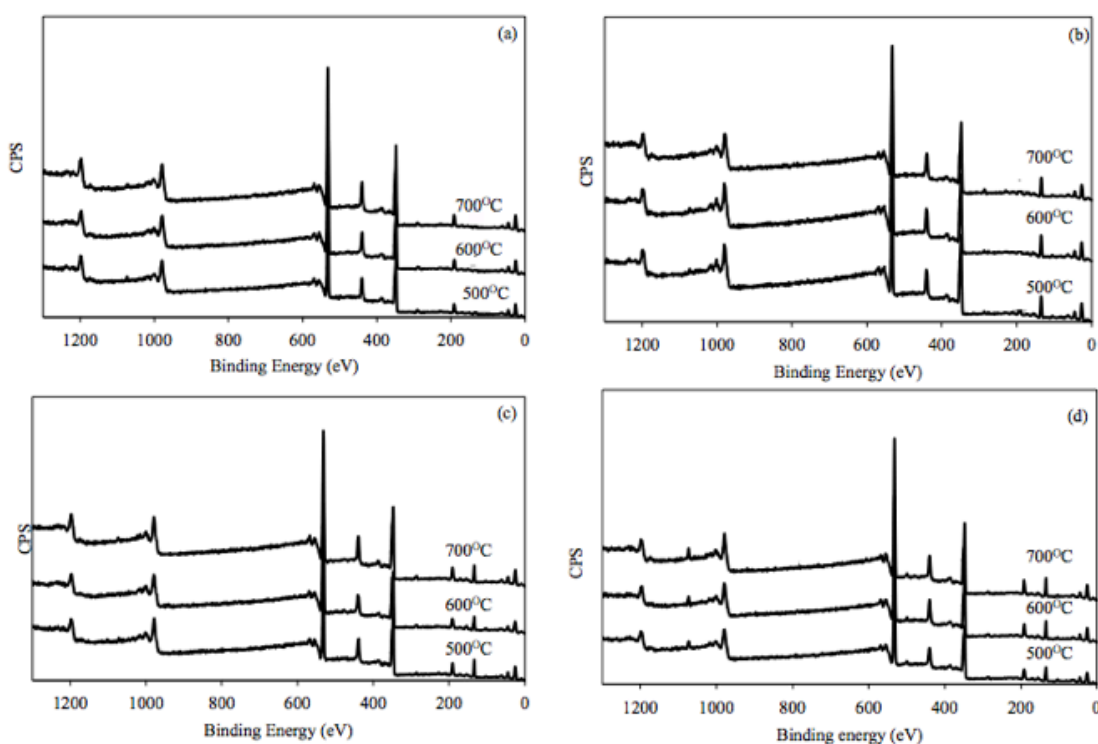


Fig. 3.7: XPS analysis of the as-calcined powders. Spectra confirmed the surface atomic compositions of the investigated powders calcined at 500-700°C; (a) CHA; (b) SiHA; (c) SiCHA-1; (d) SiCHA-2.

3.2.3.2. XRD analysis

Regardless of the specific composition, all powders remained stable in a single-phase diffraction pattern, which corresponds to hydroxyapatite (ICDD: 09-0432). Varying the calcination temperature from 500°C to 700°C shows no obvious difference between the diffraction patterns as shown in Fig. 3.8. There were eight main peaks detected *i.e.* at about $2\theta=26^\circ$ which was indexed at (002), $2\theta=32-34^\circ$ which represents three overlapped peaks of (211), (300) and (202), $2\theta=39.8^\circ$ indexed to (310), $2\theta=49.4^\circ$ for (222), and $2\theta=50$ and 53° indexed to (213) and (004), respectively. Most importantly, no other phase of calcium phosphate, such as calcite or calcium oxide (CaO) was traced (Kim et al. 2003). The main peak of CaO at $2\theta=37.347^\circ$ (ICDD= 37-1497) was absent even at high calcination temperature of 700°C for all the compositions of the as-calcined powders (Boyer et al. 2013).

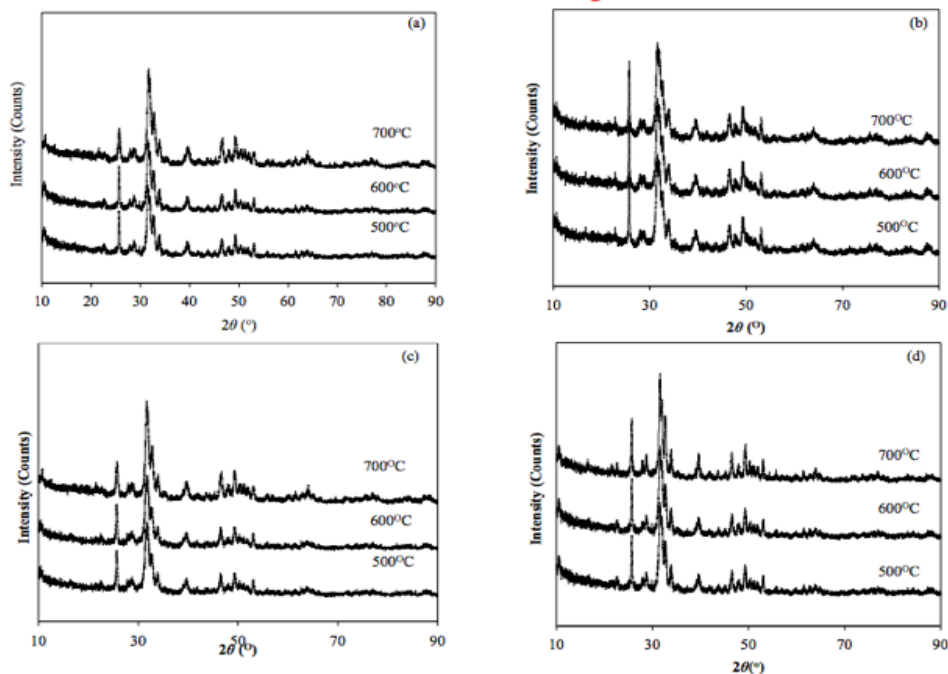


Fig. 3.8: XRD analysis of the calcined powders at 500-700°C; (a) CHA; (b) SiHA; (c) SiCHA-1; (d) SiCHA-2, demonstrating single phase of HA without the formation of secondary phase.

Although all the calcined powders remained as single phase, further refinement on the crystallographic properties showed that increasing calcination temperature from 500 to 700°C have evident effects on the lattice parameters and crystallite size of the calcined powders. Regardless of the powders composition, the crystallite size increased with increasing calcination temperature. It was also observed that the as-calcined powders still showed the same trends in the changes of the lattice parameters when compared to the as-synthesized powders as represented in Table 3.7. For instance, powders containing carbonate demonstrated a contraction in *a*-axis and expansion in *c*-axis while carbonate-free powders (SiHA) as-calcined powders showed expansions in both *a*- and *c*-axes at any calcination temperature (500-700°C).

Table 3.7: Lattice parameters and crystallite sizes of CHA, SiHA, SiCHA-1 and SiCHA nanopowders calcined at 500-700°C.

Samples	Calcination temperature (°C)	Lattice parameters (Å)		Crystallite size (nm)
		$a \pm 0.003$	$c \pm 0.003$	
CHA	500	9.389	6.918	10.02
	600	9.367	6.920	17.83
	700	9.352	6.923	20.76
SiHA	500	9.452	6.921	17.21
	600	9.455	6.923	21.02
	700	9.459	6.928	28.89
SiCHA-1	500	9.399	6.901	12.86
	600	9.391	6.912	19.87
	700	9.387	6.918	23.73
SiCHA-2	500	9.378	6.898	12.09
	600	9.372	6.893	18.92
	700	9.369	6.899	21.07

3.2.3.3. FTIR analysis

The full FTIR spectra scanned at 600-4000 cm^{-1} and their typical bands of the carbonate and silicon ions substituted into the apatite structure are represented in Fig. 3.9 for pure CHA and SiHA as-calcined powders followed by Fig. 3.10 for the multi-substituted HA. For CHA and SiHA powders calcined at 500-700°C, the typical peaks of hydroxyl groups were detected at 3570 and 1643 cm^{-1} , while only one main peak of hydroxyl was detected at 3570 cm^{-1} for SiCHA-1 and SiCHA-2 as-calcined powders (Gibson and Bonfield, 2001; Sprio et al. 2008).

All as-calcined powders showed the main characteristic bands of phosphate groups at about 960, 1020 and 1080 cm^{-1} as these are the most intense peaks in characterizing the hydroxyapatite crystals structure shown in the study conducted by Koutsopoulos (2002).

The IR spectra also confirmed that there is no other secondary phase such as calcite ~ 712 cm^{-1} , aragonite ~ 713 and 700 cm^{-1} and vaterite ~ 745 cm^{-1} were observed for all samples (Landi et al. 2004; Slosarczyk et al. 2005).

In addition to these phosphate and hydroxyl bands, the characteristic bands of carbonate and silicon ions were also detected. All CHA as-calcined powders regardless of the calcination temperature produced bands corresponding to the B-type carbonated apatites at about 870-875, 1410-130 and 1450-1470 cm^{-1} (Krajewski et al. 2005; Zhou et al. 2008; Sprio et al. 2008).

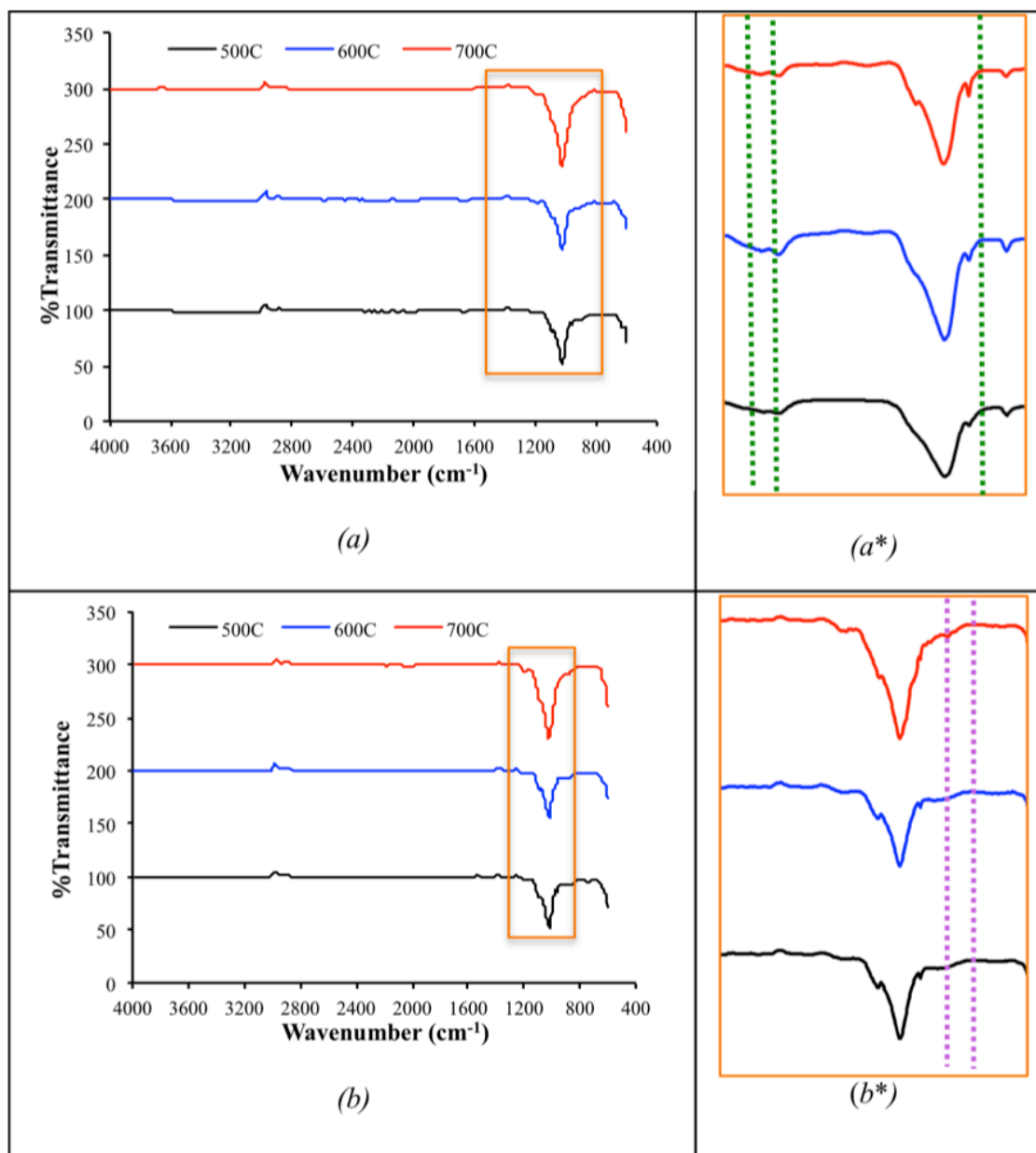


Fig. 3.9: FTIR spectra of CHA and SiHA as-calcined powders. IR spectra demonstrating the pure (a) CHA and (b) SiHA as-calcined powders at 500-700°C and their typical bands of the (a*) carbonate and (b*) silicon ions substituted into the apatite structure. Green and purple dotted lines represents the carbonate and silicon substituted HA characteristic bands.

For SiCHA-1 and SiCHA-2 as-calcined powders, a missing band of carbonate at 870-875 cm^{-1} was observed and only two main bands of carbonate were found at 1410-1430 and 1450-1470 cm^{-1} . Despite of the missing band, no carbonation occurred at the hydroxyl sites (A-type CHA) which is normally detected at 877-880, 1500 and 1540-1545 cm^{-1} (Koutsopoulos, 2002; Lafon et al. 2008) in any composition of the as-calcined powders at 700°C.

The typical bands of Si-substituted HA structure was detected at 947 and 880 cm^{-1} (Marchat et al. 2013) in the carbonated free HA (SiHA) as-calcined powders at 500-700°C. Again, the multi-substituted HA as-calcined powders demonstrated the absence of one of the Si-substituted HA band at about 947 cm^{-1} . A careful inspection of the IR spectra shows a small band of Si-substituted HA at 880-890 cm^{-1} for both SiCHA-1 and SiCHA-2 regardless the calcination temperature. Since the band of Si-substituted HA appears to be too small to be observed on the spectra, the results of FTIR analysis of as-calcined powders was listed in Table 3.8 for a clear comparison between the samples.

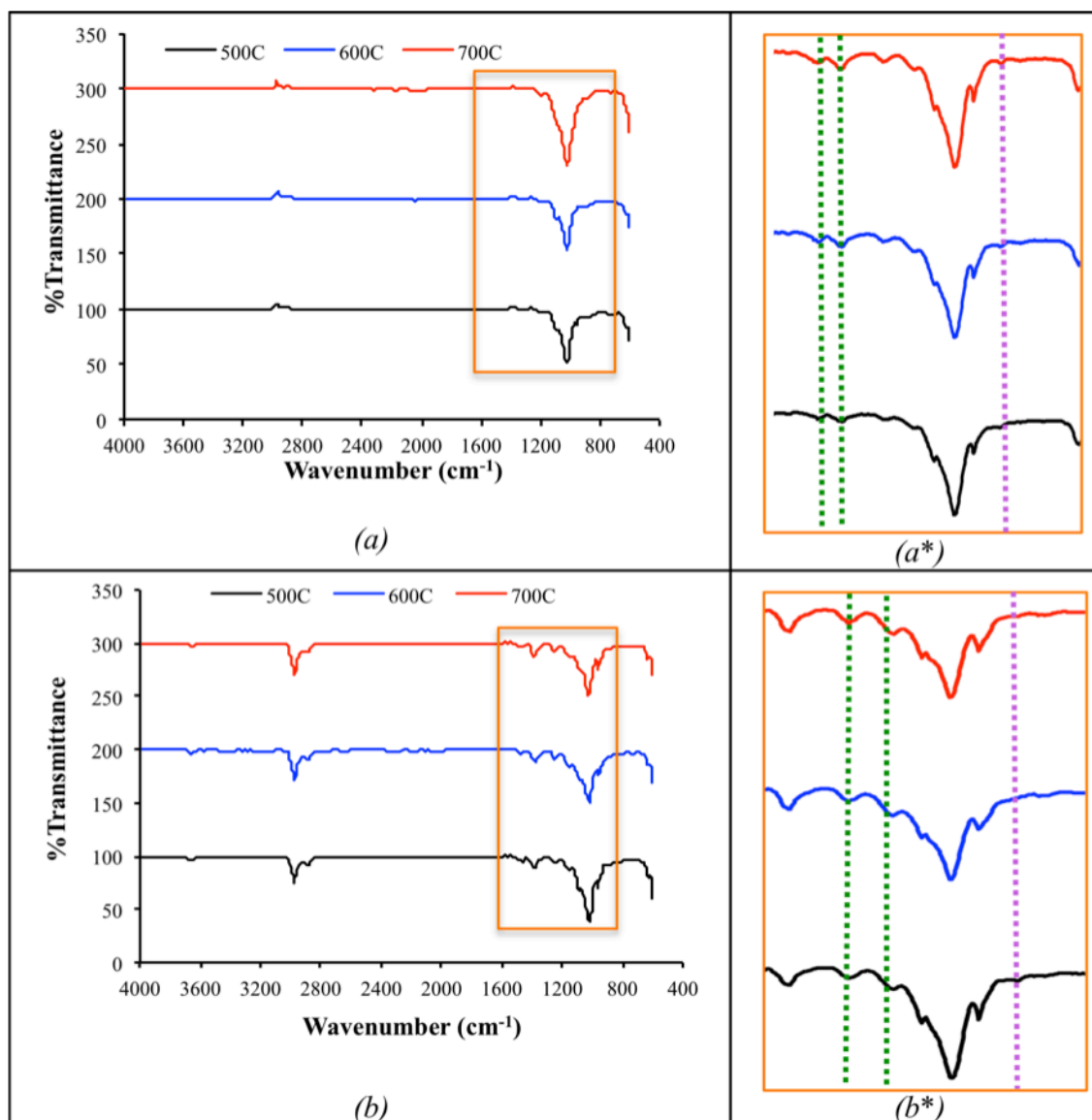


Fig. 3.10: FTIR spectra of SiCHA-1 and SiCHA-2 as-calcined powders. IR spectra demonstrating the multi-substituted HA (a) SiCHA-1 and (b) SiCHA-2 as-calcined powders at 500-700°C and their typical bands of the carbonate and silicon ions substituted into the apatite structure indicated as (a*) and (b*), respectively. Green and purple dotted lines represents the carbonate and silicon substituted HA characteristic bands.

Table 3.8: Results of FTIR analysis of as-calcined powders at 500-700°C.

<i>Samples</i>	<i>T(°C)</i>	<i>OH</i>	<i>PO₄</i>	<i>CO₃</i>	<i>Si</i>
<i>CHA</i>	500	3573.0, 1649.7	962.9, 1024.4, 1083.3	873.7, 1414.8, 1458.8	-
	600	3573.3, 1643.0	962.5, 1020.0, 1080.0	873.1, 1414.8, 1454.3	-
	700	3573.5, 1638.2	962.3, 1019.9, 1081.2	872.7, 1417.1, 1459.9	-
<i>SiHA</i>	500	3562.5, 1651.1	963.2, 1024.9, 1086.4	-	947.4, 885.7
	600	3569.7, 1635.8	962.5, 1024.7, 1089.7	-	946.9, 883.5
	700	3570.9, 1633.5	962.4, 1024.1, 1090.1	-	947.2, 884.2
<i>SiCHA-1</i>	500	3572.5	962.7, 1027.7, 1088.0	1418.2, 1461.9	883.1
	600	3570.8	962.2, 1022.9, 1087.9	1418.6, 1461.8	885.3
	700	3569.9	962.5, 1023.5, 1089.0	1413.6, 1461.9	887.7
<i>SiCHA-1</i>	500	3572.5	962.7, 1027.7, 1088.0	1418.2, 1461.9	883.5
	600	3578.7	962.2, 1022.9, 1080.0	1412.8, 1461.8	886.3
	700	3579.6	962.5, 1023.5, 1089.0	1418.2, 1461.3	884.9

3.2.3.4. TEM analysis

The TEM micrographs of the as-calcined powders at 500°C are shown in Fig. 3.11. The CHA powders appeared to be more spherical (20-30 nm length, 10-30 nm width) compared to pure SiHA, which have elongated rod-like particles (50-100 nm length, 15-30 nm width). At 500°C, the multi-substituted HA (SiCHA-1 and SiCHA-2) powders produced particles with dimensions which fall in the range of 30-50 nm length and 15-30 nm width, which perfectly matching the dimension of biological apatites. The particle sizes of the as-calcined powders correlates well with the crystallite sizes obtained from XRD analysis (section 3.2.3.2), where the same trends were seen in both analyses.

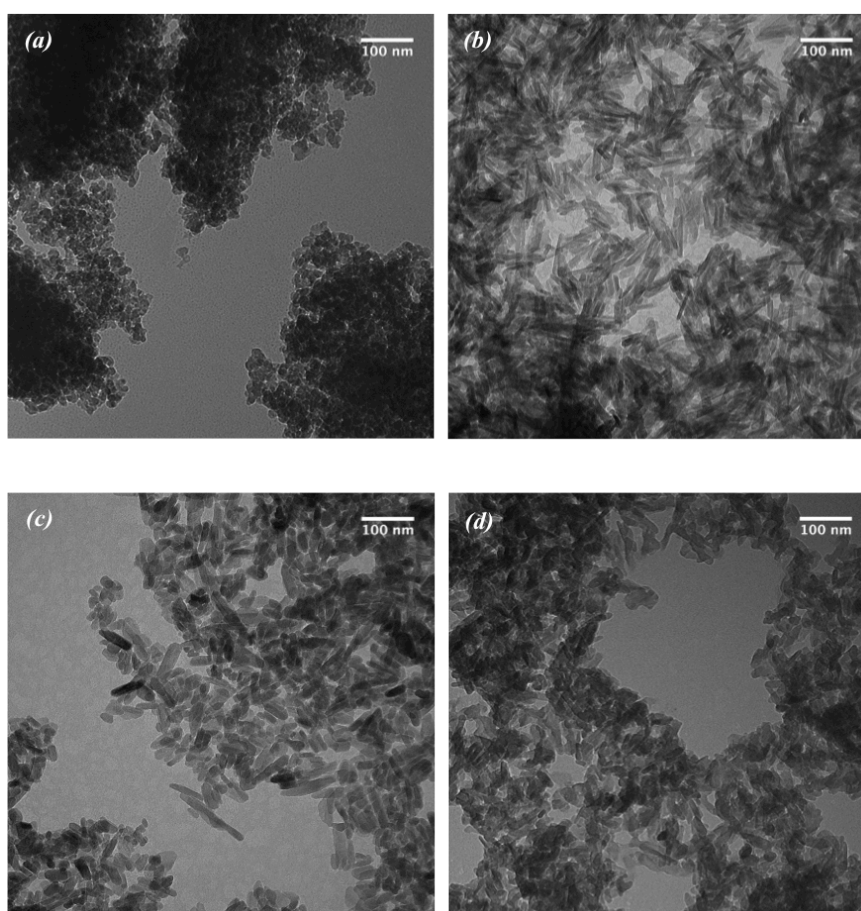


Fig. 3.11: TEM images of the investigated powders calcined at 500°C; (a) CHA; (b) SiHA; (c) SiCHA-1; (d) SiCHA-2 (scale bar = 100 nm).

3.2.3.5. CHN analysis

CHN analysis clearly demonstrated that the carbonated-substituted HA as-calcined powders, namely the CHA, SiCHA-1 and SiCHA-2 showed a similar trend of carbonate loss as the temperature increased (Table 3.9). For example, even at a low calcination temperature of 500°C, there is about 21% carbonate loss from the CHA powders; a similar trend is seen for SiCHA-1 and SiCHA-2. On the other hand, carbonated-free HA (SiHA) as-calcined powders showed an increment in the percentage of carbonate with increasing temperature. It is observed that as-calcined SiHA can potentially absorb as much as three times the relative amount of carbonate after calcination at 700°C as compared to the as-synthesized SiHA powders. The average percentage of carbonate in the as-synthesized was about 0.04wt% goes up to about 0.05, 0.08 and 0.12wt% at 500, 600 and 700°C, respectively. However, the percentage of carbonate present in the SiHA as-calcined powder is relatively low as compared to the carbonate-substituted HA powders given any calcination temperature.

Table 3.9: CHN analysis of the investigated powders at 500-700°C.

<i>Samples</i>	<i>T(°C)</i>	<i>%C (wt%)</i>	<i>%CO₃ (wt%)</i>	<i>%CO₃ changes after calcination (wt%)</i>
<i>CHA</i>	<i>500</i>	<i>1.08</i>	<i>5.80</i>	<i>-21.63</i>
	<i>600</i>	<i>0.99</i>	<i>4.95</i>	<i>-33.11</i>
	<i>700</i>	<i>0.57</i>	<i>4.15</i>	<i>-43.92</i>
<i>SiHA</i>	<i>500</i>	<i>0.01</i>	<i>0.05</i>	<i>+125.00</i>
	<i>600</i>	<i>0.02</i>	<i>0.08</i>	<i>+200.00</i>
	<i>700</i>	<i>0.02</i>	<i>0.12</i>	<i>+300.00</i>
<i>SiCHA-1</i>	<i>500</i>	<i>0.48</i>	<i>2.90</i>	<i>-24.68</i>
	<i>600</i>	<i>0.42</i>	<i>2.25</i>	<i>-41.56</i>
	<i>700</i>	<i>0.36</i>	<i>1.90</i>	<i>-50.65</i>
<i>SiCHA-2</i>	<i>500</i>	<i>0.79</i>	<i>3.98</i>	<i>-23.50</i>
	<i>600</i>	<i>0.50</i>	<i>3.25</i>	<i>-37.50</i>
	<i>700</i>	<i>0.38</i>	<i>2.98</i>	<i>-42.69</i>

Note: (-) means carbonate loss; (+) means carbonate absorb.

3.2.3.6. Elemental analyses

The ICP-OES and XRF elemental analyses shown in Table 3.10 suggest that the ionic substitutions either the CO₃ or Si or simultaneous substitution of both ions into the apatite structure have a significant effect on the ratio of Ca/P. The ratio of Ca/P obtained for all the as-calcined powders are significantly higher than the stoichiometric HA which is 1.67. The ratio of Ca/P was found to be in the range of 1.7-2.6 for the substituted-HA powders as stated in the literature (LeGeros and LeGeros, 2003; Gibson and Bonfield, 2001; Landi et al. 2010; Boyer et al. 2013; Friederichs et al. 2015).

The amount of Si measured by ICP-OES, which was given in ppm, was multiplied by 1×10^4 to convert the value to weight percentage. Results showed a slight decrease in Si wt% as the calcination temperature increased. It was stated that the amount of Si present *in vivo* within the mineralising osteoid regions was 0.5wt% by Carlisle et al. (1970). Hence, the SiCHA produced in this work could be considered comparable to the mineral content found *in vivo*.

Table 3.10: ICP-OES and XRF elemental analyses of the investigated powders at 500 - 700°C.

<i>Samples</i>	<i>T(°C)</i>	<i>Ca/P Measured value (XRF)</i>	<i>Si (wt%) Measured value (ICP-OES)</i>
<i>CHA</i>	500	1.76	-
	600	1.77	-
	700	1.79	-
<i>SiHA</i>	500	1.71	0.49
	600	1.72	0.46
	700	1.74	0.41
<i>SiCHA-1</i>	500	1.89	0.58
	600	1.91	0.47
	700	1.95	0.43
<i>SiCHA-2</i>	500	1.86	0.45
	600	1.89	0.42
	700	1.92	0.40

3.2.4. *In vitro* biological assessments

Based from physico-chemical characterizations, a calcination temperature of 500°C was chosen as the best calcination temperature to produce the multi-substituted HA powders in order to maintain the carbonate and silicon contents in the HA structure as close as possible to those presents in the natural bone mineral. *In vitro* biocompatibility assessments were conducted on the optimum powders of CHA, SiHA, SiCHA-1 and SiCHA-2. The main goal of this biocompatibility test is to explore the most osteoconductive powders when seeded with human bone marrow-derived mesenchymal stem cells (hMSCs) *in vitro*. The aim is to select the greatest biomedical materials to be used in the scaffold fabrication for bone tissue engineering (BTE) applications.

3.2.4.1. *Cell viability*

The cell viability of hMSCs in contact with the as-calcined powders was investigated using live/dead staining. Confocal laser scanning microscopy (CLSM) images for the controls and calcined powders at 500°C after 7, 14 and 21 days in culture are presented in Fig. 3.12-3.13. Cells demonstrated an elongated fibroblast-like morphology. Fig. 3.12 represents the control samples, where the viability remained high with low numbers of cell death detected at day 7 and 14 and confluence attained by day 21.

At day 7, SiCHA-1 revealed a lower proportion of live cells in comparison to SiCHA-2, SiHA and CHA powders; similar trends were observed at day 14 and 21. While, SiCHA-2, SiHA and CHA powders showed gradual increased in cell viability from day 7 to day 21. The morphology of the cells adhered to the Si-substituted HA powders was observed to be more fibroblastic (elongated morphology) compared to the cells in direct contact with CHA powders as shown in Fig. 3.13.

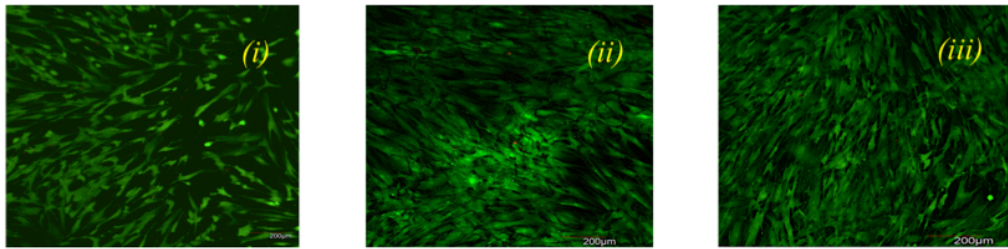


Fig. 3.12: CLSM of the positive controls; hMSCs cultured on tissue-cultured plastic at 7(i), 14(ii) and 21(iii) days. Scale bar = 200 μm.

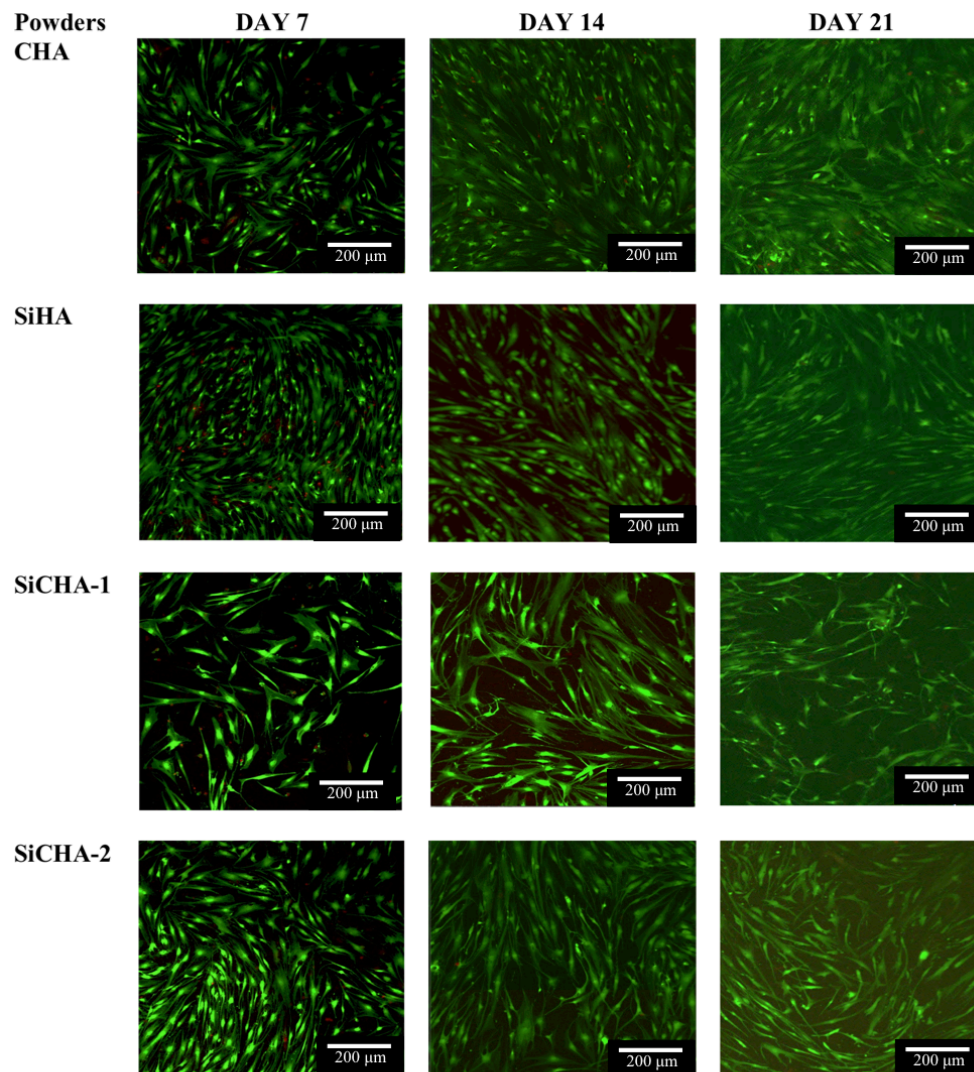


Fig. 3.13: CLSM images of CHA, SiHA, SiCHA-1 and SiCHA-2 powders cultured in osteogenic media for different time periods. Green indicates viable cells and red indicates dead cells. Scale bar = 200 μm.

3.2.4.2. *Cell proliferation and osteogenic activity*

DNA quantification was used as an indicator for cell proliferation (Fig. 3.14 a). Mean DNA concentrations increased over time for all the tested powders ($p \leq 0.0001$) and differed between the powders ($p \leq 0.0001$). There was a significant interaction between time and powder compositions ($p \leq 0.05$) suggesting that the increase in DNA concentration over time differed between powders.

Compared to the control (tissue culture plastic, TCP) the powders CHA, SiHA and SiCHA-2 showed no significant differences at day 7 ($p \geq 0.05$ for each), but at day 21 significantly increased DNA contents were detected for these powders as compared to TCP ($p \leq 0.0001$ for each). Among all the investigated powders, SiCHA-1 had the lowest mean DNA concentrations, which were $0.44 \pm 0.02 \mu\text{g/mL}$ on day 14 and $0.73 \pm 0.01 \mu\text{g/mL}$ on day 21. When comparing SiCHA-1 with TCP, significantly lower DNA concentrations were found on day 7 ($p=0.034$) and day 21 ($p=0.0082$) but no significant differences were detected at day 14 ($p=0.8466$).

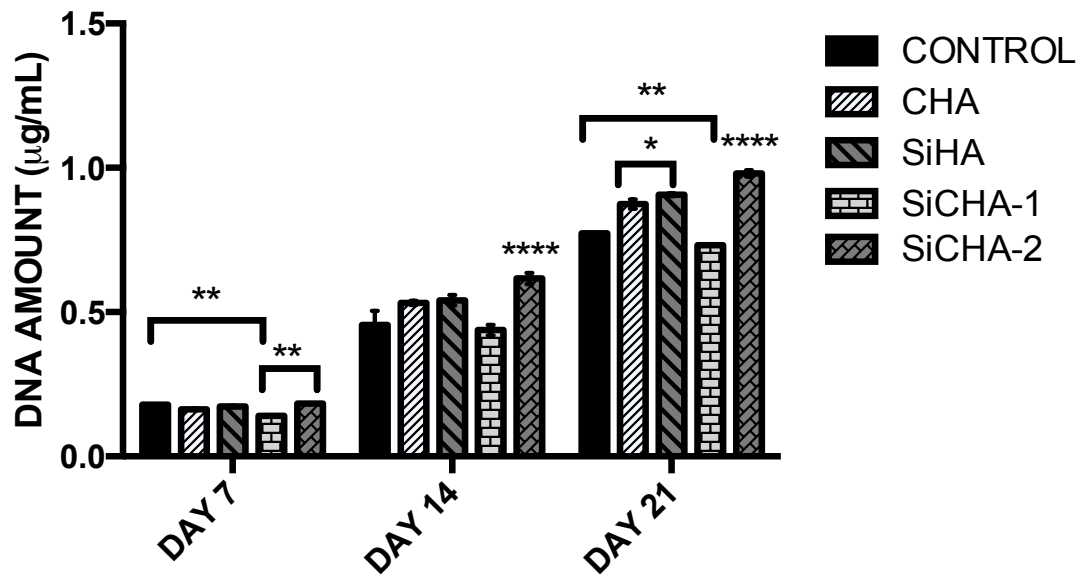
When comparing the powders with each other there was no significant difference between SiCHA-1, CHA and SiHA on day 7, but SiCHA-2 was significantly increased over SiCHA-1 ($p=0.0021$). Cells cultured on SiCHA-2 powder showed the highest DNA concentrations after 14 days and 21 days compared to all other investigated powders and were found to be significantly different ($p \leq 0.0001$ for each). On day 21, single-substituted powder SiHA was significantly higher compared to CHA ($p=0.0491$).

Overall, SiCHA-2 showed the highest DNA content compared to all other investigated groups (TCP and powders) on day 14 and day 21 ($p \leq 0.0001$ for each).

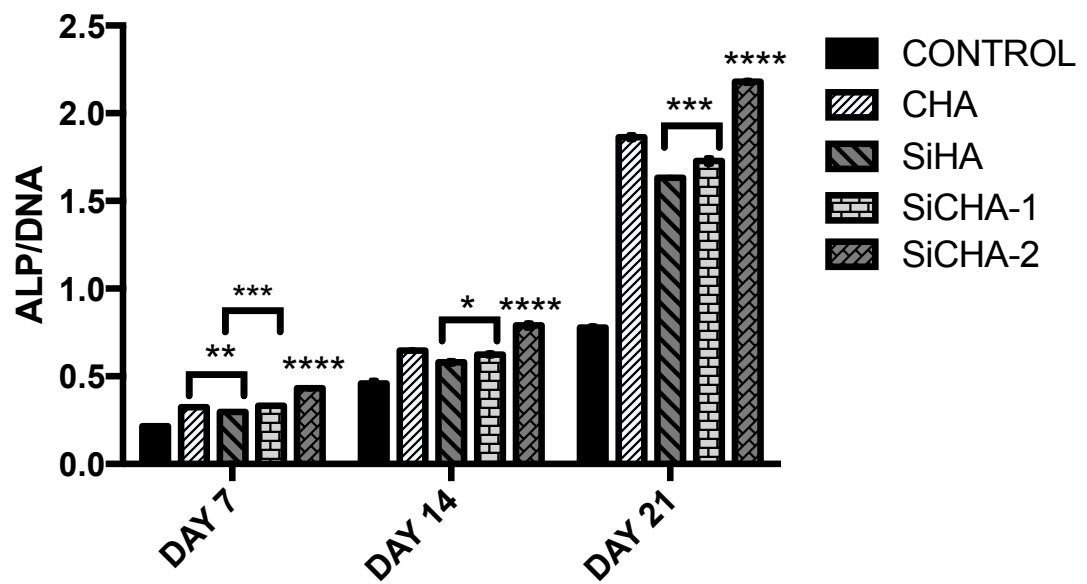
Normalizing the alkaline phosphatase (ALP) activity results to the DNA levels give an indication of the early osteogenic activity, as demonstrated in Fig. 3.14 (b). Mean ALP activity of all investigated powders showed gradual increases over time ($p \leq 0.0001$) and differed between the powders ($p \leq 0.0001$). There was a significant interaction between time and powder compositions ($p \leq 0.0001$) suggesting that the increase in ALP activity over time differed between powders.

Compared to the TCP control, all the investigated powders demonstrated significantly higher levels of ALP/DNA at 7, 14 and 21 days of culture ($p \leq 0.0001$ for each). When comparing different compositions of the tested powders, cells cultured on SiCHA-2 showed the highest mean ALP/DNA at either time-point ($p \leq 0.0001$ for each). At day 7, cells cultured on SiHA revealed significantly lower levels of mean ALP/DNA as compared to CHA ($p = 0.0098$) and SiCHA-1 ($p = 0.0003$). Between the single substitution powders, CHA showed significantly higher levels of mean ALP/DNA relative to SiHA as culture progressed ($p \leq 0.0001$ for each). SiCHA-1 demonstrated similar trend, where the levels of ALP/DNA of SiCHA-1 significantly increased on day 14 ($p = 0.0047$) and day 21 ($p = 0.0007$) as compared to SiHA.

Overall, cells cultured in direct contact with SiCHA-2 exhibited the highest level of mean ALP/DNA compared to all other investigated groups (TCP and powders) on day 7, 14 and 21 ($p \leq 0.0001$ for each).



(a)



(b)

Fig. 3.14: Effect of CHA, SiHA, SiCHA-1 and SiCHA-2 as-calcined powders on (a) cell proliferation indicated by the amount of DNA and (b) the ALP activity were measured after day 7, 14 and 21 of treatment. Control represent the tissue culture plastic. Values represent the mean \pm SD of three samples in duplicate. (* $p \leq 0.05$, ** $p \leq 0.01$, *** $p \leq 0.001$, **** $p \leq 0.0001$).

3.2.4.3. *Cell metabolic activity*

Regardless of the powder compositions, the levels of protein production increased over time ($p \leq 0.0001$) and differed between the powders ($p \leq 0.05$). There was a significant interaction between time and powder compositions ($p \leq 0.05$) suggesting that the increase in total protein production over time differed between powders.

Compared to the control (tissue culture plastic, TCP), the powders CHA, SiHA and SiCHA-2 showed significantly higher levels of mean total protein ($p \leq 0.0001$ for each) at day 7. As culture progressed, these tested powders demonstrated significantly increased levels of mean total protein produced as compared to TCP ($p \leq 0.0001$ for each). Among all the investigated powders, SiCHA-1 had the lowest levels mean total protein but still higher compared to TCP on day 7 ($p = 0.0006$) and day 14 ($p \leq 0.0001$). However, the cells in direct contact with SiCHA-1 produced lower level of total protein compared to TCP on day 21 ($p \leq 0.0001$).

When comparing the powders with each other, significantly higher levels of mean total protein was detected on SiCHA-2 than CHA powders ($p = 0.0005$) at day 7. Cells cultured on SiHA and SiCHA-1 showed no significant differences in total protein production ($p = 0.8504$) on day 7. As culture progressed, significantly higher levels of total protein detected on SiHA compared to SiCHA-1 at day 14 ($p = 0.0027$) and day 21 ($p \leq 0.0001$).

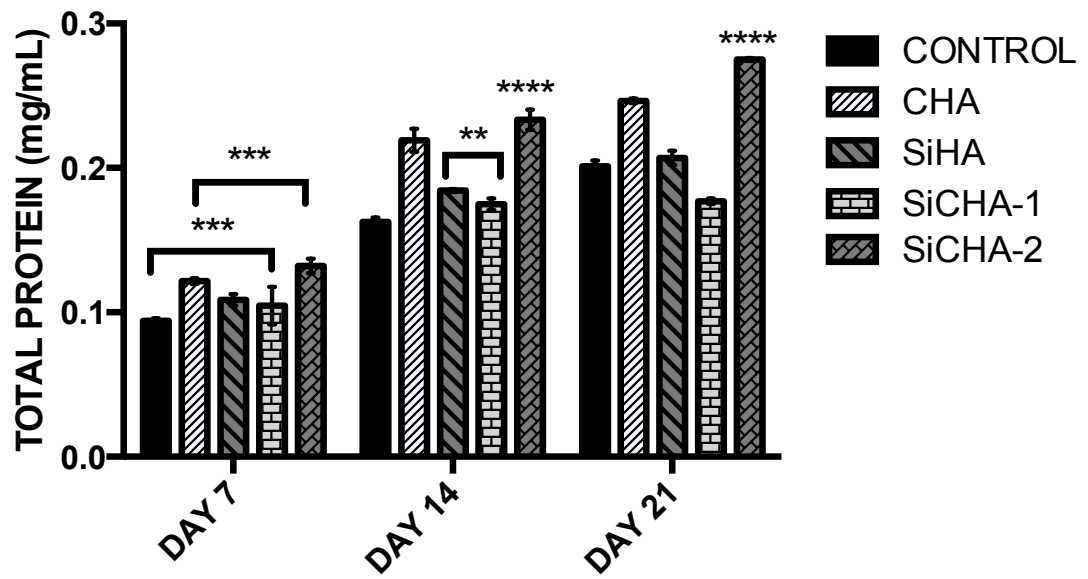
Overall, cells on SiCHA-2 produced the highest total protein compared to all other investigated groups (TCP and powders) on day 7, 14 and 21 ($p \leq 0.0001$ for each).

Alamar blue data showed consistent trend with the levels of total protein obtained. Overall, the mean levels of alamar blue increased for all the investigated powders over the culture period ($p \leq 0.0001$) and differed between the powders ($p \leq 0.05$). There was a significant interaction between time and powder compositions ($p \leq 0.05$) suggesting that the increase in levels of alamar blue over time differed between powders.

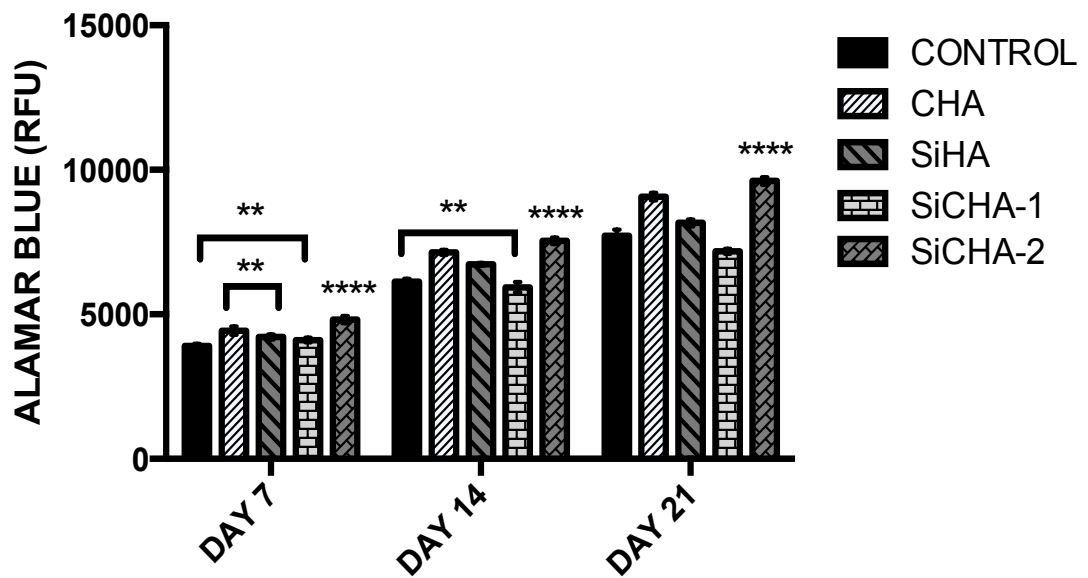
Compared to the control (tissue culture plastic, TCP), the powders CHA, SiHA and SiCHA-2 showed significantly higher levels of mean alamar blue ($p \leq 0.0001$ for each) at day 7. As culture progressed, these tested powders demonstrated significantly increased levels of mean alamar blue as compared to TCP ($p \leq 0.0001$ for each). Among all the investigated powders, SiCHA-1 had the lowest level mean alamar blue but still higher compared to TCP on day 7 ($p = 0.0062$). However, the cells in direct contact with SiCHA-1 were found to be significantly less metabolically active compared to TCP on day 14 ($p = 0.0098$) and 21 ($p \leq 0.0001$).

When comparing the powders with each other, significantly higher levels of alamar blue were obtained when cells were cultured on SiCHA-2, while SiCHA-1 remained the lowest at each time-point ($p \leq 0.0001$ for each). Between the single substitution powders, statistically higher level of metabolic activity was found when hMSCs were cultured in direct contact with CHA powders at day 7 ($p \leq 0.0029$). The metabolic activity of hMSCs on CHA remained the highest as compared to SiHA on day 14 and 21 ($p \leq 0.0001$ for each).

Overall, hMSCs cultured on SiCHA-2 powder were found to be the most metabolically active compared to all other investigated groups (TCP and powders) over the culture period ($p \leq 0.0001$ for each).



(a)



(b)

Fig. 3.15: Effect of carbonate or/and silicon-substituted HA as-calcined powders on (a) the total protein production and (b) cell metabolic activity determined by alamar blue. Values represented the mean \pm SD of three samples in duplicates. ($*p \leq 0.05$, $**p \leq 0.01$, $***p \leq 0.001$, $****p \leq 0.0001$).

3.3. Discussion

3.3.1. Preparation of as-synthesized multi-substituted HA powders

The overall aim of this chapter was to produce a selection of novel multi-substituted hydroxyapatite (SiCHA) powders and identify the most favorable composition to elicit osteogenic behaviour, before proceeding to the fabrication of final scaffolds as biomedical implants for BTE applications. In this study, powders that meet the following criteria are considered as the ideal powder formulation to be used as biomedical materials; (1) powders remained as single phase B-type CHA; (2) powders closely mirror the carbonate (2-8wt%) and silicon (<0.5wt%) contents of bone mineral and (3) powders encourage the fastest cell proliferation, produce the highest level of total protein and ALP activity over 21 days of culture period. Therefore, the focus in the first part of this study is to optimize the CO₃ and Si ions substitution into the HA structure. This is a major step in the development of new biomaterials for BTE applications as different osteogenic cells behave relatively different in response to the multi-substituted HA powders in particular when the composition and precursor used are different (Shepherd et al. 2012). The second part of this study identified the selection calcination temperature in order to complete the chemical reaction of the synthesized powders, where at the same time this temperature should remained the maximum amount of the substitution ions in the apatite structure. Finally, this study provided an interesting information on human mesenchymal stem cells behaviour as cultured in direct contact with different compositions of the powders produced.

From the physico-chemical analyses, as-synthesized powders with low carbonate contents such as 0.5-, 1.0-, and 2.0CHA remained as highly pure amorphous HA structure and no secondary phase such as calcite or calcium carbonate (CaCO₃) was detected as previously seen in 3.0CHA and 4.0CHA as-synthesized powders. Due to limited substitution, powders

with high composition of carbonate were not able to substitute all the carbonate ions at the phosphate sites in the apatite structure during the synthesis. Therefore, the excess carbonate would then react with calcium and thus forms CaCO_3 . The presence of CaCO_3 was detected at $2\theta = 29.4, 35.9$ and 43.2° . The same behaviour was reported by Lafon et al. (2008) who found the formation of secondary phase of calcite when the molar ratio of carbonate to phosphate was too high, i.e. $(\text{NH}_4)\text{HCO}_3 : (\text{NH}_4)_2\text{HPO}_4 > 3:2$ (Lafon et al. 2008). In this study, substitution of CO_3^{2-} in HA structure has resulted in smaller crystallite size. This was attributed to replacement of larger tetragonal PO_4^{3-} site by smaller trigonal planar of CO_3^{2-} . The CO_3^{2-} substitution into apatite structure can also alter the lattice parameters as compared to the synthetic HA lattice, i.e. contraction in a -axis ($< 9.418 \text{ \AA}$) and expansion in c -axis ($> 6.884 \text{ \AA}$), which gives B-type CHA; while substitution of OH^- induces a vice versa effect on the lattice parameters, which will then result in A-type CHA (Baba Ismail & Mohd Noor 2011; Kee et al. 2013; Bang et al. 2014). This indicates that CHA powders at any CO_3^{2-} content synthesized in this study are B-type CHA.

A careful inspection of the IR spectra confirmed that the CHA synthesized powders at any composition (0.5-4.0CHA) are mainly B-type CHA, where the carbonation occurred only in the phosphate sites. The hydroxyl sites were not affected by the single ion substitution into the apatite structure for these CHA powders as shown in Fig. 3.3. The typical peaks of A-type CHA at $877\text{-}880, 1500,$ and $1540\text{-}1550 \text{ cm}^{-1}$, were not visible in the spectra (He et al. 2007). This confirmed the assumption in the chemical formulation used in the making of CHA powders (as described in section 2.2.1) established in this work, where the carbonate ions were assumed to substitute the phosphate sites and no carbonation occurred in the hydroxyl crystallographic groups. This assumption is acceptable for the CHA

powders synthesized with low carbonate contents ($x \leq 2.0$) where no secondary phase was detected. Similar observation was reported by Zhou et al. (2008) who used a similar method to synthesize B-type CHA powders at room temperature. Vignoles et al. (1988) reported that under basic condition (i.e. in the presence of added ammonia) and low precipitation temperature, the probability of carbonate to substitute phosphate sites in the apatite lattice was higher. In this condition, more hydroxyl ions were present in the reaction and thus they would be more competitive to fill the apatite structure easily than the carbonate ions. As a result, carbonate ions would only substitute the phosphate sites without substituting any of the hydroxyl sites (Vignoles et al. 1988).

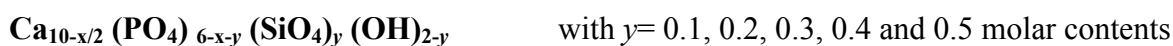
The percentage of CO_3 substituted into the structure increased with increasing molar content, indicating completion of the reaction and successful incorporation of carbonate into the apatite lattice (Lafon et al. 2008; Kee et al. 2013). Controlled amounts of carbonate substitution are crucial in order to properly mimic the mineral content of native bone, which contains B-type CHA with purely single phase HA and adequate amounts of CO_3 . The carbonate content in bone mineral has been shown to vary depending on the individual age, with an increase in the amount of A-type CHA substituted apatite in aging bone (Rey et al. 1991). Hence, B-type CHA is the most abundant inorganic minerals in bones of young people. A study on different carbonate substitution mechanisms in bulk HA conducted by Astala and Stott (2005) showed that B-type CHA (phosphate ions substitutions) is energetically preferred to A-type CHA (hydroxyl ions substitution). This can probably explain that most as-synthesized CHA reported in the literature as well as found in this current study, is the B-type CHA. For this reason, CHA with $x=2.0$ was chosen as the optimum composition because it possesses the most sufficient amount of

carbonate which is about 7.40wt% incorporated in the HA structure as compared to other compositions, typical B-type CHA and possess single phase HA.

Si-substituted HA (SiHA) powders were synthesized using the same nanoemulsion method. Varying the Si contents had no significant effect on the XRD spectrum as all compositions exhibited a pure single amorphous phase of HA. The diffraction patterns were marginally broader as more Si is incorporated into the apatite structure. The powder crystallinity decreased with the increased Si amounts substituted the apatite structure. Contradicting observations were made for synthesizing SiHA powders as compared to CHA powders, where both lattice parameters and crystallite size of the powders increased with increasing Si-substituted HA lattice. This could be explained by the replacement of smaller P^{5+} ions (0.35 \AA) with larger Si^{4+} ions (0.42 \AA) in the HA framework (Kim et al. 2003; Bianco et al. 2009). The substitution of larger SiO_4^{4-} in the PO_4^{3-} site caused crystallite strain of the HA lattice, which contributes to a larger crystallite size of SiHA powders as compared to CHA powders synthesised in the same manner. This finding is strongly supported by the previous studies reported in the literature (Kim et al. 2003; Bianco et al. 2009; Palard et al. 2008; Gomes et al. 2011). The substitution of silicon into the apatite structure has been known to induce chemical and structural changes in HA lattice that lead to changes *in vitro* response of the osteogenic cells as previously studied by Botelho et al. (2006). This is because, decreased in the crystallinity resulted in increased solubility of the powders and the higher the dissolution rate. Friederichs et al. (2015) has stated that the dissolution rates of SiHA was higher as compared to HA which may contribute to the success of SiHA as bone graft materials.

The IR spectra of the SiHA as-synthesized powders demonstrated the typical HA bands with additional band of Si detected at $880\text{-}895$ and 947 cm^{-1} . It is observed that the triplet

bands of the phosphate groups become narrower as more Si-substituted the HA lattice. One of the hydroxyl band was found missing and this indirectly showing that the Si ions have substituted both phosphate sites and also the hydroxyl groups as assumed in the chemical equation shown below:



Quantification of CO₃ content by CHN analysis in SiHA powders shows that a very small amount (<1wt%) of CO₃ present in all compositions of the as-synthesized SiHA powders. This is most likely the impurities used in the synthesis, e.g. the silicon tetraacetate, Si(CH₃COO)₄ contains carbon in the chemical structure, which possibly remained in the end products. In addition, the carbonate present in the SiHA structure might be due to the carbon dioxide in the atmosphere had dissolved in the mother-liquor solution during the synthesis, as this process take place at room temperature. Although the elemental analysis showed the present of CO₃ in the SiHA as-synthesized powder, no typical carbonate bands corresponding to either A- or B-type were evident in any of the powders. Therefore, it is likely that the carbonate present only on the surface and not incorporated into the HA lattice.

Prior to the development of multi-substituted HA (SiCHA) powders, the amounts of CO₃ and Si-substituted HA optimised to closely mimic the physiological relevant amounts of CO₃ and Si presents in the biological apatite. There is a discrepancy regarding the optimum amount of Si-substituted into HA powders. For instance, Carlisle et al. (1970) highlighted the presence of 0.5wt% silicon in the active calcification sites. However, a concentration of 0.8wt% was found to be optimal to induce the development of important bioactivity as reported by Hing et al. (2006) and Botelho et al. (2006). In order to develop SiCHA

powders where the carbonate and silicon ions are simultaneously substituted into the apatite structure, a study by Sprio et al. (2008) suggested the initial Si/P ratio should be equal to 0.05. For this reason, we chose 0.3SiHA as the optimum composition (0.3SiHA = 0.05 Si/P, 0.04% CO₃ and 1.73 Ca/P + Si).

Multi-substituted HA (SiCHA) powders were synthesized with different combinations of the highest ($x= 4.0$ and $y= 0.5$), lowest ($x= 0.5$ and $y= 0.1$), and optimum amounts ($x= 2.0$ and $y= 0.3$), of carbonate and silicon ions. Same results obtained as described in the production of CHA powders, where powders with high carbonate content ($x=4.0$) lead to the formation of a secondary phase of CaCO₃ besides the HA phase detected in the diffraction patterns.

On the other hand, at low carbonate content ($x=0.5$ and 2.0) the SiCHA as-synthesized powders in particular exhibit the XRD spectrum of an amorphous and purely single phase carbonated hydroxyapatite with corresponds to the HA standard pattern. No secondary phase of other calcium phosphate or silicate was found. This indicates the competitive substitution between carbonate and silicon ions, as both ions tend to substitute the phosphate crystallographic site as assumed in the stoichiometry empirical formula described earlier. Sprio et al. (2008) found similar phenomenon where no secondary phase detected to contaminate the multi-substituted HA, except for samples containing high carbonate ions attributed to the formation of CaCO₃. Refined analysis on the lattice parameters and crystallite size of SiCHA nano-powders showed that the crystallographic parameter falls about midway between CHA and SiHA powders. These changes in the lattice parameters clearly demonstrated that both carbonate and silicon ions are structurally incorporated into the HA framework, and not only cover the surface of HA.

The IR spectra of the SiCHA as-synthesized powders show the typical bands stretching vibration modes of phosphate. The presence of silicon can only be detected on sample 0.5:0.5SiCHA as-synthesized powders as it contained the combination of the highest silicon content with lowest carbonate content. All the other samples can be considered mainly B-type CHA as the carbonate substitution predominates. The typical peaks of A-type CHA, which typically appear at wave numbers of 877-880, 1500 and 1540-1550 cm^{-1} , were not visible in the spectra (He et al. 2007). There is also a missing band of one of the OH^- group at 1600-1700 cm^{-1} (Tang et al. 2005). This proved that the silicon ions substituted the phosphate position and partially substituted the hydroxyl position (Gibson et al. 2002) as assumed in the empirical formula.

It is noted that all SiCHA as-synthesized powders possess lower carbonate content in comparison to the pure CHA. This is due to the limitation of position occupancy as both carbonate and silicon ions trying to compete to simultaneously substitute the phosphate group. Thus, this might cause slight loss in the amount of carbonate. The results show that silicon ions have successfully substituted all the as-synthesized powders. It is observed that the amount of silicon decreased as carbonate molar content increased. Again, this is due to the competitive ion substitutions into the phosphate group.

The Si contents measured in all the as-synthesized SiCHA powders with different combinations of carbonate and silicon compositions revealed <1wt% Si presents. It was suggested in the literature that an amount of only 1wt% Si-substituted into HA was sufficient to elicit important bioactive improvements, i.e. Si has been reported to have a specific metabolic role connected to bone growth (Boanini et al. 2010). Hence, the SiCHA powders produced in this work offer the potential for enhancing bioactivity. Similar amount of Si wt% was obtained by the work reported by Bang et al. (2014) who

synthesized SiCHA via wet precipitation method. Therefore, based on physico-chemical characterization, the optimum as-synthesized powder compositions produced were 2.0:0.3SiCHA and 2.0:0.5SiCHA, because they fulfilled the ideal criteria, i.e. B-type CHA with single phase HA and yielded closely mirror the carbonate and silicon contents of bone mineral.

3.3.2. Development of multi-substituted HA powders as biomedical materials

The next phase of this study investigated the effect of calcination at low temperature (500-700°C) under atmospheric conditions (air), i.e. calcination on the optimum as-synthesized SiCHA denoted by SiCHA-1 (2.0:0.5SiCHA) and SiCHA-2 (2.0:0.3SiCHA). The main purpose of calcination is to ensure the synthesis process is completed and to remove any unreacted components incorporated during synthesis (Zhou et al. 2008). According to Ivanova et al. (2001), carbonate loss in air generally starts at 550°C and is completed above 900°C, depending on treatment-time and composition. Therefore, the calcination temperature was limited up to 700°C for 1 hour (soaking period) in this study to retain the carbonate content.

It is particularly important to ensure that the ionic substitutions remained in the structure after the heat treatment. XPS was conducted on the as-calcined powders in order to detect any possible changes that could alter the composition of the powders during calcination. Qualitatively, the XPS spectra of the calcined powders were not modified by increasing temperature from 500 to 700°C; with all profiles demonstrating similar binding energies. The analysis by XPS confirm that carbon and silicon does exist in all the as-calcined powders from 500 to 700°C. The BE of SiO_4^{4-} was detected at 102.0 ± 0.2 eV (Mekki et al., 1997; Botelho et al. 2002). While, the BE of SiO_2 was centered at 103.9 eV as stated in other study (Beshkov et al. 2002). In this study, it was conclusively confirmed that silicon

does exist as tetrahedral silicate (SiO_4), rather than in a polymeric or SiO_2 form. This was determined by the binding energy (BE) detected on the spectra, i.e. 101 eV. This important finding supports the different term between silicon or silicate substitution with the well-characterized carbonate substitution of phosphate groups in the HA structure.

The physical and chemical analyses established that simultaneous substitution of carbonate and silicon ions into the HA lattice remained as pure single phase HA as shown in the as-synthesized powders even after calcination at 500 to 700°C. The absence of (112) Miller's plane, which usually appears on a standard HA diffraction pattern is typically attributed to the substitution of the ions into the HA structure (He et al. 2007). The formation of secondary phase of CaO or CaCO_3 which normally resulted after the heat treatment of substituted-HA powders in particular the carbonate-substituted HA at temperature above 750°C in air atmosphere (Gibson & Bonfield 2002), was effectively prevented with slightly lower calcination temperature used. Regardless of the powder formulation, increasing the calcination temperature has resulted in increased crystallite size of the powders. This could easily be explained as higher calcination temperature leads to an increase in the atomic mobility, which gives rise in the grain growth resulting in a larger crystallite size.

The IR spectrum shows a clear comparison between CHA, SiHA and SiCHA after calcination. Both SiCHA as-calcined powders demonstrated similar characteristics with missing bands of carbonate and silicon ions at 870-875 cm^{-1} and 947 cm^{-1} , which is one of the typical bands of B-type CHA and Si-substituted HA, respectively. The two main carbonate bands detected in SiCHA powders calcined at 500 to 700°C belongs to the B-type CHA (Koutsopoulos 2002; Landi et al. 2010), besides the Si-substituted bands detected at 880-895 cm^{-1} (Sprio et al. 2008; Marchat et al. 2013). The main characteristic

bands of the typical carbonate and Si-substituted HA are highlighted in Fig 3.10-3.11 (inset expanded region of whole spectra). The FTIR results as listed in Table 3.8 precisely indicated the mode of ion substitutions in the apatite structure. It is clear that the missing bands in SiCHA powders provide evidence of the competitive substitutions between the carbonate and silicon ions into the phosphate sites. This provides important information regarding the simultaneous ionic substitution after calcination.

The low calcination temperature used in this work allow the powders to remain as B-type CHA and not transforming from B-type to more complex mixture of AB-type or A-type CHA. This phase transformation normally occurs when as-synthesized powders are heat treated between 700-1200°C (LeGeros et al. 1969; Gibson & Bonfield 2001; Lafon et al. 2008). This indicated that the as-calcined powders produced in this study are thermally stable up to 700°C.

Surprisingly, carbonate-free substituted HA (SiHA) powders shows an increment in the percentage of carbonate as the calcination temperature increased. At 700°C, SiHA powders contain up to three times as much carbonate compared to the as-synthesized powders. However, the carbonate presents in the SiHA powders was not detected in the IR spectra. This means that the CO₂ from the atmosphere was absorbed only on the surface of the powders during calcination and not incorporated in the crystal structure. As mentioned earlier, this small amount of CO₃ in SiHA might be due to the presence of acetate group that would have remained from the silicon acetate precursor Gibson et al. (2002). In order to prevent any carbonation in the SiHA structure, the calcination of the powders could be performed in argon atmosphere instead of ambient condition (David et al. 2013). However, it should be noted that a CO₂ atmosphere can be beneficial during calcination of carbonate-

substituted HA powders, in order to retain the substituted carbonate in the apatite structure, avoiding phase decomposition Boyer et al. (2013).

The surface morphologies of the optimised powders show a significant difference in the particle size and shape. This discrepancy is thought to be due to the differences in ionic substitutions. The presence of high carbonate concentrations in the CHA powders caused the powders to be more spherical; which is a similar observation made by Zhou et al. (2008). On the other hand, SiHA powders possess more elongated and larger particle size with about 80-100 nm in length. The multi-substituted HA (SiCHA-1 and SiCHA-2) powders produced in this study perfectly matched the dimensions of the biological apatite with particle sizes falling in the range of 30-50 nm in length and 15-30 nm in width (Wang et al. 2006). It is important to ensure that the powders produced are at the nanoscale level in particular for bone tissue engineering applications as it directly affects the mechanical and biological performances of the end products. It was shown in other studies that nanoparticles are used as to ensure the optimum strength and maximum tolerance to flaws. Furthermore, nanoparticle apatite has been shown to have a good influence on a variety of metabolic functions and remodelling processes (Dorozhkin 2009). For instance, *in vitro* tests of fibroblast and osteoblasts cells on the nanocrystalline octacalcium phosphate phosphate (OCP) coatings, proved that both cell types could adhered, formed a normal morphology, proliferated and remained viable, thus supporting a good biocompatibility and absence of any toxicity effects.

3.3.3. *In vitro* biocompatibility assessments of the optimum as-calcined powders

The optimum as-calcined powders were then tested *in vitro* using human MSCs. The aim of the last part in this study was to determine the highly osteoconductive powders formulation for use as biomedical material in bone tissue engineering applications. In this case, the most osteoconductive powders formulation can be defined as powders that can allow the fastest cell proliferation, produced the highest proteinaceous material and the ability to stimulate rapid osteogenic differentiation of the hMSCs over 21 days culture period.

Despite their composition, no sign of toxicity was evident from any of the powders using a direct contact method with hMSCs. It was previously reported that the toxicity of a material is mainly caused by either the release of ions or compounds, or worn debris from the ceramic material itself (Li et al. 1993). In the present finding, we observed that the cells in direct contact with SiCHA-1 powders were less confluent than on other powders at each time-point. This is due to the ions released from SiCHA-1 powders as it contains the highest silicon content among them. The release of the silicon ions in high proportions might have caused some cell death at the early stage of culture, which resulted in a slight loss of cells (Landi et al. 2010). As a consequence, the population of the viable cells in direct contact with SiCHA-1 remains low at every time point. However, <30% of cell death were found on all the exposed powders at 21 days. According to ISO 10993-5, a reduction of more than 30% viability is considered as cytotoxic. Thus, SiCHA-1 prepared in this study is considered as non-toxic, but is hindering the proliferation of hMSCs. Similar observation was reported by Landi et al. (2010) in their finding, where 0.8wt% Si in SiCHA powders caused a toxic effect on the human osteoblast cells, while SiCHA powders with lower Si content (0.55wt%) inhibited the proliferation of human osteoblast,

but after 7 days of culture, powders were not considered to be toxic. The higher the Si content incorporated in the HA structure, the higher the cell death. This is due to higher ion release as powders with high Si content have higher solubility (Lin et al. 2006; Ni et al. 2007). In this work, SiCHA-2 which contain <0.55wt% Si shows higher cell viability compared to SiCHA-1 with >0.55wt% Si. This observation is in agreement to the finding demonstrated by Landi et al. (2010) where although no toxicity effect found with the present of 0.55wt% Si in SiCHA powders, the cells proliferation was impeded.

The quantity of DNA was used to indicate an increase in cell population. Results supported the observations of cell viability, identifying that SiCHA-2 powders outperformed other powders at all time-points in terms of DNA quantity and viability. In contrast, SiCHA-1 with highest Si-substituted HA shows the lowest level of DNA throughout the culture. This negative behaviour of SiCHA-1 was apparently in contrast with the previous study reported in the literature (Botelho et al. 2006; Pietak et al. 2007), where good interaction of human osteoblasts was found as in contact with high Si-substituted HA (0.8wt%). The discrepancy in the results is due to different nature of the tested materials. For instance, the work conducted by Botelho et al. (2006) was based on dense, sintered SiHA pellets. Thus, the solubility-reactivity and the extent of the biomaterial-cell interactive surface were remarkably lower as compared to that of a powdered form (Landi et al. 2010).

After 21 days culture, SiCHA-2 shows the highest level of ALP/DNA ratio, which indicates the powder may stimulate osteogenic behaviour to greater extent than other powders. Botelho et al. (2006) found a similar behaviour up to 21 days and decreased in the ratio of ALP/COL I after 27 days treatment, which was related to the onset of mineralization. However, the later trend was not observed in this study as the powders

were tested only for 21 days. Further work in the future, including immunostaining, qPCR and flow cytometry would provide better indications for the osteogenic bone markers.

Carbonate-substituted HA appeared to perform better than other powders in the production of total protein after 21 days culture. This indicated that hMSCs were the most metabolically active when in contact with CHA powders. An increasing carbonate content resulted in higher metabolic activity of the particular cells/tissues as stated in the literature (Gibson et al. 1999). For instance, bone, which is very active tissue contained higher carbonate compared to almost inert enamel (LeGeros 1991; Boanini et al. 2010, Landi et al. 2010). This explained the underlying reason for the highest level of total protein produced by CHA powders, as it possesses the highest percentage of carbonate content among the investigated powders. Comparing the multi-substituted HA powders, SiCHA-2 shows relatively higher protein production than SiCHA-1. This is related to the cell number as represented by the amount of DNA obtained. Essentially, as the cell population increases in size so does the quantity of total protein. In addition, SiCHA-2 powders contained higher carbonate content as compared to SiCHA-1. Alamar blue results correlate with the total protein levels observed. This assay is typically used to evaluate cell viability and proliferation, which could be an indicator of the cell metabolic activity (Rodrigues et al. 2013). hMSCs were found to be more metabolically active as in contact with 0.45wt% Si (SiCHA-2) than 0.58wt% Si (SiCHA-1). This is in agreement with the previous study reported by Gibson et al. (1999) where higher metabolic activity was found as osteosarcoma cells were seeded on 0.8wt% SiHA than 1.6wt% SiHA and HA (Gibson et al. 1999).

At this stage of study, only one batch of the prepared powders was used for the *in vitro* biocompatibility test due to time limitation. Ideally, the test should be performed using

different batches of powders in order to ensure the reproducibility and repeatability of powder production. Besides, all different compositions of the prepared powders in this work should be tested for their *in vitro* biocompatibility in order to select the ideal powder formulation. For this particular study, the cell source used was only from one donor due to cost and time limitations. However, to fully meet the requirements of ISO 10993-5, several cell donors ($n=3$) should be used to test different batches of the prepared powders in the future.

3.4. Conclusion

The osteoblast behaviour are directly linked to the rate and amount of ions released by the multi-substituted HA structure, which in turn depends on the physico-chemical properties of the material. The solubility-reactivity and biomaterial-cell interactive surfaces are two key points in determining the cell survival and response. Thus, controlled amounts of the ionic substitutions into the apatite structure are mandatory in order to promote the desired osteoblast behaviour. In this study, powders with 3.98wt% carbonate and 0.45wt% Si-substituted HA namely, SiCHA-2, shows the closest compositions to the physiological range of ionic substitutions in bone mineral, thus, make it the most favourable growth environment for hMSCs up to 21 days culture *in vitro*. These powders were associated with the most rapid proliferation of cells showed the strongest potential for osteogenic activity (ALP/DNA ratio). hMSCs also produced more proteinaceous material and were most metabolically active in direct contact with SiCHA-2 as compared to SiCHA-1. It can be concluded at this point that, among the tested powders, SiCHA-2 was the best powder formulation and that it was suitable for the next phase in the development of a novel 3D multi-substituted HA scaffold for BTE.

Chapter 4

Development of novel coating materials assembly on Poly (lactic acid) (PLA) films to enhance cell- material interaction

4.1. Introduction

Poly (α -hydroxyl ester) in particular, poly (lactic acid) (PLA) has been used as a substrate material to support the regeneration of different tissues and organs, such as bone and articular cartilage (Chen et al. 2008; Zhao et al. 2014). It is non-toxic, possess low level of immunogenic reaction, have easily tailored mechanical properties and predictable degradation rates (Suh et al. 2001). However, the application of PLA in the biomedical field is hampered to a certain extent by its hydrophobic nature and lack of cell recognition, i.e. poor cell adhesion and proliferation (Kim et al. 2006; Jahno et al. 2007). As tissue engineering (TE) scaffolds and implants interact with the biological environment via their surface, modification on the outermost surface of the materials was considered as an effective approach (Tzoneva et al. 2008). The main aim in surface modification of a polymer substrate is to provide a surface with reactive group such as -OH, -NH₂ and -COOH to permit binding with biomolecules (Soldana et al. 1991; Yamauchi et al. 1991; Okada & Ikada, 1991; Suh et al. 1998).

Human bone is a complex organic and inorganic composite material, in which biomacromolecules such as collagen type I, proteoglycans and carbonate substituted hydroxyapatite (CHA) nanocrystals are well organized into hierarchical architecture (Liao et al. 2005). The ideal bone scaffolds designed to enhance the bone formation should closely mimic the naturally occurring environment in the bone matrix. These biomacromolecules could then form physical or chemical cross-linked networks, which regulates the expression of osteoblastic phenotype and supports osteogenesis both *in vitro* and *in vivo* (Datta et al. 2005; Yu et al. 2012). Therefore, ECM-like biomacromolecules such as hyaluronic acid or collagen type I have been incorporated into the 3D scaffolds for bone regeneration besides CHA nanocrystals (Zhang et al. 2005; Yu et al. 2012; Hoyer et

al. 2012). Since our bone comprises of both osteoconductive (CHA nanocrystals) and osteoinductive (collagen type I) components, thus, bone scaffold fabricated from such components is likely to behave in similar way as natural bone, and to be of more use compared to a monolithic scaffold (either collagen type I or CHA alone) (Wahl & Czernuszka 2006). Indeed, both collagen type I and HA as monolithic scaffold were found to enhance osteogenesis, but the combination of both collagen type I and HA as composite scaffolds has successfully accelerated osteogenic differentiation as compared to the monolithic scaffolds (Xie et al. 2004).

Therefore, the overall aim of this thesis was to fabricate a novel 3DP hybrid scaffolds, which consists of SiCHA nanocrystals, collagen type I and hyaluronic acid as a mean to fabricate an ideal bone scaffolds in order to enhance bone formation. Prior to the construction of 3DP hybrid scaffolds, the fabrication technique used in this work was firstly investigated on two-dimensional (2D) PLA films. The assembly of the ECM-like biomacromolecules onto the charged PLA film was performed using PEMs technique adapted from Zhao et al. (2014) with some modification. Hyaluronan and collagen type I were chosen as the building blocks, which acts as the carrier for the SiCHA nanopowders to be deposited on the PLA films. These polyelectrolytes helped SiCHA nanopowders to chemically bind onto the surface. Hyaluronic acid or hyaluronan is a major component in ECM and synovial fluid. It is one of the polyanions, which has been widely used in PEMs assembly (Khademhosseini et al. 2004; Zhang et al. 2005). Collagen type I is positively charged below the isoelectric point, which allows it to be used as the polycation (Zhang et al. 2005). In this study, the bilayers were finally cross-linked with and without 1-ethyl-3-(3-dimethylaminopropyl) carbodiimide hydrochloride (EDC) and N-hydroxysulfosuccinimide sodium salt (NHS) as to maximize the coating materials deposition. PLA films were coated with different number of layers followed by physical

and chemical/elemental characterizations. *In vitro* studies using human bone marrow-derived mesenchymal stem cells (hMSCs) were performed to investigate the most favourable environment for cell-material interaction, which was then selected as the optimal condition. This optimal condition was then applied in the similar manner for the fabrication of 3DP hybrid scaffolds, which will be discussed in the next chapter.

4.2. Results

4.2.1. Investigation of the novel coating materials on PLA films

Scanning electron microscopy (SEM) analysis was used to inspect the PLA films before and after surface modification. The films exhibited a smooth surface morphology before chemical modification was performed. However, post-aminolysis, the films demonstrated a rougher surface topography (Fig. 4.1). The chemically modified PLA films were deposited with one bilayer of the newly developed materials with and without the presence of EDC/NHS coupling agent. After one bilayer, PLA films with EDC/NHS surface finish (1-BL) resulted in better deposition of coating materials as compared to coated PLA films without the coupling agent (1-BL*). It was observed that without the use of the coupling agent, agglomeration of SiCHA nanopowders occurred. This agglomeration was not seen when the coupling agent was used. Essentially, the coupling agent was associated with a more homogenous distribution of the nanopowders on the surface of the PLA films.

Based from the morphological characterization, novel coating materials assembly for PEMs technique was established in this work. This coating assembly involves the dispersion of SiCHA nanopowders in two different polyelectrolytes, namely hyaluronan and collagen type I. The PEMs were finally cross-linked with EDC/NHS as the surface finish for each bilayer. To our knowledge this coating materials has not been reported anywhere else in the literature.

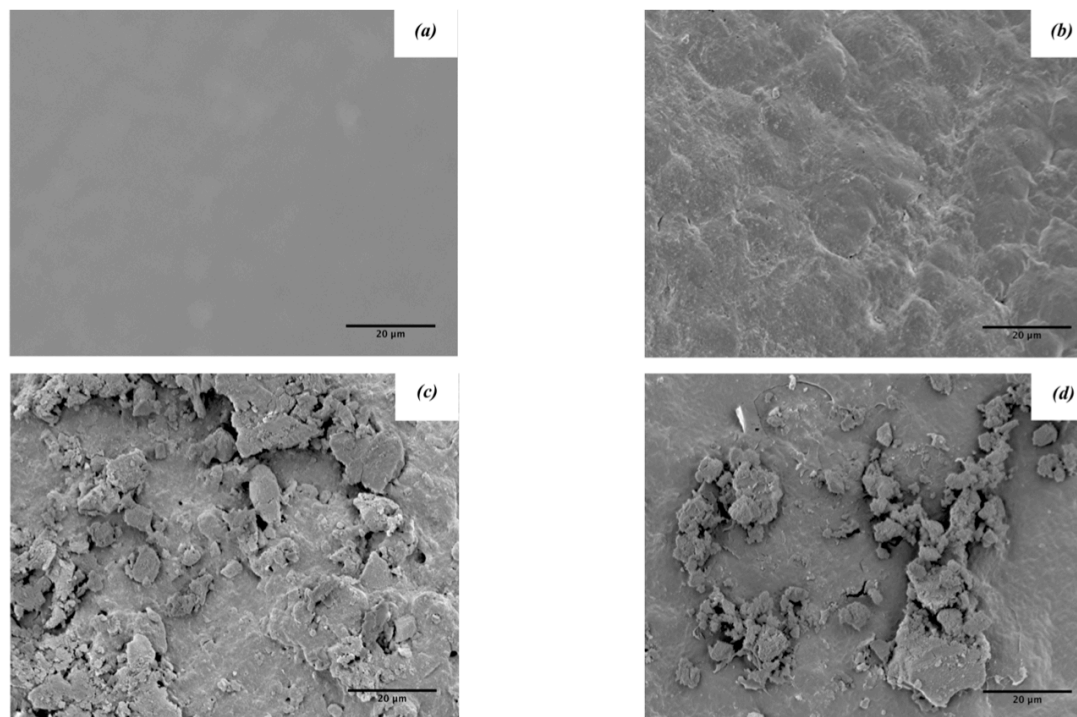


Fig. 4.1: Surface topography of the PLA films was assessed using SEM analysis. Images demonstrated different PLA surfaces, (a) control PLA (0-BL), (b) aminolyzed PLA (0-BL), (c) coated PLA with EDC/NHS coupling agent (1-BL) and (d) coated PLA without EDC/NHS coupling agent (1-BL*). The surface of 1-BL PLA films was homogenously covered with coating materials whereas, localized agglomeration of the SiCHA nanopowders formed on 1-BL* PLA films. Scale bar = 20 µm.*

4.2.2. Optimization on the number of deposition cycles

4.2.2.1. Atomic Force Microscopy analysis

The surface morphology of biomaterials plays an important role on cell attachment, proliferation and function. The changes in surface topography during PEMs process were investigated by atomic force microscopy (AFM) analysis. The surface roughness of the control and coated PLA films were measured by AFM. There was a slight difference between the roughness of the whole film and individual, localized areas on each film.

In general, the surface roughness increased with increasing number of layers up to 5-BL. The surface roughness of 1-BL PLA films was approximately twice as rough relative to the unmodified control PLA films. However, only a slight increase in surface roughness was observed after the third alternate deposition of the coating materials. Further deposition (>5-BL) resulted in a small drop in surface roughness.

Table 4.1: Surface roughness of PLA films measured on the control PLA (0-BL) and coated PLA with 1-, 3-, 5- and 10-BL, respectively.

<i>Surface roughness/ Samples</i>	<i>Whole area (nm)</i>	<i>Localized areas (nm)</i>
0-BL	52.83 ± 0.71	50.11 ± 0.91
1-BL	98.97 ± 0.97	96.48 ± 1.47
3-BL	177.33 ± 1.53	175.18 ± 2.71
5-BL	208.13 ± 0.80	214.98 ± 3.36
10-BL	186.37 ± 0.86	184.40 ± 2.10

Note: Surface roughness of the whole area was measured on each PLA films (n=3) and localized areas represent the mean of five different spots on each PLA films.

AFM topography results shown in Fig. 4.2 support the values measured for surface roughness shown in Table 4.1. The colour gradient indicates the surface roughness where dark red and light yellow represented the rough and smooth areas, respectively. It is assumed that, the rougher the surface area, the higher the percentage of coating materials deposited. After 3 deposition cycles, about 70-80% of the surface area of the films were covered with the coating materials (Fig. 4.2 c). At the end of 5 deposition cycles, the surface coverage increased to more than 90% of the entire films. However, after 5 deposition cycles, little influence on the surface roughness was observed as shown in Fig. 4.2 (e). In fact, 10-BL films showed a slight decrease in the surface covered compared with 5-BL films.

AFM images were also used to investigate the homogeneity of the coating materials on the PLA films. It is clearly seen that the surface coverage of the coating materials designated by the rough surface area was not uniformly distributed throughout the entire surface. Surfaces with 3-BL and 5-BL seems to be the most homogeneously coated surface as compared to 1-BL and 10-BL coated PLA films. The distribution of coating materials deposited on the PLA films will be further characterized in the next section.

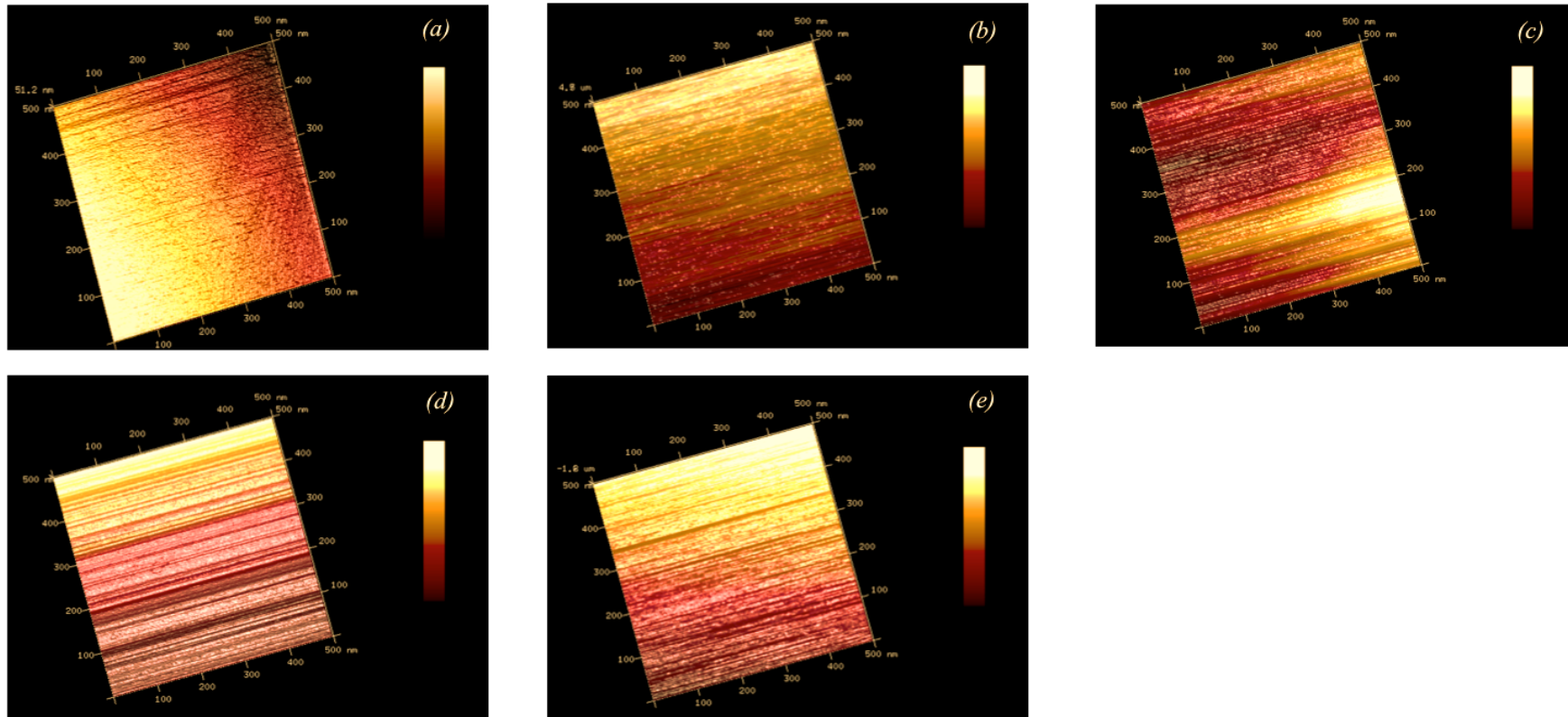


*Fig. 4.2: AFM images showing topography of (a) 0-BL; (b) 1-BL; (c) 3-BL; (d) 5-BL and (e) 10-BL PLA films. The surface roughness of the PLA films increased with increasing number of coating layers as represented by the changes of the colour bar. *Dark red = rough area and light yellow = smooth area. AFM was performed in air using RTESPA tip of spring constant of 40 N/m, 896 scans/lines, 0.32 Hz scan rates, and 1.102 V amplitude.*

4.2.2.2. *Transmission electron microscopy analysis*

Representative transmission micrographs of the surface modified PLA films deposited with 1-, 3-, 5- and 10-BL layers are shown in Fig. 4.3. Transmission electron microscopy (TEM) demonstrated that the PLA films were covered with coating materials on the surface. The distribution of particles covering the surface increased with increasing number of layers. Coating materials were found to be more homogenous and well distributed on 5-BL layers as compared to the other coated films. Results were in agreement with the observation obtained from AFM analysis.

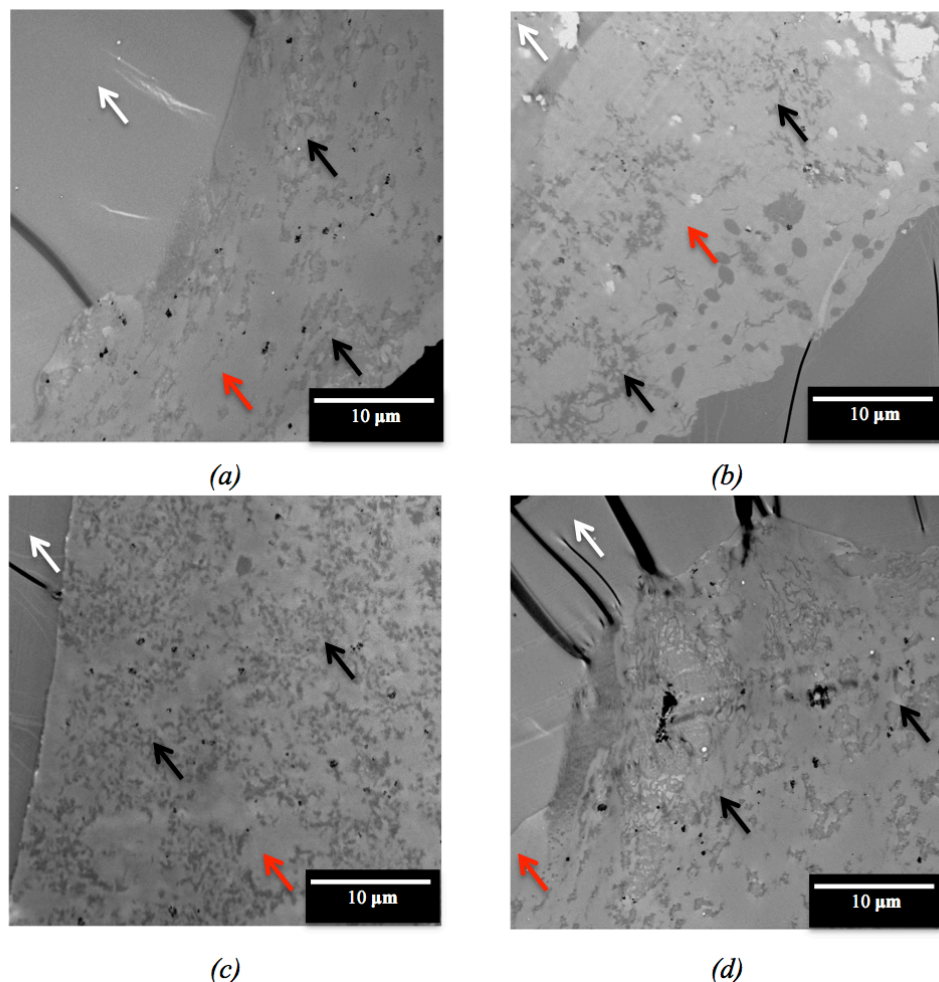


Fig. 4.3: TEM images of (a) 1-BL; (b) 3-BL; (c) 5-BL and (d) 10-BL. Red, black and white arrows on the images represent the coating materials, PLA film surface and background, correspondingly. Coating materials were found to be more homogeneously distributed on 5-BL layers compared to the other coated films. Scale bar = 10 μm.

4.2.2.3. *X-Ray Photoelectron Spectroscopy analysis*

X-Ray Photoelectron Spectroscopy (XPS) is an effective tool to confirm the formation of thin layer of coating materials deposited on the surfaces. This is achieved through the detection of the chemical composition represented by the specific peak for the elements that comprise the coating. Details on the element of interest and their respective binding energies were described in Chapter 2 (Table 2.4).

For control PLA (0-BL), only two main peaks appeared in the XPS spectra (Fig. 4.4 a), representing the elements of carbon and oxygen. These peaks were detected at binding energies of 288.9 and 533.0 eV; denoted the C1s and O1s, respectively. After surface modification (0-BL*), an additional elemental peak for nitrogen was detected at 400.0 eV as can be seen in Fig. 4.4 (b). Spectra associated with coated PLA films with 1-, 3-, 5- and 10-BL are represented in Fig. 4.5 (a-d). Two additional elemental peaks, which corresponded to calcium (Ca) and phosphorus (P), as expected for HA, were observed besides those associated with aminolyzed PLA films (Fig. 4.4 b). The intensity of the nitrogen peak increased with increasing number of bilayers coating on the surfaces; indicating more collagen deposited. However, the typical peak of silicon at binding energies of 101.0 eV was not observed. Thus, the atomic percentages of all the elements of interest on the modified PLA films were quantified (Table 4.2). The carbon content of the PLA film reduced from 77.7 at% (0-BL) to 74.6 at% (0-BL*). The increase in the number of layers has no obvious effect on the atomic percentage of carbon as compared to the aminolyzed PLA films. However, it was observed that the levels of Nitrogen (N1s) became relatively higher. Concurrently, higher calcium and phosphorus atomic percentages were observed with increasing number of layers. In addition, silicon was found to be present on the thin coating layer of the PLA films, despite the peak not being visible on the spectra (Fig. 4.5 a-d).

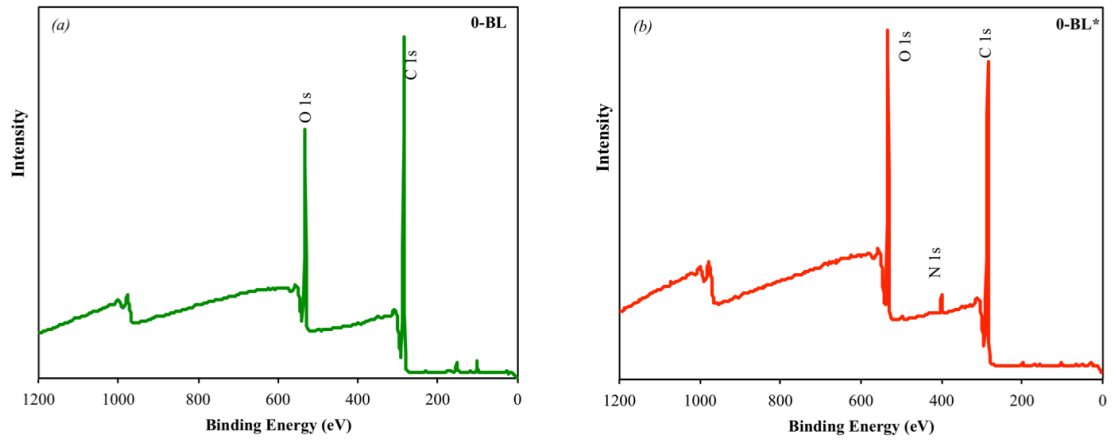


Fig. 4.4: XPS scan spectra of control PLA films, (a) before (0-BL) and (b) after (0-BL*) aminolysis. The peak intensity of the material detected on the surface is expressed in relation to the binding energy.

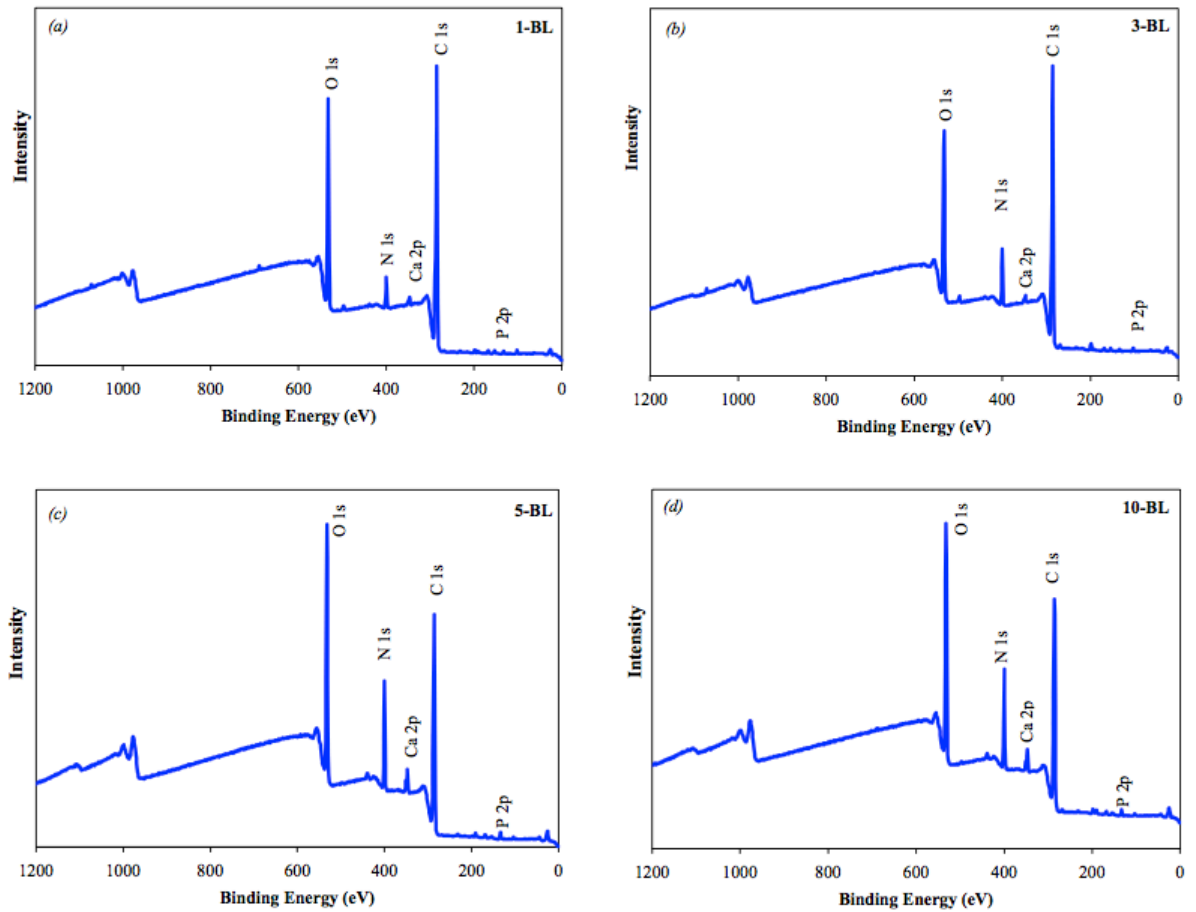


Fig. 4.5: XPS scan spectra of coated PLA films deposited with (a) 1-BL, (b) 3-BL, (c) 5-BL and (d) 10-BL, respectively.

Comparing the quantitative data within the coated PLA films, 10-BL demonstrated a slight drop in the atomic percentages of all the detected elements than 5-BL PLA films. The highest atomic percentages of calcium, phosphorus and silicon (which represent the chemical composition of the coating materials) were obtained on 5-BL PLA films.

Table 4.2: Atomic percentage (at%) of the control PLA (0-BL) and coated PLA with 1-, 3-, 5- and 10-BL, respectively.

<i>Samples</i>	<i>C_{1s}</i>	<i>O_{1s}</i>	<i>N_{1s}</i>	<i>Ca_{2p}</i>	<i>P_{2p}</i>	<i>Si_{2p}</i>
0-BL	77.74 ± 3.16	22.26 ± 3.16	-	-	-	-
0-BL*	74.62 ± 0.32	23.42 ± 0.34	1.96 ± 0.14	-	-	-
1-BL	73.83 ± 1.74	22.48 ± 1.54	2.07 ± 0.07	0.91 ± 0.03	0.47 ± 0.02	0.24 ± 0.18
3-BL	74.22 ± 1.12	19.19 ± 1.26	4.46 ± 0.51	1.21 ± 0.05	0.60 ± 0.02	0.32 ± 0.06
5-BL	74.09 ± 0.89	18.95 ± 0.66	4.92 ± 0.02	1.47 ± 0.05	1.12 ± 0.44	0.45 ± 0.26
10-BL	73.97 ± 0.97	18.86 ± 0.44	3.70 ± 0.34	1.39 ± 0.05	1.08 ± 0.05	0.42 ± 0.08

Note: values represent mean ± SD for n=3.

4.2.2.4. *Histochemical characterization of calcium and collagen deposition*

Qualitative histochemical methods were used to confirm the presence of both SiCHA nanopowders and collagen depositions on the PLA coated films. Alizarin Red (AR) staining is a commonly used histochemical technique to detect calcium deposits in mineralized tissue and cultures. In this study, AR staining was used to observe the distribution of calcium, which is the main component in SiCHA nanopowders on the PLA films with different numbers of multilayers. Positive AR staining (bright red) was obtained from all the coated PLA films as demonstrated in Fig. 4.6, indicative of the presence and distribution of calcium throughout the sample. More homogenous bright red stain was observed on the PLA film surface with increased deposition cycles as can be seen on 3-, 5- and 10-BL relative to 1-BL coated films.

The collagen deposition on the PLA films were quantified by Sirius Red (SR) staining (Rich & Whittaker 2005; Vandrovcová et al. 2011). The bright orange stain indicated a positive result for the presence of collagen. The brightness of the stain is directly proportional to the amount of collagen present within the multi-layered films (the same applies for AR stain and calcium content). All coated films demonstrated the presence of both calcium and collagen. With increasing number of multilayers deposited, brighter and more homogenous staining was apparent. For instance, after three deposition cycles, almost the whole surface area of the coated films was covered with the bright orange stain as showed in Fig. 4.6. No obvious differences in stain intensity were observed with increasing number of bilayers.

The control PLA films (0-BL), which were chemically unmodified shows the absence for both AR and SR staining. A distinct difference was observed between control and coated films; as neither calcium nor collagen was present on the control films. However, the

actual amount of calcium or collagen was not quantified, as the purpose of staining was to confirm the homogenous distribution of coating materials.

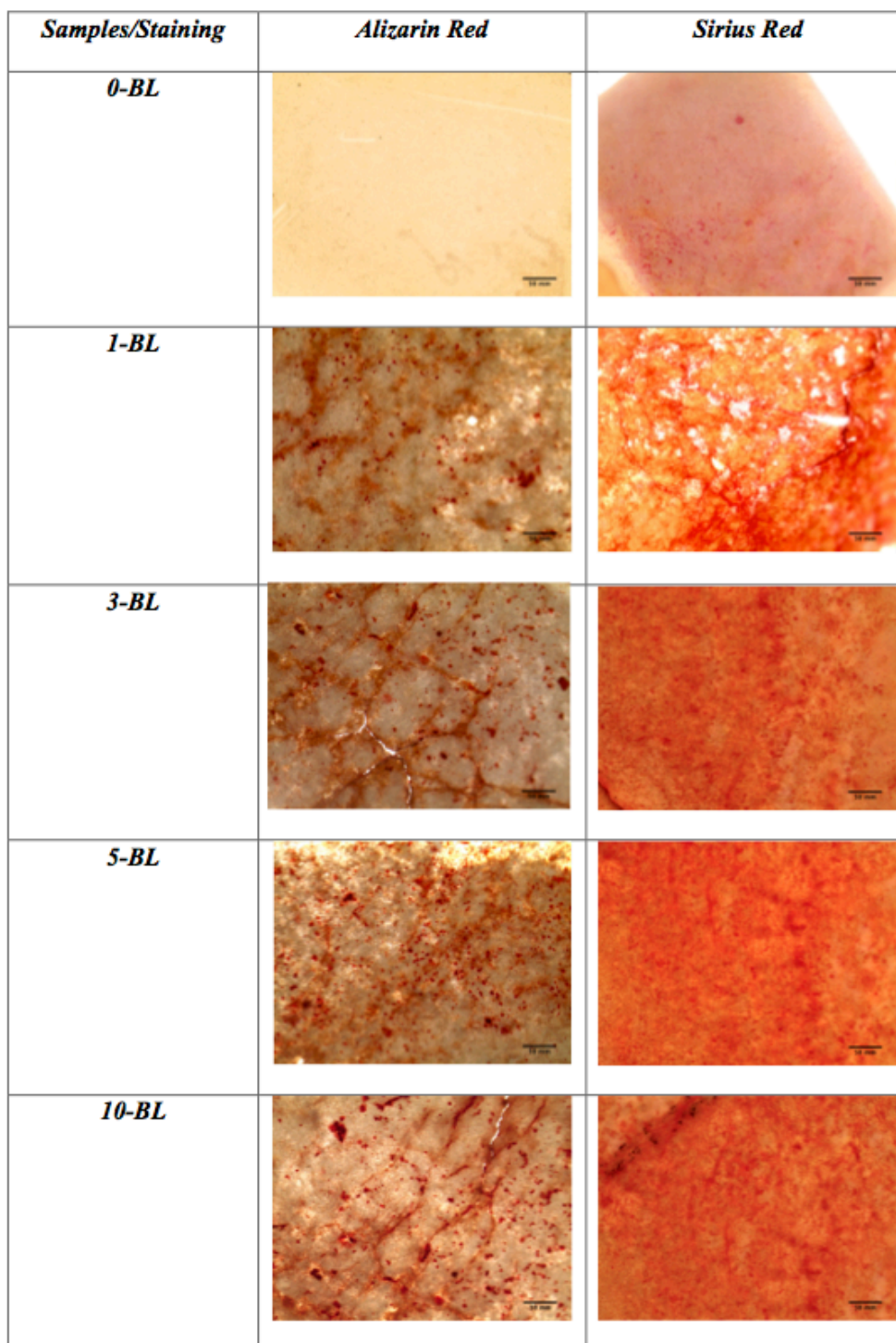


Fig. 4.6: Light microscopy imaging of Alizarin Red (AR) and Sirius Red (SR) Staining on 0-, 1-, 3-, 5- and 10-BL films. All coated PLA films showed positive stains for both AR and SR and the amount of stained material appeared to increase with the increasing number of layer, up to 5-BL. Scale bar = 50 μ m.

4.2.3. *In vitro* biocompatibility test

4.2.3.1. *Cell viability*

The viability of hMSCs seeded on different surfaces of the PLA films was observed after 7 and 14 days of culture, as shown in Fig. 4.7. Confocal Laser Scanning Microscopy (CLSM) images demonstrated that cells were homogeneously distributed on the surface of all coated PLA films. On the other hand, the cell density appeared to be considerably lower on unmodified, control PLA films, relative their coated counterparts.

CLSM images also indicate diverse proliferation ability of hMSCs as a function of number of multilayers deposition. The proliferation of hMSCs onto the modified PLA films with the newly developed coating materials assembly were greatly augmented compared to the unmodified PLA films (0-BL). In addition, cellular proliferation was considerably enhanced with the number of deposited multilayers. Close observation on the CLSM images suggested that 5-BL PLA films revealed the highest proportion of cell attached and proliferated onto the surface after 7 days in culture.

Over the culture period of 14 days, hMSCs seeded on the coated films reached confluence regardless the deposition cycles applied to the PLA films. Very few dead cells (stained red) were found on any of the PLA films including the control. However, cells seeded on the control PLA films were associated with a slower proliferation rate as fewer cells found on the surface compared to the coated PLA films. These results clearly highlighted that all the modified PLA films could effectively increase the cell viability, proliferation and provide better surface for efficient cell adhesion as compared to the control PLA films.

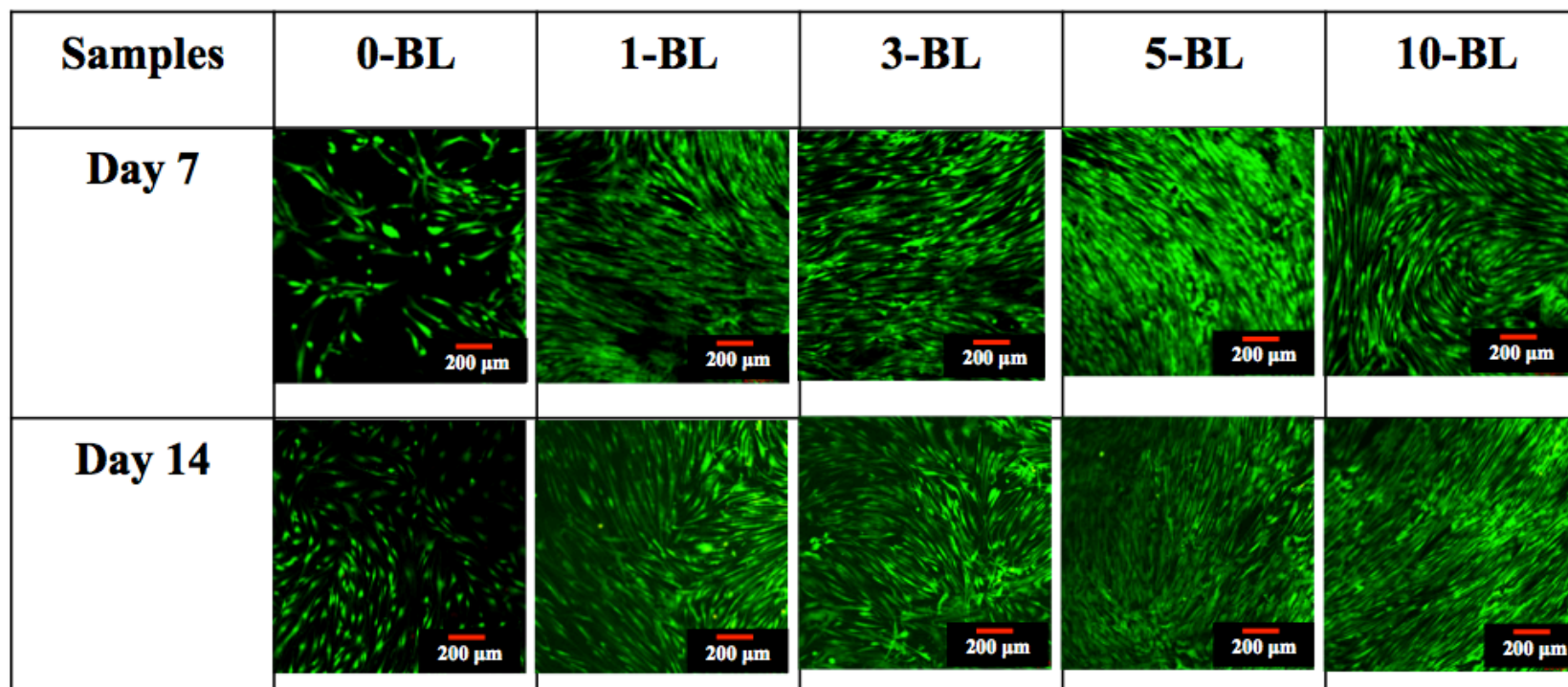


Fig. 4.7: CLSM images of control and coated PLA films. Cell viability of hMSCs cultured on different PLA surfaces namely the control (0-BL) and coated PLA films deposited with 1-, 3-, 5-, and 10-BL on 1 mm X 1 mm PLA films. Scale bar = 200 μ m.

4.2.3.2. *Cell proliferation and differentiation*

The extent of cell proliferation was estimated by DNA quantification. Overall, the deposition of the innovative coating materials assembly on the PLA films resulted in increased cell proliferation over the culture period ($p \leq 0.0001$) and differed between the coated films ($p \leq 0.0001$). There was a significant interaction between time and coated film ($p \leq 0.05$) suggesting that the increase in DNA concentration over time differed between coated films.

Compared to the control (non-coated PLA films), cells cultured on all coated films demonstrated significantly increased DNA content at day 7 and day 14 ($p \leq 0.0001$ for each). No significant differences were observed in the cell proliferation of hMSCs seeded on the control PLA films over the culture period ($p = 0.9999$), as shown in Fig. 4.8.

Among the coated films, hMSCs cultured on 5-BL coated films showed the highest DNA concentration at each time-point ($p \leq 0.0001$). Cells cultured on 10-BL showed no significant differences in DNA content as compared to 3-BL coated films at 7 days ($p = 0.062$) but significantly higher on 14 days ($p = 0.0013$). No significant differences were observed in the cell proliferation of hMSCs seeded on 1-BL and 3-BL coated films on day 14 ($p = 0.9981$).

Overall, the highest DNA contents were obtained by culturing hMSCs in direct contact with 5-BL coated films compared to all tested films (non-coated and coated films) on day 7 and day 14 ($p \leq 0.0001$ for each).

The early osteogenic differentiation of the hMSCs cultured on the control (non-coated) and coated PLA films was assessed by measuring their ALP activity after culturing for 7 and 14 days in proliferation media. The ALP activity shown in Fig. 4.9 represented the values of ALP normalised to DNA concentration. The mean ALP activity of all the investigated films significantly increased over time ($p \leq 0.0001$) and differed between films ($p \leq 0.0001$). There was a significant interaction between time and all the investigated films ($p \leq 0.05$) suggesting that the increase in ALP activity over time differed between these films.

Regardless of the number of deposition cycles on the PLA films, significantly higher levels of mean ALP activity were obtained when hMSCs were cultured on the coated films than the control (non-coated films) on day 7 and day 14 ($p \leq 0.0001$ for each).

When comparing the coated films with each other, the highest levels of mean ALP activity were found when cells were cultured on 5-BL coated films at each time-point ($p \leq 0.0001$). At 7 days, the mean ALP activity of cells cultured on 3-BL coated films was statistically higher than those on 1-BL ($p = 0.0005$) and this trend was also observed on 14 days ($p \leq 0.0001$). Cells cultured on 10-BL revealed statistically higher level of mean ALP activity than those on 3-BL films after 14 days ($p = 0.0036$), although no significant differences were detected on day 7 ($p = 0.1892$).

Overall, hMSCs cultured on 5-BL coated films exhibited the highest levels of mean ALP activity on day 7 and 14 ($p \leq 0.0001$ for each) as compared to all other tested films (non-coated and coated PLA films).

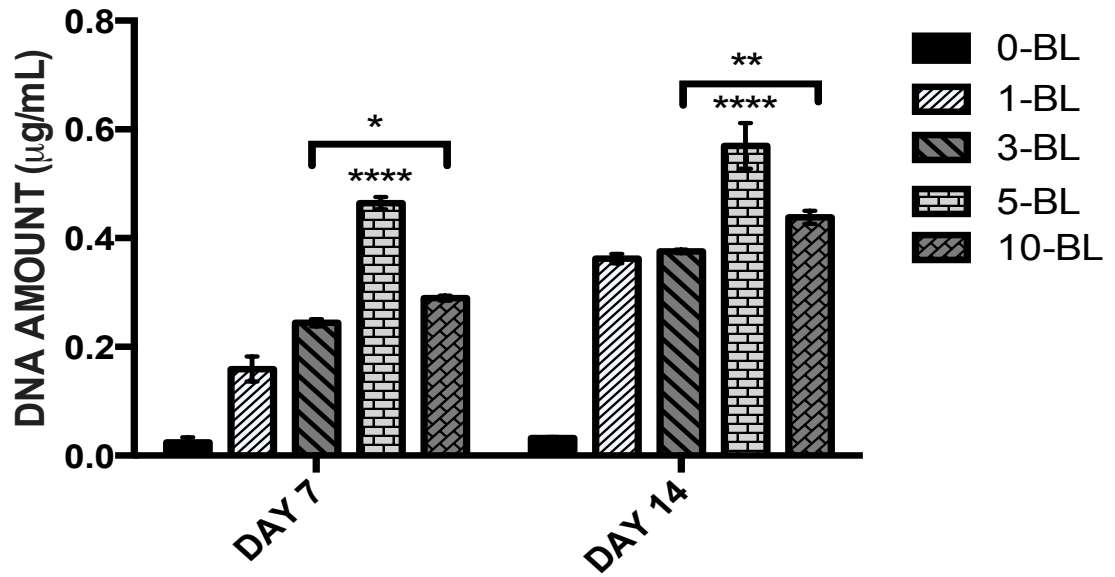


Fig. 4.8: Cell proliferation of hMSCs indicated by the DNA contents after 7 and 14 days cultured on control PLA (0-BL) and PLA films deposited with different number of coating layers of 1-, 3-, 5- and 10-BL, respectively. 5-BL shows significantly higher DNA concentrations after 7 and 14 days in culture compared to other films ($p \leq 0.0001$). Regardless of the number of deposition cycles, cells seeded on all coated films demonstrated significant increased in the DNA concentration from day 7 to day 14 ($p \leq 0.0001$). Cells cultured on control PLA films showed no significant differences over time ($p = 0.9999$).

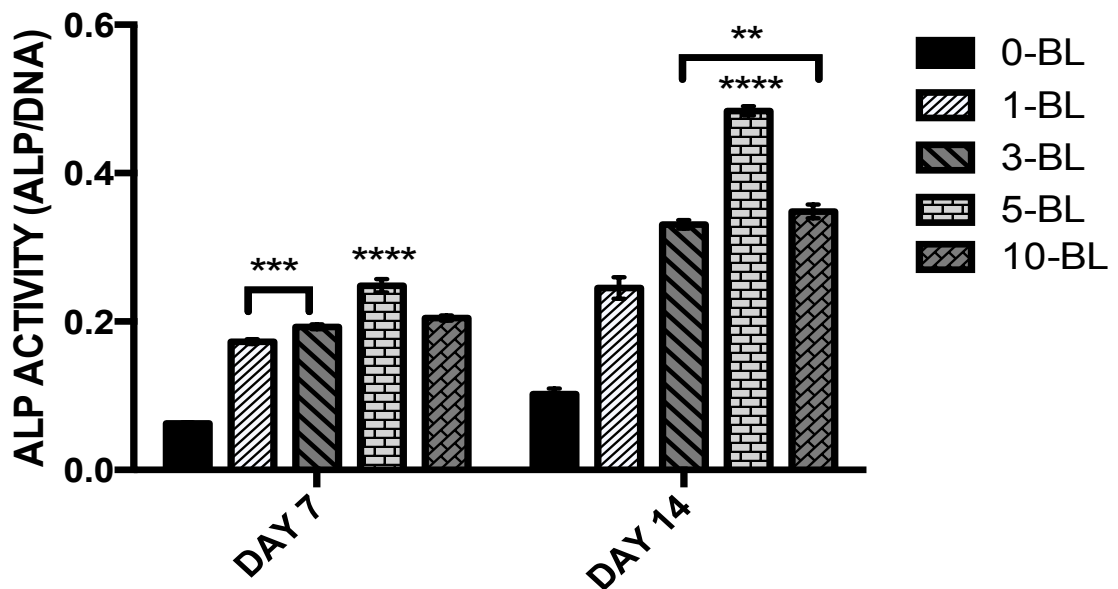


Fig. 4.9: The ALP activity of hMSCs seeded on control PLA (0-BL) and PLA films deposited with different number of coating layers of 1-, 3-, 5- and 10-BL, respectively. The highest levels of ALP activity were found when cells were cultured on 5-BL films ($p \leq 0.0001$). Cells cultured on 3-BL and 10-BL films showed no significant differences after 7 days ($p = 0.1892$) but as culture progressed, cells cultured on 10-BL revealed statistically higher levels of ALP activity ($p = 0.036$).

The levels of total protein produced by hMSCs cultured on control PLA (0-BL) and PLA films deposited with different number of coating layers of 1-, 3-, 5- and 10-BL, respectively are shown in Fig. 4.10. The levels of total protein production steadily increased over the culture period for all the coated PLA films ($p \leq 0.0001$) and differed between these films ($p \leq 0.0001$). There was a significant interaction between time and all the coated films ($p \leq 0.05$) suggesting that the increase in total protein over time differed between these films.

Compared to the control (non-coated PLA films), cells cultured on all coated films demonstrated significantly increased levels of mean total protein production at day 7 and day 14 ($p \leq 0.0001$ for each). However, hMSCs cultured on the control PLA films showed no significant differences in the levels of total protein produced as culture progressed ($p = 0.1367$).

When comparing the coated films with each other, no significant differences were observed when hMSCs were cultured on 5-BL and 10-BL coated films at day 7 ($p = 0.8486$). As culture progressed, significantly increased levels of mean total protein was observed on 5-BL compared to 10-BL on day 14 ($p = 0.0005$). At early 7 days of culture, higher levels of total protein produced when cells were cultured on 3-BL than 1-BL ($p = 0.0031$), but significantly higher levels of mean total protein produced on 10-BL compared 3-BL ($p = 0.0001$).

Overall, hMSCs cultured on 5-BL coated film produced the highest levels of mean total protein on day 14 ($p \leq 0.0001$ for each) compared to all other tested films (non-coated and coated films).

4.2.3.3. *Cell metabolic activity*

The metabolic activity of hMSCs on control and coated PLA films after 7 and 14 days was measured using the alamar blue assay (Fig. 4.11). Over time, hMSCs in direct contact with coated films showed significant increase in the levels of alamar blue ($p \leq 0.0001$) and differed between these films ($p \leq 0.0001$). There was a significant interaction between time and all the coated films ($p \leq 0.05$) suggesting that the increase in alamar blue over time differed between these films.

Compared to the control (non-coated PLA films), cells were found to be more metabolically active on the coated films independent of the number of deposition cycles at both time-points ($p \leq 0.0001$ for each).

When comparing the coated films with each other, increasing number of deposition cycles on the PLA films resulted in higher levels of alamar blue at each all time-points ($p \leq 0.0001$ for each). At 7 days, cells cultured on 10-BL showed statistically higher level of metabolic activity than those on 5-BL ($p = 0.0046$). However, after 14 days in culture, hMSCs showed no significant differences in the metabolic activity when cultured on 5-BL and 10-BL films ($p = 0.9920$).

Overall, the highest levels of alamar blue were obtained when cells were cultured on 5-BL and 10-BL on day 14 ($p \leq 0.0001$ for each) as compared to all other tested films (non-coated and coated films).

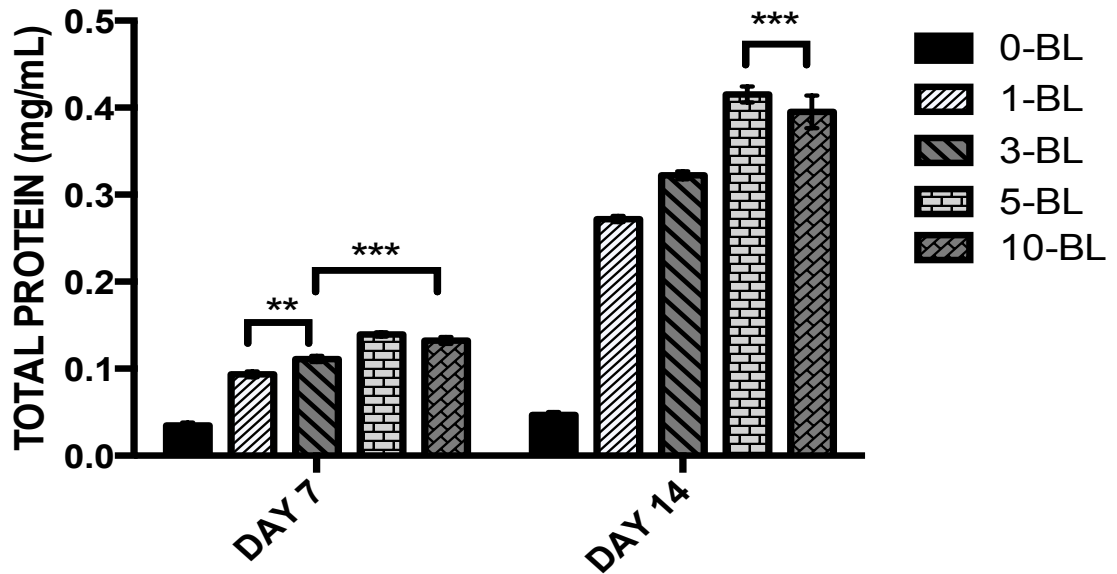


Fig. 4.10: The levels of total protein produced by hMSCs cultured on control PLA (0-BL) and PLA films deposited with different number of coating layers of 1-, 3-, 5- and 10-BL, respectively. The levels of total protein production steadily increased over the culture period for all the coated PLA films ($p \leq 0.0001$). After 7 days, no significant differences were found when cells were cultured on 5-BL and 10-BL films ($p = 0.8486$). As culture progressed, more total protein produced by hMSCs on 5-BL films compared to those cultured on 10-BL ($p \leq 0.001$).

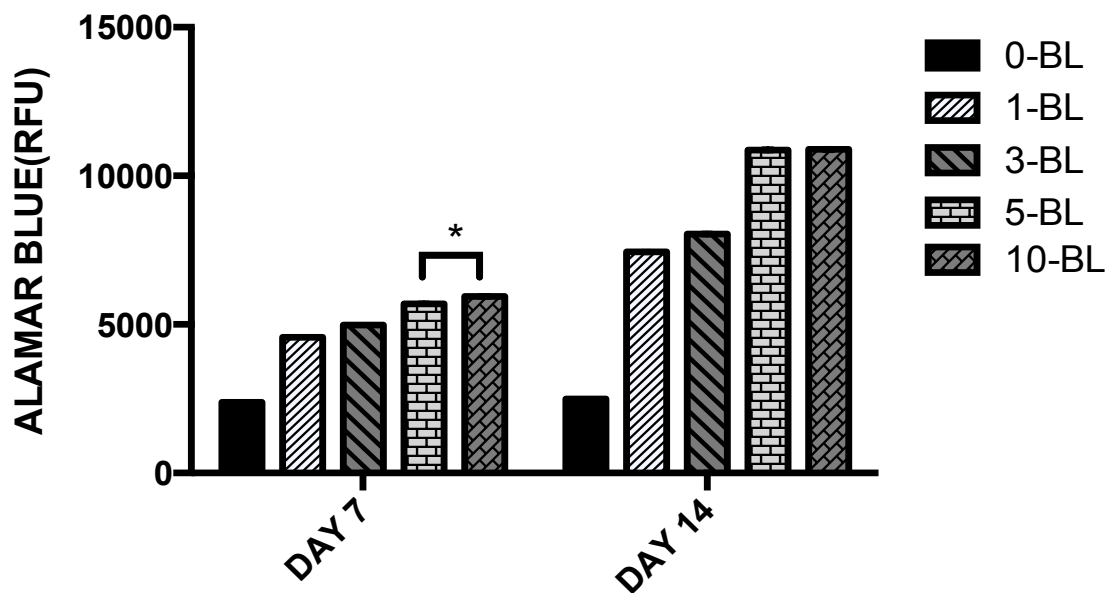


Fig. 4.11: Metabolic activity of hMSCs seeded on control and coated PLA films at 7 and 14 days of culture. The levels of alamar blue of hMSCs on all coated films were found to be statistically higher than the control after 7 days with cells seeded on 10-BL shows the highest levels of alamar blue. After 14 days, no significant differences were observed on the levels of alamar blue of hMSCs cultured on 5-BL and 10-BL films ($p = 0.9920$).

4.3. Discussion

4.3.1. The effect of coupling agent in PEMs assembly

In the current study, novel coating materials assembly for PEMs technique has been established. To our knowledge, this combination of coating materials assembly has not been reported anywhere else in the literature. The rationale underpinning the selection of this coating materials assembly was to closely mimic the bone composition and ECM environment. The novel multi-substituted HA (SiCHA) nanopowders used in this work possess similar composition to the mineral content of bone as discussed in the previous chapter. Collagen type I was chosen as a component for the polycations in PEMs as it remains positively charged in solution, below the isoelectric point which is close to pH 5.0 (Zhao et al. 2014). In this work, collagen type I was used as a carrier to bind the SiCHA powders on the PLA films. By incorporating collagen type I into the assembly, it provides more cell recognition sites, thus enhanced the cellular adhesion and proliferation on the PLA films surface (Wang et al. 2014). It is known to have a variety of cell adhesive peptide moieties (i.e. Arg-Gly-Asp, RGD) for anchoring cells and act as structural cue for stimulating cell growth. Therefore, surface chemical and topographical cues created by hydroxyapatite-based nanoparticles and collagen multilayer deposition mimicked the natural ECM (Kim et al. 2010). Moreover, many reports have focused on osteogenic differentiation of MSCs cultured on collagen type I. The activation of specific integrins by collagen type I was reported to mediate the osteogenic response of hMSCs (Mizuno & Kuboki 2000; Salaszyk et al. 2004; Dawson et al. 2008). In order to allow PEMs assembly, hyaluronan was used as the polyanion. Hyaluronan is also called hyaluronic acid, a major component of the ECM and synovial fluid. Thus, in this study we proposed the combination of SiCHA nanopowders, collagen type I and hyaluronan as attractive innovation in the development of coating materials assembly for osteogenesis applications.

Firstly, the validity in the use of EDC/NHS as coupling agent was verified. Since collagen type I and hyaluronan are the major ECM proteins, it is possible to covalently immobilize these ECM proteins using coupling agents such as hexamethylene diisocyanate (HMDIC), 1, 6-dimethyl suberimidate dihydrochloride (DMS) (Higuchi et al. 2005) or EDC/NHS (Melkounian et al. 2010). EDC is a water-soluble carbodiimide that is generally used at pH 4.0-6.0 (Melkounian et al. 2010). It is critically important to preserve the pH throughout the multi-layered depositions in order to avoid degrading the efficiency of the coating materials in PEMs. Besides HMDIC, DMS and EDC/NHS, glutaraldehyde is one of the typical cross-linking agents used in PEMs. Glutaraldehyde is not commonly used in tissue engineering as it can cause a toxic effect to the stem cells. EDC/NHS promotes cross-linking between carboxylic acids and amino groups in ECM proteins. Thus, EDC/NHS was chosen as the coupling agent in this work because it functions at approximately pH 5.0, similar to both the polyelectrolytes used in the PEMs and it has limited toxicity (Higuchi et al. 2012). Therefore, it was used to immobilize the functional coating materials onto PLA films.

SEM images have demonstrated that PLA films coated with one bilayer of coating materials having EDC/NHS as the outermost layer (1-BL) showed significantly better distribution of the coating materials throughout the surface than those without EDC/NHS surface finished (1-BL*). The introduction of EDC/NHS was believed to successfully immobilize the coating materials onto the films surfaces. EDC/NHS had firmly bound the bilayers deposited on the 1-BL PLA films, evidenced by the retention of the coating after washing was performed. On the other hand, some of the coating materials on the 1-BL* PLA films were slightly washed off at the final stage where the films were rinsed in dH₂O before proceeding with the next deposition cycles, resulting in localized agglomerated coating materials on the surface as seen in SEM images (Fig. 4.1 d). This observation

highlighted the importance of using EDC/NHS in PEMs and appears as an innovative way to improve the surface modification of the hydrophobic nature of PLA films. Thus, the newly developed coating materials assembly consists of novel SiCHA powder in hyaluronan, SiCHA powder in collagen type I and EDC/NHS deposition cycles was then adapted in the following study.

4.3.2. The effect of different number of bilayers on surface properties

The effect of these novel coating materials assembly with different number of layers deposited on the PLA films was studied in terms of physical, chemical and biological properties. It is known that the surface properties of a biomaterial such as topography, chemical composition and hydrophilicity can affect cell-biomaterial interaction (Chesmel et al. 1995; Lincks et al. 1998). Surface properties greatly influence the viability and functional activity of anchorage-dependent cells such as osteoblasts, upon implantation of TE constructs into the body. Cells directly get in contact with the implant surface before the interaction throughout the entire construct could occur, i.e. cells adhere to the protein adsorb layer on the implant surface and proliferate, followed by migrating over the entire construct over time (Zhao et al. 2014).

The surface roughness and topography of the unmodified and modified PLA films were evaluated using AFM. Amino functional groups were introduced onto PLA films surface through aminolysis (Bunnett & Davis, 1960). This process provides a positive charged on the surface, which allows the alternate absorption of polyanion (i.e. SiCHA in hyaluronan) followed by polycation (i.e. SiCHA in Collagen type I) solutions. The introduction of the coating materials assembly induces a rougher surface area on the films compared to the control PLA films (unmodified). This is due to the presence of the aggregates of SiCHA nanopowders deposited on the surface of the film with increasing number of layers. This

could influence the cell behaviour in contact with the coated PLA films (Deligianni et al. 2001). It is well known that cell adhesion and proliferation are sensitive to the surface topography of the biomaterial (Brunette, 1988). It has been demonstrated that human osteoblast-like cells cultured on titanium alloy surfaces with rougher surfaces resulted in greater cell spreading and proliferation relative to smoother surfaces of the same material (Schwartz et al. 2008).

In this work, 5-BL coated films possess the highest surface roughness of all the groups tested. However, after 5 deposition cycles, there was a small drop in the surface roughness of the 10-BL coated films. This result was consistent with the findings by Zhu et al. (2003). Subsequent deposition of polyelectrolytes serves to fill voids and defects present in previous layers of the coating, effectively creating a smoother surface (Lowman & Buratto 2002). It is also believed that after finite n -layers deposition (which varies depending on the materials used), the electrostatic force binding the polyelectrolytes become weaker and the surface might have reached the saturated level of absorption; no further absorption occurs (Szilagyi et al. 2014). Thus, increasing number of coating layers could cause collapse of the layers formed as the coating materials fail to properly bind to the surface.

The distribution of coating materials on the surface was further observed using TEM. The images acquired support the surface topography observed under AFM. The surface was covered with more coating materials as a function of the increase in number of layers. Coating materials were found to almost cover the entire surface of 5-BL coated films and seemed reduced on 10-BL PLA films as coating materials assembly possibly reached saturated adsorption point after 5-BL deposition cycles. This explained why 5-BL has the highest surface roughness compared to the other coated films.

In the current investigation, the chemical compositions of the coating deposited on the PLA films were also evaluated. XPS analysis confirmed that the hydrophobic PLA films were effectively modified by aminolysis process, as identified by the presence of N1s peak. Increasing number of layers means more collagen deposited on the surface, which associated with the increased of amino acid residues (from collagen) on the surface. As a consequence, the intensity of N1s peak appeared higher on the coated PLA films with increasing deposition cycles compared to the aminolyzed PLA films (Zhang et al. 2006).

The composition of the coating materials assembly deposited on the PLA films was further assessed qualitatively by histochemical staining. Both Alizarin Red and Sirius Red showed positive stains, which confirmed the presence of calcium and collagen deposited on the surfaces. Brighter and more homogenous stains were obtained as more coating materials were deposited on the surface. After three deposition cycles, no obvious differences in SR staining were observed. This indicates that the adsorption of the coating materials on the surface is approaching the saturation level. Comparing 5 deposition cycles with 10 cycles, less AR stain was observed on 10-BL than 5-BL films. This suggests that the surface has become saturated and could not adsorb more deposition of the coating materials.

4.3.3. *In vitro* hMSCs growth and osteogenic differentiation

The final aim of this work was to investigate the cytotoxicity effect of the newly developed coating materials assembly on hMSCs behaviour particularly, the SiCHA nanopowders and PLA films, which are the major components of the hybrid system. While, collagen type I and hyaluronic acid were only the carriers for SiCHA nanopowders to allow these powders to be chemically bound to the PLA films. Therefore, only unmodified PLA films was used as control in this study. Ideally, PLA films coated with either collagen type I or hyaluronic acid alone should be tested in the future for determining the most favourable

growth environment for hMSCs on PLA films. This will also provide a better understanding for the role of each component used in the hybrid system that could affect the outcome.

For an ideal bone scaffolds, the construct itself should be able to provide a cell-favourable microenvironment for supporting cellular adhesion and proliferation (Kim et al. 2010). The seeded hMSCs on the control and coated PLA films deposited with different number of bilayers showed no toxicity effects after 14 days. There was no evident difference in the cell morphology on different substrates; hMSCs showed an elongated fibroblast-like morphology on all tested films. However, more viable cells were found on the coated PLA films than the control PLA films (unmodified). Rodrigues et al. (2013) reported similar observation upon culturing MG63 osteoblast-like cells on collagen-nano HA scaffolds and collagen scaffolds. These results confirmed that the coating materials invented are biocompatible and lead to better cell viability. It is believed that cell adhesion was likely to have improved as a result of increasing number of deposited layers (Kim et al. 2010).


The amount of DNA as a function of culture period was used to assess the proliferation of hMSCs. The presence of the multilayer coating played an important role in favouring the cellular adhesion and proliferation on the surface. As expected, 5-BL coated films seem to have prominent effects on cell proliferation. 5-BL surfaces have the highest surface roughness and well-distributed coating materials on the surface. This proved that the rougher the surface area, the better the cellular adhesion and proliferation (Schwartz et al. 2008; Rodrigues et al. 2013). As mentioned above, the surface roughness increased with the layer of deposition cycle (up to 5-BL), means larger specific surface area available that subsequently, might promote more proteins interaction on the surface (i.e. adsorption, conformation and bioactivity), which further enhanced the cell adhesion and proliferation

(Kim et al. 2010; Laranjeira et al. 2010; Ribeiro et al. 2010; Rodrigues et al. 2013). However, there are discrepancies in the literature on the effect of surface roughness on cell attachment, proliferation and differentiation. These inconsistencies may be due to differences in the cell type used, culture conditions, serum concentration, surface fabrication methods, sterilization technique and type of substrate as highlighted by Osathanon et al. (2011).

Besides surface roughness, the chemical composition also plays an important role in cell responses. Among the multilayer components, collagen is known to contain an adhesion sequence (RGD), which favours cell attachment and proliferation (Bisson et al. 2002; Becker et al. 2002; Ma et al. 2005). A study using SaOS-2 osteosarcoma cell line on PLLA with apatite and apatite/collagen composite coating reported in the literature found that the presence of collagen assisted cell attachment and proliferation when it was combined with apatite crystals (Chen et al. 2008). It was also discovered that a favourable matrix for cell attachment and growth was provided by grafted collagen type I (Suh et al. 2001). The benefits of collagen have also been investigated using other cell types than osteoblast-like cells. For instance, Ma et al. (2005) cultured chondrocytes on collagen immobilized PLLA surfaces and reported that the surfaces displayed considerably enriched cell spreading and growth. In the current study, cell adhesion and proliferation were facilitated with the presence of collagen as polycations in PEMs assembly. The composition of the newly developed coating materials assembly is closely resembled the bone mineral composition. This may be the main reason for the observation that the highest cell proliferation level had been obtained on the coated PLA films compared to the control (unmodified PLA) (Chen et al. 2008). Regardless the deposition cycles, all coated PLA films encourage rapid cell proliferation.

ALP production by hMSCs increased overall with the culture period. In consistency with hMSCs viability, adhesion and proliferation, ALP activity increased with number of deposited cycles. This indicated that the coating materials assembly are both osteoconductive and osteoinductive as they provide a suitable basis that could accelerate matrix-mediated intracellular signalling related to osteoblastic activity (Kim et al. 2010). Moreover, this result demonstrated the efficacy of the SiCHA nano aggregates formed on the surface, which not only improved cell adhesion by providing rougher surface but also enriched the osteoblastic phenotype. Considering a patient with large bone defects, the implanted scaffold should be both osteoconductive and osteoinductive by itself. Indeed, a monolithic scaffold fabricated either from osteoconductive material (i.e. HA-based nanocrystals) or osteoinductive material (i.e. collagen type I) could favour osteogenesis, but having composite scaffolds of collagen-HA has been proven to accelerate the new bone formation leading to rapid recovery. Previously, Tsai et al. (2008) cultured MG63 osteosarcoma cell line on collagen-HA composite beads and discovered that HA increased the ALP activity of the cells when cultured on collagen-HA composite beads than they were cultured on collagen alone. In addition, osteoblast responses to gelatin-HA nanocomposites were investigated over 14 days in culture. It was determined that the ALP levels were significantly higher on the nanocomposite when compared to pure gelatine (Kim et al. 2005). This is due to the good osteoconductive properties of HA (Tang et al. 2005; Fathi et al. 2008). Several studies have demonstrated that calcium ions (a major component of HA) are directly involved in boosting the proliferation and osteoblast cell type phenotype expression through membrane-mediated ion transfer, which is a possible explanation for the here observed results (Rodrigues et al. 2013). This highlighted the benefits of having both collagen type I and HA-based material as the major components in fabricating a hybrid scaffold with the aim to enhance bone formation.

In consistence with the DNA contents, hMSCs cultured on coated PLA films showed an increased protein release when compared to the control unmodified PLA films. The levels of total protein increased as a function of deposition cycles up to 5-BL. The unmodified PLA films produced the lowest levels of total protein at either time-point compared to the coated films ($p \leq 0.0001$). After 14 days, hMSCs cultured on 5-BL films produced the highest levels of total protein, meaning more proteinaceous materials produced as in direct contact to 5-BL films than others. The trend for the levels of total protein production for different number of deposition cycles is as follows:

$$5\text{-BL} > 10\text{-BL} > 3\text{-BL} > 1\text{-BL} > 0\text{-BL}$$


Decreasing trend of total protein production

Coated PLA films demonstrated enhancement in the cell metabolic activity as compared to the unmodified PLA films; which is the similar response to the levels of total protein produced. Cells were found to be the most metabolically active when cultured on 5-BL and 10-BL PLA films with no significant differences were observed ($p \geq 0.05$) after 14 days in culture. This showed that increasing number of deposition cycles after 5-BL has no improvement on the cell metabolic activity.

4.4. Conclusions

In this study, the hydrophobic PLA films were successfully modified with different layers of novel coating materials assembly. The use of EDC/NHS coupling agent has effectively immobilized the coating layers onto the PLA substrate. Surface roughness, topography and chemical compositions of the coatings deposited on the PLA films increased with increasing the number of deposition cycles. It was found that 5-BL PLA films possess the highest surface roughness and homogenous distribution of coating materials assembly.

In vitro tests confirmed that the newly developed coating material is biocompatible and able to support cell adhesion and proliferation over the surface of the materials. The coated PLA films were able to encourage faster cell proliferation and functional activity as compared to the unmodified PLA films, as determined by DNA quantification and cell activity markers, i.e. metabolism, protein production and ALP activity. This finding proved that the aminolysis process followed by deposition of PEMs with different deposition cycles of coating materials assembly have efficiently enhanced the surface properties of PLA films. PLA films deposited with 5 deposition cycles of coating materials provided more adequate environment for cell adhesion, proliferation and improving cell response after 14 days and this is likely to be as a consequence of increased surface roughness and homogenous distribution of coating materials on 5-BL materials.

By considering all the aforementioned physical, chemical and cell behaviour on different surface of the PLA films, finding leads to conclusion that 5-BL of PEMs assembly are potentially ideal deposition cycles to fabricate hybrid three-dimensional printed (3DP) scaffolds for BTE applications. Taken into account that the hybrid 3DP scaffolds will be fabricated in a large scale, it is critically important to ensure that the fabrication technique involved is simple, easily reproducible and most importantly time and cost-effective.

Minimum manufacturing consumption with maximum performances is always the goal in the production line. Again, 5-BL perfectly fulfilled this requirement. Increasing the number of deposition layers after 5 deposition cycles had no improvement on the performance of the coating material. Instead, the production time taken and chemicals used for 5-BL was half as required for 10-BL PLA films. Thus, 5-BL coating layers consist of newly developed coating materials assembly of SiCHA in hyaluronan, SiCHA in collagen type I and EDC/NHS was established and implemented in further investigation for the fabrication of 3DP hybrid scaffolds discussed in the following chapter.

Chapter 5

How does the structural and functional design of three-dimensional printed scaffolds affect the stem cells fate?

5.1. Introduction

The tremendous demand for a bone graft substitutes to treat patients with congenital defects, tumour or non-union fracture is still alarming. Limited availability of suitable bone graft has driven the development of tissue engineering (TE) approaches to overcome the limitations of bone regeneration (Sheyn et al. 2010). There are three proposed approaches in bone TE: (i) the use of isolated cells or cell substitutes to replace the defective tissues, (ii) the delivery of tissue-inducing substances such as growth factors, to the targeted locations and (iii) growing cells in three-dimensional (3D) scaffolds which is also known as scaffold-based TE (Langer & Vacanti 1993; Bloch et al. 2001; Peterson et al. 2002). The first two approaches are mostly employed when the defects are small and well confined. However, for large bone defects, these two approaches have serious limitations (Song et al. 2008). An intervention is usually required to heal the majority of the large bone defects and the ability to heal these sizes of injuries is limited (Stevens 2008). Therefore, researchers worldwide have been focussed on the third approach e.g. scaffold-based TE, which involves the combination of scaffolds, cells and potentially an appropriate 3D culture environment as regenerative strategy (Hutmacher et al. 2004).

A biodegradable scaffolds is a temporary substrate for cell growth and activity as well as encourage cells to synthesize their extracellular matrix (ECM) and other biological cues that could facilitate the formation of functional tissues/ organs (Salgado et al. 2004; Song et al. 2008). Several kinds of scaffolds have been fabricated using polymer, ceramic or natural based materials for example poly (lactic acid) (PLA), poly (glycolic acid) (PLGA), hydrogel, chitosan, hydroxyapatite (HA), and so forth by various fabrication techniques (Hutmacher 2000; Sachlos & Czernuszka 2003). Recently, the Rapid Prototyping (RP) techniques have become an attractive alternative to fabricate an intricate scaffolds design

for bone TE, as it allows customization of scaffold designs to treat the variable needs of patients. For instance, a section of bone defect from the patient can be imaged using Magnetic Resonance Imaging (MRI) or X-Ray computed tomography (CT scan), which can then be converted to the file format for RP manufacturing (usually in stereolithographic or .STL format). The final stage is to print a customized 3D scaffolds for that individual patient (Bagaria et al. 2011). The 3D scaffolds can be constructed using different types of RP techniques such as fused deposition modeling (FDM) (also known as fused filament fabrication, FFF), 3D plotter and 3D printing (Subia et al. 2010).

In order to induce a 3D pattern of cell ingrowth and differentiation, a 3D scaffold alone is insufficient. The addition of progenitor cells can promote more rapid growth when delivered to the patient. The growth of these 3D constructs requires specialized growth chambers termed bioreactors. These chambers enhance mass transfer throughout the scaffold and provide optimized conditioning of the constructs with tailored biomechanical conditions related to the implant site (El Haj & Cartmell 2010). Previous research has demonstrated that preconditioning with mechanical forces can lead to scaffolds and matrices being remodeled and therefore being adapted to the implant site (Baas et al. 2010). In our experiments where we have designed a 3DP hybrid scaffold with aligned channels there is more of a need for a culture environment that supports larger TE constructs and promotes cell proliferation and differentiation such as the rotary bioreactor selected for this study.

Bioreactors technologies are the most commonly used for dynamic cell culture studies (Rauh et al. 2011; Yeatts & Fisher 2011). Ideally, a bioreactor should enable controlled biochemical and/or biological processes. One example of an early bioreactor design still commercially available today is the rotating wall vessels (RWVs) bioreactor, which was

originally developed by NASA for space research. The aim of these bioreactors was to protect cell cultures from the high shear forces generated during launch and landing of the space transport, however, the system has also been found to provide a good growth environment for TE which requires improved mass transport without mechanical conditioning. In this system, cell constructs are able to rotate in the vessels with minimal disruptive shear stresses, thus simulating microgravity conditions and essentially free from turbulence (Granet et al. 1998). RWVs are used to support high-density and large scale 3D cell cultures and provide controlled supply of oxygen and nutrients needed for cell growth (Gao et al. 1997).

There have been various studies on the effects of microgravity in the culture of osteoblast-like cells have been investigated (Sikavitsas et al. 2002; Facer et al. 2005; Sheyn et al. 2010). However, contradictory results have been described. Some authors reported that microgravity inhibits the proliferation and osteogenic differentiation of mesenchymal stem cells (MSCs) (Dai et al. 2008; Zayzafoon et al. 2013). On the other hand, Nakamura et al. (2003) found that the viability of human osteoblasts cells were not affected by the microgravity conditions even after several days in culture. In fact positive impacts of using RWVs bioreactor were demonstrated by Sheyn et al. (2010) and Araujo et al. (2010) where the improved mass transfer provided by the bioreactor in combination with the appropriate substrate were thought to be a decisive factor for stimulating osteogenic differentiation. However, it is known that the cell viability and ingrowth are not solely dependent on the cell culture conditions. There are other important parameters, which should be taken into consideration such as the scaffold surface properties in particular the surface roughness, chemical composition and porosity. These properties could greatly affect the cell attachment and activity (Salgado et al. 2004). Alongside the microgravity effect, the chemical cues and the rotating speed might also contribute to the different outcomes in the

cell response. The interplay between these factors must be optimized for the best outcome of tissue growth prior to implantation.

The aim of this study was to investigate the fate of human bone marrow derived-mesenchymal stem cells (hMSCs) cultured on different structural and functional designs of three-dimensional printed (3DP) hybrid scaffolds in static and dynamic conditions with the use of the rotary bioreactor (RCCS systems, Cellon, Synthecon, Texas). The 3DP scaffolds were initially fabricated by Fused Filament Fabrication technique followed by surface modification using Polyelectrolyte Multilayers (PEMs) assembly. The optimized coating technique described in the previous chapter was adapted to engineer the 3D hybrid scaffolds. The effect of the chemical cues in the culture medium were also investigated in this study by culturing the cellular scaffolds in two differences culture medium i.e. the osteogenic media (OM) and proliferation media (PM) for both conditions. Pure hydroxyapatite (HA) scaffolds purchased from Ceramisys (Sheffield, United Kingdom) was used as the experimental control since this product is commercially available and has a supporting clinical data. It should be noted that the clinical data is not shown in this study since it is highly confidential.

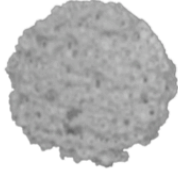



5.2. Results

5.2.1. Scaffold designs for bone TE

In this study, three different scaffold designs were fabricated by FDM technique followed by PEMs (as described in Chapter 4) in order to produce 3DP hybrid scaffolds. Commercially available scaffolds of pure sintered HA scaffolds were used as the experimental control. The basic properties of commercial HA, 2 channels (designated as 2C), 4 channels (designated as 4C) and mesh scaffolds are summarized in Table 5.1. The

examples of three-dimensional drawing for 2- and 4-channel scaffolds are illustrated in Fig. 5.1.

Table 5.1: Summary of the basic properties of HA, 2C, 4C and mesh scaffold.

Scaffolds	HA	2C	4C	Mesh
Appearances				
Diameters (mm)	10	10	10	10
Thickness (mm)	2	2	2	2
SA:V (mm ⁻¹)	0.95	0.26	0.55	0.86
Pores/channels size (µm)	200-300	1500	1500	500
Porosity (%)	70-85	20	40	60
Nature of materials	Ceramic (100% Pure HA)	Composite (PLA based scaffolds coated with SiCHA nanopowders and collagen type I)	Composite (PLA based scaffolds coated with SiCHA nanopowders and collagen type I)	Composite (PLA based scaffolds coated with SiCHA nanopowders and collagen type I)

** SA: V= surface area to volume ratio.

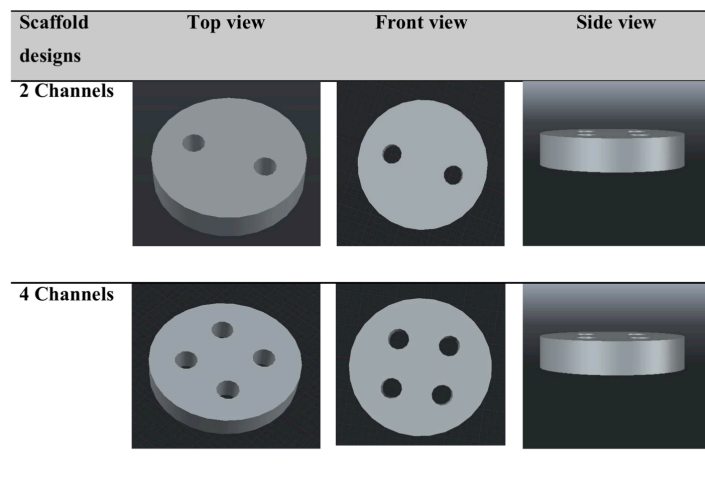


Fig. 5.1: Examples of three-dimensional drawing for 2- and 4-channel scaffolds.

5.2.2. Seeding efficiency on three-dimensional scaffolds

The concept of Bone tissue engineering (BTE) holds great promise for the treatment of clinical defects. However, much optimization is required before BTE can be broadly applied clinically. This study evaluated various cell seeding methods on the different designs of 3D scaffolds i.e. the HA, 2C, 4C and mesh scaffolds seeded with different volume of cell suspensions (20 and 40 μL) in coated and non-coated well plates. The seeding efficiency on different scaffolds is represented in terms of percentages of cell attachment onto the scaffolds as shown in Table 5.2.

Table 5.2: Percentages of cell attachment onto the scaffolds with different cell volume suspensions on different scaffold designs.

Scaffolds	Coated well plates		Non-coated well plates	
	20 μL	40 μL	20 μL	40 μL
HA	55%	47%	46%	45%
2C	87%	80%	56%	48%
4C	85%	77%	60%	52%
Mesh	80%	75%	48%	40%

Note: Coated well plates = 1 w/v% Pluronic F-127 coated 24-well cell culture plates; non-coated well plates = normal 24-well cell culture plates. The volumes indicate 5×10^4 cells in 20 and 40 μL delivered to the scaffolds.

The results suggested that scaffolds seeded with small cell volume suspension of 20 μL have higher percentages of cell attachment onto the scaffolds as compared to 40 μL cell volume suspension. Regardless of the scaffold designs, lower cell attachment was found on scaffolds seeded in the non-coated well plates. Overall, HA scaffolds exhibited the lower percentages of cell attachment as compared to the 3DP hybrid scaffolds. In order to further optimize the seeding efficiency, scaffolds were then seeded in two different methods using 20 μL volume suspension and coated well plates.

The cells were seeded either on one-side or two-sides on all scaffolds types. MTT stain was used to qualitatively determine the cell distribution throughout the scaffolds. Images are shown in Fig. 5.1. A positive MTT stain forms a blue formazan upon reduction at the site of metabolically active viable cells (Stoddart 2011).

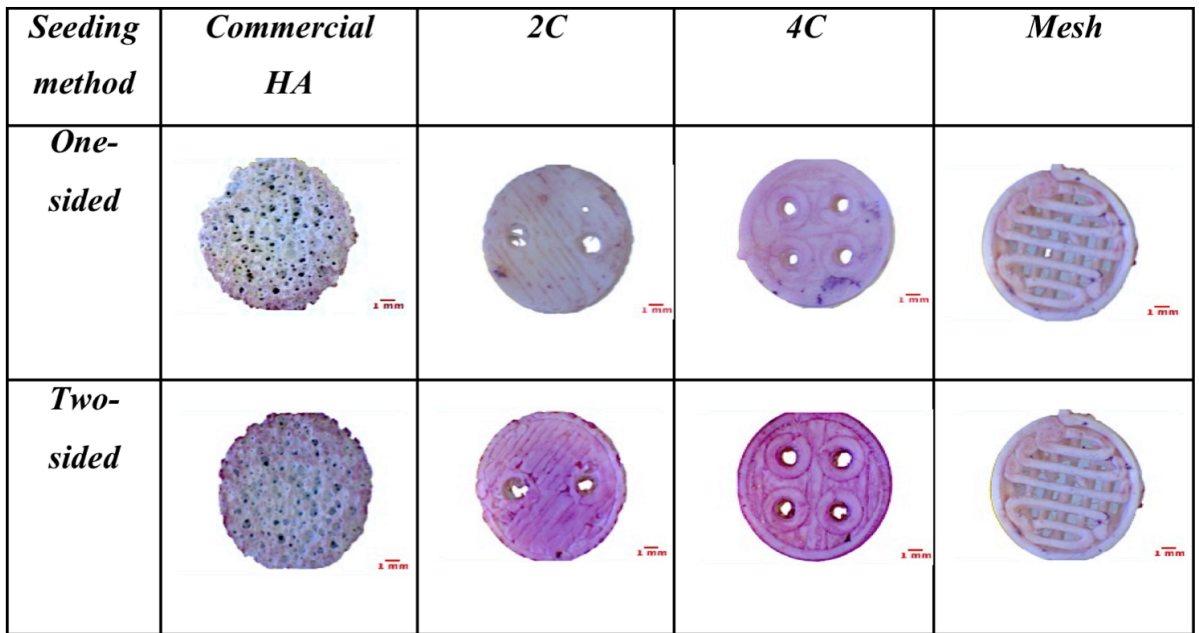


Fig. 5.2: Cell distribution on different scaffold designs seeded with one-sided and two-sided seeding method. Scale bar = 1 mm.

MTT staining indicates that two-sided cell seeding resulted in better cell distribution across the surface of the scaffold than one-sided seeding represented by the purple stained (Fig. 5.2). After 6 hours incubation, cells were found to have attached and were more homogenously spread over the entire scaffolds when seeded on both sides of the scaffolds (data not shown). It was observed that 2C and 4C scaffolds showed brighter stains compared to the porous HA and mesh scaffolds. This indicates that the former scaffolds have better cell attachment and distribution compared to the latter.

5.2.3. Optimization on the rotational speed of the rotary bioreactor

In our initial experiments, the rotational speed of the rotary bioreactor has been optimized. To achieve this, the cellular scaffolds with the most optimal seeding method (small volume suspension of about 20 μL with cell seeded in two-sided method in a coated well plate) were cultured in the 50 mL vessels of the rotary bioreactor then rotated at 20 and 40 rpm for 24 hours. The cell viability was then observed by live/dead staining under confocal laser scanning microscope (CLSM) as shown in Fig. 5.3. The images indicated that more viable cells were found on the cellular scaffolds cultured at 20 rpm compared to 40 rpm. This indicates that the lower rotational speed allows for a better cell attachment across the scaffolds whilst the cells tend to detach from the scaffolds when they were rotated at higher speed. At a higher speed of 40 rpm, scaffolds started to collide with each other and the wall of the chamber, resulted in some loss of cells. At lower speed than 20 rpm, scaffolds sediment at the bottom of the chamber and stick to each other (data not shown). Thus, 20 rpm was chosen as the ideal speed to study the effect of dynamic condition on the hMSCs fate cultured on different structural design of 3DP hybrid scaffolds.

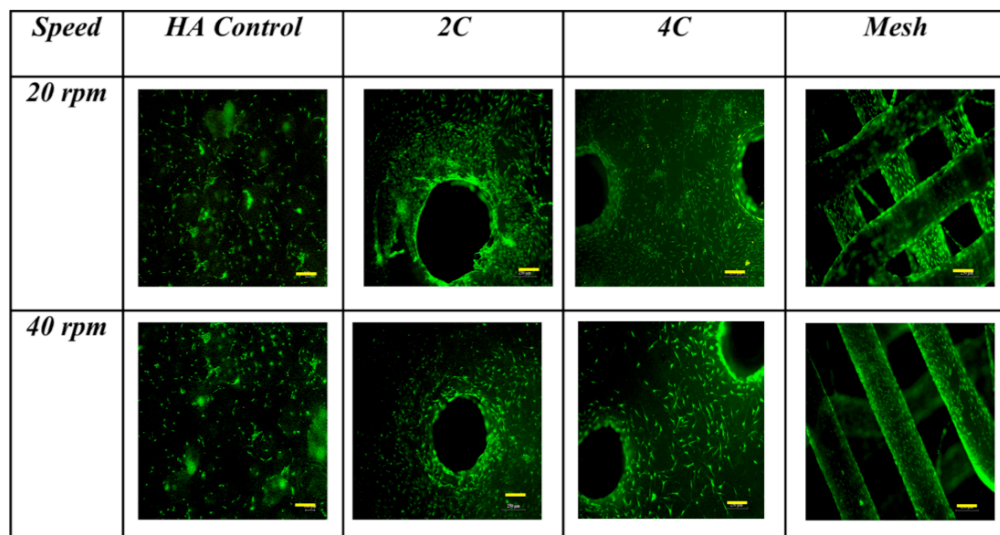


Fig. 5.3: Cell viability on different structural designs of 3DP hybrid scaffolds at 20 and 40 rpm, respectively. Results suggested more viable cells were found as cells were cultured at 20 rpm where the scaffolds were free floating in the rotary bioreactor. Scale bar= 500 μm .

5.2.4. Determining the fate of cellular scaffolds in several culture conditions

Having determined the best seeding and growth conditions for the cellular scaffolds, e.g. cells were seeded onto the scaffolds using the two-sided seeding method in which each scaffold was seeded with about 20 μL cell volume suspension contains 5×10^4 hMSCs on each side of the scaffold, the fate of the cells with time in culture was determined.

The results did demonstrate a difference, however, in terms of the incubation time (before transferring to the bioreactor) required for the 3DP hybrid scaffolds and the control HA scaffolds. For the 3DP hybrid scaffolds, the cellular scaffolds were cultured in static condition for 24 hours before transferring them to the rotary bioreactor. However, the HA scaffolds needed longer incubation time in static before they can be transferred to the bioreactor in order to allow for cell adhesion. As suggested by the manufacturer, these scaffolds should be incubated at least for 72 hours post-seeding before the same dynamic condition use for the 3DP hybrid scaffolds can be applied.

In this study, we have two hypotheses; (1) the dynamic flow and the use of osteogenic media are expected to enhance the bone formation *in vitro* compared to those cultured under static condition and in proliferation media; and (2) Our second hypothesis was the novel designed of the 3DP hybrid scaffolds are assumed to promote better bone formation than the commercial HA scaffolds. While, our null hypothesis was the designs of 3DP hybrid scaffolds have no effect on bone formation *in vitro*. The role of the osteogenic media versus culture environment was evaluated by assessment of the chemical cues from the culture medium. Cellular scaffolds were cultured in osteogenic media (OM) and proliferation media (PM) for both conditions. The cellular scaffolds were then characterized qualitatively and quantitatively after 7, 14 and 21 days in culture. The cell viability of the hMSCs seeded on different scaffold were observed using live/dead staining.

To determine the early osteogenic differentiation, ALP kits were used to determine the level of alkaline phosphatase expression on the cellular scaffolds. Furthermore, biochemical assays were performed to quantitatively determine the scaffolds cellularity, the capability to produce extracellular matrix and protein, the early indicator for osteogenic differentiation as well as cell death. Finally, the scaffolds were analysed using μ CT to estimate the formation of the mineralized matrix on the cellular scaffolds in different culture conditions.

5.2.4.1. Cell seeding and cell viability

Live/dead staining was performed before the cellular scaffolds were transferred into the rotary bioreactor to confirm that the cells were attached to scaffolds before any stimulation was applied. This allowed confirmation that all scaffolds were comparably seeded prior to the application of dynamic culture, ensuring that any differences could be attributed to the culture condition, rather than differences in the initial cell seeding density. The CLSM images (Fig. 5.4) showed that higher proportions of viable cells were found on 3DP hybrid scaffolds than the HA scaffolds one day after seeding. However, no quantitative analysis was performed to determine the actual proportion of viable cells attached on each scaffold.

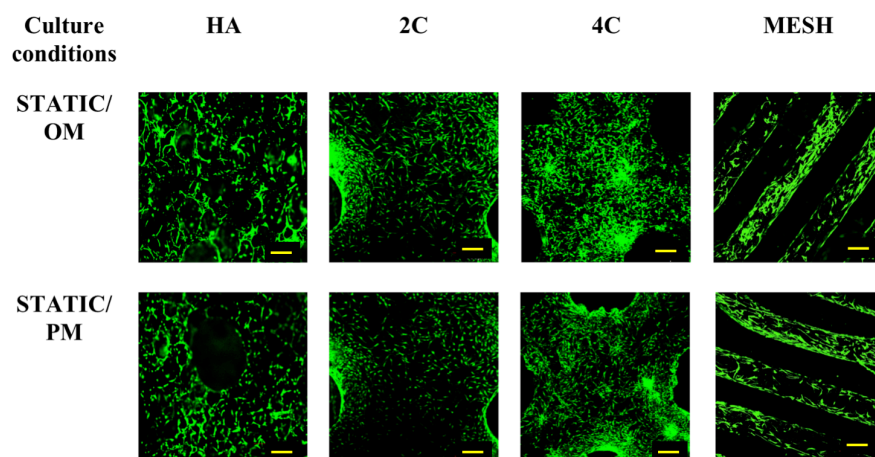


Fig. 5.4: CLSM of hMSCs seeded on all four scaffold designs cultured under static condition OM and PM after 1 day (for 3DP hybrid scaffolds) and 3 days (for HA scaffolds). Green indicates the live cells and red represents the dead cells. Yellow scale bar = 500 μ m.

The obtained CLSM images showed in Fig. 5.5 revealed that hMSCs seeded on HA scaffolds were only able to attach when scaffolds were cultured in static condition. Regardless of the culture medium, no cells were found on the HA scaffolds in the rotary bioreactor up to 21 days.

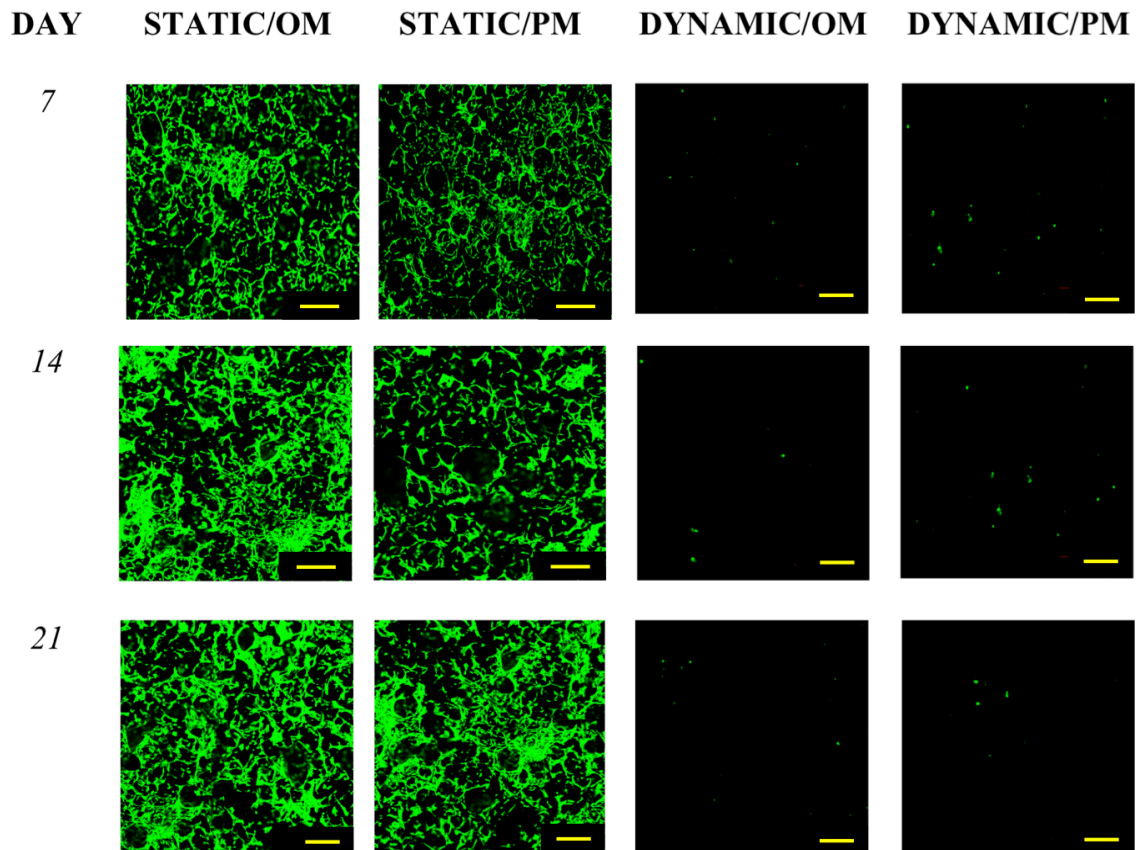


Fig. 5.5: CLSM images of hMSCs seeded on HA scaffolds cultured either under static or dynamic conditions in OM and PM for different time periods of 7, 14 and 21 days. Green indicates the live cells and red represents the dead cells. Yellow scale bar = 500 μ m.

Cells were able to proliferate throughout the HA scaffolds in static condition over the culture period. On the other hand, cells seeded on the 3DP hybrid scaffolds remained viable over the culture period in all culture conditions. Very few dead cells (<30%) were detected on these cellular scaffolds for all three designs as shown in Fig. 5.6-5.8.

The cell viability of hMSCs seeded on 2C scaffolds is represented in Fig. 5.6. Cells were able to attach and proliferate throughout the entire scaffolds over time. In addition, the hMSCs started to form bone-like nodules (as indicated by arrows in Fig. 5.6) on the surface of the 2C scaffolds after 14 days cultured with the use of the rotary bioreactor in osteogenic media. However, no aggregates were detected when the cellular scaffolds were cultured in the bioreactor without the presence of the osteogenic supplements in the culture media. Similar observations were obtained as the cellular scaffolds cultured in static conditions for both media. Under static conditions, cells were able to proliferate and fully cover the surface of the scaffolds in particular after 21 days in culture.

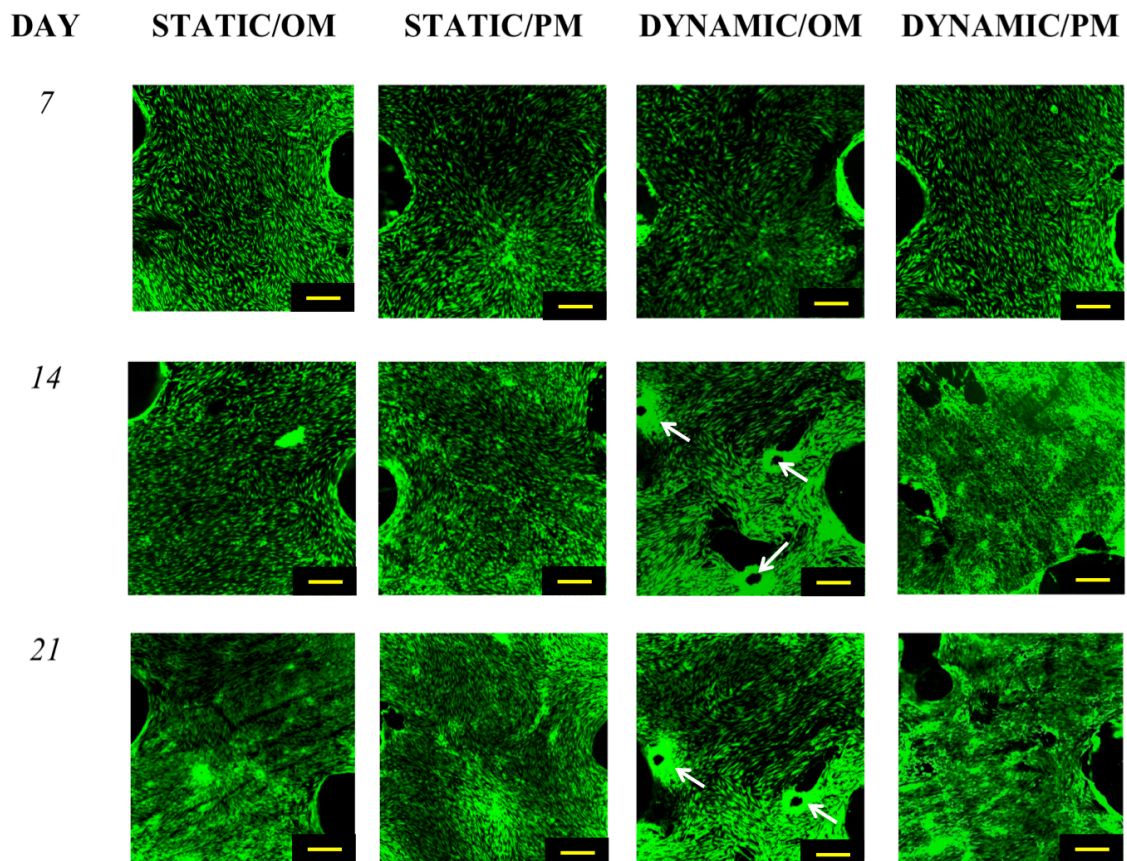


Fig. 5.6: CLSM images of hMSCs seeded on 2C scaffolds cultured either under static or dynamic conditions in OM and PM for different time periods of 7, 14 and 21 days. Green indicates the live cells and red represents the dead cells. Bone-like nodules (indicated by the white arrows) were observed as the cellular scaffolds were cultured in the rotary bioreactor with the use of osteogenic media after 14 days in culture. Yellow scale bar = 500 μ m.

The hMSCs were able to proliferate on 4C scaffolds in both static and dynamic conditions as shown in Fig. 5.7. Interestingly, the bone-like nodules (indicated by the white arrows) were detected in both static and dynamic condition as the 4C cellular scaffolds were cultured after 21 days in osteogenic media. However, a distinct outcome obtained when the 4C cellular scaffolds were cultured in proliferation media. After 21 days, the hMSCs were found to reach confluence when the 4C cellular scaffolds were cultured under static conditions whereas cell detachment was observed from the surface when grown in the rotary bioreactor.

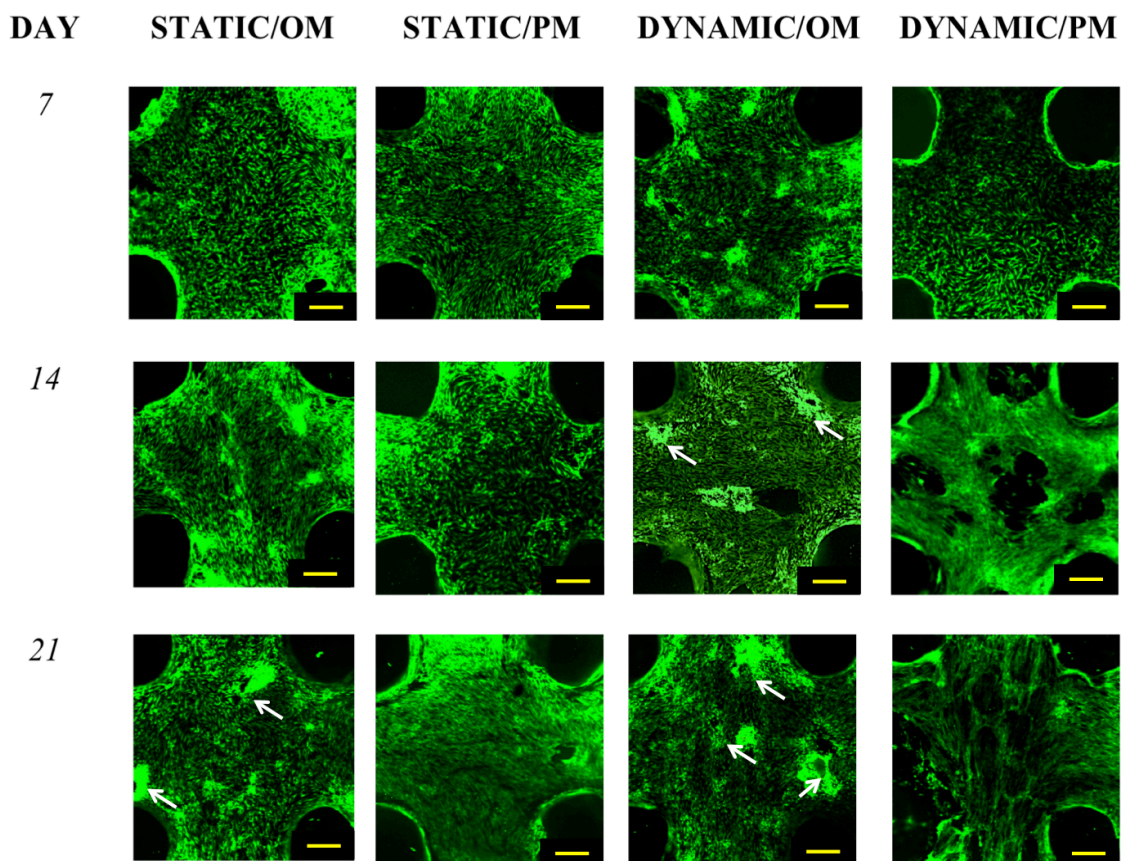


Fig. 5.7: CLSM images of hMSCs seeded on 4C scaffolds cultured either under static or dynamic conditions in OM and PM for different time periods of 7, 14 and 21 days. Green indicates the live cells and red represents the dead cells. Bone-like nodules (indicated by the white arrows) were observed as the cellular scaffolds were cultured in the osteogenic media for both static and dynamic culture conditions after for 21 days. Yellow scale bar = 500 μ m.

Similar to the 2C and 4C 3DP hybrid scaffolds demonstrated earlier, cells were able to attach to the mesh scaffolds and remained viable throughout the culture period of 21 days (Fig. 5.8). However, less viable cells were found when the cellular scaffolds were cultured in Dynamic/PM with increasing culture periods, i.e. a deleterious effect was seen after 21 days when most of the cells detached from the scaffolds. The opposite outcome was obtained when the cellular scaffolds were cultured in Dynamic/OM. The cells homogenously distributed across the scaffolds after 21 days. For the cellular scaffolds grown in static conditions, regardless of the culture medium, the cells were able to attach and proliferate along the struts of the mesh scaffolds.

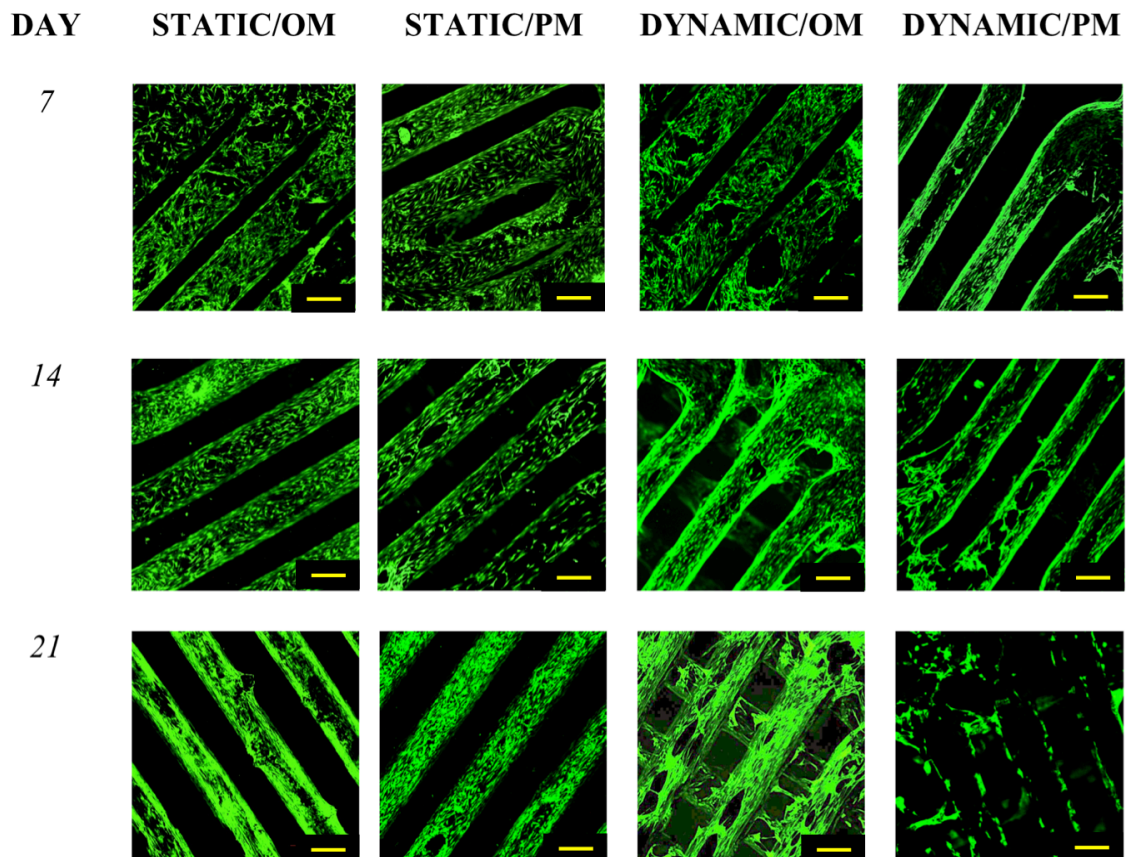


Fig. 5.8: CLSM images of hMSCs seeded on mesh scaffolds cultured either under static or dynamic conditions in OM and PM for different time periods of 7, 14 and 21 days. Green indicates the live cells and red represents the dead cells. Cells were stretched out across the struts of the mesh scaffolds after 21 days cultured in Dynamic/OM. Negative effect of microgravity was seen in Dynamic/PM as the cells were found to detach from the scaffolds. Yellow scale bar = 500 μ m.

The end goal of this study is to select the ideal scaffold design from our studies to translate for bone TE applications in the clinic. To do so, the results obtained after 21 days of culture was used to compare the impact of culture condition on different scaffold designs. In terms of cell viability, the results demonstrate that the 3DP hybrid scaffolds outperformed the HA scaffolds (experimental control) as seen in Fig. 5.9. The formations of bone-like nodules were found on the 3DP hybrid scaffolds in particular the 2C and 4C scaffolds in Dynamic/OM. While, cells seeded on HA scaffolds were not able to survive once they had been exposed in the rotary bioreactor regardless of the culture medium used.

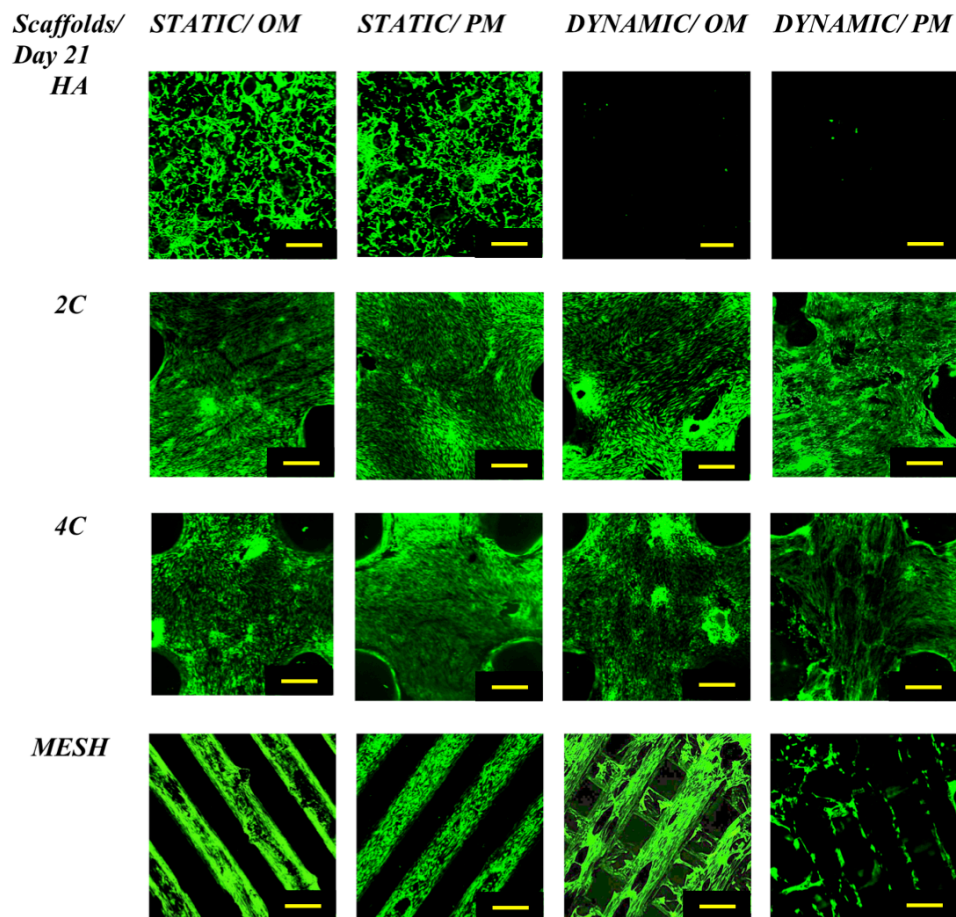


Fig. 5.9: Comparison of cell viability for different scaffold designs after 21 days cultured under static and dynamic conditions in OM and PM. For the HA scaffolds, cells were only able to attach in static condition while, better cells attachment and proliferation were obtained when the cells were seeded on the 3DP hybrid scaffolds for all culture conditions except for 4C and mesh scaffolds in Dynamic/PM where some lost of cells were detected after 21 days. Yellow scale bar = 500 μm .

5.2.4.2. *Cell proliferation on different scaffold designs*

The cell proliferation of hMSCs on HA, 2C, 4C and mesh scaffolds, cultured in different conditions were assessed by their amounts of DNA after 7, 14 and 21 days (Fig. 5.10).

For HA cellular scaffolds, mean DNA concentrations increased when cultured in static condition ($p \leq 0.0001$) in OM and PM, however, decreased in dynamic condition ($p \leq 0.0001$) for both culture media over time and differed between cultured conditions and media ($p \leq 0.05$). There were significant interactions between time, culture condition and media ($p \leq 0.05$), suggesting that the increase/decrease in DNA concentrations over time differed between culture conditions and media.

Comparing the culture conditions, HA cellular scaffolds in static culture showed significant increase in DNA concentrations in both OM and PM over time ($p \leq 0.0001$ for each). While, exposing these scaffolds in dynamic condition independently of used culture media, significantly reduced DNA concentrations were detected on day 14 ($p \leq 0.0001$). No significant differences in DNA concentrations were observed for scaffolds in Dynamic/OM, while, cellular scaffolds in Dynamic/PM continuously decreased ($p = 0.0007$) on day 21. Culturing hMSCs on HA scaffolds in static condition regardless of the culture media resulted in significantly higher mean DNA concentrations compared to dynamic at each time-point ($p \leq 0.0001$ for each).

When comparing different culture media, no significant differences were observed when these scaffolds were cultured in Dynamic/OM and Dynamic/PM on day 7 ($p = 0.9989$) and day 14 ($p = 0.9976$). Mean DNA concentration was significantly lower when cultured in Dynamic/PM relative to Dynamic/OM on day 21 ($p = 0.0010$). In static condition,

culturing HA cellular scaffolds in Static/OM resulted in higher DNA concentrations than Static/PM on day 7 ($p = 0.0052$), day 14 ($p = 0.036$) and day 21 ($p \leq 0.0001$).

Mean DNA concentrations for HA cellular scaffolds in static condition for both OM and PM increased as culture progressed ($p \leq 0.0001$ for each). While, no significant differences were observed when these scaffolds were cultured in dynamic condition regardless of culture media used ($p \leq 0.0001$ for each).

Overall, culturing HA cellular scaffolds in Static/OM resulted in the highest mean DNA concentration on day 21 compared to all other culture conditions and media ($p \leq 0.0001$ for each).

For the 2C cellular scaffolds, mean DNA concentrations increased when cultured in static condition for both culture media ($p \leq 0.0001$) over time and differed between culture media ($p \leq 0.0001$). There was significant interaction between time, culture condition and media ($p \leq 0.0001$), suggesting that the increase/decrease in DNA concentrations over time differed between culture conditions and media.

Comparing the culture conditions, 2C cellular scaffolds revealed significantly higher mean DNA concentrations when cultured in static condition over time ($p \leq 0.0001$ for each). While, when these scaffolds were cultured in dynamic condition both OM and PM, mean DNA concentrations reached the peak on day 14 and dropped afterwards on day 21 ($p \leq 0.0001$ for each).

When comparing scaffolds in different culture media, cells cultured on 2C scaffolds in Static/PM resulted in higher DNA concentrations as compared to Static/OM at each time-point ($p \leq 0.0001$ for each). At 7 days, no significant differences were detected when the scaffolds when exposed in dynamic condition for both OM and PM ($p = 0.8380$).

However, culturing these scaffolds in Dynamic/OM showed significantly higher mean DNA concentrations than those in Dynamic/PM on day 14 and day 21 ($p \leq 0.0001$ for each).

Mean DNA concentrations for 2C cellular scaffolds in static condition for both OM and PM increased as culture progressed ($p \leq 0.0001$ for each). When these scaffolds were cultured in dynamic condition regardless of culture media used, mean DNA concentrations increased until 14 days and eventually decreased on day 21 ($p \leq 0.0001$ for each).

Overall, 2C cellular scaffolds in Static/PM exhibited the highest mean DNA concentrations compared to all other tested culture condition and media (Static/OM, Dynamic/OM and Dynamic/PM) ($p \leq 0.0001$ for each) at each time-point.

Growing cells on 4C scaffolds resulted in the same trend and interactions between time, culture condition and media as 2C scaffolds ($p \leq 0.0001$ for each). Mean DNA concentrations increased when cultured in static condition for both culture media ($p \leq 0.0001$) over time and differed between culture media ($p \leq 0.0001$). There was significant interaction between time, culture condition and media ($p \leq 0.0001$), suggesting that the increase/decrease in DNA concentrations over time differed between culture conditions and media.

Comparing the culture conditions, significantly higher mean DNA concentrations were obtained when 4C cellular scaffolds were cultured in static compared to dynamic for both OM and PM ($p \leq 0.0001$ for each) at either time-point. For instance, when cultured in PM, 4C cellular scaffolds in static showed significantly higher DNA concentration compared to dynamic on day 14 ($p = 0.0004$).

When comparing between OM and PM in static condition, higher mean DNA concentrations were obtained when 4C cellular scaffolds were cultured in Static/PM at day 7 ($p \leq 0.0001$), day 14 ($p = 0.0003$), and day 21 ($p \leq 0.0001$). Culturing these scaffolds in dynamic condition resulted in higher mean DNA concentrations in OM than PM on day 7 ($p \leq 0.0001$) and day 21 ($p = 0.0005$). However, mean DNA concentrations were found to be significantly higher for Dynamic/PM as compared to Dynamic/OM ($p \leq 0.0001$) on day 14.

Over time, 4C cellular scaffolds revealed gradual increased in mean DNA concentrations when cultured in Static/PM ($p \leq 0.0001$ for each). While, those in Static/OM showed increased in DNA concentration till day 14 ($p \leq 0.0001$), but no significant differences were observed on day 21 ($p = 0.9998$). In dynamic condition, mean DNA concentrations reached maximum at day 14 and significantly declined on day 21 ($p \leq 0.0001$ for each) for both OM and PM.

Overall, 4C cellular scaffolds in Static/PM exhibited the highest mean DNA concentrations compared to all other tested culture condition and media ($p \leq 0.0001$ for each) over the culture period.

Similar trends were obtained by culturing hMSCs on mesh scaffolds as compared to 2C and 4C scaffolds. Comparing the culture conditions, significantly higher mean DNA concentrations were obtained when mesh cellular scaffolds were cultured in static compared to dynamic in PM ($p \leq 0.0001$ for each) at either time-point. However, no significant differences were detected when these scaffolds were cultured in Static/OM and Dynamic/OM at day 7 ($p = 0.4619$) and day 21 ($p = 0.6123$); only on day 14 higher DNA concentration was obtained in Dynamic/OM compared to Static/OM ($p \leq 0.0001$).

When comparing the culture media, culturing cells on mesh scaffolds in Static/PM resulted in higher mean DNA concentrations compared to Static/OM ($p \leq 0.0001$) at either time-point. Under dynamic condition, those cultured in OM showed significantly higher DNA concentration than PM ($p \leq 0.0001$) over the culture period. Over the 21 days, cells cultured on mesh scaffolds in static condition for both OM and PM showed gradual increases ($p \leq 0.0001$ for each). Similar to 2C and 4C cellular scaffolds, culturing cells on mesh scaffolds independently of culture media reached the highest DNA concentration on day 14 and ultimately dropped on day 21 ($p \leq 0.0001$ for each).

Overall, the highest mean DNA concentration was presented by mesh cellular scaffolds in Static/PM ($p \leq 0.0001$ for each) compared to all other culture condition and media.

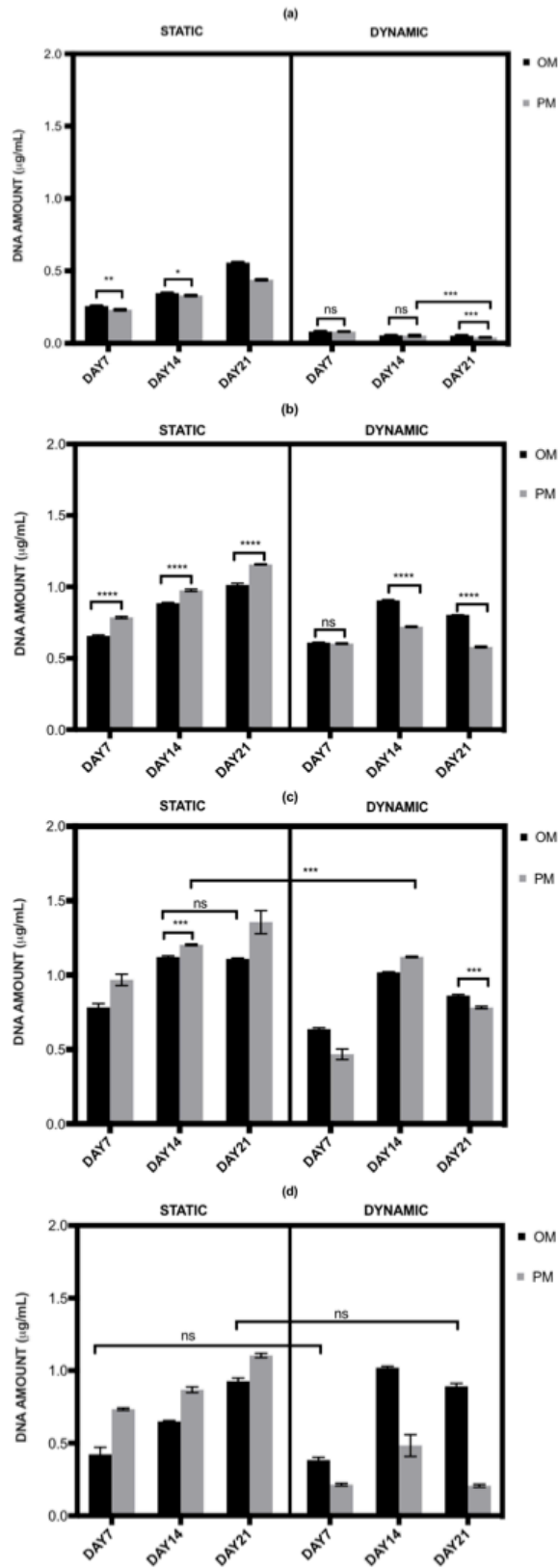


Fig. 5.10: The amount of DNA of hMSCs growing on (a) HA; (b) 2C; (c) 4C and (d) mesh scaffolds under different culture conditions. Error bars represent means \pm SD for $n=3$. (ns ≥ 0.05 ; * $p \leq 0.05$, ** $p \leq 0.01$, *** $p \leq 0.001$, **** $p \leq 0.0001$).

The amounts of DNA released by the hMSCs cultured on HA, 2C, 4C and mesh scaffolds under different culture conditions were evaluated after 21 days as shown in Fig. 5.11. The aim here is to determine which scaffold design and under which culture condition/medium composition could encourage the fastest cell proliferation.

After 21 days, mean DNA concentrations were significantly higher for static condition both OM and PM for the entire tested scaffold designs ($p \leq 0.05$) and differed between scaffold designs ($p \leq 0.0001$). There was significant interaction between culture condition/media and scaffold designs ($p \leq 0.05$), suggesting for all tested scaffold designs, significantly higher mean DNA concentrations were obtained in static condition ($p \leq 0.0001$). Culturing the 3DP hybrid scaffolds in dynamic condition for both OM and PM resulted in significantly lower DNA concentrations compared to static condition, particularly in Dynamic/PM ($p \leq 0.0001$ for each).

Comparing to the control (HA cellular scaffolds), all 3DP hybrid scaffolds showed significantly higher DNA concentrations regardless of the culture condition/media ($p \leq 0.0001$ for each).

When comparing the 3DP hybrid scaffold designs, the highest mean DNA concentrations were observed on 4C scaffolds in static for both OM and PM as compared to 2C and mesh scaffolds ($p \leq 0.0001$ for each). When cells were cultured in Static/PM, significantly higher mean DNA concentration was obtained on 2C scaffolds compared to mesh ($p = 0.0064$). No significant differences were observed when cells were cultured on 4C and mesh scaffolds in Dynamic/OM ($p = 0.6283$). In Dynamic/PM, culturing cells on 4C scaffolds resulted in the highest mean DNA concentration, while; the lowest mean DNA concentration was obtained by culturing on mesh scaffolds ($p \leq 0.0001$ for each).

Overall, 4C scaffolds in Static/PM revealed the highest mean DNA concentrations compared to all other investigated groups (scaffolds designs and culture condition/ media) on day 21 ($p \leq 0.0001$ for each).

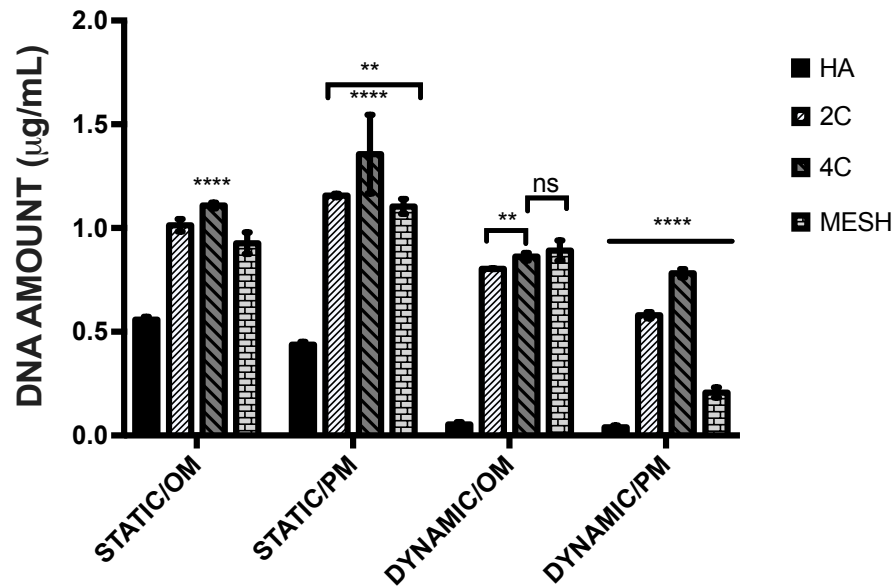


Fig. 5.11: Comparison of the amount of DNA associated with hMSCs after 21 days cultured on HA, 2C, 4C and mesh scaffolds in different culture conditions. In static conditions, 4C scaffolds revealed the highest DNA contents for both OM and PM compared to other scaffold designs ($p \leq 0.0001$). No significant differences were found in the DNA contents when 4C and mesh scaffolds were cultured in Dynamic/OM ($p = 0.6283$). DNA content was statistically lower when 2C scaffolds were cultured in Dynamic/OM compared to 4C scaffolds ($p = 0.0020$). In Dynamic/PM, 4C scaffolds showed the highest DNA contents ($p \leq 0.0001$). DNA contents remained the lowest for the HA scaffolds under all culture conditions. ($ns \geq 0.05$; $*p \leq 0.05$, $**p \leq 0.01$, $***p \leq 0.001$, $****p \leq 0.0001$).

5.2.4.3. *Total protein production*

For HA cellular scaffolds (Fig. 5.12 a), mean total protein produced concentrations increased when cultured in static condition ($p \leq 0.0001$), however, decreased in dynamic condition ($p \leq 0.05$) for both culture media (OM and PM) over time and differed between cultured conditions and media ($p \leq 0.05$). There was significant interaction between time, culture condition and media ($p \leq 0.05$), suggesting that the increase/decrease in mean total protein over time differed between culture conditions and media.

Comparing the culture conditions, HA cellular scaffolds in static showed significant increased in mean total protein when cultured in both OM and PM over time ($p \leq 0.0001$ for each). While, culturing these scaffolds in dynamic condition independent of culture media used, significantly reduced the mean total protein over culture period ($p \leq 0.0001$).

When comparing scaffolds in different culture media, no significant differences were observed when these scaffolds were cultured in Dynamic/OM and Dynamic/PM on day 7 ($p = 0.4485$) and day 14 ($p = 0.1922$). Mean DNA concentration was significantly lower when cultured in Dynamic/PM relative to Dynamic/OM on day 21 ($p = 0.0045$). In static condition, culturing HA cellular scaffolds in Static/OM resulted in higher mean total protein than those in Static/PM at either time-point ($p \leq 0.0001$ for each).

Over time, mean total protein for HA cellular scaffolds in static condition for both OM and PM increased as culture progressed ($p \leq 0.0001$ for each). When cultured in Dynamic/OM, cells produced significantly increased mean total protein up to day 14 ($p = 0.0260$), but no significant differences were observed on day 21 ($p = 0.9915$). HA cellular scaffolds cultured in Dynamic/PM showed no significant differences in the mean total protein on day 14 ($p = 0.9915$) and day 21 ($p = 0.1221$).

Overall, culturing HA cellular scaffolds in Static/OM produced the highest mean total protein on day 21 compared to all other culture conditions and media ($p \leq 0.0001$ for each).

For the 2C cellular scaffolds (Fig. 5.12 b), mean total protein increased over time for all tested culture conditions and media ($p \leq 0.0001$) and differed between culture conditions and media ($p \leq 0.0001$). There was a significant interaction between time, culture condition and media ($p \leq 0.0001$) suggesting that the increase in mean total protein over time differed between culture condition and media.

Comparing the culture conditions, 2C cellular scaffolds cultured in Static/OM were found to be significantly higher than Dynamic/OM on day 7 ($p = 0.0013$) but the former were significantly lower than the later on day 14 and day 21 ($p \leq 0.0001$ for each). While, cells cultured on 2C in PM showed significantly higher mean total protein produced in static compared to dynamic at either time-point ($p \leq 0.0001$ for each).

When comparing scaffolds in different culture media, cells cultured on 2C scaffolds in OM regardless in static or dynamic conditions produced significantly higher mean total protein compared to those in PM ($p \leq 0.0001$ for each) at each time-point.

Mean total protein for 2C cellular scaffolds cultured in static and dynamic condition independent of the culture media gradually increased ($p \leq 0.0001$ for each) as culture progressed.

Overall, culturing 2C cellular scaffolds in Dynamic/OM produced the highest mean total protein on day 14 and day 21 ($p \leq 0.0001$ for each) compared to all other culture conditions and media. While, those in Dynamic/PM remained the lowest throughout the culture period ($p \leq 0.0001$ for each) compared to all other culture conditions and media.

For the 4C cellular scaffolds (Fig. 5.12 c), mean total protein increased over time for all tested culture conditions and media ($p \leq 0.0001$) and differed between culture conditions and media ($p \leq 0.0001$). There was a significant interaction between time, culture condition and media ($p \leq 0.0001$) suggesting that the increase in mean total protein over time differed between culture condition and media.

Comparing the culture conditions, 4C cellular scaffolds in Dynamic/OM always revealed significantly higher mean total protein compared to Static/OM. For instance, 4C cellular scaffolds cultured in Dynamic/OM were found to be significantly higher than Static/OM ($p = 0.0001$) on day 21. While, when cells were cultured on 4C scaffolds in PM, static condition exhibited significantly higher mean total protein than dynamic condition at all time-points ($p \leq 0.0001$ for each).

When comparing scaffolds in different culture media, cells cultured on 4C scaffolds in OM regardless in static or dynamic conditions produced significantly higher mean total protein compared to those in PM ($p \leq 0.0001$ for each) at each time-point. The highest mean total protein produced when 4C cellular scaffolds were cultured in Dynamic/OM, while, culturing in Dynamic/PM resulted in the lowest mean total protein at each time-point ($p \leq 0.0001$ for each).

Mean total protein for 4C cellular scaffolds cultured in static and dynamic condition independent of the culture media gradually increased ($p \leq 0.0001$ for each) over time.

Overall, culturing 4C cellular scaffolds in Dynamic/OM produced the highest mean total protein on all time-points ($p \leq 0.0001$ for each) compared to all other culture conditions and media.

For the mesh cellular scaffolds (Fig. 5.12 d), mean total protein increased over time for all tested culture conditions and media ($p \leq 0.0001$) and differed between culture conditions and media ($p \leq 0.0001$). There was a significant interaction between time, culture condition and media ($p \leq 0.0001$) suggesting that the increase in mean total protein over time differed between culture condition and media.

Comparing the culture conditions, mesh cellular scaffolds cultured in Static/OM were found to be significantly higher than Dynamic/OM on day 7 ($p = 0.0718$) but the former were significantly lower than the later on day 14 and day 21 ($p \leq 0.0001$ for each). While, cells cultured on mesh scaffolds in PM showed significantly higher mean total protein produced in static compared to dynamic at either time-point ($p \leq 0.0001$ for each).

When comparing scaffolds in different culture media, cells cultured on mesh scaffolds in OM regardless in static or dynamic conditions produced significantly higher mean total protein compared to those in PM ($p \leq 0.0001$ for each) at each time-point.

Mean total proteins for mesh cellular scaffolds cultured in static (both OM and PM) and Dynamic/OM steady increased ($p \leq 0.0001$ for each) as culture progressed. However, mean total protein produced by mesh cellular scaffolds in Dynamic/PM showed a significant decreased on day 21 ($p \leq 0.0001$).

Overall, culturing mesh cellular scaffolds in Dynamic/OM produced the highest mean total protein on day 14 and day 21 ($p \leq 0.0001$ for each) compared to all other culture conditions and media. While, those in Dynamic/PM remained the lowest throughout the culture period ($p \leq 0.0001$ for each) compared to all other culture conditions and media.

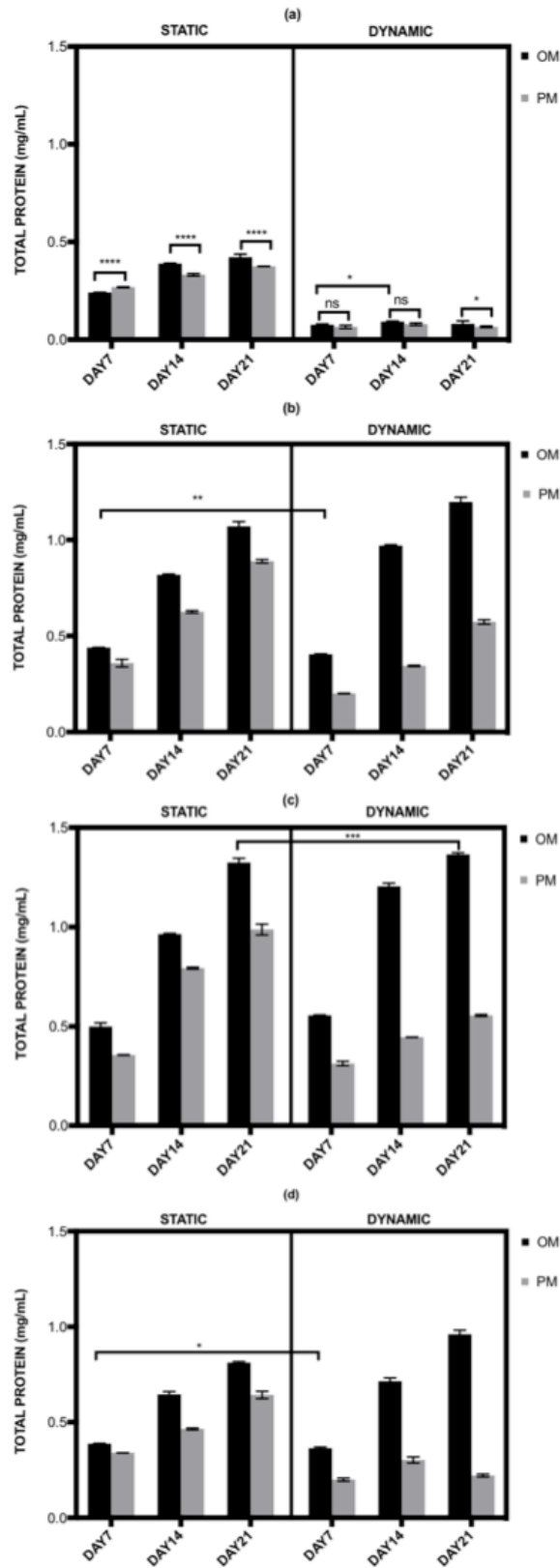


Fig. 5.12: The levels of total protein produced by hMSCs cultured on (a) HA; (b) 2C; (c) 4C and (d) mesh scaffolds under different culture conditions. Error bars represent means \pm SD for n=3. (ns \geq 0.05, * $p \leq$ 0.05, ** $p \leq$ 0.01, *** $p \leq$ 0.001, **** $p \leq$ 0.0001).

The mean total protein produced by the hMSCs cultured on HA, 2C, 4C and mesh scaffolds under different culture conditions were evaluated after 21 days as shown in Fig. 5.13.

Mean total proteins were significantly higher when cultured in OM than PM both in static and dynamic conditions for all the tested scaffold designs ($p \leq 0.05$) and differed between scaffold designs ($p \leq 0.0001$). There was significant interaction between culture condition/media and scaffold designs ($p \leq 0.05$), suggesting for all the tested scaffold designs, significantly higher mean total proteins were obtained in OM ($p \leq 0.0001$).

Comparing to the control (HA cellular scaffolds), all 3DP hybrid scaffolds showed significantly higher mean total proteins regardless of the culture condition/media ($p \leq 0.0001$ for each). No significant differences were observed by culturing HA scaffolds in dynamic condition both in OM and PM ($p = 0.9643$).

When compared between the 3DP hybrid scaffold designs, cells on 4C scaffolds revealed the highest mean total proteins in static for both OM and PM and Dynamic/OM as compared to 2C and mesh scaffolds ($p \leq 0.0001$ for each). However, no significant differences were observed between 2C and 4C scaffolds when cultured in Dynamic/PM ($p = 0.8652$). Among the 3DP hybrid scaffolds, cells cultured on mesh scaffolds produced the lowest mean total proteins compared to 2C and 4C scaffolds in all culture condition/media ($p \leq 0.0001$ for each). Culturing hMSCs on 4C scaffolds showed the highest mean total protein when cultured in Dynamic/OM than Static/OM ($p = 0.0004$).

Overall, 4C scaffolds in Dynamic/OM revealed the highest mean total proteins compared to all other investigated groups (scaffolds designs and culture condition/ media) on day 21 ($p \leq 0.0001$ for each).

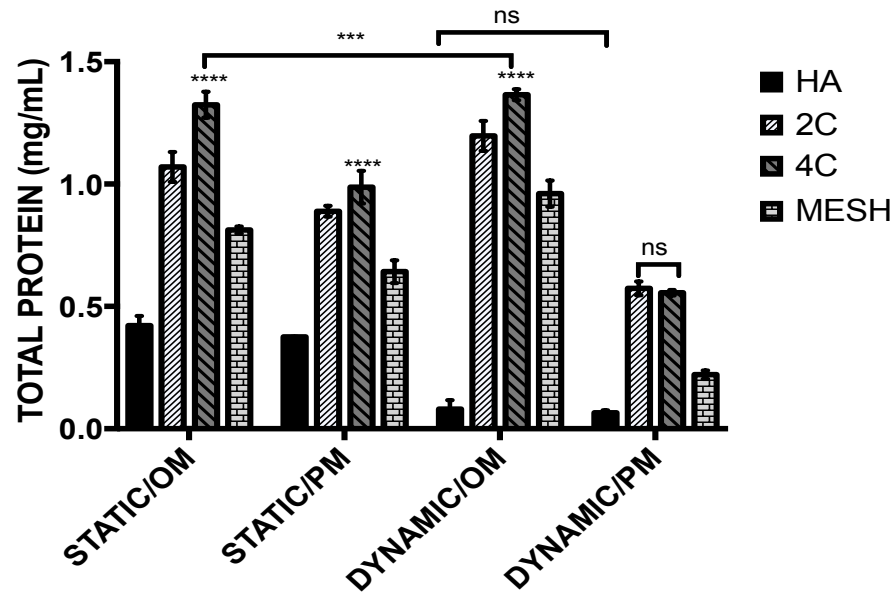


Fig. 5.13: Comparison of the levels of total protein produced by hMSCs after 21 days cultured on HA, 2C, 4C and mesh scaffolds in different culture conditions ($ns \geq 0.05$, $*p \leq 0.05$, $**p \leq 0.01$, $***p \leq 0.001$, $****p \leq 0.0001$).

5.2.4.4. Measuring the percentage of cytotoxicity

The percentages of cytotoxicity of hMSCs cultured on HA and 3DP hybrid scaffolds under different culture conditions were determined by measuring the amount of lactate excreted in the culture medium using Equation 2.4. The percentages of cytotoxicity (denoted as %LDH activity) were then calculated using Equation 2.5 (Section 2.3.8.4). Higher percentages (i.e.100%) indicate that the scaffolds or conditions were toxic to the cells and caused, or were likely to cause cell death. While, lower percentages (i.e. 0%) indicate that conditions were favourable to maintaining cell viability.

For HA cellular scaffolds (Fig. 5.14 a), mean %LDH activity increased when cultured in static condition ($p \leq 0.0001$) in OM and PM, however, decreased in dynamic condition ($p \leq 0.0001$) for both culture media over time and differed between cultured conditions and media ($p \leq 0.05$). There were significant interactions between time, culture condition and

media ($p \leq 0.05$), suggesting that the increase/decrease in %LDH activity over time differed between culture conditions and media.

Comparing the culture conditions, HA cellular scaffolds in static culture showed significant increase in mean %LDH activity in both OM and PM over time ($p \leq 0.05$ for each). While, exposing these scaffolds in dynamic condition independently of used culture media, significantly reduced mean %LDH activity was detected as culture progressed ($p \leq 0.0001$). Culturing hMSCs on HA scaffolds in dynamic condition regardless of the culture media resulted in significantly higher mean %LDH activity compared to static at each time-point ($p \leq 0.0001$ for each). For instance, Dynamic/OM showed significantly higher mean %LDH activity than Static/OM ($p = 0.0141$) on day 21 and Dynamic/PM also resulted in higher mean %LDH activity compared to Static/PM ($p = 0.0006$) on day 21.

When comparing different culture media, HA cellular scaffolds cultured in Static/PM showed significantly higher mean %LDH activity than those in Static/OM ($p \leq 0.0001$) at day 7. No significant differences were observed when these scaffolds were cultured in Static/OM and Static/PM at day 14 ($p = 0.9979$) and day 21 ($p = 0.9816$). Similar trends were observed in dynamic condition, where Dynamic/PM showed significantly higher mean %LDH activity than those in Dynamic/OM ($p \leq 0.0001$) at day 7. No significant differences were observed when these scaffolds were cultured in Dynamic/OM and Dynamic/PM at day 14 ($p = 0.9929$) and day 21 ($p = 0.5318$).

Over time, mean %LDH activity for HA cellular scaffolds in static condition for both OM and PM increased as culture progressed ($p \leq 0.0001$ for each). While, decreasing trend of mean %LDH activity were observed when these scaffolds were cultured in dynamic condition regardless of culture media used ($p \leq 0.0001$ for each).

Overall, culturing HA cellular scaffolds in Dynamic/PM resulted in the highest mean %LDH activity on day 7 compared to all other culture conditions and media ($p \leq 0.0001$ for each).

For the 2C cellular scaffolds (Fig. 5.14 b), mean %LDH activity increased when cultured in PM for both static and dynamic conditions ($p \leq 0.0001$) over time and differed between culture conditions ($p \leq 0.0001$). Culturing these scaffolds in OM showed no significant differences for both static ($p = 0.1946$) and dynamic ($p = 0.0120$) conditions on day 21. There was significant interaction between time, culture condition and media ($p \leq 0.05$), suggesting that the increase in %LDH activity over time differed between culture conditions and media.

Comparing the culture conditions, 2C cellular scaffolds revealed significantly higher means %LDH activity when cultured in dynamic condition than static in OM and PM on day 7 ($p \leq 0.0001$). No significant differences were observed in Static/OM and Dynamic/OM ($p = 0.4543$) on day 14. The mean %LDH activity was significantly increased in Dynamic/OM compared to Static/OM ($p = 0.0472$) on day 21. 2C cellular scaffolds cultured in Dynamic/PM showed significantly higher mean %LDH activity than those in Static/PM at each time-point ($p \leq 0.0001$ for each).

When comparing scaffolds in different culture media, cells cultured on 2C scaffolds in PM exhibited significantly higher mean %LDH activity than OM for both static and dynamic conditions at either time-point ($p \leq 0.0001$ for each).

Mean %LDH activity for 2C cellular scaffolds in static condition for both OM and PM and Dynamic/PM increased as culture progressed ($p \leq 0.0001$ for each). When these scaffolds

were cultured in Dynamic/OM, no significant differences were observed on day 14 ($p = 0.9034$), but the mean %LDH activity was significantly increased on day 21 ($p = 0.0120$).

Overall, 2C cellular scaffolds in Dynamic/PM exhibited the highest mean %LDH activity compared to all other tested culture condition and media ($p \leq 0.0001$ for each) at each time-point.

Cells cultured on 4C scaffolds (Fig. 5.14 c) resulted in the same trend and interactions between time, culture condition and media as 2C scaffolds ($p \leq 0.05$ for each). Mean %LDH activity increased when cultured in static condition for both culture media ($p \leq 0.05$ for each) over time and differed between culture media ($p \leq 0.05$). There was significant interaction between time, culture condition and media ($p \leq 0.0001$), suggesting that the increase in %LDH activity over time differed between culture conditions and media.

Comparing the culture conditions, 4C cellular scaffolds revealed significantly higher means %LDH activity when cultured in dynamic condition than static in OM and PM on day 7 ($p \leq 0.0001$ for each). The mean %LDH activity was significantly increased in Dynamic/OM compared to Static/OM ($p = 0.0241$) on day 14. No significant differences were observed in Static/OM and Dynamic/OM ($p = 0.9998$) on day 21. 4C cellular scaffolds cultured in Dynamic/PM showed significantly higher mean %LDH activity than those in Static/PM at each time-point ($p \leq 0.0001$ for each).

When comparing scaffolds in different culture media, cells cultured on 4C scaffolds in PM exhibited significantly higher mean %LDH activity than OM in dynamic conditions at either time-point ($p \leq 0.0001$ for each). In static conditions, significantly higher mean %LDH activity was obtained in Static/PM compared to Static/OM on day 7 ($p = 0.0002$), day 14 ($p \leq 0.0001$) and day 21 ($p \leq 0.0001$).

As culture progressed, mean %LDH activity for 4C cellular scaffolds in Dynamic/PM increased over time ($p \leq 0.0001$ for each). When these scaffolds were cultured in Dynamic/OM, no significant differences were observed on day 14 ($p = 0.9964$) and day 21 ($p = 0.6266$). Means %LDH activity in Static/OM was significantly increased on day 14 ($p = 0.0002$) and day 21 ($p \leq 0.0001$). When these scaffolds were cultured in Static/PM, means %LDH activity gradually increased on day 14 ($p \leq 0.0001$) and day 21 ($p = 0.0004$).

Overall, 4C cellular scaffolds in Dynamic/PM exhibited the highest mean %LDH activity compared to all other tested culture condition and media ($p \leq 0.0001$ for each) at each time-point.

For the mesh cellular scaffolds (Fig. 5.14 d), mean %LDH activity showed no significant differences in OM for both culture conditions ($p \geq 0.05$) and no differences between culture conditions ($p \geq 0.05$). There was no significant interaction between time, culture condition and media ($p \geq 0.05$) suggesting that over time, there was no effect in culture condition when mesh scaffolds were cultured in OM. Linear increases were observed when these scaffolds were cultured in Static/PM and Dynamic/PM ($p \leq 0.0001$ for each) as culture progressed.

Comparing the culture conditions, mesh cellular scaffolds revealed significantly higher means %LDH activity when cultured in dynamic condition than static in PM at either time-point ($p \leq 0.0001$ for each). No significant differences were observed in Static/OM and Dynamic/OM on day 7 ($p = 0.3280$), day 14 ($p = 0.0883$) and day 21 ($p = 0.1584$).

When comparing scaffolds in different culture media, cells cultured on mesh scaffolds in Static/OM and Static/PM showed no significant differences on day 7 ($p = 0.5043$). As culture progressed, scaffolds in Static/PM exhibited significantly higher mean %LDH

activity than Static/OM on day 14 ($p = 0.0079$) and day 21 ($p \leq 0.0001$). In dynamic condition, significantly higher mean %LDH activity was obtained in Dynamic/PM compared to Dynamic/OM at each time-point ($p \leq 0.0001$ for each).

As culture progressed, no significant differences were observed in the mean %LDH activity of mesh scaffolds cultured in Static/OM on day 14 ($p = 0.2012$) and day 21 ($p = 0.4469$). Culturing these scaffolds in Dynamic/OM showed no significant differences on day 14 ($p = 0.0871$) and day 21 ($p = 0.6182$). When cultured in Static/PM and Dynamic/PM, mean %LDH activity significantly increased over time ($p \leq 0.0001$ for each).

Overall, culturing mesh scaffolds in Dynamic/PM resulted in the highest mean %LDH activity compared to all other tested culture condition and media ($p \leq 0.0001$ for each) over the culture period.

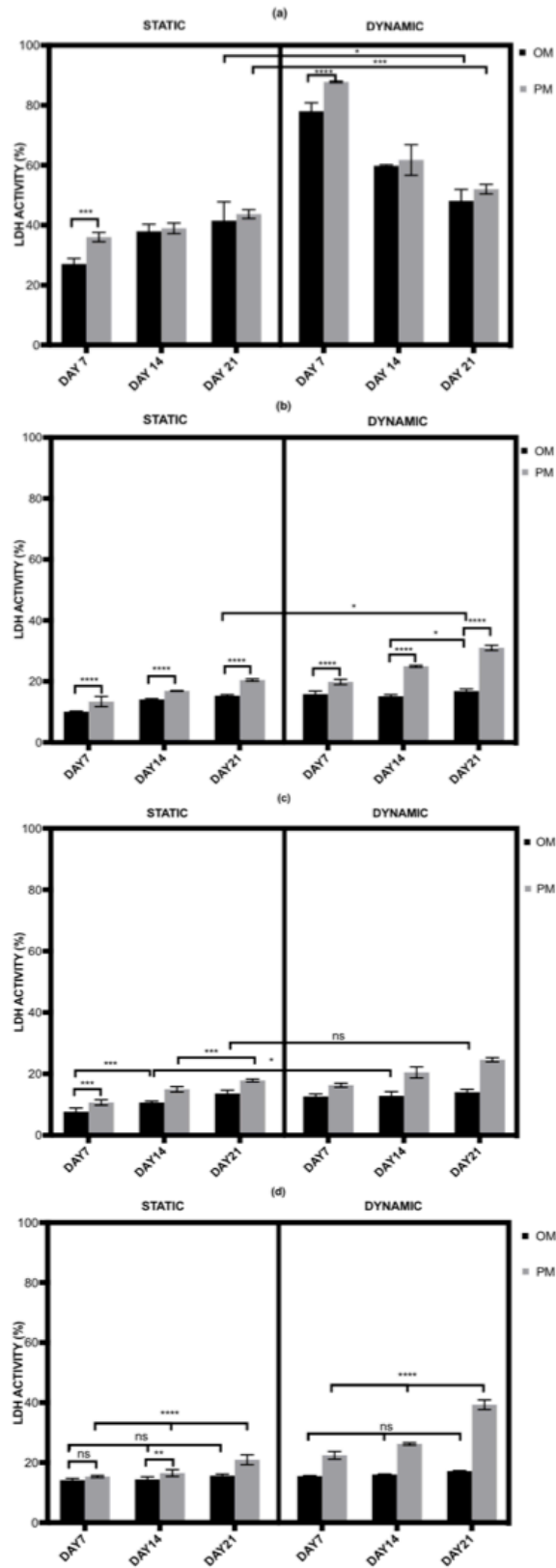


Fig. 5.14: The percentages of LDH activity of hMSCs cultured on (a) HA; (b) 2C; (c) 4C and (d) mesh scaffolds under different culture conditions. Error bars represent means \pm SD for $n=3$. ($ns \geq 0.05$, $*p \leq 0.05$, $**p \leq 0.01$, $***p \leq 0.001$, $****p \leq 0.0001$).

The %LDH activity of all the investigated scaffolds after 21 days cultured in different conditions is demonstrated in Fig. 5.15.

After 21 days, the highest mean %LDH activity were obtained in Dynamic/PM for all the tested scaffold designs ($p \leq 0.0001$) and differed between scaffold designs ($p \leq 0.0001$). There was significant interaction between culture condition/media and scaffold designs ($p \leq 0.05$), suggesting for all tested scaffold designs, significantly higher means %LDH activity were obtained in PM ($p \leq 0.0001$).

Comparing to the control (HA cellular scaffolds), all 3DP hybrid scaffolds showed significantly lower %LDH activity regardless of the culture condition/media ($p \leq 0.0001$ for each).

When comparing the 3DP hybrid scaffold designs, no significant differences in the mean %LDH activity were detected when 2C, 4C and mesh cellular scaffolds were cultured in static condition regardless of the culture media ($p \leq 0.0001$ for each). When cultured in Dynamic/OM, 4C scaffolds showed significantly lower mean %LDH activity compared to 2C ($p \leq 0.0001$) and mesh scaffolds ($p = 0.0008$). Similar trend was observed in Dynamic/PM where significantly lower %LDH activity was obtained on 4C scaffolds than 2C and mesh scaffolds ($p \leq 0.0001$ for each). Culturing the 3DP hybrid scaffolds in PM for both static and dynamic condition resulted in higher mean %LDH activity. For instance, 2C, 4C and mesh cellular scaffolds showed significantly higher means %LDH activity in Static/PM compared to Static/OM at $p = 0.0036$, $p = 0.0416$ and $p = 0.0022$, respectively.

Overall, HA cellular scaffolds showed the highest mean %LDH activity compared to all other investigated groups (scaffolds designs and culture condition/ media) on day 21 ($p \leq 0.0001$ for each).

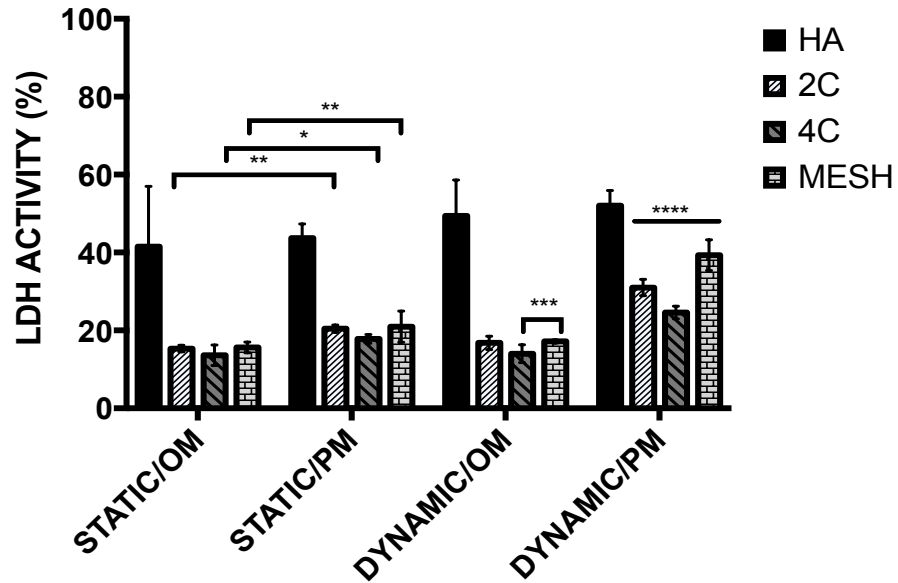


Fig. 5.15: The percentages of LDH activity on HA, 2C, 4C and mesh scaffolds in different culture conditions after 21 days. This graph demonstrates the comparison of the percentage of lactate dehydrogenase activity (%LDH activity) of hMSCs after 21 days cultured on HA, 2C, 4C and mesh scaffolds in different culture conditions ($ns \geq 0.05$, $*p \leq 0.05$, $**p \leq 0.01$, $***p \leq 0.001$, $****p \leq 0.0001$).

5.2.4.5. *Cell phenotypic expression*

Alkaline phosphatase (ALP) staining was used to qualitatively identify the osteoblastic phenotype expression. A positive ALP stain appeared red. All scaffolds stained for ALP at day 0 showed the absence of stains as shown in Fig. 5.16.

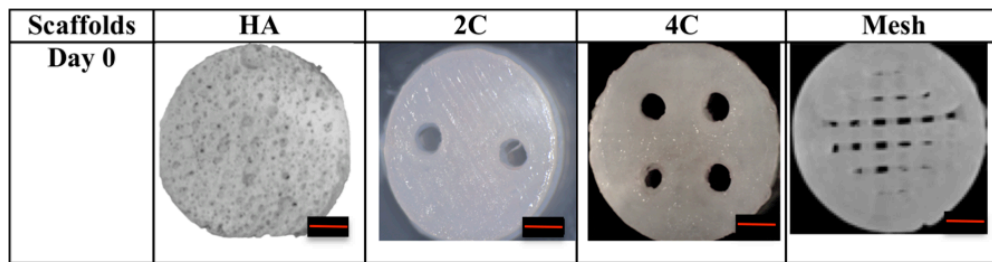


Fig. 5.16: ALP staining for all scaffold designs at day 0. Scale bar = 1mm.

The HA scaffolds demonstrated less growth over the culture periods as indicated by a reduced staining pattern. Images of the alkaline phosphatase (ALP) stains are represented in Fig. 5.17. Even after 21 days cultured in OM, low levels of stain were observed for both culture conditions.

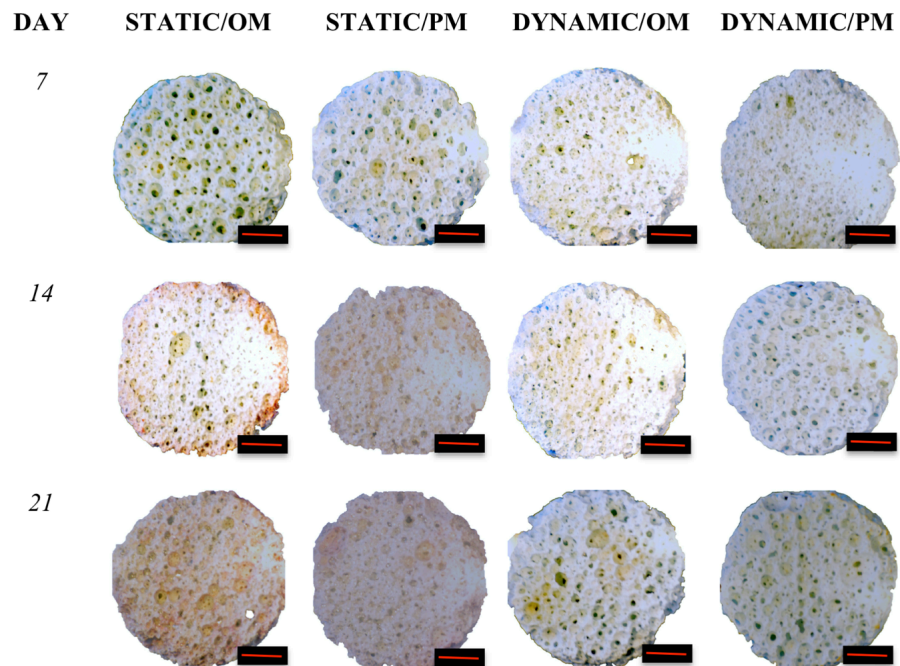


Fig. 5.17: ALP staining of the HA scaffolds after 7, 14 and 21 days under static and dynamic conditions in both OM and PM. Red scale bar = 1mm

After 14 days in OM, more positive stains across the scaffolds were observed on the 2C scaffolds for both culture conditions (Fig. 5.18). A small area of the scaffolds was faintly stained for ALP expression for 2C scaffolds in Static/PM after 21 days in culture. However, no stains were observed on the 2C scaffolds culture in Dynamic/PM over time.

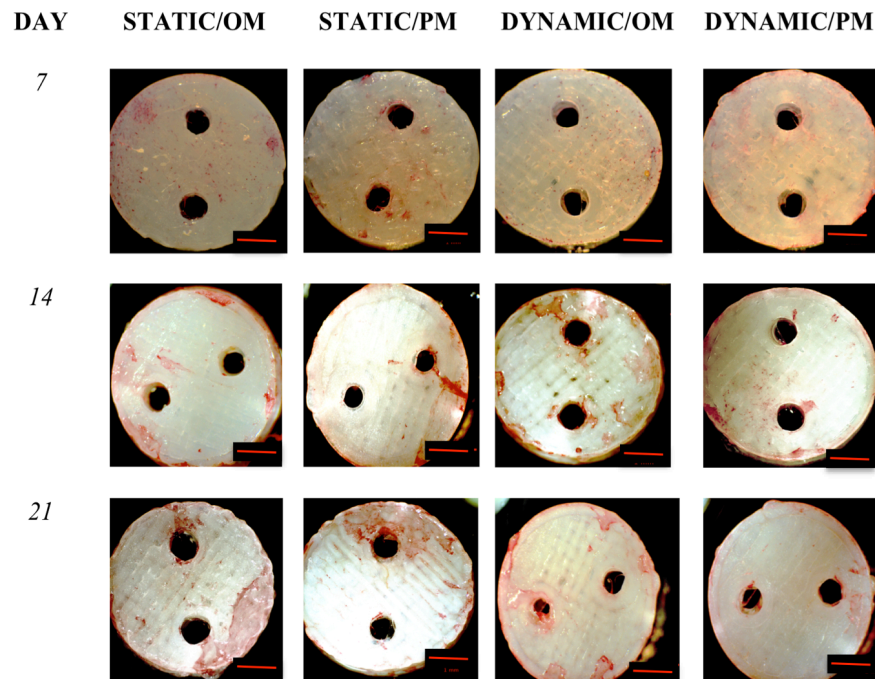


Fig. 5.18: ALP staining of the 2C scaffolds after 7, 14 and 21 days under static and dynamic conditions in both OM and PM. More localized stains were observed on 2C cellular scaffolds cultured in OM compared to PM for both static and dynamic conditions. Red scale bar = 1mm.

The ALP expressions of 4C cellular scaffolds (Fig. 5.19) was greater across the scaffolds after 21 days when they were cultured in the osteogenic media for both conditions. Scaffolds cultured in Static/PM exhibited pale ALP expressions and absolutely no stains were observed on Dynamic/PM at all time-points.

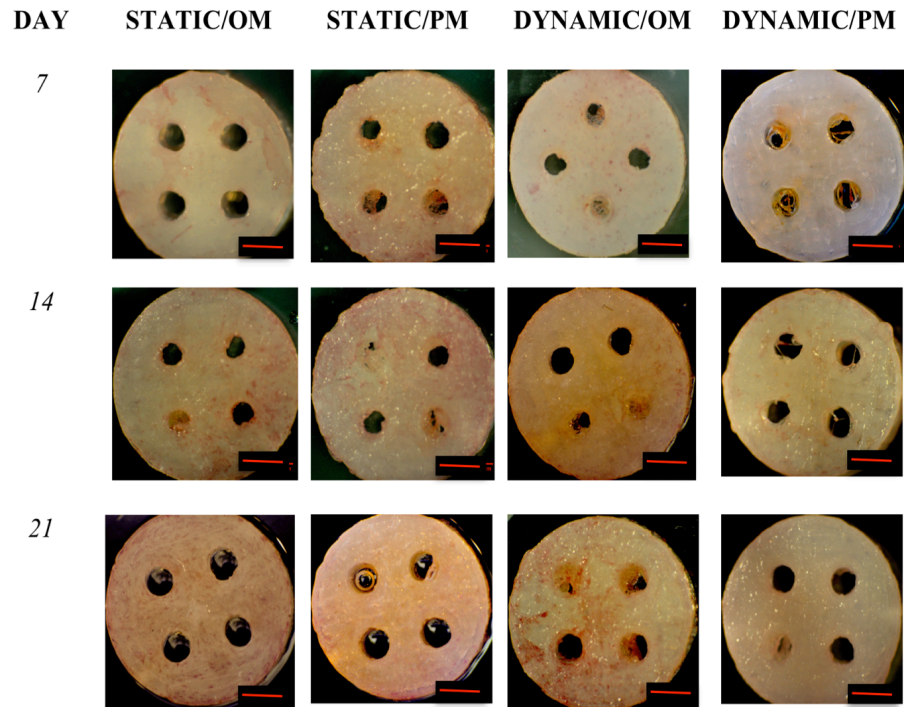


Fig. 5.19: ALP staining of the 4C scaffolds after 7, 14 and 21 days under static and dynamic conditions in both OM and PM. Positive stains were observed when hMSCs cultured on 4C scaffolds in OM under both static and dynamic conditions. Almost negligible stain was observed on 4C cellular scaffolds under Dynamic/PM at all time-points. Red scale bar = 1mm.

No ALP expressions were obtained after 7 days in culture for all conditions. Similar to the 2C and 4C cellular scaffolds, more positive stain was observed when the mesh scaffolds were cultured in osteogenic media for both static and rotary bioreactor particularly after 21 days. ALP stain on Static/OM-cultured scaffolds was observed purely on the scaffold surface, whereas scaffolds cultured in Dynamic/OM were more homogenously stained across the scaffold and its pores (Fig. 5.20).

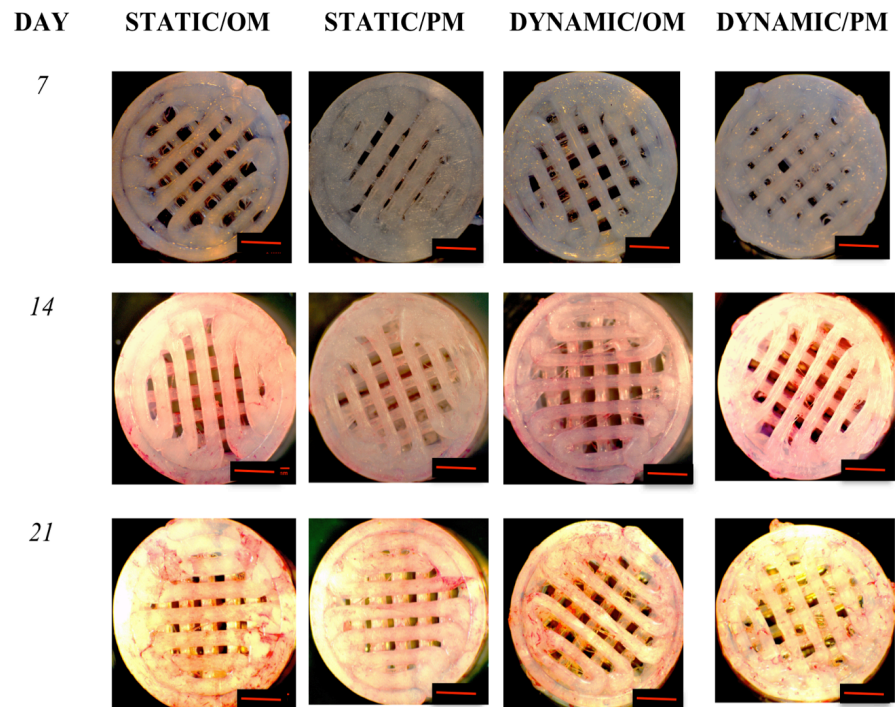


Fig. 5.20: ALP staining of the mesh scaffolds after 7, 14 and 21 days under static and dynamic conditions in both OM and PM. Red scale bar = 1mm.

In summary, no positive ALP stains were observed on the HA scaffolds for all culture conditions after 21 days. While, positive ALP stains were obtained from the 3DP hybrid scaffolds in particular with the presence of OM. Differences were seen between the three scaffolds designs. In Static/OM, the 4C cellular scaffolds showed the most homogenous ALP expression across the entire scaffolds as compared to the 2C and the mesh scaffolds. When the cellular scaffolds were exposed to the dynamic condition in the rotary bioreactor, ALP expression of the 4C and mesh scaffolds seems the higher compared to the 2C scaffold. Localized ALP expressions were observed on 2C scaffolds in both culture conditions in OM after 21 days.

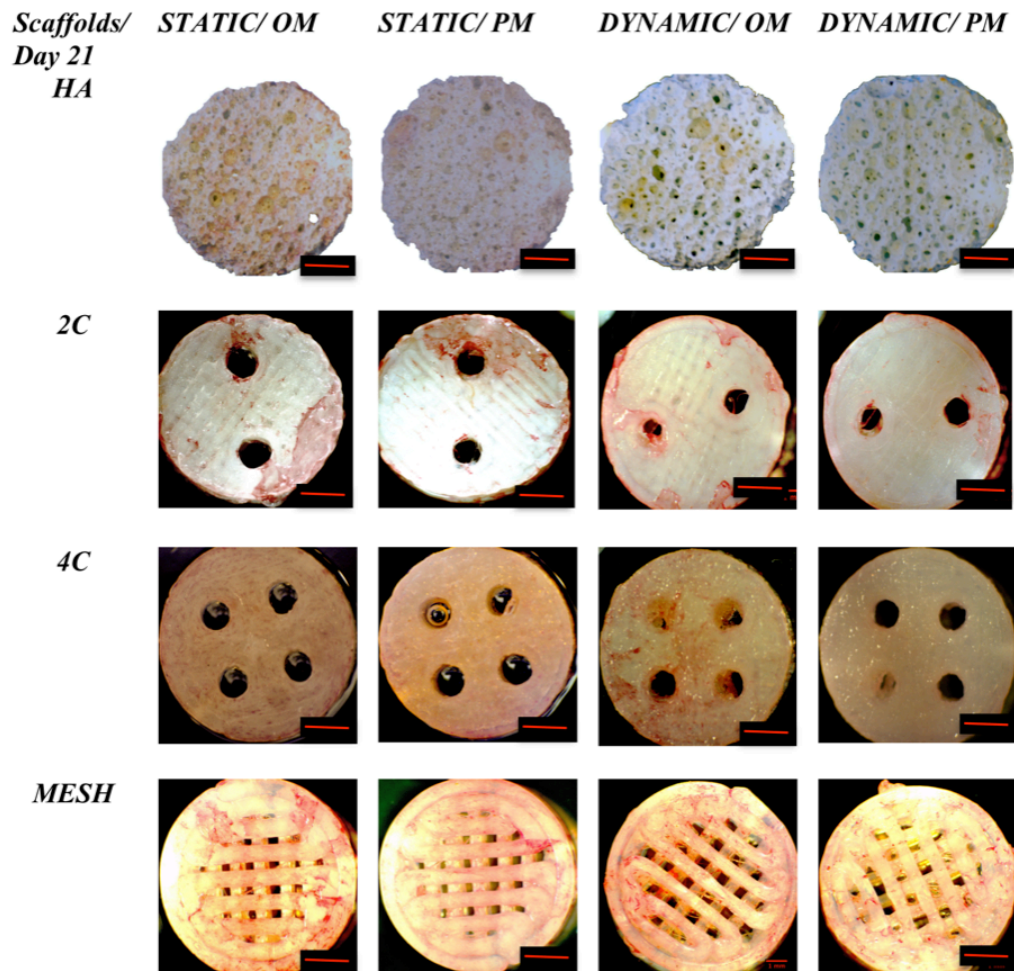


Fig. 5.21: ALP staining for different scaffold designs after 21 days cultured under static and dynamic conditions in OM and PM. Red scale bar = 1mm.

5.2.4.6. *Early osteogenic differentiation*

The Alkaline Phosphatase (ALP) enzyme activity was determined using a fluorescence assay, where metabolism of a phosphate-based substrate permits the release of a fluorescent marker. Therefore, higher enzyme activity is associated with an increased level of fluorescence from a sample. Because the ALP activity will ultimately be related to the number of cells, ALP/DNA can be a useful metric for relative comparison of different samples.

For HA cellular scaffolds (Fig. 5.22 a), mean ALP activity increased when cultured in static condition ($p \leq 0.0001$) in OM and PM, however, showed no significant differences in dynamic condition ($p \leq 0.0001$) for both culture media over time and differed between cultured conditions and media ($p \leq 0.05$). There was significant interaction between time, culture media ($p \leq 0.05$) in static condition, suggesting that the increase in mean ALP activity over time differed between culture conditions and media. However, there was no significant interaction between time, culture condition and media ($p \geq 0.05$) in dynamic condition.

Comparing the culture conditions, culturing hMSCs on HA scaffolds in static condition regardless of the culture media resulted in significantly higher mean ALP activity compared to dynamic at each time-point ($p \leq 0.0001$ for each).

When comparing different culture media, no significant differences were observed when HA cellular scaffolds were cultured in Dynamic/OM and Dynamic/PM ($p \geq 0.05$ for each) at each time-points. In static conditions, scaffolds cultured in OM showed higher mean ALP activity compared to those in PM at day 7 ($p = 0.0118$), day 14 ($p = 0.0170$), and day 21 ($p \leq 0.0001$).

Over time, no significant differences were observed in the ALP activity for all culture conditions and media. For instance, HA cellular scaffolds showed no significant differences in Static/OM on day 14 ($p = 0.9926$) and day 21 ($p = 0.4646$).

Overall, culturing HA cellular scaffolds in Static/OM resulted in the highest mean ALP activity on day 21 compared to all other culture conditions and media ($p \leq 0.0001$ for each).

For the 2C cellular scaffolds (Fig. 5.22 b), mean ALP activity showed a bell-shaped trend for all the tested culture condition and media ($p \leq 0.05$) over time and differed between culture condition and media ($p \leq 0.05$). There were significant interactions between time, culture condition and media ($p \leq 0.0001$), suggesting that the increase/decrease in ALP activity over time differed between culture conditions and media.

Comparing the culture conditions, 2C cellular scaffolds presented significantly higher mean ALP activity when cultured in dynamic condition compared to static over time ($p \leq 0.05$ for each). For instance, 2C cellular scaffolds exhibited significantly higher ALP activity when cultured in Dynamic/OM than Static/OM on day 7 ($p = 0.037$). When these scaffolds were cultured in PM, significantly lower means ALP activity were obtained in static compared to dynamic on day 7 ($p = 0.0003$), day 144 ($p = 0.0020$) and day 21 ($p \leq 0.0001$).

When comparing scaffolds in different culture media, significantly higher level of means ALP activity were detected when these scaffolds were cultured in OM compared to PM for both static and dynamic condition at each time-point ($p \leq 0.0001$ for each).

Regardless of culture condition and media, all 2C cellular scaffolds showed significant dropped in mean ALP activity on day 21 after reaching the peak on day 14 ($p \leq 0.05$ for

each). For instance, when cultured in Dynamic/OM, mean ALP activity was significantly increased and reached the maximum on day 14 ($p \leq 0.0001$) and eventually dropped on day 21 ($p = 0.0005$).

Overall, 2C cellular scaffolds cultured in Dynamic/ OM showed the highest mean ALP activity compared to all other tested culture condition and media ($p \leq 0.05$ for each) at each time-point.

For the 4C cellular scaffolds (Fig. 5.22 c), mean ALP activity showed a bell-shaped trend for all the tested scaffolds in OM ($p \leq 0.05$) over time and differed between culture condition and media ($p \leq 0.05$). There were significant interactions between time, culture condition and media ($p \leq 0.05$), suggesting that the increase/decrease in ALP activity over time differed between culture conditions and media. However, culturing 4C cellular scaffolds in PM showed no significant differences in mean ALP activity over time, but differed between culture conditions ($p \leq 0.05$).

Comparing the culture conditions, no significant differences were detected when 4C cellular scaffolds were cultured in Static/PM and Dynamic/PM on day 7 ($p = 0.5510$). These scaffolds then showed the lowest mean ALP activity when cultured in Dynamic/PM on day 14 and day 21 ($p \leq 0.0001$ for each) compared to Static/PM. Culturing 4C cellular scaffolds in OM resulted in significantly higher mean ALP activity over time, with those in Dynamic/OM were found to be significantly higher compared to Static/OM at each time-point ($p \leq 0.0001$ for each).

When comparing scaffolds in different culture media, significantly higher level of means ALP activity were detected when these scaffolds were cultured in OM compared to PM for both static and dynamic condition at each time-point ($p \leq 0.0001$ for each).

As culture progressed, mean ALP activity of the 4C cellular scaffolds cultured in OM increased and reached the peak on day 14 and finally dropped on day 21. For instance, when cultured in Static/OM, mean ALP activity showed significant increased on day 14 ($p \leq 0.0001$) and eventually dropped afterwards on day 21 ($p = 0.0008$). Similar trend was observed in Dynamic/OM, where mean ALP activity was significantly declined on day 21 ($p = 0.0091$). No significant differences were observed in the mean ALP activity when 4C cellular scaffolds were cultured in Static/PM on day 14 ($p = 0.1321$) and day 21 ($p = 0.7875$). Similar trend was observed for those in Dynamic/PM, where no significant differences were observed in the mean ALP activity on day 14 ($p = 0.2510$) and day 21 ($p = 0.5392$).

Overall, 4C cellular scaffolds cultured in Dynamic/ OM showed the highest mean ALP activity compared to all other tested culture condition and media ($p \leq 0.0001$ for each) at each time-point.

Growing cells on the mesh cellular scaffolds resulted in the same trend and interaction between time, culture condition and media as 4C scaffolds (Fig. 5.22 d), where mean ALP activity showed a bell-shaped trend for all the tested scaffolds in OM ($p \leq 0.05$) over time and differed between culture condition and media ($p \leq 0.05$). There were significant interactions between time, culture condition and media ($p \leq 0.05$), suggesting that the increase/decrease in ALP activity over time differed between culture conditions and media. However, culturing mesh cellular scaffolds in PM showed a fluctuating trend in dynamic condition ($p \leq 0.05$) while, increasing pattern in static condition ($p \leq 0.05$) over time.

Comparing the culture conditions, no significant differences were detected when 4C cellular scaffolds were cultured in Static/PM and Dynamic/PM on day 14 ($p = 0.8060$) and day 21 ($p = 0.2955$). These scaffolds then showed the lowest mean ALP activity when

cultured in Dynamic/PM on day 14 and day 21 ($p \leq 0.0001$ for each) compared to Static/PM. Culturing 4C cellular scaffolds in OM resulted in significantly higher mean ALP activity over time, with those in Dynamic/OM were found to be significantly higher compared to Static/OM at each time-point ($p \leq 0.0001$ for each).

When comparing scaffolds in different culture media, significantly higher level of means ALP activity were detected when these scaffolds were cultured in OM compared to PM for both static and dynamic condition at each time-point ($p \leq 0.0001$ for each).

Over time, the mean ALP activity for scaffolds cultured in Static/PM showed significant increased on day 14 ($p = 0.0290$), but no significant differences were observed on day 21 ($p = 0.9952$). When cultured in Dynamic/PM, mean ALP activity was significantly dropped on day 14 ($p = 0.0086$), but increased again on day 21 ($p = 0.0003$). When cultured in OM, 4C cellular scaffolds cultured in dynamic condition reached maximum on day 14 and significantly dropped on day 21 ($p \leq 0.0001$ for each). Similar trend was obtained for Static/OM, where maximum mean ALP activity was attained on day 14 ($p \leq 0.0001$) and significantly lower mean ALP activity was showed on day 21 ($p = 0.0002$).

Overall, the highest mean ALP activity was obtained when mesh cellular scaffolds were cultured in Dynamic/OM compared to all other tested culture condition and media ($p \leq 0.0001$ for each) at each time-point.

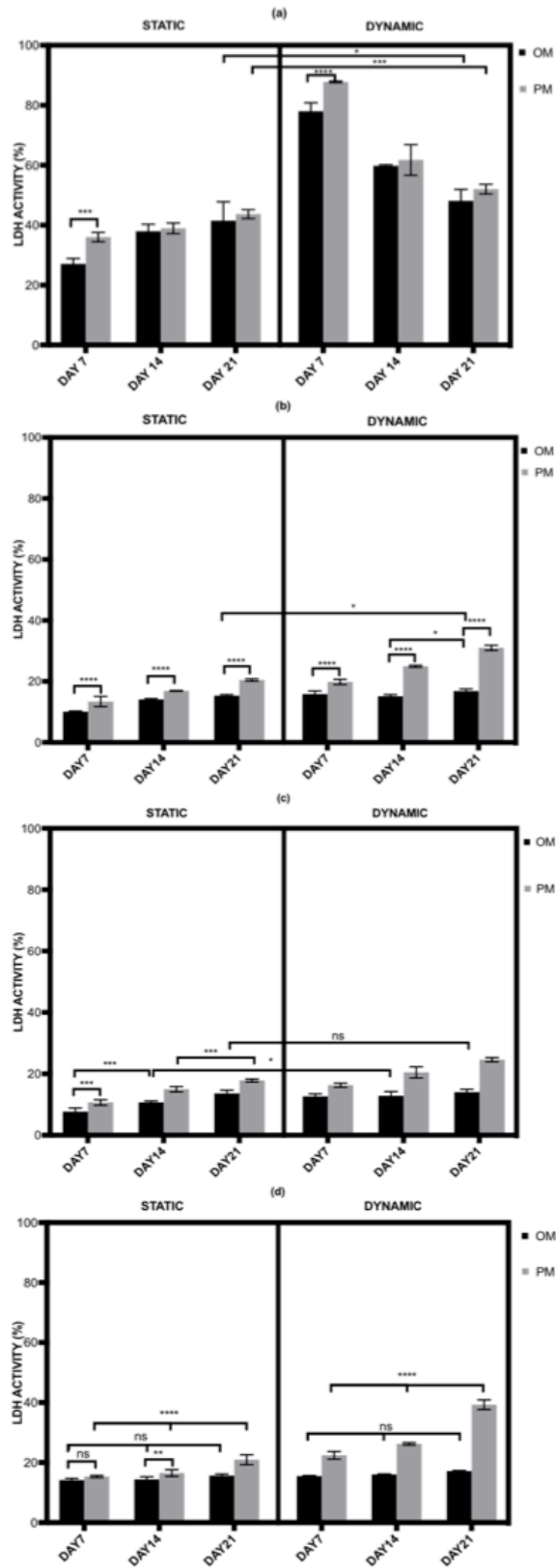


Fig. 5.22: The levels of ALP activity of hMSCs growing on (a) HA; (b) 2C; (c) 4C and (d) mesh scaffolds under different culture conditions. Error bars represent means \pm SD for $n=3$. ($ns \geq 0.05$, $*p \leq 0.05$, $**p \leq 0.01$, $***p \leq 0.001$, $****p \leq 0.0001$).

The mean ALP activity of hMSCs cultured on HA, 2C, 4C and mesh scaffolds under different culture conditions were evaluated after 21 days as shown in Fig. 5.23. The aim here is to determine which scaffold design and under which culture condition/medium composition could encourage the fastest osteogenic differentiation.

Mean ALP activity was significantly higher when cultured in OM than PM both in static and dynamic conditions for all the tested scaffold designs ($p \leq 0.0001$) and differed between scaffold designs ($p \leq 0.0001$). There was significant interaction between culture condition/media and scaffold designs ($p \leq 0.05$), suggesting for all the tested scaffold designs, significantly higher means ALP activity were obtained in OM ($p \leq 0.0001$).

Comparing to the control (HA cellular scaffolds), all 3DP hybrid scaffolds showed significantly higher mean ALP activity regardless of the culture condition/media ($p \leq 0.0001$ for each). No significant differences were observed by culturing HA scaffolds in dynamic condition both in OM and PM ($p = 0.9699$).

When compared between the 3DP hybrid scaffold designs, cells on 4C scaffolds revealed the highest mean ALP activity in OM for both static and dynamic conditions as compared to 2C and mesh scaffolds ($p \leq 0.0001$ for each). In Static/OM, no significant differences were detected in the mean ALP activity of 2C and mesh scaffolds ($p = 0.9917$). Similar trend was obtained by culturing 2C and mesh scaffolds in Static/PM, where no significant differences were observed ($p = 0.9210$). 4C cellular scaffolds showed significantly higher mean ALP activity compared to 2C ($p = 0.045$) when cultured in Static/PM. While, cells cultured on mesh scaffolds exhibited significantly lower mean ALP activity compared to 4C scaffolds ($p = 0.0003$). When cultured in Dynamic/OM, no significant differences were shown by 2C and mesh scaffolds ($p = 0.7464$). 4C scaffolds demonstrated significantly higher mean ALP activity compared to 2C and mesh scaffolds ($p \leq 0.0001$ for each) in

Dynamic/OM. However, when 4C scaffolds were cultured in Dynamic/PM, significantly lower mean ALP activity was obtained as compared to 2C ($p \leq 0.0001$) and mesh scaffolds ($p = 0.0002$). Between 2C and mesh scaffolds, no significant differences were detected when cultured in Dynamic/PM ($p = 0.7464$).

Overall, 4C scaffolds in Dynamic/OM revealed the highest ALP activity compared to all other investigated groups (scaffolds designs and culture condition/ media) on day 21 ($p \leq 0.0001$ for each).

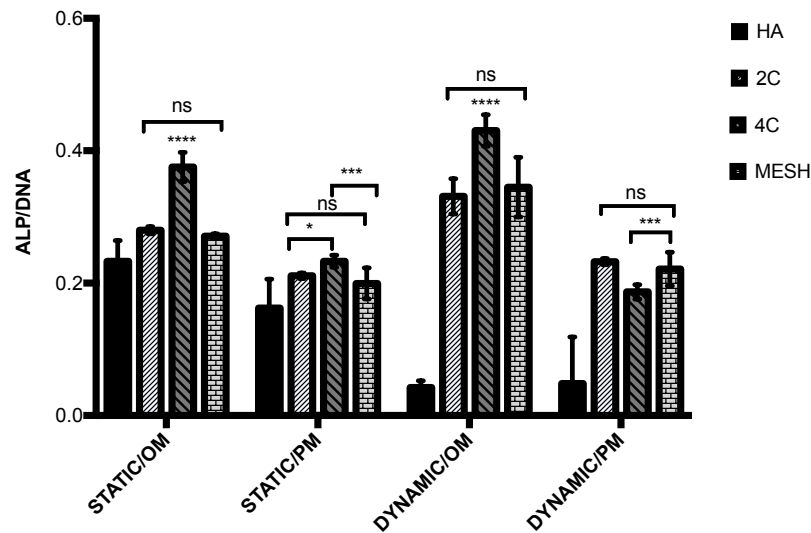


Fig. 5.23: The comparison of the levels of ALP activity of hMSCs after 21 days cultured on HA, 2C, 4C and mesh scaffolds in different culture conditions. (ns ≥ 0.05 , * $p \leq 0.05$, ** $p \leq 0.01$, *** $p \leq 0.001$, **** $p \leq 0.0001$).

5.2.4.7. *Micro-computed tomography analysis*

Micro-computed tomography (Micro-CT) analysis was used to evaluate the formation of the mineralized matrix on different scaffold designs. Prior to cell seeding, all scaffolds were scanned at different thresholds (HA scaffolds: 50/1000 and 3DP hybrid scaffolds: 42/1000) as demonstrated in Appendix (Fig. A5). The cellular scaffolds were scanned at two density thresholds (HA scaffolds: 60/1000 and 120/1000; 3DP hybrid scaffolds: 55/1000 and 120/1000), firstly to determine the total volume and connectivity density of each scaffold and secondly at a higher threshold to estimate the mineralized portion formed on all scaffold designs after 7, 14 and 21 days cultured under different culture conditions. Typical Micro-CT density maps of the whole area and cross-sections of the cellular scaffolds are demonstrated in Fig. 5.24-5.27. The colour density bar shown in the images represented different density values, where lower density area is designated with minimum value while higher density is denoted by the maximum value. Higher density represents mineralized areas, lower density represents non-mineralized areas.

The density maps obtained from Micro-CT analysis of the HA cellular scaffolds showed that no mineralized matrix was found in any culture conditions. As demonstrated in Fig. 5.24, the majority of the scanned images were only the scaffold (denoted by green areas). However, a small area of the scaffold appeared red at higher threshold values particularly after 21 days.

The 2C cellular scaffolds showed mineralized matrix formed after 21 days cultured in Static/OM as demonstrated in Fig. 5.25. Only a small portion of mineralized matrix was seen on the surface of these cellular scaffolds.

Evidence of the formations of mineralized matrix was shown when hMSCs were cultured on 4C hybrid scaffolds particularly in OM. Denser areas were found on 4C cellular

scaffolds as early as 14 days in Static/OM and Dynamic/OM. After 21 days in Dynamic/OM, channels on the 4C cellular scaffolds were partially filled with the mineralized matrix as can be clearly seen in the cross-section image shown in Fig. 5.26. The denser area of the cellular scaffolds under Static/OM was only found on the surface of the scaffolds. Almost negligible mineralized portion was detected by growing hMSCs on 4C cellular scaffolds in PM for both culture conditions even after 21 days.

Similar to 2C cellular scaffolds, a very limited portion of mineralized matrix formed on the mesh scaffolds under all culture conditions (Fig. 5.27). For instance, a small portion of mineralized matrix was detected on the cellular scaffolds cultured in Dynamic/OM after 21 days. However, the denser area was only found on the surface of the scaffold.

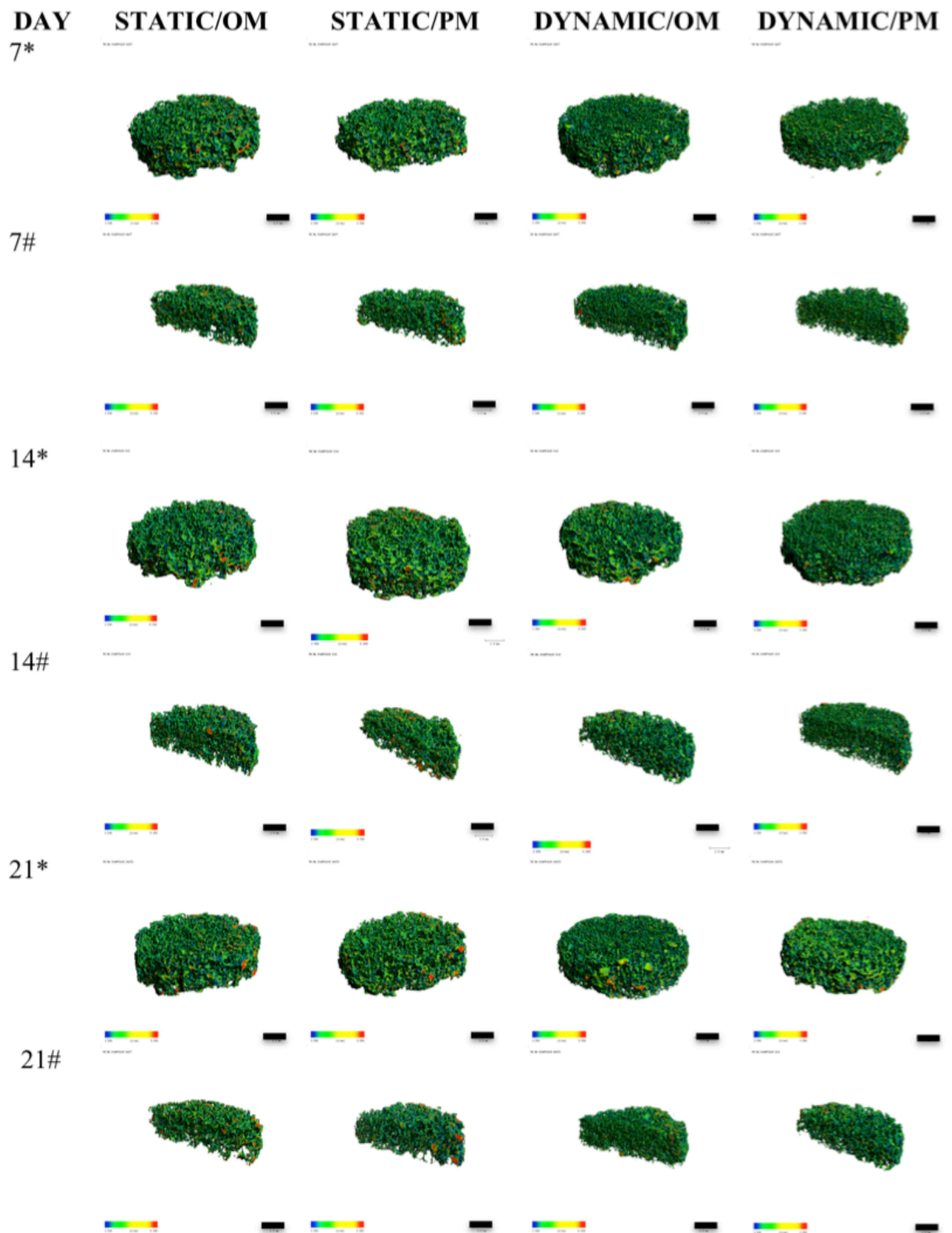


Fig. 5.24: Density maps of HA cellular scaffolds in different culture conditions after 7, 14 and 21 days obtained from Micro-CT analysis. No mineralized matrix was found in any culture conditions even after 21 days when hMSCs were cultured on HA scaffolds (control). (*=Whole area; #= cross-section of the scaffolds). Black scale bar = 1 mm. Colour density bar = 3.5 (min)-5.0 (max)/cm.

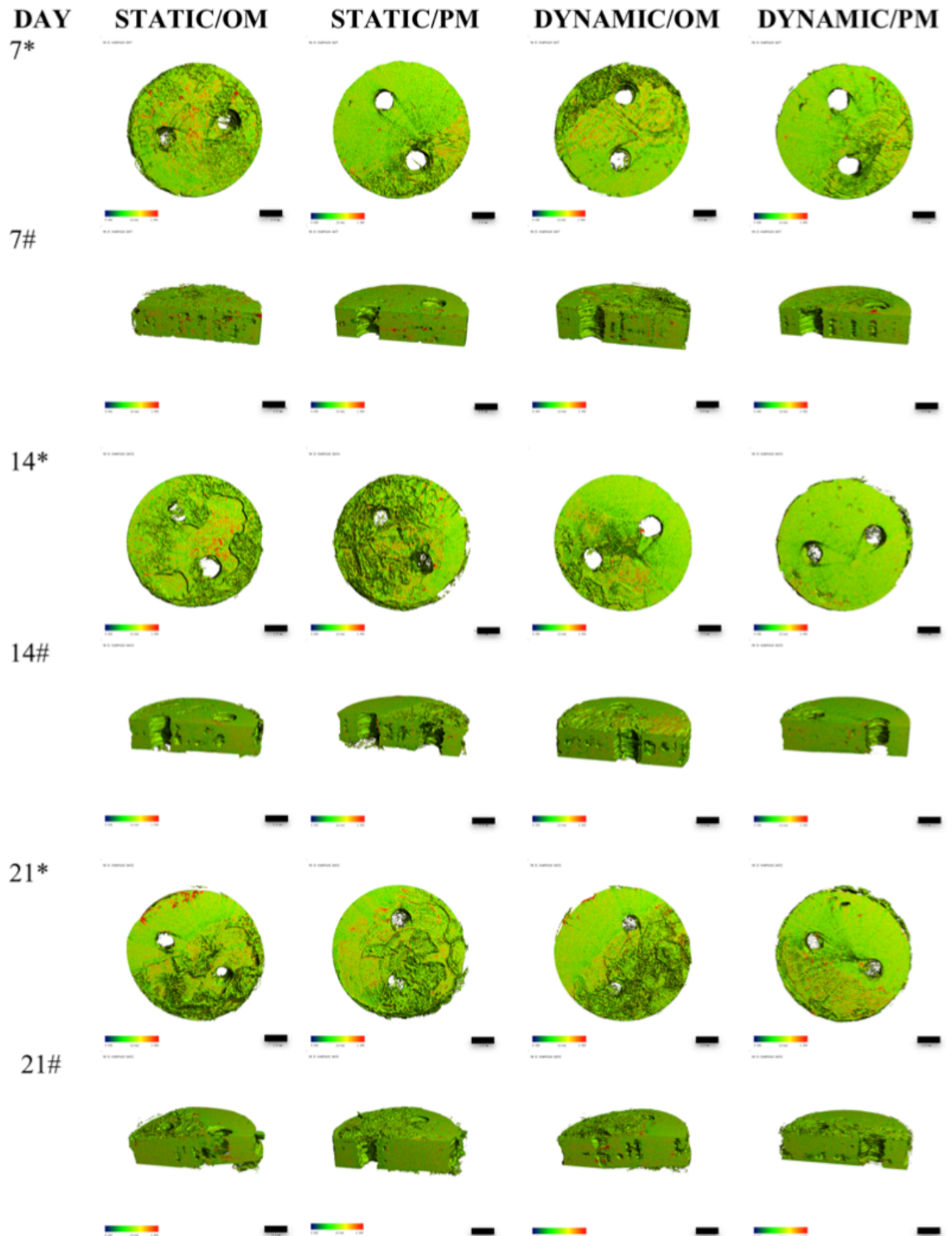


Fig. 5.25: Density maps of 2C cellular scaffolds in different culture conditions after 7, 14 and 21 days obtained from Micro-CT analysis. Small amount of mineralized matrix was found after 21 days culture in Static/OM, where hMSCs started to form mineralized matrix on the surface of the scaffolds. (*=Whole area; #= cross-section of the scaffolds). Black scale bar = 1 mm. Colour density bar = 3.5 (min)-5.0 (max)/cm.

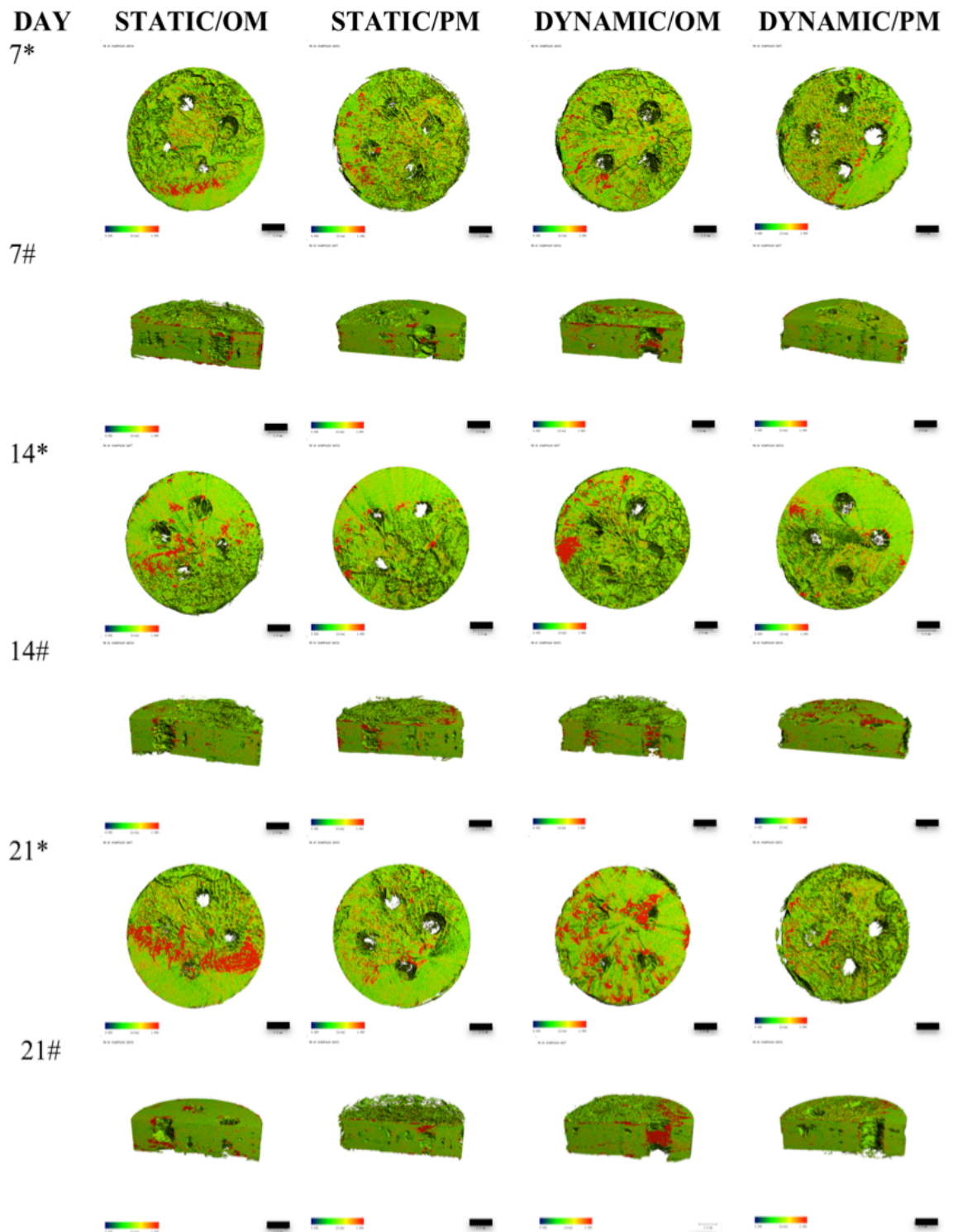


Fig. 5.26: Density maps of 4C cellular scaffolds in different culture conditions after 7, 14 and 21 days obtained from Micro-CT analysis. hMSCs were able to form mineralized matrix on 4C scaffolds as early as 14 days in osteogenic media for both conditions and these amounts increased over time. (*=Whole area; #= cross-section of the scaffolds). Black scale bar = 1 mm. Colour density bar = 3.5 (min)-5.0 (max)/cm.

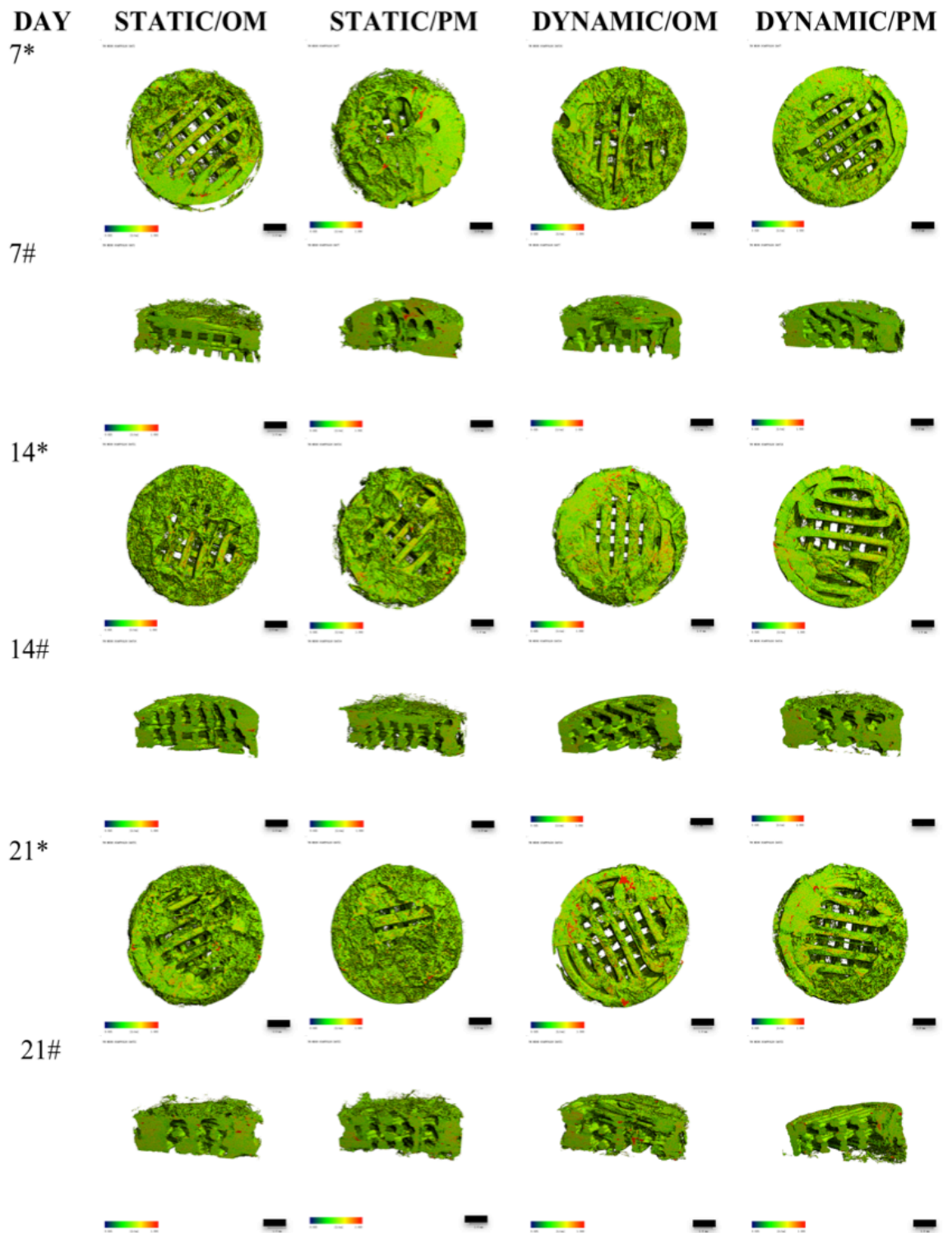


Fig. 5.27: Density maps of mesh cellular scaffolds in different culture conditions after 7, 14 and 21 days obtained from Micro-CT analysis. Only a small portion of mineralized matrix was found on mesh cellular scaffolds culture in Dynamic/OM after 21 days. (*=Whole area; #= cross-section of the scaffolds). Black scale bar = 1 mm. Colour density bar = 3.5 (min)-5.0 (max)/cm.

By comparing the four scaffold designs, it is clearly seen that higher portion of the denser area, which was assumed as the mineralized matrix was exhibited by 4C cellular scaffolds in osteogenic media for both culture conditions. In fact, more mineralized matrix was detected as the 4C cellular scaffolds were cultured in the dynamic environment as demonstrated in Fig. 5.28.

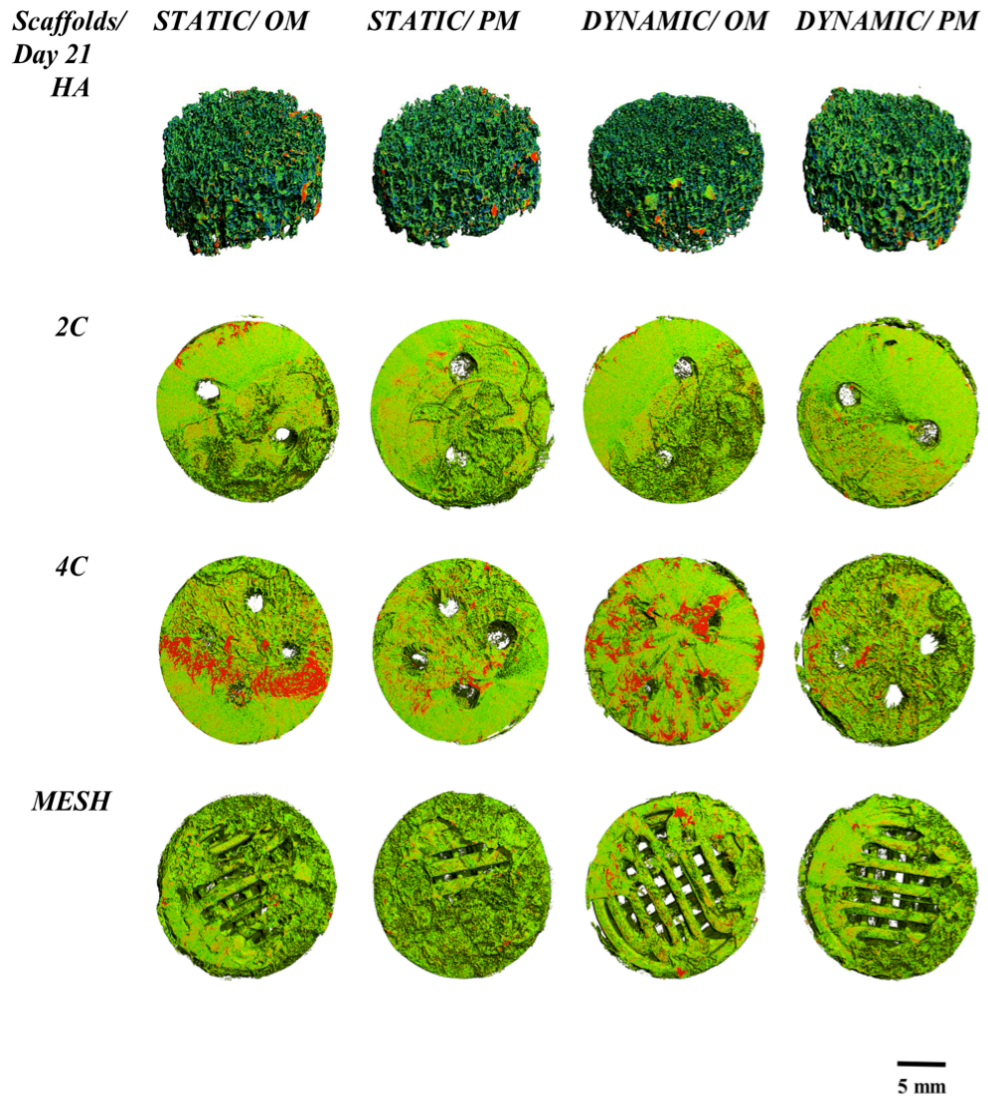


Fig. 5.28: Density maps of HA, 2C, 4C and mesh scaffolds after 21 days in different culture conditions. This figure demonstrated the comparisons of the formation of mineralized matrix (designated by red dense area) by hMSCs on different scaffold designs under different culture conditions. It was more apparent that more dense areas were associated with 4C scaffolds in OM for both culture static and dynamic conditions compared to other scaffold designs.

Quantitative Micro-CT analysis was then performed to determine the changes in the total volumes and percentages of mineralization formed on the cellular scaffolds. Table 5.3 represented the total volume of the dry scaffolds (before seeding) for all scaffold designs. It is apparent that HA scaffolds exhibited the lowest amount of total volume as compared to the 3DP hybrid scaffolds.

Table 5.3: Total volume of the dry scaffolds (before seeding) obtained from Micro-CT analysis.

Dry scaffolds	HA	2C	4C	Mesh
Total volume (mm³)	35.27	80.20	81.90	80.77

Overall, the total volumes of all the cellular scaffolds increased in all culture conditions over 21 days as demonstrated in Table 5.4. Despite, 4C cellular scaffolds in all culture conditions exhibited the highest increase in the total volumes as compared to other scaffold designs except mesh scaffolds in Dynamic/OM. All cellular scaffolds cultured in osteogenic media revealed higher total volume than in proliferation media for both static and dynamic conditions. This become more apparent when the cellular scaffolds were cultured in the dynamic environment. For instance, mesh cellular scaffolds were found to have the highest total volume when cultured in Dynamic/OM.

Results suggested that the highest percentage of mineralization was obtained when hMSCs were cultured on 4C hybrid scaffolds in Dynamic/OM. On the other hand, HA cellular scaffolds exhibited the lowest percentage of mineralization as compared to the 3DP hybrid scaffolds under all culture conditions after 21 days. These results are consistent with the density maps shown earlier (Fig. 5.28).

Table: 5.4: The total volumes and percentages of mineralization of the cellular scaffolds under different culture conditions after 21 days.

		HA	2C	4C	Mesh
Static/OM	Total volume (mm ³)	38.71 (3.45)	90.30 (10.1)	93.72 (11.82)	86.67 (5.9)
	Mineralization (%)	2.07	12.06	22.64	11.65
		HA	2C	4C	Mesh
Static/PM	Total volume (mm ³)	37.38 (2.11)	82.91 (2.71)	85.06 (3.16)	83.49 (2.72)
	Mineralization (%)	2.15	8.43	8.59	7.98
		HA	2C	4C	Mesh
Dynamic/OM	Total volume (mm ³)	36.18 (0.91)	88.85 (8.65)	95.41 (13.51)	96.13 (15.36)
	Mineralization (%)	0.53	12.31	26.94	16.38
		HA	2C	4C	Mesh
Dynamic/PM	Total volume (mm ³)	35.49 (0.22)	82.14 (1.94)	83.89 (1.99)	82.36 (1.59)
	Mineralization (%)	0.39	4.63	5.15	4.81

Note: The values in bracket represent the increase of total volume of the cellular scaffolds relative to their dry scaffolds (before seeding). The represented values are the mean, n= 2.

Growing hMSCs on 3DP hybrid scaffolds in OM under microgravity environment have increased the percentages of mineralization as compared to the static culture condition. However, contradictory effects were seen when these cellular scaffolds were cultured in Dynamic/PM where the percentages of mineralization was about 75% lower compared to those in Dynamic/OM condition.

The overall performances of each scaffold in different culture conditions are summarized in Table 5.5. Relative to the HA cellular scaffolds, all the 3DP hybrid cellular scaffolds performed better in producing mineralized matrix. Results suggested that scaffold designs with different nature of materials and pore/channel size have great impacts on the cells behaviour particularly when cultured under microgravity simulation. This difference has resulted in different cell responses between these two scaffolds, where 4C cellular scaffolds exhibited the highest scores in all culture conditions relative to 2C cellular scaffolds. On the other hand, HA cellular scaffolds showed the lowest scores regardless of the culture conditions.

Culture condition does play an important role in determining the cell proliferation and differentiation. It was observed that cellular scaffolds cultured in osteogenic media under both conditions revealed higher scores in the overall performances than those cultured in proliferation media. However, variations in scaffold performance were observed when comparing static versus dynamic culture conditions. For instance, 4C cellular scaffolds showed the best overall performances in osteogenic medium under dynamic culture condition compared to static. However, while in proliferation media, higher scores were achieved by culturing 4C cellular scaffolds in static rather than in microgravity environment.

Table 5.5: Summary of the overall performances for HA, 2C, 4C and mesh scaffolds under different culture conditions.

	Overall performances	HA	2C	4C	Mesh
Static/OM	Cell viability	2	4	4	3
	Proliferation	2	4	4	3
	Protein production	2	3	4	3
	Differentiation	1	3	4	3
	% Cytotoxicity	3	2	1	2
	%Mineralization	1	2	3	2
	Total score	11	18	20	16
Static/PM	Overall performances	HA	2C	4C	Mesh
	Cell viability	2	3	4	3
	Proliferation	3	3	4	3
	Protein production	2	3	3	2
	Differentiation	1	2	2	2
	% Cytotoxicity	3	1	1	1
	%Mineralization	1	1	1	1
Total score	12	13	15	12	
Dynamic/OM	Overall performances	HA	2C	4C	Mesh
	Cell viability	1	3	4	4
	Proliferation	1	3	4	4
	Protein production	1	3	4	3
	Differentiation	1	3	4	3
	% Cytotoxicity	4	2	1	1
	%Mineralization	1	2	4	3
Total score	9	16	21	18	
Dynamic/PM	Overall performances	HA	2C	4C	Mesh
	Cell viability	1	3	3	2
	Proliferation	1	3	3	2
	Protein production	1	1	2	1
	Differentiation	1	1	2	1
	% Cytotoxicity	4	3	2	3
	%Mineralization	1	1	1	1
Total score	9	12	13	10	

Note: Scores are given from scale 1-4 in ascending order of performances. (1 = <25% of best, 2 =25 to 50% of best, 3 = 50-75% of best, 4 = >75% best).

5.3. Discussion

5.3.1. The effect of seeding efficiency on establishing a 3D culture

Cell seeding of scaffolds involves the distribution of a cell suspension across the surface of a scaffold and potentially growth within the pores (Martin et al. 2004). Thus, seeding efficiency is the first step in establishing a 3D culture and this might be a determining factor for the development of tissue formation (Vunjak-Novakovic et al. 1998). The distribution of tissue, which subsequently forms within engineered construct, is highly associated to the initial distribution of the cells within the scaffold after seeding (Freed et al. 1998; Ishaug-Riley et al. 1998; Kim et al. 1998; Holy et al. 2000). Therefore, it has been highlighted that homogenous cell seeding can be considered as the beginning to uniform tissue formation. However, even for a small scaffold (e.g. 2 mm X 10 mm as have been used in this study), it is a critical challenge to distribute a high density of cells efficiently and homogeneously throughout the entire scaffold. Thus, it is important to firstly optimize the cell seeding method on the 3DP hybrid and HA scaffolds in order to obtain the maximum amount of mineralized matrix formed by placing the cellular scaffolds in different culture conditions.

In this study, it was found that placing a small volume of cell suspension (20 μ L) directly onto the scaffold resulted in higher percentage of cells adhered to the scaffold compared to higher volume of cell suspension (40 μ L). This result is in agreement with the study reported by Jones & Cartmell (2006) where a higher proportion of cell adhesion was obtained when small volume of cell suspension was seeded directly onto the gelatine scaffolds compared to larger volume suspension. Using small volume cell suspension allows the cell to retain on the surface of the 3DP hybrid scaffolds and in the porous structure of the HA scaffolds. While, larger volume of cell suspension could easily flow

through the channels/pores of the scaffolds and cells would then rather adhere to the well plate than to the scaffolds. Thus, smaller volume suspension was found to be better on a small scaffold in order to avoid overflowing of the cell suspension around the scaffold, which could lead to the loss of cells that should attached to the scaffolds.

The percentages of cell attachment was found to be higher on 3DP hybrid scaffolds as compared to the HA scaffolds. This showed that the coating materials used to fabricate the 3DP hybrid scaffolds were more suitable for cell attachment than pure HA scaffolds. This proved the role of collagen as one of the elements in the coating materials. The presence of collagen on the 3DP hybrid scaffolds has effectively contributed towards better support for cell attachment (Gelse et al. 2003; Wahl & Czernuszka 2006; Liu et al. 2008). While, pure HA scaffolds needed longer pre-wetting time with higher concentration of serum (20% FBS) before seeding compared to the 3DP hybrid scaffolds. This was to create a thin layer of protein on the surface as to provide better cell attachment.

To further improve the seeding efficiency, scaffolds were seeded with hMSCs on different culture substrates. The first was a commercially available 24-well cell culture plate; a hydrophobic surface denoted as non-coated well plates. The second substrate was the same type of plate coated with 1 w/v% of Pluronic F-127, denoted as coated well plates. Pluronic F-127 has been used as biological coating in particular to prevent cells adherent to the culture well plate (Dang et al. 2002). Pluronic F-127 is a polypropylene oxide-polyethylene oxide (PPO-PEO) tri-block copolymer with two hydrophilic ethylene oxide chains and a hydrophobic propylene oxide chain in the middle, which provides Pluronic F-127 with very flexible molecular chains and high capacity to hydration (Wanka et al. 1994; Deegan et al. 2014). Studies have shown that coating substrates with Pluronic F-127 reduces protein and hence cell adhesion, which prevents seeded cells from adhering to the

substrate (Freij-Larsson et al. 1996; Nejadnik et al. 2008). The results obtained shows that hMSCs seeded on all scaffold designs in the coated well plates resulted in higher percentages of cell attachment compared to the non-coated well plates. This finding highlighted the beneficial use of Pluronic F-127 in improving seeding efficiency.

Seeding method is another crucial key towards efficient seeding. The distribution of cells on each scaffold seeded by one-sided and two-sided method was analysed using MTT stains. It was found that cells were more homogenously spread over the entire scaffolds when hMSCs were seeded on the scaffolds by the two ways method. The use of two ways seeding method is indirectly helping the cells to migrate faster throughout the entire scaffolds. While, the one way seeding method requires longer time for the cells to migrate and infiltrate from one side of the scaffold to the other. This explains the rationale of previous studies reported in the literature for using two-sided seeding method in culturing cells on 3D scaffolds (Leukers et al. 2005; Song et al. 2008).

Thus, three main parameters improving cell seeding efficiency were established in this study: (1) small volume suspension, (2) using coated well plates during cell seeding and (3) seed cells by the two-sided method.

5.3.2. The impact of rotating speed on cell survival

Rotary bioreactor was used in this study to investigate the impact of a microgravity environment on cells fate upon cultured on different scaffold designs. The aims of using this type of bioreactor were to minimize shear force and maximize the fluid flow throughout the scaffolds to provide enhanced mass transfer across large scaffolds for bone TE (El Haj & Cartmell 2010; Rauh et al. 2011). In this study, two different speeds (20 and 40 rpm) were used for our initial optimization using all scaffold designs.

Slower rotational speed (20 rpm) was found to exhibit better cell attachment and viability on all scaffold designs. This speed allowed the scaffolds to be in continuous state of free fall in the culture vessel. While, increasing the speed to 40 rpm caused the scaffolds to collide with each other and collide with the wall of the vessels. Consequently, more cells detached from the scaffolds over time. This explains why more viable cells were found on the scaffolds cultured at slower speed of 20 rpm than 40 rpm. For this reason, the typical speed used for the rotary bioreactor system falls in the range of 3-18 rpm as demonstrated in many studies (Qiu et al. 2001; Song et al. 2006; Bucaro et al. 2007; Song et al. 2008; Araujo et al. 2010). For instance, Song et al. (2008) used two different speeds, 5 and 10 rpm. The first speed was used to expand the rat osteoblast cells isolated from cranium (3 days old) on suspension microcarrier system. These expanded cells were then seeded on 3D human bio-derived bone scaffolds (BDBS) and cultured again in the rotary bioreactor (at speed of 10 rpm) and some were placed in spinner flask (at speed of 25 rpm). The results demonstrated that after 3 weeks show that more collagen fibres mineralized nodules and new osteoid tissue formed as the scaffolds were cultured in the rotary bioreactor compared to those in spinner flasks.

However, the speed used in this study was relatively high as compared to those reported in the literature. The coating materials deposited on the 3DP scaffolds has considerably increased the total density of the scaffolds making them heavier so higher speeds were needed to keep the scaffolds from falling to the bottom of the flask and being exposed to high levels of shear. As a result, higher rotational speed was required in order to maintain the scaffolds in the free fall state. It was observed that when scaffolds were cultured below 20 rpm (results not shown in this study), due to gravity sedimentation at one side of the vessel occurred and the scaffolds potentially experienced high shear stress as the vessels were rotated. It was then considered that the cellular scaffolds suffered from friction between each other, as they were settling at one side of the vessel at slower rotation speed. Thus, in this study, the rotating speed of the bioreactor was kept constant at 20 rpm for culturing the four scaffold designs. These conditions were selected in order to avoid the collision of the scaffolds with the bioreactor walls and to facilitate the mass transfer (Araujo et al. 2010).

5.3.3. The fate of hMSCs cultured on several structural and functional designs of 3DP hybrid scaffolds under different culture conditions

This study investigated the behaviour of hMSCs cultured on different scaffold designs in simulated microgravity. The final aim of this study was to select the best scaffold design, which could enhance bone formation *in vitro*. The vascular network within matured bone could be likened to channels, through which nutrients can be supplied to cells and tissues. In order to re-create this vascular network, millimetre-size channels (diameter = 1.5 mm) were created on the 2C and 4C scaffolds. These channels were designed with the aim to facilitate the dispersion of hMSCs throughout the scaffolds and encourage nutrient exchange in order to promote differentiation particularly under dynamic culture conditions. Apart from the channel scaffolds, mesh scaffolds were also fabricated using the same technique with different structural design as shown in Table 5.1.

Pure sintered HA scaffolds was used as the experimental controls. The HA scaffold is commercially available and has been investigated for its clinical relevance (clinical data not shown due to confidentiality) thus was assumed as the “golden standard” in this study. The in house fabricated 3DP hybrid scaffolds were compared to the pure HA scaffolds in order to select the best scaffold that serves as the optimum structural and functional design for potential BTE applications. To do so, a rotary bioreactor was used to create the dynamic effect based on microgravity simulation.

The live/dead stain indicated that 3DP hybrid scaffolds allow greater cell attachment than the pure HA scaffolds during the seeding period. It takes only 24 hours for the cells to properly attach to the former scaffolds while the later scaffold requires at least 72 hours. Collagen is known to be an adhesion protein, which favours cell attachment and proliferation (Bisson et al. 2002; Becker et al. 2002; Ma et al. 2005). The results obtained

in this study are consistent with Chen et al. (2008) who cultured SaOS-2 osteosarcoma cell line on PLLA with apatite and apatite/collagen composite coating. This study found that the presence of collagen assisted cell attachment and proliferation when it was combined with apatite crystals. Suh et al. (2001) discovered that the grafted type I collagen provided a favourable matrix for cell attachment and growth. Thus, the present of collagen on 3DP hybrid scaffolds allowed easier and faster cell attachment compared to pure HA scaffolds.

Cells seeded on HA scaffolds were able to survive only in static condition and were found to be completely detached once cultured in the rotary bioreactor. Culturing scaffolds in OM and PM does make the differences for the 3DP hybrid scaffolds in particular under microgravity simulation. For instance, after 21 days in OM, cells started forming aggregates/bone-like nodules on 4C cellular scaffolds, which indicates the early sign of osteogenic differentiation.

Quantification of DNA for experimental groups demonstrated a gradual increase when all scaffolds were cultured under static conditions in PM over time, which indicated that the cells were actively proliferating, increasing cell numbers and therefore increasing the amount of DNA. However, when exposed to microgravity in PM, lower DNA contents were obtained compared to other culture conditions. Without osteogenic supplements, proliferation media can only help in cells expansion to achieve into higher cell number (Jung et al. 2012; Rupani et al. 2012). Thus, as culture progress, these scaffolds with greater cell density than the surrounding medium started to sediment to the side of the vessel and experienced repeated frictions with the vessel wall (Goldstein et al. 2001; Sikavitsas et al. 2002). As a result, some cells detached from the scaffolds and were floating in the culture media. For instance, when HA scaffolds were cultured in dynamic compared to static condition, majority of the cells had detached from the scaffolds at an

early stage of culture, thus resulted in negligible amount of DNA detected at every time-points. hMSCs is known to be an anchorage-dependent cells, thus, they need a substrate to attach and survive in culture (Jung et al. 2012; Chen et al. 2013). It is assumed that when the hMSCs were in suspension state, the detached cells were floating in the continuously rotating culture media, which has eventually cause cell death. This explained why we obtained lower DNA contents and higher percentage of LDH activity for scaffolds cultured under dynamic flow in PM. Whereas, cells in osteogenic media for both culture conditions seem to survive better than those in PM. The presences of dexamethasone, β -glycerolphosphate and ascorbic acid in OM, has driven the cells towards osteoblastic differentiation over time (Birmingham et al. 2012; Langenbach & Handschel 2013). It is believed that better cell adhesion was provided since more ECM being produced as the cells undergoes differentiation. As a result, less cells detached from the scaffolds cultured in Dynamic/OM compared to Dynamic/PM, which was represented by the low %LDH activity.

Over time, more proteinaceous materials were produced particularly when hMSCs started to differentiate into osteogenic lineage. This is observed when the cellular scaffolds were cultured in OM and more apparently in Dynamic/OM. It has been reported that an early stage of osteogenic differentiation is the expression of collagen type I matrix onto which the mineral is deposited (Quarles et al. 1992). While, in final stage from day 14 to 28 high expression of osteocalcin and osteopontin usually obtained. This is followed by the deposition of calcium and phosphate (Huang et al. 2007; Hoemann et al. 2009). However, in this work the total protein produced by the cellular scaffolds were not analysed in details to classify the different types of bone-synthesized proteins.

Lactate dehydrogenase (LDH) assay was performed in order to quantify the percentage of cytotoxicity in the culture medium as to predict the phenomena happening in Dynamic/PM culture condition. Lactate is mainly produced from glucose metabolism. Glutamine can also excrete small amount of lactate. The concentration of lactate depends on the glucose concentration, cellular activity and bioreactor operation. Higher shear induced by the bioreactor resulted in higher concentration of lactate in the culture medium (Ozturk et al. 1992; Schneider et al. 1996). The presence of lactate is then likely to impede cell growth and metabolism and decrease the productivity (Cruz et al. 2000). This is due to the changes in the osmolarity of the media where lactate attributed to media acidification (Eagle, 1973). Consequently, growth may be restricted by lactate even at constant pH. This phenomenon resulted in down-regulation of cell activity and total protein production of the cellular scaffolds in Dynamic/PM culture condition. The LDH assay also confirmed that high percentage of cytotoxicity detected at early culture of hMSCs on HA scaffolds under dynamic condition in both culture media. The trend obtained for HA cellular scaffolds was reciprocal to the 3DP cellular scaffolds, where the percentage of cytotoxicity decreased as the culture progress. This is because majority of the cells were already detached from the early culture (7 days), consequently a lower cell density remained as the culture progressed.

With regards to the onset of mineralization, the levels of ALP/DNA of hMSCs cultured on all 3DP hybrid scaffolds in Dynamic/OM relatively dropped at 21 days. This reciprocal relationship between cell proliferation and osteoblast phenotype development is consistent with the model of the relationship between growth and differentiation of osteoblast development sequence proposed by Stein et al. (1990) and Aubin et al. (2006). The differentiation of hMSCs *in vitro* can be divided into three stages; (1) peak in number of cells (usually designated by increased in amount of DNA), (2) early cell differentiation

(shows peak levels of ALP expression) and (3) down-regulation of ALP expression (Huang et al. 2007). This trend can be clearly seen for 4C scaffolds cultured in Dynamic/OM.

hMSCs cultured on 3DP hybrid scaffolds exhibited the typical bell-shaped trend of the ALP activity. In consistency to the ALP expression, 4C cellular scaffolds in osteogenic media for both culture conditions showed the highest levels of ALP activity after 14 days. This indicates that 4C scaffold is the most favourable substrate for hMSCs cultured in microgravity simulation, as cells were able to proliferate and differentiate the fastest in this condition. On the other hand, HA scaffolds showed almost negligible amount of ALP expression when cultured under microgravity simulation in both culture media. This is due to the cell detachment from the scaffolds at early stage of culture. As culture progresses, hMSCs started to differentiate into osteogenic lineage with cells become alkaline phosphatase (ALP) positive histochemically in particular for the 3DP hybrid scaffolds under dynamic condition in osteogenic media after 14 days of culture, i.e. 4C in Dynamic/OM. ALP histochemical analysis is considered as one of the earliest phenotypic markers of the osteoblastic lineage, which indicates the onset of mineralization (Lian & Stein 1995). Back in middle 1990s, a study conducted by Stein et al. (1996) found that osteoblast differentiation involve a multistep series of events modulated by an integrated cascade of gene expression that initially supports proliferation, differentiation and mineralization of the bone extracellular matrix. This study also proposed that the onset of matrix production begins at 14 days in culture.

Micro-CT analysis is an effective tool to monitor the mineralized matrix formation within 3D tissue-engineered constructs *in vitro* and *in vivo* (Cartmell et al. 2004; Henstock et al. 2013; Reinwald et al. 2015). In this study, Micro-CT analysis was used to further detect if

any mineralization formed on the cellular scaffolds after the exposure to different culture conditions. Micro-CT analysis revealed the formation of denser area on 4C cellular scaffolds in OM after 21 days. The density maps of the whole and cross-sectional area of 4C scaffolds in Dynamic/OM showed the most coverage with denser area compared to other investigated scaffolds. Correlating these results with the formation of bone-like nodules observed in live/dead staining and positive ALP expression, these denser areas can be assumed as mineralized matrix formation. A denser mineralized layer at the surface of cellular constructs is a common observation in tissue engineering (Ishaug-Riley et al. 1998; Cartmell et al. 2004; Hagenmüller et al. 2007). Quantitative Micro-CT analysis supported this observation, where 4C scaffolds in OM exhibited huge increments in the total volume and highest percentages of mineralization compared to other scaffold designs in different culture conditions.

Based from the results obtained, the finding supports our hypothesis made in this study where the combination of dynamic flow and OM is assumed to promote better bone formation compared to other culture conditions. Our second hypothesis is also accepted as the 3DP hybrid scaffolds performed better in enhancing the bone formation *in vitro* than the HA scaffolds in all culture conditions over 21 days. However, based from our findings, the null hypothesis is then rejected since scaffold designs were found to have significant effects in enhancing bone formation *in vitro* particularly when cultured under dynamic condition. This study also underlines a number of critical parameters in creating 3D scaffolds for bone tissue engineering applications. Chemical composition, channel/pore size, structural designs and culture conditions all work hand-in-hand to create a functional scaffold. An ideal 3D scaffold should be able to recreate the natural extracellular matrix of bone. In order to do so, a scaffold must have an appropriate 3D architecture enhancing

initial cell attachment and subsequently migration into the matrix (Hutmacher et al. 2004; Jones et al. 2010).

The results obtained in this study demonstrated that the 3DP hybrid scaffold are better compared to the pure HA in all culture conditions. HA alone is insufficient to enhance cell attachment and induce osteogenic differentiation particularly in dynamic condition even with the help of biochemical cues from the osteogenic media. Native bone tissue is comprised of two core components; the first of which is the mineralized inorganic phase consisting mainly of calcium phosphate with multiple ionic substitutions, and the second is the non-mineralized organic phase, which is predominantly collagen type I (Weiner & Wagner, 1998; Best et al. 2008; Hannink & Arts, 2011). Therefore, natural bone is more accurately referred as carbonated hydroxyapatite to as carbonate ions are the most abundant rather than solely hydroxyapatite (Spence et al. 2008). It is believed that there was lack of cell recognition when cells were cultured on HA scaffolds although it is known to be osteoconductive materials. This might also explain the weak bonding between cells and HA scaffolds in dynamic culture. The 3DP hybrid scaffolds were built up from the combination of both osteoconductive and osteoinductive materials, in which, multi-substituted HA and collagen type I are the major components of the coating materials. These scaffolds resemble closely the compositions of natural bone. Thus, they are more likely to behave in similar way to bone as compared to monolithic scaffolds (Rodrigues et al. 2003; Wahl & Czernuszka 2006). In addition, the presence of multi-substituted HA powders has influenced the cellular responses of the hMSCs on the 3DP hybrid scaffolds. It is known that multi-substituted HA powders can provide better bioactivity by raising its solubility compared to pure HA (Palard et al. 2008; Sprio et al. 2008).

Pore and channel size is another key factor in affecting cell response. Channel size plays an important role in cell migration and diffusion of nutrients/waste products (Jones et al. 2010). For bone tissue engineering purposes, pore size that is well accepted should be in the range of 200-900 μm (Maquet & Jerome, 1997; Burg et al. 2000; Yang et al. 2001). However, Holy et al. (2000) proposed that in order to achieve successful bone reconstruction, the 3D substrate should have a macroporous structure with pore sizes ranging from 1.2-2.0 mm to facilitate cell, tissue and blood vessel ingrowth throughout the scaffolds by having high surface to volume ratio. This study demonstrated the relationship between scaffold pore size and cells activity within tissue engineering constructs. Smaller pore sizes, as shown on HA scaffolds prevented cellular penetration and extracellular matrix production (Salgado et al. 2004). While, larger pore sizes were seen to improve the overall performances of the hMSCs cultured on 3DP hybrid scaffolds particularly under dynamic environment. It is believed that the presence of larger pores might have allowed for homogenous fluid flow in the bioreactor hence, minimizing shear and turbulences around the scaffold peripheries, which facilitate cell penetration and migration throughout the entire scaffolds. Among the 3DP hybrid scaffolds, 4C scaffolds was considered as the best scaffold design under the here investigated culture conditions. Indeed, mesh scaffolds possess higher SA: V ratio as compared to 2C and 4C scaffolds since they have the highest porosity, which is important for cell penetration. However, cells are subjected to excessive fluid shear particularly when they were exposed in dynamic culture. As a result, cells adhered on the struts of the mesh scaffolds were washed off. In this case, channel scaffolds, which have relatively smaller SA: V ratio (as shown in Table 5.1), offered some shelter for the cells from excessive fluid shear and at the same time still permit suitable nutrient flow. Therefore, the key finding in this study emphasized that scaffold design should balance the SA: V ratio. At this stage of study, it can be concluded that 4C scaffolds

is the most promising scaffold design as compared to 2C and mesh scaffolds. This is because 4C scaffolds possess a SA: V ratio, which lies between 2C and mesh scaffolds and provides suitable surface area for cell attachment and porosity to allow mass transfer.

This study also highlighted the impact of rotary bioreactor in bone formation *in vitro*. Conflict results have been reported in the literature. Some authors reported that microgravity has a negative influence on the behaviour of osteoblast by decreasing the cell viability (Sarkar et al. 2000; Sarkar et al. 2000; Rucci et al. 2003). Other authors found positive outcomes of microgravity on osteoblast development. Previous study has shown that culturing MG63 osteosarcoma cells on biomimetic calcium phosphate-coated poly (caprolactone) nano fibre meshes (BCP-NMs) and poly (caprolactone) nanofibre meshes (PCL-NMs) in rotary bioreactor at 16 rpm for two weeks showed higher levels of protein production and ECM genes for BCP-NMs constructs in dynamic compared to static condition (Araujo et al. 2010). Other than rotary bioreactor, different kinds of bioreactor have been used to enhance bone development. For instance, cyclic hydrostatic pressure has been shown to promote bone growth and mineralization of foetal chick femur model and play an important role in regulating bone development and remodelling *in vivo* (Henstock et al. 2013). From the result obtained thus far, we believed that the enhancement of bone growth *in vitro* is not solely dependent on the culture condition but may be related to other properties of the structure that support cell growth during culture particularly the scaffold designs and materials as well as culture medium, which have great impacts on the stem cells fate. Ideally, the coating materials assembly deposited on each 3DP scaffolds should be consistent for each particular layer as this could directly affect the cell attachment and cell activity. Therefore, it is beneficial to stain each deposition layer on the 3DP hybrid scaffolds with Alizarin Red (AR) and Sirius Red (SR) followed by de-staining as to quantify the amount of calcium and collagen type I deposited on each layer. This will

function as quality control for the fabrication of 3DP hybrid scaffolds and will enhance the overall scaffold performance *in vitro* aiding in the selection of the best scaffold design for BTE application.

5.4. Conclusion

The structural design of the scaffolds has a pronounced impact on the behaviour of hMSCs *in vitro*. In addition, the combination of dynamic culture condition based on microgravity simulation and different culture media also plays important role in determining cells fate. Overall the utilization of the in-house fabricated 3DP hybrid scaffolds as cell culture substrates resulted in enhanced cell proliferation and differentiation compared to the control scaffold in all culture conditions. In addition, 4C hybrid scaffolds showed best performance among the scaffold designs investigated. Furthermore, the comparison of different culture conditions (static versus dynamic, OM versus PM) resulted in the identification of overall best culture conditions for this study, namely 4C Dynamic/OM. Here, hMSCs were able to produce the highest levels of proteins, DNA content and mineralization. This study determined that by creating a millimeter-size aligned channels on the scaffold structure aiming to resemble a vascular structure has greatly facilitated the cell migration, proliferation and differentiation under dynamic environment in osteogenic media. However, further studies should be performed to improve the vascularization of the entire scaffolds in particular the 4C hybrid scaffolds. Hopefully, the presence of a vascular network within the scaffolds would then augment and facilitate the osteogenesis of hMSCs on these in-house fabricated 3DP hybrid scaffolds.

Chapter 6

Does the crosstalk between human mesenchymal stem cells and human umbilical vein endothelial cells promote pre-vascularization of bone constructs?

6.1. Introduction

Bone is a complex tissue, interpenetrated with a highly vascularized network in the human body (Duttenhoefer et al. 2013; Salgado et al. 2004). In large bone defects not only is the bone tissue damaged, but the surrounding vascular network is often markedly disrupted as well, which can consequently affect the repair response of the tissue (Johnson et al. 2011). During bone regeneration, new capillaries derived from the pre-existing surrounding blood vessels, invade the site through angiogenesis (Carano & Filvaroff 2003). Typically, areas with the highest level of vascularization resulted in rapid healing rates (Deleu & Trueta 1965; Novosel et al. 2011).

No doubt, various kinds of constructs have been fabricated by several advanced techniques such as biomimetic, electrospinning and rapid prototyping, but none have provided full clinical benefit in tissue engineering (TE). In bone TE, multiple cell types with new biomaterials have been combined to promote repair. Common approaches in bone tissue engineering include culturing osteogenic cells on a scaffold *in vitro*, i.e. culturing murine fibroblastic cells on hydroxyapatite scaffolds (Leukers et al. 2005) and human bone marrow-derived mesenchymal stem cells (hMSCs) on β -Tricalcium Phosphate (β -TCP) scaffolds (Hasegawa et al. 2010). It has been established that a key to the development of bone tissue does not rely solely on the use of osteoprogenitor cells, but also the inclusion of a functional vascular network. This is an essential pre-requisite for the survival and integration of the constructs to the host tissue. A lack of blood supply remains to be one of the major limitations in bone tissue engineering. Inadequate vascularization was attributed to be the cause of cell death in the constructs as a result of limited nutrients supply, hypoxia and accumulation of waste products, toxic and non-functional substances greatly

affects the remodelling process followed by total failure of the constructs biologically (Kanczler & Oreffo 2008; Grellier et al. 2009; Aguirre et al. 2010).

Several approaches for improving the vascularization of the tissue-engineered constructs have been described (Moon & West 2008). Improvements to scaffold design, in particular the pore size and interconnectivity or by combining the gene and cellular therapies are key strategies. For example, transfecting cells to over-express key angiogenic growth factors such as vascular endothelial growth factor (VEGF) as to deliver specific biological factors that could direct the recruitment of endothelial cells (ECs) progenitors and their differentiation has been proposed by Jabbarzadeh et al. (2008). The *in vivo* evaluation on transfected adipose-derived stromal cells (ADSCs) with adenovirus encoding the cDNA of VEGF combined with ECs on 3D poly (lactide-co-glycolide), PLGA sintered microsphere scaffold showed that this combination resulted in formation of vascular network within the PLGA scaffolds after 21 days implantation in SCID mice (Jabbarzadeh et al. 2008). Other strategies include *in vivo* pre-vascularization of implants using vascular pedicles as well as creating pre-vascularized three-dimensional (3D) tissue constructs *in vitro* using a co-culture system of vascular ECs and bone cells or mesenchymal stem cells (MSCs) primarily spheroid co-culture model and hydrogel materials (Rouwkema et al. 2006; Unger et al. 2007). This involved less complex processes compared to constructing vascular networks in 3D porous scaffolds, as hydrogels provide an environment that is manipulated by vascular forming cells (Au et al. 2008; Chen et al. 2009; Laschke et al. 2009; Allen et al. 2010; Lee & Niklason 2010; Melero-Martin et al. 2010). In addition, cells are directly incorporated into the hydrogel before gelation and hence distributed throughout. However, gel-like materials are well known for its poor mechanical properties thus, with less applicable for load-bearing bone defects.

A key element in engineering vascularized bone tissue is to rapidly creating functional blood vessels within the constructs to supply cells with nutrients and oxygen as well as to remove the waste products (Rouwkema et al. 2006). Various different co-culture conditions have been investigated. However, the culture medium and the cell ratio remain a debating issue among researchers. For instance, McFadden et al. (2013) demonstrated that a ratio of 4:1, HUVECs:hMSCs in complete endothelial growth media (EM) increased vascularization within the 3D porous scaffolds, as the main aim was to create a vascular construct. Kaigler et al. (2005) investigated the effect of various cell ratio (1:1-10:1) of hMSCs:HUVECs co-cultured in proliferation media, PM: EM on osteogenesis and found highest ALP activity in the ratio of 1:1. Interesting cell behaviours in different culture media were discovered by Rouwkema et al. (2006) where, hMSCs was found to have highest proliferation rate in mix media, while HUVECs proliferate well in EM and exhibit intermediate result in mix media; the optimal CD31 staining in the 50:50 of co-culture systems in mix media. Apart from these debating issues, cell-seeding technique is a major concern. Most of the studies described in literature were based on immediate simultaneous seeding of HUVECs and hMSCs (Rouwkema et al. 2006; Rao et al. 2012; Gershovich et al. 2013). According to McFadden et al. (2013) who made a comparison between immediate co-culture and delayed addition of hMSCs to HUVECs network, whereas the former resulted in cellular regression and limited vascular formation. It was reported that delayed addition of hMSCs after 3 days of post-HUVECs seeding showed a well-developed vessel-like structure 3 days later. The rationale with this approach was to replicate the event that occurs *in vivo*, whereby HUVECs form the initial vascular structures followed by recruitment of perivascular cells in order to maintain and stabilize the newly formed vessel (McFadden et al. 2013). For this study, the cell ratio and culture medium of 1:1, HUVECs:hMSCs and EM:OM were chosen based on the literature.

On the other hand, hMSCs produced high levels of VEGF. This growth factor plays an important role in the survival and proliferation of HUVECs and further development of the premature vessel structure. In this study, we focussed on the quantification of PDGF and VEGF production, as these are the two most important pro-angiogenic growth factors.

The main aim of this study was to investigate the potential for *in vitro* pre-vascularization of bone TE constructs. The design of the scaffolds features large pores, which aim to promote vascular channels integrating the bone scaffold. The model used in this study employed a co-culture model consisting of HUVECs and hMSCs. The scaffolds were designed as a cylindrical disk with four channels in the middle fabricated by Fused Deposition Modelling method. In our previous study, the four channels (4C) scaffold revealed the highest percentage of mineralization in OM for a culture period of 21 days both in static and dynamic culture as compared to two channel (2C), mesh and hydroxyapatite (HA) scaffolds. The concept is to take the best design for induction of osteogenesis and add HUVECs to the channels to promote vascularization. HUVECs were embedded in a Matrigel solution and seeded directly into the channels aiming to create a vessel-like network throughout the scaffolds. Matrigel was used to facilitate HUVECs growth and promote proliferation. This study aims to provide insight into the crosstalk between the HUVECs and hMSCs within the 4C scaffolds by means of the early osteogenic and angiogenic expression as well as the secretion of the pro-angiogenic growth factors in particular Vascular Endothelial Growth Factor (VEGF) and Platelet Derived Growth Factor (PDGF).

6.2. Results

6.2.1. Imaging labelled cells on the 3DP hybrid scaffolds

After optimizing the 3DP hybrid scaffolds in the previous chapter, it was concluded that 4C scaffold showed the best overall performances as compared to HA, 2C- and mesh scaffolds. hMSCs cultured on 4C scaffolds in the presence of osteogenic media (OM) showed enhanced migration, proliferation and differentiation into osteogenic lineage, as well as increased mineralization. Thus, 4C scaffolds were chosen for this study to create a pre-vascularized bone construct *in vitro* by introducing a co-culture model of HUVECs and hMSCs.

To observe the distribution of the cells throughout the 4C scaffold by hMSCs alone, HUVECs alone and HUVECs: hMSCs co-cultured, samples were imaged using confocal laser scanning microscopy (CLSM). The cells were fluorescently labelled with blue and red dyes for hMSCs and HUVECs, respectively, which enabled observations of cells with time in culture. The CLSM images (Fig. 6.2) shows that both cell types remained viable and increased in cell number over the entire scaffolds throughout culture. The same observation was obtained for the controls.

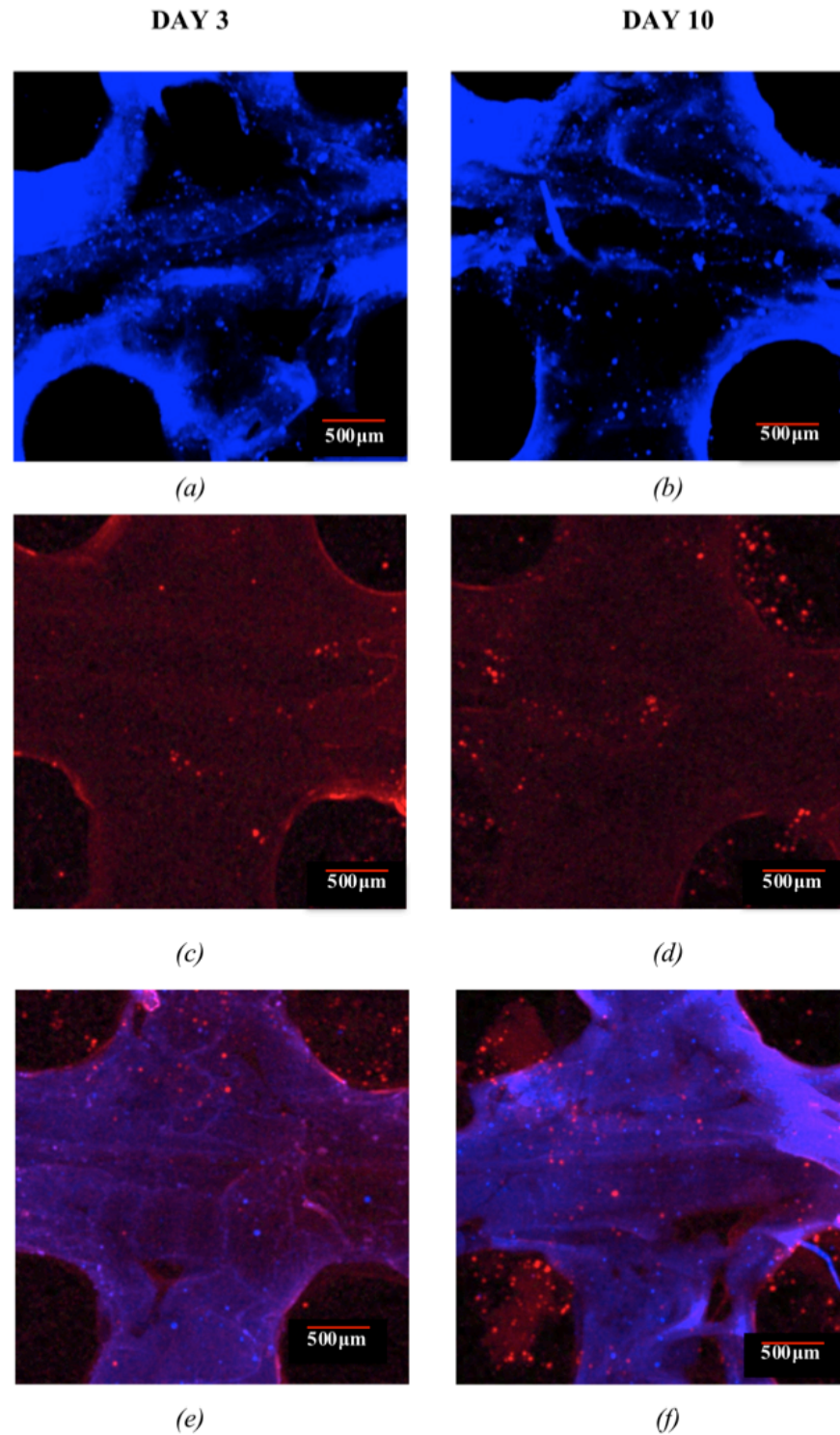


Fig. 6.2: CLSM images showing the fluorescent labelling of the hMSCs (labelled blue) and HUVECs (labelled red) on 4C scaffolds on different samples after day 3 and 10 post hMSCs addition; (a-b) hMSCs alone, (c-d) HUVECs alone and (e-f) hMSCs: HUVECs co-culture model. Scale bar = 500 μ m.

To further characterize the events happening in the channel, the channels were imaged at higher magnification using CLSM. It was observed that, after 3 days post-hMSCs addition, HUVECs formed aggregate-like structures in the channels. hMSCs on the other hand remained at the periphery of the channels. After 10 days in culture, HUVECs spread out and started to organize themselves throughout the channels as shown in Fig. 6.3 (b). HUVECs in the channels also migrated to the surface and towards the hMSCs especially the cells close to the periphery of the channels. In addition, a small number of hMSCs migrated into the channels.

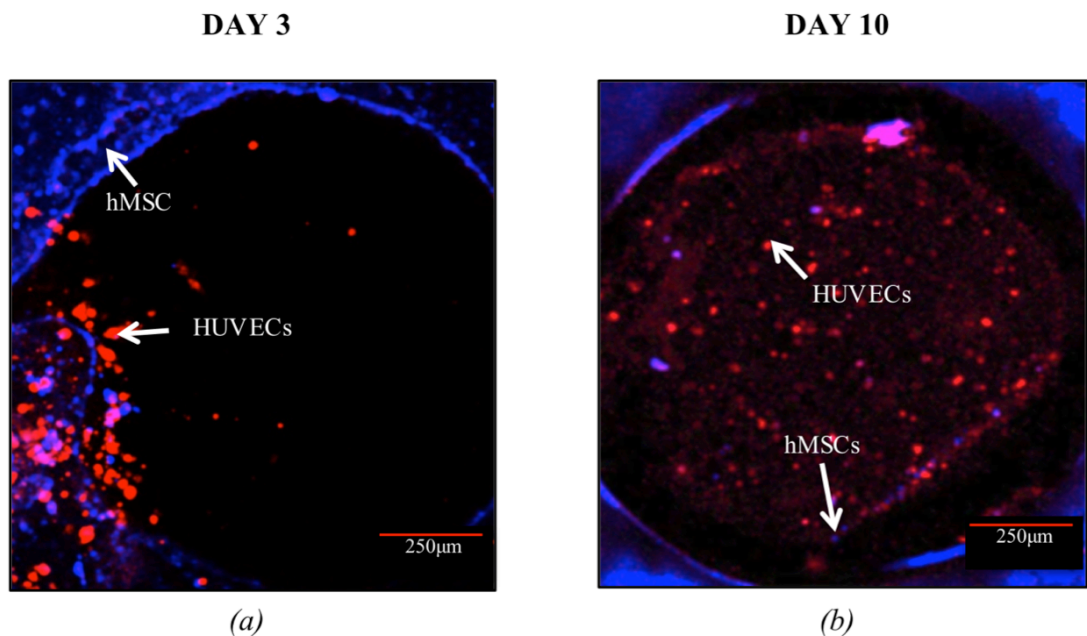


Fig. 6.3: Cell morphology of the co-culture system in the channel of the 4C scaffolds after 3 and 10 days post-hMSCs addition. HUVECs were distributed in the entire channels after 10 days post hMSCs addition. Scale bar = 250 μm.

6.2.2. Immunocytochemistry staining

In order to observe the expression of pro-osteogenic and angiogenic markers RUNX-2 and CD31 were investigated as the early osteogenic and angiogenic marker, respectively.

The RUNX-2 expression (labelled by the green fluorescent dye) of hMSCs alone, HUVECs alone and co-culture model are represented in Fig. 6.4. For hMSCs controls, a very small amount of RUNX-2 was expressed as early as 3 days after seeding and increased over time with enhanced fluorescence intensity. Highest level of the relative intensity for the green signals was detected on the hMSCs alone after 10 days in culture.

The co-culture samples showed a similar trend to the hMSCs controls. This indicated that a low level of RUNX-2 expression occurred during the early stage of culture. The expression of RUNX-2 was significantly greater after 10 days of hMSCs addition to the pre-seeded cellular scaffolds as shown in Fig. 6.4 (h). The co-culture model shows only about half the levels of relative intensity of hMSCs alone (control). Over time, the relative intensity of the co-culture model (both green and blue) increased to about double the levels of their initial relative intensity (after 3 days post-hMSCs addition). This indicates highest levels of RUNX-2 expression obtained when more hMSCs found on the scaffolds.

In order to obtain a three-dimensional observation of the events happening in the channels, the samples were scanned layer-by-layer through the channels to a depth of 2 mm. Results demonstrated that the HUVEC cells were distributed throughout the channels and demonstrated an absent for RUNX-2 expression at all time-points. This is confirmed quantitatively as no green fluorescent signal was detected from HUVECs alone.

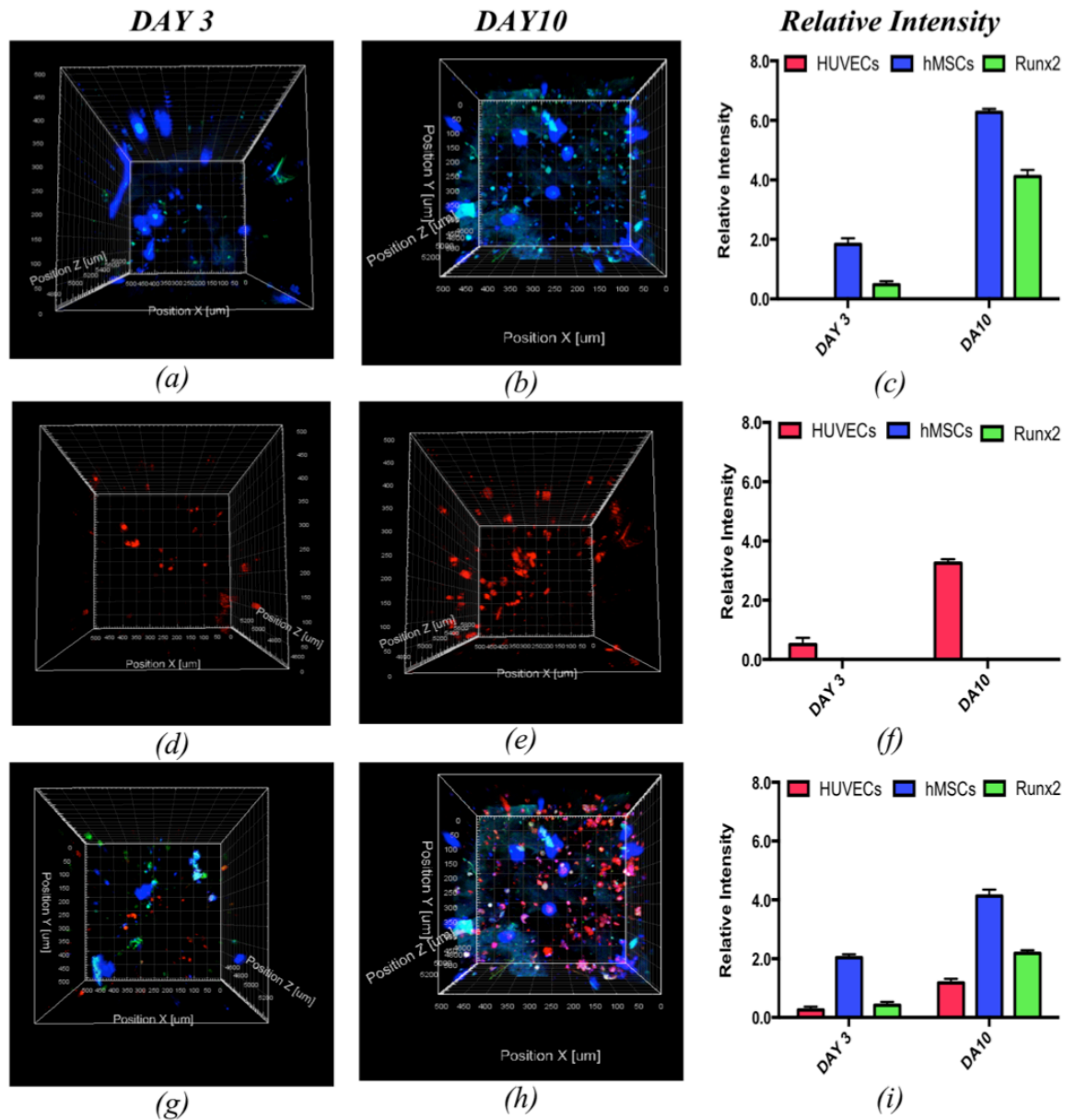


*Fig. 6.4: Immunostaining of the RUNX-2 expression on the surface of the scaffolds after 3 and 10 days post-hMSCs addition and their relative fluorescence intensity, respectively; (a-c) hMSCs alone, (d-f) HUVECs alone and (g-i) hMSCs: HUVECs co-culture model. *Fluorescent labelled of green, blue and red designated for RUNX-2 expression, hMSCs and HUVECs, respectively. hMSCs alone and co-culture system showed positive stains of RUNX-2 expression indicating early osteogenic differentiation occurred as early as 10 days. Absent of stained was detected in HUVECs alone as expected. Relative fluorescence intensity obtained from IMARIS software demonstrated that hMSCs on the surface of the scaffolds started to differentiate into osteoblastic lineage over time with the increased of the relative intensity. The results also showed that HUVECs migrated and proliferated to the surface after 10 days post-hMSCs addition as more fluorescence detected for both HUVECs alone and co-culture model. Scale bar = 250 μ m.*

Human-specific CD31 antibody was used to test *in vitro* vessel formation within the 4C scaffolds. In the hMSCs alone group, no expression of CD31 was observed at all time-point, as represented in Fig. 6.5 (a-c). A low level of cells was detected in the channels especially after 10 days post-hMSCs addition although hMSCs were initially seeded only on the surface of the scaffolds. After 6 days post-HUVEC seeding, HUVECs alone showed positive staining for CD31. Cell number increased and was more distributed compared to 3 days post-HUVECs seeding as shown earlier in Fig. 6.3. After 10 days in culture, HUVECs alone demonstrated relatively higher CD31 expression than those after 6 days post-HUVEC seeding. The staining was also found to be more homogenous throughout the channels rather than localized staining as seen at early stage of culture. However, no proper vascular network was observed at this time-point.

To confirm whether the interaction between HUVECs and hMSCs in the co-culture model resulted in the formation of newly developed vascular networks, the channels of the co-culture samples were imaged. It was observed that in the co-culture model, HUVECs expressed CD31 and that its expression increased over time. However, the expression of CD31 in the co-culture model was more localized as compared to HUVECs alone group. Again, no vessel networks were detected after 10 days post-hMSCs addition. Typically, HUVEC takes about 10 days to form a 3D well-developed vessel-like network in the co-culture model (Rouwkema et al. 2006; McFadden et al. 2013). Unfortunately, this trend was not seen in this work as no vessel-like network was formed at the time-points investigated.

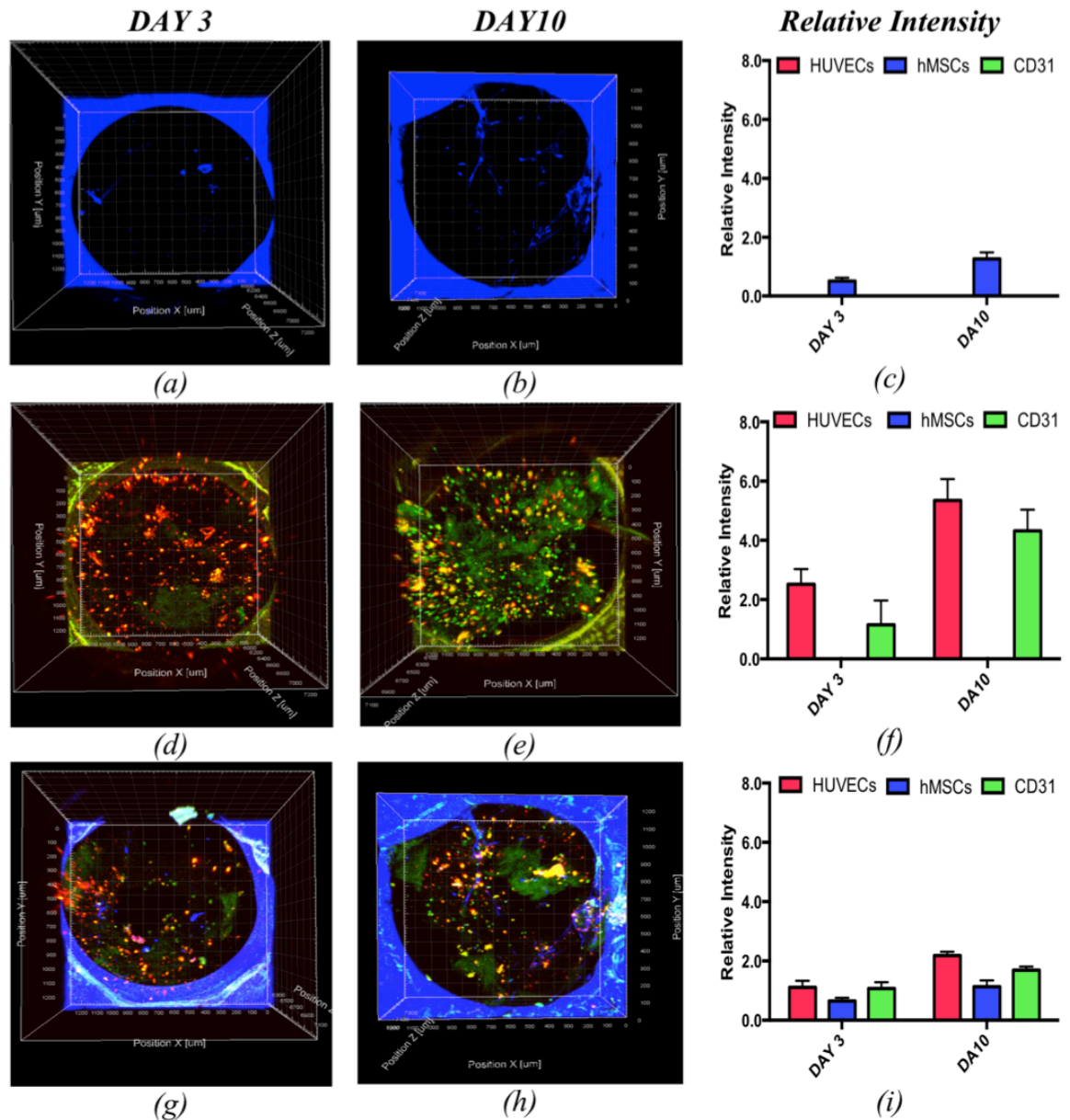


Fig. 6.5: Immunostaining of the CD31 expression in the channel of the scaffolds after 3 and 10 days post-hMSCs addition and their relative fluorescence intensity, respectively; (a-c) hMSCs alone, (d-f) HUVECs alone and (g-i) hMSCs: HUVECs co-culture model. *Fluorescent labelled of green, blue and red designated for CD31 expression, hMSCs and HUVECs, respectively. Both HUVECs alone and co-culture model expressed CD31 after 3 days post-hMSCs addition. IMARIS only detected the relative intensity of the blue fluorescence from the hMSCs alone, which indicates the cells migrated into the channels over time. Increasing trends of relative intensity of the red and green fluorescence were obtained for both HUVECs alone and co-culture model. Relative intensity of blue fluorescence was also detected in the co-culture system. Scale bar= 250 μ m.

6.2.3. Quantification of secretion of pro-angiogenic growth factors

The secretion of pro-angiogenic signalling molecules, PDGF and VEGF into the cell culture media by hMSCs alone, HUVECs alone and co-culture model were quantified using ELISA and the results are represented in Fig. 6.6. The release of both signal proteins is critically essential in the vessel formation and stabilization. The results can also be used to draw a comparison between monoculture (hMSCs alone and HUVECs alone) and co-culture model.

The levels of PDGF-BB differed between culture groups ($p \leq 0.0001$) at each time-points. There were different interactions between time and the secretion of PDGF-BB depending on the culture groups, where HUVECs alone group demonstrated linear increases over the culture period ($p \leq 0.0001$). When hMSC and HUVEC were co-cultured, the levels of PDGF-BB decreased with increasing cultivation period ($p \leq 0.0001$).

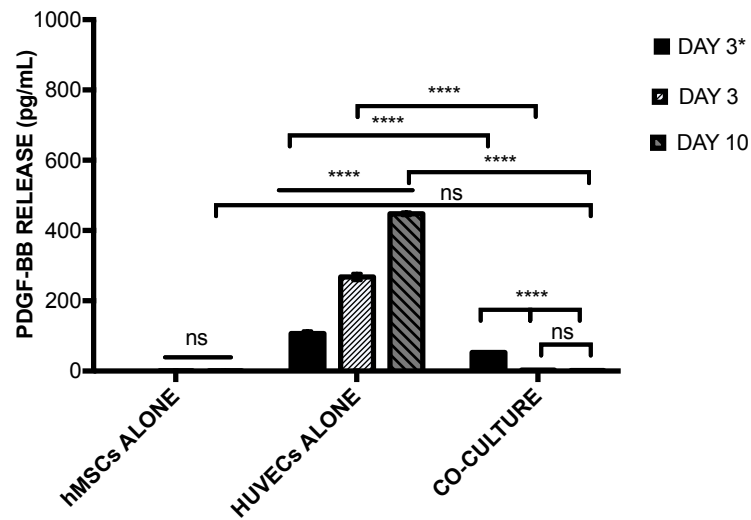
Comparing the culture groups, HUVECs alone released the highest levels of mean PDGF-BB compared to hMSCs alone and co-culture groups at either time-point ($p \leq 0.0001$ for each). For the co-culture group the levels of PDGF-BB decreased at day 3 post-hMSCs additions to the pre-seeded cellular scaffolds ($p \leq 0.0001$) and eventually diminished, where no significant differences were observed at day 10 ($p = 0.9787$). hMSCs alone showed no significant differences in the secretion of PDGF-BB on day 10 ($p = 0.9999$).

Overall, HUVECs alone group released the highest PDGF-BB on day 10 compared to hMSCs alone and co-culture groups ($p \leq 0.0001$ for each).

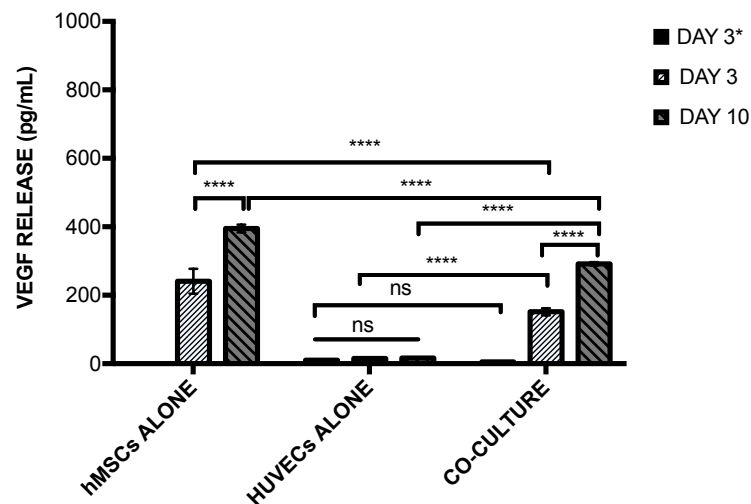
Mean VEGF released increased over time for both hMSCs alone and co-culture groups ($p \leq 0.0001$) and differed between the culture groups ($p \leq 0.0001$). There was a significant interaction between time and VEGF released ($p \leq 0.0001$), suggesting that the increase in VEGF released over time differed between culture groups.

Among the culture groups, hMSCs released significantly higher levels of mean VEGF at day 3 ($p \leq 0.0001$) and day 10 ($p \leq 0.0001$) compared to HUVECs alone and co-culture. No significant differences were observed in the production of VEGF in the HUVECs alone group at day 3 ($p = 0.7278$) and day 10 ($p = 0.9999$). The co-culture group demonstrated similar trends compared to the hMSCs monoculture. Before the addition of hMSCs, post-HUVECs seeded scaffolds produced as negligible level of VEGF as the HUVECs alone ($p = 0.5370$). The levels of VEGF increased drastically with the addition of hMSCs after 3 days post-HUVECs seeding. The co-culture group continues to secrete more VEGF over the culture period ($p \leq 0.0001$ for each).

Overall, hMSCs alone secreted relatively higher levels of VEGF as compared to the co-culture I and HUVECs alone groups at day 3 and day 10 ($p \leq 0.0001$ for each).



(a)



(b)

Fig. 6.6: The level of (a) PDGF-BB and (b) VEGF produced by hMSCs alone, HUVECs alone and co-culture model after day 3 HUVECs seeding only, day 6 and 10 post-hMSCs additions. PDGF-BB production was increased from day 3 to 10 for HUVECs alone group ($p \leq 0.0001$) while co-culture model demonstrated declined in PDGF-BB production post-hMSCs addition and no longer detectable afterwards. hMSCs alone showed almost negligible PDGF-BB production at any time-points. In the co-culture model, significant increase of VEGF production at day 3 and 10 post-hMSCs addition ($p \leq 0.0001$) was observed. Similar trend was observed for hMSCs alone group, which showed significant inclined in VEGF production from day 3 to day 10 ($p \leq 0.0001$).

6.3. Discussion

To date, tissue engineering strategies for bone have yet to deliver fully functional clinical approaches. The development of a vascular network surrounding the constructs is insufficient, resulting in cell death and tissue necrosis, as there are limited nutrients and oxygen supply to the cells within the constructs (Novosel et al. 2011; Ma et al. 2011). Thus, providing sufficient blood supply in the initial phase after implantation is crucial for success of bone constructs (Grellier et al. 2009). Recent findings have suggested that one of the effective solutions to overcome this limitation is pre-vascularization. In this study, the aim was to undertake the proof of concept work to closely mimic the bone structure by using a 3DP hybrid scaffold with pre-determined channel size and co-culture of HUVECs and hMSCs. Four channels (4C) scaffolds with each individual channel diameter of 1.5 mm were selected from previous criteria (as described in Chapter 5) in order to create the pre-vascularized bone construct. From the literature, it is suggested that delayed addition of hMSCs to pre-seeded HUVECs scaffolds is the optimum condition to create a pre-vascularized constructs (McFadden et al. 2013). According to McFadden and co-workers (2013), delayed addition of hMSCs after 3 days of post-HUVECs seeding was reported to enhance vessel formation within the scaffolds, with increased, cell migration and distribution and structural organization evident. The rationale behind this is the formation of vascular structure occurred in spatio-temporal pattern. The initial stage of vessel formation requires endothelial cells assembly followed by maturation and stabilization recruitment of perivascular cells, i.e. the secretion of growth factors such as VEGF which is crucial in the maintenance and stabilization of the new blood vessels (Grellier et al. 2009). Therefore, delayed hMSCs seeding pronounced a better method to closely replicate the *in vivo* process as it is widely agreed that vascularization occurs before osteogenesis take place during both embryonic development and bone healing for an adult (Roux et al.

2015). Thus, the balance in growth conditions between osteogenic and angiogenic cues are one of the challenges in developing vascularized bone constructs.

However, in this study, the vascular networks have not yet been found after 10 days co-culture. This is due to the relatively low cell density seeded on the scaffolds. Thus, culture period of 10 days after hMSCs addition as suggested by McFadden and co-workers (2013) seems insufficient for this work. McFadden et al. (2013) demonstrated that high cell number (5×10^5 /scaffold) and cell ratio of 4:1 (HUVECs: hMSCs) cultured in OM successfully induced the formation of vessel-like structure after 10 days post-hMSCs seeding (McFadden et al. 2013). Since the formation of vascular networks depends on space and time, the low cell density used in this study may require a longer culture period for the cells to migrate, proliferate and assemble to form vessel-like structure before the addition of hMSCs to the co-culture system. It is possible that, in this study, HUVECs were still proliferating with only minimal communication between the neighbouring cells, as there is more area to fill. It is also possible that the addition of hMSCs to the system might interfere with the natural process of vessel formation as the physically larger hMSCs may impede the self-assembly of HUVEC networks, thus hindering adequate formation of these early vascular structure (Jain 2003; Chen et al. 2007).

Positive stains for RUNX-2 and CD31 in the co-culture system indicated the expression of early osteogenic and angiogenic markers. RUNX-2 is the most specific transcription factor in early osteoblastic differentiation of hMSCs (Kanczler & Oreffo 2008; Rupani et al. 2012). In both conditions, hMSCs alone and HUVECs: hMSCs co-culture model, RUNX-2 markers were expressed, which indicates that the hMSCs started to differentiate towards osteoblastic lineage. It was observed that HUVECs alone demonstrates higher expression of CD31 compared to the co-culture system. This clearly highlights that HUVECs were

able to achieve cell-cell contact and maintain phenotype before hMSCs were added to the culture. According to the literature, endothelial cells of all origins are able to form tube-like structures *in vitro* when grown in appropriate ECM components such as Matrigel or collagen type I. Matrigel is a tumor basement membrane matrix extract enriched with laminin. During angiogenesis, the proliferating and migrating ECs are eventually organized into newly formed capillary structures (Grant et al. 1985; Madri et al. 1988). Unfortunately, in this study the vessel-like structure was not formed at these time-points. It is believed that embedding HUVECs in the Matrigel might have restricted the cell proliferation and activity. To overcome this problem in the future, a further study on the use of Matrigel in culturing HUVECs in 3D structure should be conducted. For instance, instead of embedding HUVECs in the Matrigel, the cells should be cultured on the top layer of the Matrigel, applying the common method for Matrigel angiogenic assay. This could possibly promote cell survival, proliferation, migration and formation of new vessel-like structure.

In addition, there are difficulties with imaging the vessel-like structures using confocal microscopy, which may cause issue with the detection of the vessel-like structures even using higher magnification. This is because the newly formed vessels are relatively small and the confocal microscope might not be able to provide sufficient resolution/magnification to detect smaller structures. Two-photon fluorescence light microscopy was recently used to detect the vascular-like structure in particular for a thick three-dimensional constructs as suggested in the literature (McFadden et al. 2013). Although, confocal and two-photon microscopy techniques are very much alike, two-photon microscopy has a number of advantages. Firstly, the excitation wavelength of two-photon is twice as high/powerful as one-photon excitation. Secondly, two-photon microscopy is predominantly suited for imaging thick specimens. This is because the near

infrared light used in two-photon excitation has orders of magnitude less absorption in biological specimens than UV or blue/green light. Finally, two-photon microscopy requires no pinhole aperture and minimizes the signal loss. Unlike two-photon microscopy, confocal requires the use of emission pinhole aperture to eliminate out of focus light. However, scattering of the fluorescent photons inside thick specimens is unavoidable. The divergence of the resultant path causes a significant loss of these photons at the confocal pinhole (So 2002).

Platelet-derived growth factor (PDGF) family members and vascular endothelial growth factor (VEGF) are the most essential pro-angiogenic growth factors and are closely related (Rouwkema et al. 2006; Rouwkema et al. 2008; Novosel et al. 2011). PDGF-BB is a critical factor produced by HUVECs and is principally involved in the recruitment and migration of perivascular cells to the site of vessel assembly (Ball et al. 2007). Results revealed that HUVECs alone continued to release PDGF up to day 10 in culture and in an attempt to recruit perivascular cells to stabilize neo-vascular structures. HUVECs require time to release PDGF before hMSCs addition, thus allowing for superior, more functional formation of vessel-like structure. This has then a knock-on effect on vessel-like structure migration into the scaffold and mitigates vessel regression (Carmeliet & Conway 2001; Chen et al. 2007; Lee & Niklason 2010).

On the other hand, hMSCs primarily released VEGF in order to influence vessel assembly (Kanczler & Oreffo 2008; Rouwkema et al. 2008). The co-culture model shows increased expression of VEGF at day 6 post-addition of hMSCs at day 3. Concurrently, PDGF production was diminished once the hMSCs were added to the system. These data are consistent with the literature. Similar phenomenon was observed by Lee & Niklason (2010), whereby PDGF was only released by the rat aortic endothelial cells (RAECs)

cultured alone; however, no PDGF was released in the co-culture of RAECs and rat hMSCs alone. The availability of this chemotactic agent to the newly added hMSCs may be the reason that enhanced vessel formation occurs and faster recruitment may be permitted to the site of the vessel wall assembly followed by incorporation of the vessel wall (Jain 2003; Merfeld-Clauss et al. 2010). Once the hMSCs localize to the site of the HUVEC vessels, they can then stabilize this structure explaining the cessation of the PDGF production in the co-culture system. As for this study, two primary reasons HUVECs have not yet formed the vascular network is due to low cell density and insufficient PDGF secretion. This is because the production of VEGF by the hMSCs has inhibited the production of PDGF by the HUVECs once hMSCs were added to the pre-seeded HUVECs scaffolds. Even for the monoculture system, HUVECs alone was still producing PDGF and no vessel-like structure seems to form at these time-points. Our data highlights the important of spatio-temporal relationship between these two growth factors and their respective influences on both cell types. It has been reported in literature that the size of the new vessels was affected by the spatial delivery of VEGF, but depended primarily on the presence of PDGF. In addition, vessel maturation increased over time, and was enhanced by the delivery of PDGF (Chen et al. 2007). Controlled delivery of both growth factors is important in the formation, stabilization and maturation of the vessel within the scaffolds. To author knowledge, vessel formation and maturation is time-dependent and to date no exact time has been reported in the literature as this varies on several parameters, i.e. cell ratio, culture medium, culture period, seeding technique and culture substrate materials (i.e. soft-gel, spheroid or scaffolds).

6.4. Conclusions

The concept for pre-vascularization of engineered bone construct can be tested by co-culture in defined regions of the channel scaffolds. The co-culture model shows that both HUVECs and hMSCs were able to proliferate throughout the scaffolds despite the low density of cells seeded. The quantification of the relative fluorescence intensity provides a better understanding of the cell-cell interaction. Both osteogenic and angiogenic markers were positively expressed by the co-culture model. Further work should include the use of higher cell densities, which may result in a higher production of PDGF and VEGF in the co-culture model compared to monoculture systems leading potentially to a successful pre-vascularized bone construct. However, results highlight the need to optimize the co-culture model within the 3DP scaffolds. Seeding technique, cell density, cell ratio, total cell number, culture medium and culture period require further optimization.

Chapter 7

General discussion, Concluding Remarks and Future Work

7.1. General Discussion

Bone tissue engineering (BTE) is a vast diverse field, which provides new concepts for bone regeneration. There are a number of new strategies based on this concept including cell-based therapies, scaffold-based therapies and various examples of combinations of both therapies with the aim to guide cells to form functional tissue (Burg et al. 2000; Hutmacher et al. 2004; Meijer et al. 2007). A range of materials has been used in BTE mainly for making scaffolds, including natural and synthetic polymers, bioglass and a number of calcium phosphate-based bioceramics such as hydroxyapatite (HA) and tricalcium phosphate (TCP) (Rose et al. 2004). Besides bioceramics, synthetic polymers such as poly (lactic acid) (PLA) and poly (lactic-co-glycolic acid) (PLGA) have been widely used as architectural supports for cells since these polymers are known to be biodegradable, biocompatible, mechanically durable and capable of being formed into desired shapes (Rezwan et al. 2006). Many different scaffolds have been fabricated using numerous materials and techniques; but none has actually met the clinical needs.

Therefore, this study aims to fabricate novel 3DP hybrid scaffolds to enhance bone formation *in vitro*. In order to achieve the research goal, this study was divided into four main phases which includes the production of newly develop multi-substituted HA powders and development of novel coating materials assembly followed by fabrication of 3DP hybrid scaffolds. The cell behaviour on 3DP hybrid scaffolds was then investigated, i.e. hMSCs cultured on several structural and functional scaffold designs in different culture conditions (static versus dynamic and OM versus PM). The primary aim of this thesis was to fabricate a functional scaffold design that could bring us a step closer to the clinical needs particularly for osteoarthritis cases. The final phase of this study undertake the proof of concept work to closely mimic the bone structure by introducing the co-

culture model of HUVECs/hMSCs into the best scaffold design as to create pre-vascularized scaffolds, which could benefit both osteogenesis and angiogenesis during repair.

For many years, synthetic HA has been used as bone substitute material in medical applications due to its osteoconductive properties, similarity in the composition to the mineral phase of bone and in conjunction with their FDA approval for clinical use (Ducheyne & Qiu 1999). However, the use of HA as a biomedical material has been hindered as synthetic HA is slower to resorb than the endogenous form and may possibly remain at the site of implantation for many years (Bohner 2000; Brydone et al. 2010). The difference in composition makes biological apatites different to synthetic HA; thus it is more accurately referred to as multi-substituted HA (Sprio et al. 2008; Spence et al. 2008; Landi et al. 2010).

The function of the ionic substitutions in the HA lattice on biological responses has been documented in the literature for both *in vitro* and *in vivo*. The presence of B-type CHA has been shown to cause a decrease in crystallinity and increase in solubility both *in vitro* and *in vivo* (Landi et al. 2003; Murugan & Ramakrishna 2006; Shepherd et al. 2012). *In vivo* tests using an ovine model demonstrated that more dissolution was observed from the CHA, at the bone implant interface and within the implant, when compared to pure HA (Porter et al. 2005). In addition, the presence of carbonate may also play an important role in metabolic activity where a higher carbonate leads to a higher metabolic activity. For example, tissues containing higher carbonate content like bone and dentin are known to be more bioactive than enamel, which is a nearly inert tissue due to relatively low carbonate content (Landi et al. 2010).

Besides carbonate, silicon (Si) also plays an essential role of for normal bone and cartilage growth and development (Carlisle 1970; Schwarz & Milne 1972; Carlisle 1979). Si content varies widely dependant on the bone age and site. It has been reported that Si up to 0.5wt% was localized in the active calcification sites of the young mice and rats and the value varies in concentration for the enamel of young humans (1.3-504 $\mu\text{g/g}$) (Carlisle 1970; Healy 1998). Studies have shown the benefits of delivering controlled levels of Si to a wound healing site in order to promote bone repair (Hing et al. 2006). Si plays an important role in bone and cartilage systems as it influences cartilage synthesis and the integration of the ECM as well as the bio-mineralization process (Gibson et al. 1999; Landi et al. 2010). However, there is still a discrepancy on the effect of Si-HA on biological responses, which has been reported in the literature. This is mainly because Si substitution into HA lattice is known to have a dose-dependent effect on the proliferation, differentiation and collagen synthesis of osteoblast, with a direct influence on the remodelling process and osteoclast development and resorption activities (Pietak et al. 2007). For instance, Landi et al. (2010) found that higher silicon content ($\geq 0.8\text{wt}\%$) incorporated in the HA structure resulted in higher cell death *in vitro*. Literature has suggested that this is due to higher ion release as powders with high silicon content have higher solubility (Lin et al. 2006; Ni et al. 2007); the same trend was observed in this study. Our study has highlighted that the incorporation of carbonate and silicon ions in the HA lattice in controlled amounts plays an important role in improving the cell response. However, very limited studies on the benefits of simultaneous ionic substitutions into HA lattice (mainly in nanopowders forms) on human osteogenic cells have been demonstrated in the literature. This study not only aims to produce a novel biomedical material but hopefully the findings would be beneficial to other groups manufacturing materials for bone TE.

In this study, different degrees of the newly developed substituted HA nanopowders have been successfully produced by a nanoemulsion method. Two groups of multi-substituted HA (SiCHA) nanopowders have been produced, namely SiCHA-1 and SiCHA-2 besides a single substitution (either carbonate or Si) nanopowders, i.e. CHA and SiHA. Among the powders produced, SiCHA-2 was chosen as the ideal biomedical material since it provided the most favourable growth environment for hMSCs *in vitro* compared to the other investigated powders. The distinct cell responses observed can be explained by the differences in the powder formulations. This evidence was observed when hMSCs were seeded on SiCHA-1 and SiCHA-2. hMSCs in direct contact with SiCHA-2 showed the fastest cell proliferation and production of proteinaceous materials. This can be explained by having the closest compositions of carbonate and silicon ions substituted HA lattice relative to natural bone. hMSCs cultured on SiCHA-2 show statistically higher cell responses (i.e. DNA content, protein production, metabolic activity) compared to SiCHA-1 ($p \leq 0.0001$). In contrast, SiCHA-1 show the worst cell responses compared to the single substituted CHA and SiHA nanopowders. The use of high Si concentration in SiCHA-1 produced powders, which contain silicon as the major substitution with limited carbonate incorporated in the HA structure. This behaviour gives evidence of the competition arising between these two ions for the occupation of the same crystallographic site of phosphate group (Sprio et al. 2008). Having too high Si concentration in the HA lattice, have no toxic effect found in this study, but SiCHA-1 hinder the proliferation of hMSCs. This finding highlights the importance of controlled amounts of ionic substitutions in the HA structure as they can be the determining factor in the cell responses. To date, no such study has been published using the same production route according to the author's knowledge.

The substituted HA powders can be used in several different ways, i.e. powder forms, compact sintered discs, coating materials and composite scaffolds (Gross et al. 1998; Murugan & Ramakrishna 2006; Habibovic et al. 2010; Shepherd et al. 2012; Rodrigues et al. 2013). In this study, a novel coating materials assembly for Polyelectrolyte Multilayers (PEMs) technique has been established using multi-substituted HA nanopowders, hyaluronan, collagen type I and EDC/NHS on 2D PLA films prior to 3DP hybrid scaffolds fabrication. In nature, the biological world is built up by precise self-assembly of bio-macromolecules. This has inspired the researchers to explore an engineered scaffold via macromolecules self-assembly (Kim & Bruening 2003; Huang et al. 2012). PEMs have been used to modify the polymer surface and re-create the ECM environment on biopolymer surface (Mhanna et al. 2011; Mathews et al. 2012). In this study, the combinations of osteoconductive (SiCHA nanopowders) and osteoinductive (collagen type I) materials as the polyelectrolytes resulted in positive outcome with 5-bilayers (BL) depositions of the innovative coating materials serving as the most favourable milieu for hMSCs attachment and activity. This coating materials assembly resembles the composition of natural bone which contains mainly CHA and many natural ECM-like macromolecules such as hyaluronan and collagen type I (Zhao et al. 2014). No researchers have ever reported on the same coating materials assembly as used in this study based on author's knowledge. This coating technique was firstly developed by Decher (1997) and has been used in many applications such as biosensors, separation or dialysis membranes, and surface modification of various different materials due to its simplicity and versatility. Among other coating materials used in TE applications were poly (L-lysine)/alginate, hyaluronic/collagen type I and chitosan/hydroxyapatite (Detzel et al. 2011).

As well as material type, the design of scaffolds is important to facilitate cell and tissue growth. Factors governing scaffold design are complex and involve considerations on the

architecture design, pore/channel size and morphology, surface properties, mechanical durability and most importantly biological influence (Hutmacher 2000). One common problem encountered in scaffold-based TE is the rapid formation of tissue on the outer edge of the scaffolds while the tissue in the inner part of the scaffold undergoes necrosis. (Rose et al. 2004; Silva et al. 2006). A common approach to overcome this problem is by altering the culture conditions with the use of sophisticated bioreactors such as perfusion or rotary bioreactors. This will help to provide effective nutrients and oxygen supply as well as waste removal; nutrients are able to reach the cells in the centre of the scaffolds, which improves cell survival (El Haj & Cartmell 2010; Yeatts & Fisher 2011). Although, these bioreactors have shown successful outcomes and are increasingly used in tissue engineering *in vitro*, this field is still emerging in order to ensure that the host tissue can penetrate through the entire scaffold as to guarantee satisfactory integration of the scaffold (Stevens et al. 2005).

Alternative approach to address this issue is to incorporate a design within the scaffold, which will improve nutrient and oxygen supply to the inner part or core of the scaffold. This approach has potential benefits both *in vitro* and *in vivo* culture conditions. In order to achieve this goal, recent studies have incorporated aligned channels on a solid material (Hollister et al. 2002; Lin et al. 2003; Silva et al. 2006). This design of scaffolds has been fabricated using several techniques such as modified slip casting, phase separation and rapid prototyping (RP) (Taboas et al. 2003; Rose et al. 2004; Wilson et al. 2004; Silva et al. 2006). In this study, Fused Deposition Modelling, which is one of RP techniques, was used to fabricate the 3DP PLA scaffolds with aligned channels. This technique was chosen as it has been used for fabricating complex shaped scaffolds. The intended size of the aligned scaffolds can be easily designed using a CAD system and allows in precisely creating the predetermined forms and internal structure. In addition, it is highly

reproducible and can be customized to the patient needs in the future (Hutmacher 2000; Hollister 2005; Sobral et al. 2011). Previous studies have reported the positive influence of incorporating design within the scaffolds on cell and tissue ingrowth. This is thought to improve nutrients and cell transfer to the core of the scaffold, both *in vitro* and *in vivo* (Ma & Zhang 2001; Hollister et al. 2002; Gabriel et al. 2002; Rose et al. 2004; Silva et al. 2006).

From a scaffold-based TE point of view, improved tissue formation in 3D is closely may be related to the initial cell adhesion on the scaffolds. The cell growth in a scaffold is largely dependent on the scaffold architecture typically the pore/channel size and their orientation (Galban & Locke, 1999; Sobral et al. 2011). In general, the higher the porosity of a scaffold, the higher its surface area to volume ratio, which could allows better cell attachment and migration throughout the entire scaffolds (Salgado et al. 2004). However, in this study we found that mesh scaffolds having too large pore size (i.e. 500 μm) with struts perpendicular to each other resulted in less support is available for the cells to attach to the scaffold. In addition, most cells found at the bottom of the scaffolds as cells were easily slides down. This is the major issue encountered in this study when hMSCs were seeded on the mesh scaffolds. To address this problem, the cell culture well plates were coated with Pluronic F-127 beforehand to create non-adhesive regions as suggested in the literature (Dang et al. 2002; Deegan et al. 2014). This method is very simple, uses commercially available reagents and is generally applicable to substrates including tissue culture plastic (TCP) surface with unlimited geometric constrains. The results obtained in this study have demonstrated that better cell attachment was obtained when the cells were seeded on the 3DP hybrid scaffolds using pluronic coated cell culture well plates.

It is also possible to coat the culture plate using ethylene glycol-functionalized alkanethiols as this polymer resists protein adsorption and cell adhesion. The disadvantage of ethylene glycol-functionalized alkanethiols is that it is not commercially available (Tan et al. 2004; Aydin et al. 2011). The use of suspension culture plates would be another potential option in the future. It is believed it would be better to use suspension culture plates rather than ordinary TCP, which has been plasma treated. The well in the suspension plate has a layer of hydrogel that is hydrophilic and neutrally charged. This will inhibit cell attachment, as the proteins and other biomolecules are passively adhering to the surface through hydrophobic and ionic interactions.

The combination of osteoconductive and osteoinductive materials on the 3DP hybrid scaffolds have a significant impact on the cell response as compared to the pure HA scaffold. The presence of collagen type I plays an important role as an adhesion protein, which favours cells attachment and proliferation (Bisson et al. 2002; Becker et al. 2002; Ma et al. 2005). Thus, cells adhered to the 3DP hybrid scaffolds are deemed to have stronger bonding compared to the pure HA scaffolds. It is assumed that the HA scaffolds were sintered at high temperature, resulting in a highly crystalline structure with small pore sizes that affected the protein adsorption. This decreased cell adhesion and detachment strength (Gariboldi & Best 2015). Consequently, the weakly bonded cells were easily detached from HA scaffolds once exposed to microgravity simulation. Although the HA scaffolds have good interconnectivity and are highly porous, the HA scaffolds have the smallest pores (200-300 μm) compared to the 3DP hybrid scaffolds and majority of the pores were blind-ended. It has been demonstrated in the literature that blind-ended porosity decreased cell penetration into HA scaffolds core when compared to open porous scaffolds with aligned channels both *in vitro* and *in vivo*, suggesting tortuosity and closed pores reduced cell penetration (Silva et al. 2006). Besides, blind-ended structure also prevent

cellular infiltration and ECM production of the inner core of the HA scaffolds (Salgado et al. 2004). However, HA cellular scaffolds in static conditions were able to attach, migrate and proliferate over time as typically found in the literature (Li et al. 2012). It is believed that culturing HA cellular scaffolds in the rotary bioreactor exposed the weak bonded cells to high shear stress induced by the collision with the vessel wall, as the rotational speed was kept constant at 20 rpm. Numerous studies of particles dynamics in a rotating bioreactor have demonstrated that the density difference between the microcarrier and the culture medium resulted in an increase in shear stress on the microcarrier. For instance, ceramic materials, which in general have high density, would experience a high shear stress, affecting cell attachment and causing cell damage. In addition, denser microcarrier tend to bounce off from the walls of the vessel, thereby causing a detrimental effect on the cell viability (Gao et al. 1997; Qiu et al. 1998).

Commercial HA scaffolds used in this study appeared pale blue instead of white (which is the typical appearance of pure HA) (Leukers et al. 2005). It is assumed that there were some impurities in the structure or material of the scaffolds. Upon culture, it is believed that these impurities might have reacted with the cells and resulted in negative impact on the overall cell responses. In order to ensure the HA scaffolds are free from any impurities, it would be beneficial to characterize the scaffolds (i.e. the actual composition, crystallinity and surface roughness) before further studies could be performed in the future.

A principal concern of the *in vitro* 2D cell culture is that cells tend to grow in a monolayer even when cultured on 3D biodegradable scaffolds. Cells cultured in static condition are not allowed to pile on top of one another, but are forced into flat layers, which do not accurately replicate the *in vivo* model (Sheyn et al. 2010). Tissues or organs are cellular 3D well-organized structures with sophisticated cell-cell and cell-matrix interactions and

intricate transport dynamics for nutrients and cells (Antoni et al. 2015). The effect of 3D culture on collagen-sponge network in bone has been demonstrated by Masi et al. (1992) who discovered that it was able to induce osteocalcin synthesis even in the absence of vitamin D in the human osteoblast-like SaOS-2 cells whereas, osteocalcin was not expressed by these cells when they were cultured on collagen type I coated dishes (Masi et al. 1992).

Moreover, high density, 3D *in vitro* growth of mammalian cells is challenging owing to the nutrients diffusion and lack of oxygenation in the classic *in vitro* cell culture (Granet et al. 1998). Thus, a dynamic cell culture system is required to engineer a 3D pattern of growth and differentiation as well as closely mimic the *in vivo* environment (Martin et al. 2004; Rauh et al. 2011). To overcome this problem, a rotary bioreactor seems a promising dynamic culture system as it was designed to reduce the shear stress as compared to perfusion system (El Haj & Cartmell 2010). Studies have shown that the use of the rotating bioreactor increases the protein production in comparison to perfusion or static conditions after 28 days (Pound et al. 2006). The 3D dynamic flow environment induced by the microgravity simulation from the rotary bioreactor was reported to affect the bone cell distribution in 3D cultures even at early stage of culture (4 and 7 days) enhancing osteoblastic phenotypic expression and mineralized matrix synthesis within tissue-engineered constructs. This is believed to be due to the improvement in mass transport between the cells seeded within the scaffolds and the culture media (Yu et al. 2004). For this reason, the rotary bioreactor was selected as to address the fundamental issues facing bone remodelling and formation, in particular, regarding the effect of dynamic flow in a 3D environment on bone cell biology and bone formation *in vitro* (Granet et al. 1998; Song et al. 2006).

This study provides important basic information to elucidate the effect of dynamic flow on hMSCs proliferation, osteoblast phenotype development and generation of early stage of mineralized matrix on different scaffold designs. Interesting findings were obtained when the 3DP hybrid scaffolds were cultured in the rotary bioreactor in different culture medium, namely the OM and PM. Regardless of the scaffold designs, cell seeded scaffolds under dynamic flow in PM demonstrated the least cell growth compared to the other growth environment e.g. Dynamic flow in OM and Static in OM and PM. As culture progressed, the cell seeded scaffold in PM continuously expanded and increased in cell number with the enhancement following addition of serum into the media. Without any osteogenic supplements, hMSCs proliferate to higher cell numbers without differentiation occurring (Jung et al. 2012). Over time, cell seeded scaffolds with greater cell density than the surrounding medium suffer repeated impacts with the bioreactor wall, imposing a mixture of non-quantifiable mechanical disruptions to cultured cells. These repeated collisions have a detrimental effect by limiting the cell density and mineralized matrix synthesis during cultivation in the rotary bioreactor (Goldstein et al. 2001; Sikavitsas et al. 2002). In addition, some of the hMSCs were detached from the scaffolds and resulted in suspended cells present in the media. Being an anchorage-dependent cells, hMSCs need a substrate to attach and survive (Jung et al. 2012; Chen et al. 2013). It is assumed that when the detached cells were in suspension, they were floating and eventually undergoes cell death. This may explain why we obtain higher percentage of LDH activity for cell seeded scaffolds under dynamic flow with PM.

This trend was less severe when 3DP hybrid cellular scaffolds were cultured in OM than PM. With the presences of dexamethasone, β -glycerolphosphate and ascorbic acid in OM, cells were able to differentiate towards osteogenic lineage (Birmingham et al. 2012; Langenbach & Handschel 2013). Once the cells started to differentiate, the rate of

proliferation is slowed down concurrently following the model of the reciprocal relationship between proliferation and differentiation during osteoblast development as proposed by Lian & Stein (1992). As differentiation progressed, more ECM is produced by the hMSCs. This is thought to provide a better cell adhesion to the cell seeded scaffolds and help in cell survival. Consequently, less cells detached from the scaffolds, which resulted in fewer cell death represented by lower percentage of LDH activity. In this study, cell seeded scaffolds under dynamic flow in OM showed positive outcomes. The pre-designed aligned channels on the 3DP hybrid scaffolds (2C and 4C scaffolds) have allowed the culture medium to be distributed throughout the scaffolds while the vessels were rotating. This has facilitated the transport of nutrients and waste removal as well as oxygen supply to the cell seeded scaffolds. As a result, more bone-like nodules and early-mineralized matrix formed when the 3DP hybrid scaffolds were cultured under dynamic flow in OM. The combinations of the pre-designed aligned channels on the 3DP hybrid scaffolds, OM and dynamic culture condition have greatly enhanced the overall cell responses. This finding was found to be contradictory to the study by Sikavitsas et al. (2002), who found that after 21 days of culturing rat MSCs on 75: 25 PLGA biodegradable scaffolds in OM, in spinner flask bioreactor and in static culture conditions, scaffolds showed higher ALP activity, osteocalcin secretions and calcium depositions compared to those cultured in the rotary bioreactor. The discrepancy in the results can be easily explained by the obvious difference in the rotational speed used. In this study, 20 rpm was selected as the optimum speed in order to minimize the shear stress while maintaining the cellular scaffolds free floating in the vessels. A higher speed of 30 rpm was used by Sikavitsas et al. (2002) and this has caused detrimental effect on the cellular scaffolds. Here we highlighted three important fundamental findings discovered in this study, which

controlled the cells behaviour under dynamic flow in a 3D environment; (1) scaffold designs, (2) culture medium and (3) rotational speed applied.

The ultimate goal of BTE is to create a living scaffold that could survive after implantation, where this engraftment sought a rapid formation of a stable and functional vascular network (Unger et al. 2010; Ma et al. 2011; Gershovich et al. 2013). During *in vitro* culture, nutrients can be supplied to the larger tissue-engineered scaffolds using the advanced technology of bioreactors and pre-designed aligned channel scaffolds as demonstrated in this study. However, after implantation cells can only survive with a limited distance of about 100-200 μm (the diffusion limit of oxygen) from the next capillary network for the supply of nutrients and oxygen and for the removal of waste products (Rouwkema et al. 2008).

One approach to create pre-vascularized tissue-engineered scaffold, which involves the paracrine communication between endothelial cells (i.e. HUVECs) and hMSCs (Rouwkema et al. 2006; Gershovich et al. 2013; Dahlin et al. 2014). The main aim of this study was to develop a proof of concept study that could closely replicate the bone structure by directly filling in the aligned channels with HUVECs and covering the surface with hMSCs. The cellular crosstalk between the major pro-angiogenic cells (HUVECs) and the perivascular cells (hMSCs) could result in the establishment of functional vasculature that can mature and stabilized (McFadden et al. 2013). To obtain a well-organized vascular network within the 3DP hybrid cellular scaffolds, the cell ratio of 1:1 mix of HUVECs: hMSCs was chosen based on previous studies (Rouwkema et al. 2006; Gershovich et al. 2013). However, there is discrepancy in the optimum culture medium (i.e. EM, OM and mix of both two) used for this particular system. Rouwkema et al. (2006) discovered interesting cell behaviour in different culture media where, hMSCs was found

to have highest proliferation rate in mix media, while HUVECs proliferate well in EM and exhibit intermediate result in mix media. With regard to this finding, mix media of EM and OM with 1:1 ratio was used in this study.

Besides cell ratio and culture medium, the seeding technique is another important parameter. Most studies directly seeded both cells simultaneously, which not accurately imitate *in vivo* occurrences (Gershovich et al. 2013; Dahlin et al. 2014). According to McFadden et al. (2013) the *in vivo* phenomena can be replicated by the delayed addition of hMSCs to the HUVECs seeded scaffolds; the seeding technique was adapted in this work with some modification. According to the literature, the most important pro-angiogenic growth factors for this co-culture system are VEGF and PDGF expressions as the secretion of both growth factors would influence the vessel assembly and mineralization as a whole (Ball et al. 2007; Kaigler et al. 2010). Typically, HUVECs would take roughly about 10 days to develop a proper vasculature in the co-culture system (Rouwkema et al. 2006; McFadden et al. 2013). However, no vasculature was evident in this study, which may result from a lower cell density as compared to those in the literature. For instance, with high cell ratio (4:1) and total cells (5×10^5) on a scaffold, McFadden et al. (2013) has shown the detection of optimal vessel formation even as early as 6 days of hMSCs post-implantation. Despite the low cell density used, cells used in this co-culture model were still able to secrete both pro-angiogenic factors. It is thought that the addition of hMSCs to the pre-seeded HUVECs scaffolds was probably too early which impede the proliferated HUVECs to form a stable vessel assembly. Another possible reason why vessel formation could not be seen in this study is due to the imaging technique used. Alternatively, two-photon fluorescence light microscopy was recently used to detect the newly small vessel formation in particular for a thick three-dimensional scaffold as suggested in the literature (McFadden et al. 2013).

7.2. Concluding Remarks

Overall, this thesis has investigated the potential application of 3DP hybrid scaffolds for enhanced bone formation. The first phase of the study involved the production of a range of newly developed multi-substituted HA nanopowders using nanoemulsion method followed by heat treatment (calcination). Among the various different compositions of powders produced, good hMSCs behaviour was found on direct contact with SiCHA-2 nanopowders, which consists of 3.98 wt% carbonate and 0.45 wt% silicon substituting the HA lattice. SiCHA-2 was chosen as the ideal powder formulation as these powders closely mimic the composition of bone mineral. Thus, SiCHA-2 was suitable for next phase in the development of a novel 3DP hybrid scaffold for BTE applications. The optimum SiCHA nanopowder was then used as a major component in the innovative coating materials assembly for Polyelectrolyte Multilayers (PEMs) technique, which was established in the second phase of this study. Five bilayers (5-BL) coating was chosen as the finest deposition cycles as they provide the highest surface roughness and homogenous distribution of coating materials, which offered the best milieu for the hMSCs adhesion, growth and proliferation.

Fused Deposition Modelling is a useful technique in making different structural and functional designs of 3D scaffolds with precise aligned channels and pores. The coating materials assembly established was then adapted for the fabrication of 3DP hybrid scaffolds in the third phase of this study. Dynamic flow has effectively facilitated the mass transport to pass through the entire scaffolds and enhance the overall cell responses on the 3DP hybrid scaffolds in OM. The biochemical cues in OM have encouraged rapid cell differentiation and produced a stronger matrix between the cells and scaffolds. While, the lack of biochemical cues in PM allowed the fluid flow induced from the rotary bioreactor

to be easily washed off the cells on the scaffolds as they experienced higher shear stress by colliding with the vessel walls. Finally, this study has provided a proof of concept of co-culture system to closely resemble the bone structure. The positive indications given by the expression of both pro-angiogenic markers show that the concept applied may be capable of supporting vessel formation *in vitro*. However, more experiments should be done in the future to optimize the co-culture parameters for this particular scaffold design as to create a pre-vascularized 3DP hybrid scaffold that could be beneficial help for osteoarthritis cases in particular.

7.3. Future Work

To address the aims of this study, the production of 3DP hybrid scaffolds enhancing bone formation, a thorough understanding of the background materials specifically related to bone tissue engineering is required. Therefore, studying the properties of natural human bone or bone similar in composition (sheep or bovine bone) should be performed to provide an understanding of the composition and structure of the natural bone and to be used as “gold-standard” for future studies.

In this work, the 3DP hybrid scaffolds were fabricated manually by PEMs assembly technique. For large-scale production in the future, an automatic coating system using the same coating materials assembly would be helpful to maintain the high level of quality control and consistency between batches and to be more time efficient.

In order to fabricate large scale of 3DP hybrid scaffolds, multi-substituted HA nanopowders needs to be produced at large scale. The application of these powders is not limited to coating materials; they can also be used to fabricate a 3D scaffold using other technique, i.e. 3D printing, selective laser sintering or laminated object manufacturing (Seitz et al. 2005). The fabricated ceramic scaffolds could potentially be used as an

experimental control to this study. Alternatively, to ideally compare the performances of the 3DP hybrid scaffolds, a control scaffold should have the same structure and functional design. A commercial HA powder could be used as the osteoconductive materials (replacing the in house SiCHA nanopowders) to coat the 3DP scaffolds in exactly the same manner as the 3DP hybrid scaffolds produced in this study.

Besides the materials properties, the structural design of a scaffold also plays an important role in determining the stem cells fate. For instance, altering the orientation of the struts across the mesh scaffold could maximize the cell attachment on the scaffold. Instead of having the struts perpendicular to each other, some researchers have designed the scaffolds with inclined layers of 45°. This design shows enhance cell attachment because the cells are hindered from sliding down of the structure (Leukers et al. 2005). There are other several 3DP technical parameters that could be optimized to obtain better cell attachment on the scaffolds such as the layer thickness, window size and pore/channel size (Silva et al. 2006; Asadi-Eydivand et al. 2016). Further work, including qPCR would help to quantify the differentiation state of hMSCs seeded on different scaffold designs and allow the investigation of further osteogenic and chondrogenic markers. In the future, it would be interesting as well to investigate the impacts of dynamic flow on the 3DP hybrid scaffolds using different bioreactor such as perfusion system. Animal model testing would also be a very interesting future direction. Since the fabricated scaffold is made of biodegradable materials, it is also essential to investigate the degradation rate and mechanical properties of the scaffolds over longer cultivation time (3-6 months). The degradation rate of the 3DP hybrid scaffolds could be easily determined by measuring the weight loss of the scaffolds) or by checking the changes in the molecular weight and Polydispersity Index (PDI) using Gel Permeation Chromatography (GPC) analysis. It is also crucial to investigate mechanical properties of the scaffold such as compression strength as well as the

mechanical compatibility of the scaffolds with cells particularly the stiffness as it is an important cue for the stem cell fate.

In order to successfully create pre-vascularized scaffolds using the same concept applied in this study, more detailed optimizations on the cell ratio, culture medium, seeding technique and culture period should be performed. In the future, it would be interesting to further investigate the co-culture system not only *in vitro* and but also *in vivo*. As an alternative to animal model, Chick Embryo Chorioallantoic Membrane (CAM) can be used to study the impact of angiogenesis in stimulating rapid bone mineralization. CAM assay is probably the most widely used *in vivo* assay for studying angiogenesis as it is relatively simple and inexpensive, suitable for large-scale screening (Staton et al. 2004). The in-house fabricated 3DP hybrid scaffolds could also potentially be used for osteochondral defects. Thus, it would be beneficial to study the crosstalk between chondrogenic and osteogenic cells on the 3DP hybrid scaffolds in the future.

References

References

- Aguirre, A., Planell, J.A., Engel, E., 2010. Dynamics of bone marrow-derived endothelial progenitor cell/ mesenchymal stem cell interaction in co-culture and its implications in angiogenesis. *Biochemical and Biophysical Research Communications*, 400: 284-291.
- Albrektsson, T. & Johansson, C., 2001. Osteoinduction, osteoconduction and osseointegration. *European Spine Journal*, 10: S96-S101.
- Albert, A., Leemrijse, T., Druetz, V., Delloye, C., Cornu, O., 2006, Are bone autografts still necessary in 2006? A three-year retrospective study of bone grafting. *Acta Orthopaedica Belgica*, 72(6): 734–740.
- Allen, P., Melero-Martin, J., Bischoff, J., 2010. Type I collagen, fibrin and PuraMatrix matrices provide permissive environments for human endothelial and mesenchymal progenitor cells to form neovascular networks. *Journal of Tissue Engineering and Regenerative Medicine*, 5: 74–86.
- Ana, I.D., Matsuya, S. Ishikawa, K., 2010. Engineering of Carbonate Apatite Bone Substitute Based on Composition-Transformation of Gypsum and Calcium Hydroxide. *Engineering*, 2(5): 344–352.
- Antoni, D., Burckel, H., Josset, E., Georges, N., 2015. Three-dimensional cell culture: a breakthrough in vivo. *International journal of molecular sciences*, 16(3): 5517–27.
- Araujo, J.V., Reis, C.C., Rada, T., da Silva, M.A., Gomes, M.E., Yang, Y., Ashammakhi, N., Reis, R.L., El Haj, A.J., Neves, N.M., 2010. Dynamic Culture of Osteogenic Cells in Biomimetically Coated Poly (Caprolactone) Nanofibre Mesh Constructs. *Tissue Engineering Part A*, 16(2): 557-563.
- Arthritis Research UK, Osteoarthritis booklet. Available from: <<http://www.arthritisresearchuk.org/arthritis-information.aspx>> [15 October 2015].
- Asadi-Eydivand, M., Solati-Hashjin, M., Farzad, A., 2015. Effect of technical parameters on porous structure and strength of 3D printed calcium sulfate prototypes. *Robotics and Computer-Integrated Manufacturing*, 37: 57–67.
- Ashton, B.A., Allen, T.D., Howlett, C.R., Eaglesom, C.C., Hattori, A., Owen, M., 1980. Formation of bone and cartilage by marrow stromal cells in diffusion chambers *in vivo*. *Clinical Orthopaedics Related Research*, 151: 294–307.
- Astala, R. and Stott, M.J., 2005. First Principles Investigation of Mineral Component of Bone: CO₃ Substitutions in Hydroxyapatite. *Chemistry of Materials* 17(16): 4125-4133.
- Athanasiou, K. A., Niederauer, G.G., Agrawal, C.M., 1996. Sterilization, toxicity, biocompatibility and clinical applications of polylactic acid/polyglycolic acid copolymers. *Biomaterials*, 17(2): 93–102.
- Au, P., Daheron, L.M., Duda, D.G., Cohen, K.S., Tyrrell, J.A., Lanning, R.M., Fukumura, D., Scadden, D.T., Jain, R.K., 2008. Differential in vivo potential of endothelial progenitor cells from human umbilical cord blood and adult peripheral blood to form functional long-lasting vessels. *Blood*, 111: 1302–5.

Aubin, J.E., Lian, J.B., Stein, G.S., 2006. Bone formation: maturation and functional activities of osteoblast lineage cells. In: Murray, J.F., ed. Primer on the metabolic bone diseases and disorders of mineral metabolism. *The American society for bone and mineral research*, Washington, D.C.

Audigé, L., Griffin, D., Bhandari, M., Kellam, J., Rüedi, T.P. 2005. Path analysis of factors for delayed healing and nonunion in 416 operatively treated tibial shaft fractures. *Clinical Orthopaedics Related Research*, 438:221-232.

Aydin, H.M., Hu, B., Sulé Suso, J., El Haj, A., Yang, Y., 2011. Study of tissue engineered bone nodules by Fourier transform infrared spectroscopy. *The Analyst*, 136(4): 775–80.

Bab, I., Ashton, B.A., Gazit, D., Marx, G., Williamson, M.C., Owen, M.E., 1986. Kinetics and differentiation of marrow stromal cells in diffusion chambers in vivo. *Journal of Cell Science*, 84: 139–151.

Baba Ismail, Y.M. & Mohd Noor, A.F., 2011. Effect of a novel approach of sintering on physical properties of carbonated hydroxyapatite. *Journal of Materials Science and Engineering B*, 1(2), pp.157–163.

Bagaria, V., Rasalkar, D., Bagaria, S.J., Ilyas, J., 2011. Medical Application Of Rapid Prototyping - A New Horizon. *Advanced Applications of Rapid Prototyping Technology In Modern Engineering*, 1–21.

Ball, S.G., Shuttleworth, C.A., Kielty, C.M., 2007. Vascular endothelial growth factor can signal through platelet-derived growth factor receptors. *The Journal of cell biology*, 177(3): 489–500.

Bang, L.T., Long, B.D. & Othman, R., 2014. Carbonate hydroxyapatite and silicon-substituted carbonate hydroxyapatite: synthesis, mechanical properties, and solubility evaluations. *The Scientific World Journal*, 2014: 969876.

Baron F, Lechanteur C, Willems E, Bruck, F., Baudoux, E., Seidel, L., Vanbellinghen, J-F., Hafraoui, K., Lejeune, M., Gothot, A., Fillet, G., Beguin, Y., 2010. Cotrans-plantation of mesenchymal stem cells might prevent death from graft-versus-host disease (GVHD) without abrogating graft-versus-tumor effects after HLA-mis-matched allogeneic transplantation following nonmyeloablative conditioning. *Biology of Blood and Marrow Transplant*, 16: 838-847.

Becker, D., Geibler, U., Hempel, U., Bierbaum, S., Scharnweber, D., Worch, H., Wenzel, K.W., 2002. Proliferation and differentiation of rat calvarial osteoblasts on type I collagen-coated titanium alloy. *Journal of Biomedical Materials Research*, 59(3): 516–527.

Berenbaum, F., 2013. Osteoarthritis as an inflammatory disease (osteoarthritis is not osteoarthrosis!). *Osteoarthritis and Cartilage*, 21: 16-21.

Bergsma, E.J., Rozema, F.R., Bos, R.R.M., Debruijn, W.C., 1993. Foreign body reaction to resorbable poly(L-lactic) bone plates and screws used for the fixation of unstable zygomatic fractures. *Journal of Oral Maxillofacial Surgery*, 51: 666–670.

Beshkov, G., Krastev, V., Grigorov, K., Maciel, H., Tang, T-A, Huang, V., 2002. X-Ray photoelectron spectroscopy study of phosphorus silicate glasses. *Surface and Coatings Technology*, 161 (1): 11-19.

Best, S.M., Porter, A.E., Thian, E.S., Huang, J., 2008. Bioceramics: Past, present and for the future. *Journal of European Ceramic Society*, 28 (7): 1319-1327.

Bianco A, Cacciotti I, Lombardi M, Montanaro L., 2009. Si-substituted hydroxyapatite nanopowders: synthesis, thermal stability and sinterability. *Materials Research Bulletin*, 44: 345–54.

Birmingham, E., Niebur, G.L., McHugh, P.E., Shaw, G., Barry, F.P., McNamara, L.M., 2012. Osteogenic differentiation of mesenchymal stem cells is regulated by osteocyte and osteoblast cells in a simplified bone niche. *European Cell and Materials*, 23(353): 13–27.

Bisson, I., Kosinski, M., Ruault, S., Gupta, B., Hilborn, J., Wurm, F. Frey, P., 2002. Acrylic acid grafting and collagen immobilization on poly(ethylene terephthalate) surfaces for adherence and growth of human bladder smooth muscle cells. *Biomaterials*, 23(15): 3149–3158.

Boanini, E., Gazzano, M., Bigi, A., 2010. Ionic substitutions in calcium phosphates synthesized at low temperature. *Acta biomaterialia*, 6(6): 1882–94.

Bohner, M., 2000. Calcium orthophosphates in medicine: from ceramics to calcium phosphate ce- ments. *Injury*, 31(S4): S37–S47.

Bonfield W., 2006. Designing porous scaffold for tissue engineering. *Philosophical Transaction of The Royal Society A*, 364: 227-232.

Botelho, C.M., Lopes, M.A., Gibson, I.R., Best, S.M., Santos, J.D., 2002. Structural analysis of Si-substituted hydroxyapatite: zeta potential and X-ray photoelectron spectroscopy. *Journal of materials science. Materials in medicine*, 13(12): 1123–7.

Botelho, C.M., Brooks, R.A., Spence, G., McFarlane, I., Lopes, M.A., Best, S.M., Santos, J.D., Rushton, N., Bonfield, W., 2006. Differentiation of mononuclear precursors into osteoclasts on the surface of Si-substituted hydroxyapatite. *Journal of Biomedical Material Research Part A* 78A: 709–720. 12.

Botelho, C.M., Brooks, R.A., Best, S.M., Lopes, M.A., Santos, J.D., Rushton, N., Bonfield, W., 2006. Human osteoblasts response to silicon-substituted hydroxyapatite. *Journal of Biomedical Materials Research Part A*, 79(3): 723-730.

Boxall, S. A. & Jones, E., 2012. Markers for characterization of bone marrow multipotential stromal cells. *Stem cells International*, 2012: 1-12.

Boyer, A., Marchat, D., Bernache-Assollant, D., 2013. Synthesis and characterization of Cx-Siy-HA for bone tissue engineering application. *Key Engineering Materials*, 529-530: 100-104.

Bradford, M.M., 1976. A rapid and sensitive method for the quantitation of microgram quantities of protein utilizing the principle of protein-dye binding. *Analytical biochemistry*, 72: 248–254.

- Breuls, R.G.M., Jiya, T.U., Smit, T.H., 2008. Scaffold stiffness influences cell behaviour: opportunities for skeletal tissue engineering. *The Open Orthopaedics Journal*, 2: 103-109.
- Brouwer, P., 2010. Theory of XRF. Getting acquainted with the principle. *PANalytical*, The Netherland.
- Brundle, C.R., Evans, Jr., C.A., Wilson, S., 1992. Encyclopedia of Material Characterization. *Butterworth-Heinemann*, Boston.
- Brunette, D.M., 1988. The effects of implant surface topography on the behavior of cells. *The International Journal of Oral and Maxillofacial Implants*, 3(231): 246-53.
- Brydone, a S., Meek, D., Maclaine, S., 2010. Bone grafting, orthopaedic biomaterials, and the clinical need for bone engineering. *Proceedings of the Institution of Mechanical Engineers, Part H: Journal of Engineering in Medicine*, 224(12): 1329–1343.
- Buckwalter, J.A., Glimcher, M.J., Cooper, R.R., Recker, R., 1995. Bone Biology. *The Journal of Bone and Joint Surgery*, 77: 1256-1275.
- Burg, K.J.L., Porter, S., Kellam, J.F., 2000. Biomaterial developments for bone tissue engineering. *Biomaterials*, 21: 2347-2359.
- Caplan, A.I., 1991. Mesenchymal stem cells. *Journal of Orthopaedic Research*, 9(5): 641-50.
- Caplan, A.I., 1994. Mesenchymal stem cells in bone development, bone repair, and skeletal regeneration therapy. *Journal of Cellular Biochemistry*, 56(3): 283-94.
- Carano, R.A. & Filvaroff, E.H., 2003. Angiogenesis and bone repair. *Drug Discovery Today* 8: 980-989.
- Carlisle, E.M., 1970. Silicon: A possible factor in bone calcification. *Science*, 167: 279–280.
- Carlisle, E.M., 1979. Biochemical and morphological changes associated with long bone abnormalities in Si deficiency. *Journal of Nutrition*, 110: 1046–1055.
- Carmeliet, P. & Conway, E.M., 2001. Growing better blood vessels. *Nature Biotechnology*, 19:1019–1020.
- Cartmell, S., Huynh, K., Lin, A., Nagaraja, S., Guldberg, R., 2004. Quantitative microcomputed tomography analysis of mineralization within three-dimensional scaffolds in vitro. *Journal of biomedical materials research Part A*, 69(1): 97–104.
- Castro-Malaspina, H., Gay, R.E., Resnick, G., Kapoor, N., Meyers, P., Chiarieri, D., McKenzie, S., Broxmeyer, H.E., Moore, M.A.S., 1980. Characterization of human bone marrow fibroblast colony-forming cells (CFU-F) and their progeny. *Blood*, 56: 289–301.
- Chamberlain, G., Fox, J., Ashton, B., Middleton, J., 2007. Concise Review: Mesenchymal Stem Cells: Their Phenotype, Differentiation Capacity, Immunological Features, and Potential for Homing. *Stem Cells*, 25(11): 2739–2749.

- Chen, G., Ushida, T., Tateishi, T., 2001. Development of biodegradable porous scaffolds for tissue engineering. *SPECIAL ISSUE: Containing Papers from the Bionic Design Workshop 2000, Tsukuba, Japan, November 16-17*, 17(1–2): 63–69.
- Chen, G., Ushida, T., Tateishi, T., 2002. Scaffold Design for Tissue Engineering. *Macromolecular Bioscience*, 2: 67-77.
- Chen, R.R., Silva, E.A., Yuen, W.W., Mooney, D.J., 2007. Spatio-temporal VEGF and PDGF Delivery Patterns Blood Vessel Formation and Maturation. *Pharmaceutical Research*, 24(2): 258–264.
- Chen, Y, Mak, A.F.T., Wang, M., Li, J.S., Wong, M.S., 2008. In vitro behavior of osteoblast-like cells on PLLA films with a biomimetic apatite or apatite/collagen composite coating. *Journal of Materials Science: Materials in Medicine*, 19(6): 2261–2268.
- Chen X., Aledia A.S., Ghajar C.M., Griffith C.K., Putnam A.J., Hughes C.C., George, S.C., 2009. Prevascularization of a fibrin-based tissue construct accelerates the formation of functional anastomosis with host vasculature. *Tissue Engineering Part A*, 15: 1363–71.
- Chen, A.K-L., Reuveny, S., Oh, S.K.W., 2013. Application of human mesenchymal and pluripotent stem cell microcarrier cultures in cellular therapy: Achievements and future direction. *Biotechnology Advances*, 31: 1032-1046.
- Chesmel, K.D., Clark, C.C., Brighton, C.T., Black, J., 1995. Cellular response to chemical and morphologic aspects of biomaterial surface. II. The biosynthetic and migratory response of bone cell populations. *Journal of Biomedical Material Research*, 29 (9): 1101-10.
- Chevallay, B. & Herbage, D., 2000. Collagen-based biomaterials as 3D scaffold for cell cultures: applications for tissue engineering and gene therapy. *Medical & biological engineering & computing*, 38(2): 211–218.
- Choi, K.-M., Seo, Y-K., Yoon, H-H., Song, K-Y., Kwon, S-Y., Lee, H-S., Park, J-K., 2008. Effect of ascorbic acid on bone marrow-derived mesenchymal stem cell proliferation and differentiation. *Journal of bioscience and bioengineering*, 105(6): 586–594.
- Chow, D.C., Wenning, L.A., Miller, W.M., Papoutsakis, E.T., 2001. Modeling pO₂ distributions in the bone marrow hematopoietic compartment. II. Modified Kroghian models. *Biophysical Journal*, 81: 685–696.
- Cima, L.G., Vacanti, J.P., Vacanti, C, Ingber, D., Mooney, D., Langer, R., 1991. Tissue engineering by cell transplantation using degradable polymer substrates. *Journal of Biomechanical Engineering*, 113: 143-151.
- Coelho, M.J. & Fernandes, M.H., 2000. Human bone cell cultures in biocompatibility testing. Part II: effect of ascorbic acid, beta-glycerophosphate and dexamethasone on osteoblastic differentiation. *Biomaterials*, 21(11): 1095–1102.

Consolo, F., Bariani, C., Mantalaris, F., Redaelli, A., Morbiducci, U., 2012. Computational modelling for the optimization of a cardiogenic 3D bioprocess of encapsulated embryonic stem cells. *Biomechanics and Modeling Mechanobiology*, 11(1-2): 261-77.

Croisier, F. & Jérôme, C., 2013. Chitosan-based biomaterials for tissue engineering. *European Polymer Journal*, 49(4): 780–792.

Crump, S. S. 1992. Apparatus and method for creating three-dimensional objects. U.S. Patent 5 (121): 329.

Daculsi, G., LeGeros, R.Z., Nery, E., Lynch, K., Kerebel, B., 1989. Transformation of biphasic calcium phosphate ceramics in vivo: ultrastructural and physiochemical characterization. *Journal of Biomedical Materials Research*, 23(8): 883-94.

Dahlin, R.L., Gershovich, J.G., Kurtis Kasper, F., Mikos, A.G., 2014. Flow perfusion co-culture of human mesenchymal stem cells and endothelial cells on biodegradable polymer scaffolds. *Annals of biomedical engineering*, 42(7): 1381–90.

Dana, J.D., 1977. Manual of Mineralogy, 19th edition, *John Wiley & Sons*, United States of America.

Dang, S.M., Kyba, M., Perlingeiro, R., Daley, G.O., Zandstra, P.W., 2002. Efficiency of embryoid body formation and hematopoietic development from embryonic stem cells in different culture systems. *Biotechnology and Bioengineering*, 78(4): 442–453.

Datta, N., Holtorf, H.L., Sikavitas, V.I., Jansen, J.A, Mikos, A.G. 2005. Effect of bone extracellular matrix synthesized in vitro on the osteoblastic differentiation of marrow stromal cells. *Biomaterials*, 26(9): 971–977.

David, M., Guénaële, B., Aline, L., Maria, Z., Luc, M., Stéphanie, S., Nicolas, D., Didier, B-A, Jérôme, C., 2013. Physico-chemical characterization and in vitro biological evaluation of pure SiHA for bone tissue engineering application. *Key Engineering Materials*, 529-530: 351–356.

Dawson, J.I., Wahl, D.A., Lanham, S.A., Kanczler, J.M., Czernuszka, J.T., Oreffo, R.O.C., 2008. Development of specific collagen scaffolds to support the oetogenic and chondrogenic differentiation of human bone marrow stromal cells. *Biomaterials*, 29: 3105-3116.

Decher, G., 1997. Fuzzy Nanoassemblies: Toward Layered Polymeric Multicomposites. *Science*, 277(5330): 1232–1237.

Deegan, A.J., Aydin, H.M., Hu, B., Konduru, S., Kuiper, J.H., Yang, Y., 2014. A facile in vitro model to study rapid mineralization in bone tissues. *Biomedical engineering online*, 13(1): 136.

Deleu J. & Trueta J., 1965. Vascularisation of bone grafts in the anterior chamber of the eye. *Journal of Bone and Joint Surgery*, 47: 319-329.

Detzel, C.J., Larkin, A.L., Rajagopalan, P., 2011. Polyelectrolyte multilayers in tissue engineering. *Tissue engineering. Part B, Reviews*, 17(2): 101–113.

Deligianni, D.D., Katsala, N.D., Koutsoukos, P.G., Missirlis, Y.F., 2001. Effect of surface roughness of hydroxyapatite on human bone marrow cell adhesion, proliferation, differentiation and detachment strength. *Biomaterials*, 22: 87–96.

Dhandayuthapani, B., Yoshida, Y., Maekawa, T., Kumar, D.S., 2011. Polymeric Scaffolds in Tissue Engineering Application: A Review. *International Journal of Polymer Science*, 2011: 1–19.

DiMarino, A.M., Caplan, A.I., Bonfield, T.L., 2013. Mesenchymal Stem Cells in Tissue Repair. *Frontiers in Immunology*, 4(201): 1–9.

Dimitriou, E., Jones, E., McGonagle, D., Giannoudis, P.V., 2011. Bone regeneration: current concepts and future directions. *BioMedical Central Medicine*, 9: 66.

Dominici, M., Le Blanc, K., Mueller, I., Slaper-Cortenbach, I., Krause, D., Deans, R., Keating, A., Prockop, D.J., Horwitz, E., 2006. Minimal criteria for defining multipotent mesenchymal stromal cells. The International Society for Cellular Therapy position statement. *Cytotherapy*, 8(4): 315–7.

Doreau, F., Chaput, C. & Chartier, T., 2000. Stereolithography for manufacturing ceramic parts. *Advanced Engineering Materials*, 2 (8): 493-496.

Dorozhkin, S.V., 2009. Calcium orthophosphates in nature, biology and medicine. *Materials* 2: 399-498.

Driessens, F., Verbeeck, R.M.H., Kiekens, Lc. P., 1983. Mechanism of substitution in carbonated apatites. *Journal of inorganic and General Chemistry*, 504(9): 195-200.

Ducheyne, P. & Qiu, Q., 1999. Bioactive ceramics: the effect of surface reactivity on bone formation and bone cell function. *Biomaterials*, 20: 2287–303.

Duttenhoefer, F., Lara de Freitas, R., Meury, T., Loibl, M., Benneker, L.M., Hermann, M., Richards, R.G., Alini, M., Verrier, S., 2013. 3D scaffolds co-seeded with human endothelial progenitor and mesenchymal stem cells: Evidence of prevascularisation within 7 days. *European Cells and Materials*, 26: 49–65.

Einhorn, T.A., 1998. The cell and molecular biology of fracture healing. *Clinical Orthopaedics Related Research*, 355(Suppl): S7-21.

El-Amin, S.F., Lu, H.H., Khan, Y., Burems, J., Mitchell, J., Tuan, R.S., Laurencin, C.T., 2003. Extracellular matrix production by human osteoblasts cultured on biodegradable polymers applicable for tissue engineering. *Biomaterials*, 24: 1213–1221.

El Haj, A.J., Wood, M.A., Thomas, P., Yang, Y., 2005. Controlling cell biomechanics in orthopaedic tissue engineering and repair. *Pathologie Biologie*, 53: 581-589.

El Haj, A.J. & Cartmell, S.H., 2010. Bioreactors for bone tissue engineering. *Proceedings of the Institution of Mechanical Engineers, Part H: Journal of Engineering in Medicine*, 224(12): 1523–1532.

- Engler, A.J., Sen, S., Sweeney, H.L., Discher, E., 2006. Matrix elasticity directs stem cell lineage specification. *Cell*, 126 (4): 677-689.
- Fairley, N. 2009. Introduction to XPS and AES Casa XPS Manual 2.3.15, *NEXUS*, United Kingdom: 4-7.
- Fatherazi, S., Matsa-Dunn, D., Foster, B.L., Rutherford, R.B., Somerman, M.J., Presland, R.B., 2009. Phosphate regulates osteopontin gene transcription. *Journal of Dental Research*, 88:39–44.
- Fathi, M.H., Hanifi, A., Mortazavi, V., 2008. Preparation and bioactivity evaluation of bone-like hydroxyapatite nanopowder. *Journal of Materials Processing Technology*, 202: 536-542.
- Franceschi, R.T., Iyer, B.S., 1992. Relationship between collagen synthesis and expression of the osteoblast phenotype in MC3T3-E1 cells. *Journal of Bone and Mineral Research*, 7:235–246.
- Freed, L.E. & Vunjak-Novakovic, G., 1998. Culture of organized cell communities. *Advances Drug Delivery Reviews*, 33: 15-30.
- Freed, L.E. & Vunjak-Novakovic, G. Tissue Engineering Bioreactors. In: Lanza, R.P., Langer, R., and Vacanti, J., eds. *Principles of Tissue Engineering*. San Diego, CA: Academic Press: 143-156.
- Friedenstein, A.J., Petrakova, K.V., Kurolesova, Al, Frolova, G.P., 1968. Heterotopic of bone marrow. Analysis of precursor cells for osteogenic and hematopoietic tissues. *Transplantation*, 6(2): 230-47.
- Friedenstein, A.J., Gorskaja, J.F., Kulagina, N.N., 1976. Fibroblast precursors in normal and irradiated mouse hematopoietic organs. *Experimental Hematology*, 4: 267–274.
- Friederichs, R.J., Brooks, R.A., Ueda, M., Best, S.M., 2015. *In vitro* osteoclast formation and resorption of silicon-substituted hydroxyapatite ceramics. *Journal of biomedical materials research*. Part A, 103(10): 3312–22.
- Frost, H.M., 1994. Wolff's Law and Bone's Structural Adaptations to mechanical usage: an overview for clinicians. *The Angle Orthodontist*, 64 (3): 175-188.
- Foster, B.L., Nociti, F.H. Jr., Swanson, E.C., Matsa-Dunn, D., Berry, J.E., Cupp, C.J., Zhang, P., Somerman, M.J., 2006. Regulation of cementoblast gene expression by inorganic phosphate in vitro. *Calcified Tissue International*, 78:103–112.
- Gabriel Chu, T.M., Orton, D.G., Hollister, S.J., Feinburg, S.E., Halloran, J.W. 2002. Mechanical and in vivo performance of hydroxyapatite implants with controlled architectures. *Biomaterials*, 23: 1283–93.

- Galban, C.J. & Locke, B.R., 1999. Effects of spatial variation of cells, nutrient and product concentrations coupled with product inhibition on cell growth in a polymer scaffold. *Biotechnology Bioengineering*, 64: 633–43.
- Gao, H., Ayyaswamy, P., Ducheyne, P., 1997. Dynamics of a microcarrier particle in the simulated microgravity environment of a rotating wall vessel. *Microgravity Science and Technology*, 10(3): 154-65.
- Gariboldi, M.I. & Best, S.M., 2015. Effect of Ceramic Scaffold Architectural Parameters on Biological Response. *Frontiers in Bioengineering and Biotechnology*, 3(10): 1–11.
- Gaur, T., Lengner, C.J., Hovhannisyan, H., Bhat, R.A., Bodine, P.V., Komm, B.S., Javed, A., van Wijnen, A.J., Stein, J.L., Stein, G.S., Lian, J.B., 2005. Canonical WNT signaling promotes osteogenesis by directly stimulating Runx2 gene expression. *Journal of Biological Chemistry*, 280 (39): 33132-33140.
- Gerber, H.P. & Ferrara, N., 2000. Angiogenesis and bone growth. *Trends Cardiovascular Medicine*, 10: 223-228.
- Gershovich, J.G., Dahlin, R.L., Kurtis Kasper, F., Mikos, A.G., 2013. Enhanced Osteogenesis in Cocultures with Human Mesenchymal Stem Cells and Endothelial Cells on Polymeric Microfiber Scaffolds. *Tissue Engineering Part A*, 19(23-24): 2565–2576.
- Giannoudis, P.V., Dinopoulos, H., Tsiridis, E. 2005. Bone substitutes: an update. *Injury*, 36 (Suppl 3): S20-27.
- Giannoudis, P.V., Einhorn, T.A., Schmidmaier, G., Marsh, D., 2008. The diamond concept-open question. *International Journal of The Care of The Injured*, 39S2: S5-S8.
- Giannoudis, P.V. & Einhorn, T.A., 2009. Bone morphogenetic proteins in musculoskeletal medicine. *Injury*, 40(Suppl 3): S1-3.
- Gibson, I.R., Best, S.M., Bonfield, W., 1999. Chemical characterization of silicon-substituted hydroxyapatite. *Journal of Biomedical Materials Research*, 44: 422-428.
- Gibson, I.R. & Bonfield, W., 2002. Novel synthesis and characterization of an AB-type carbonate-substituted hydroxyapatite. *Journal of Biomedical Materials Research*, 59(4): 697–708.
- Gibson I.R., Best S.M., Bonfield W., 2002. Effect of silicon substitution on the sintering and microstructure of hydroxyapatite. *Journal of the American Ceramic Society*, 85: 2771–7.
- Gleeson, J.P., Plunkett, N.A., O’ Brien, F.J., 2010. Addition of Hydroxyapatite improve stiffness, interconnectivity and osteogenic potential of a highly porous collagen-based scaffold for Bone Tissue Regeneration. *European Cells and Materials*, 20: 218-230.

Goldstein, A.S., Juarez, T.M., Helmke, C.D., Gustin, M.C., Mikos, A.G., 2001. Effect of convection on osteoblastic cell growth and function in biodegradable polymer foam scaffolds. *Biomaterials*, 22(11): 1279-88.

Gomes, M.E., 2004. Biodegradable polymers and composites in biomedical applications: from catgut to tissue engineering Part 2 Systems for temporary replacement and advanced tissue regeneration. *International Materials Reviews*, 49: 274-285.

Gómez-Barrena, E., Rosset, P., Lozano, D., Stanovici, J., Ermthaller, C., Gerbhard, F., 2015. Bone fracture healing: Cell therapy in delayed unions and nonunions. *Bone*, 70: 93–101.

Glowacki, J., Mizuno, S., Greenberger, J.S., 1998. Perfusion Enhances Functions of Bone Marrow Stromal Cells in Three-Dimensional Culture. *Cell Transplant*, 7, 319-326.

Granet, C., Laroche, N., Vico, L., Alexandre, C., Lafage-Proust, M.H., 1998. Rotating-wall vessels, promising bioreactors for osteoblastic cell culture: Comparison with other 3D conditions. *Medical and Biological Engineering and Computing*, 36: 513–519.

Grant, D.S., Kleiman, H.K., Leblong, C.P., Inoue, S., Chung, A.E., Martin, G.R., 1985. The basement-membrane-like matrix of the mouse EHS tumor. Immunochemical quantification of six of its components. *Journal of Anatomy*, 174(4): 387-398.

Grellier, M., Bordenave, L., & Amédée, J., 2009. Cell-to-cell communication between osteogenic and endothelial lineages: implications for tissue engineering. *Trends in Biotechnology*, 27(10), 562–71.

Green, S.A., Jackson, J.M., Wall, D.M., Marinow, H., Ishkanian, J. 1992. Management of segmental defects by the Ilizarov intercalary bone transport method. *Clinical Orthopaedics Related Research*, 280:136-142.

Gross, K. A, Berndt, C.C., Iacono, V.J., 1998. Variability of hydroxyapatite-coated dental implants. *The International journal of oral & maxillofacial implants*, 13(5): 601–610.

Gross, B.C., Erkal, J.L., Lockwood, S.Y., Chen, C., Spence, D.M., 2014. Evaluation of 3D printing and its potential impact on biotechnology and the chemical sciences. *Analytical Chemistry*, 86(7): 3240-3253.

Habibovic, P., Juhl, M.V., Clyens, S., Martinetti, R., Dolcini, L., Theilgaard, N., van Blitterswijk, C.A., 2010. Comparison of two carbonated apatite ceramics in vivo. *Acta biomaterialia*, 6(6): 2219–26.

Hamidouche, Z., Hay, E., Vaudin, P., Charbord, P., Schule, R., Marie, P.J., Fromiguet, O., 2008. FHL2 mediates dexamethasone-induced mesenchymal cell differentiation into osteoblasts by activating Wnt/beta-catenin signaling-dependent Runx2 expression. *Faseb Journal*, 22:3813–3822.

Hammond, P.T., 2011. Engineering materials layer-by-layer: Challenges and opportunities in multilayer assembly. *AIChE Journal*, 57: 2928–2940.

- Hannink, G. & Chris, Arts, J.J., 2011. Bioresorbability, porosity, and mechanical strength of bone substitutes: what is optimal for bone regeneration. *Injury*, 42: S22-S25.
- Harrison, J.S., Rameshwar, P., Chang, V., Bandari, P., 2002. Oxygen saturation in the bone marrow of healthy volunteers. *Blood*, 99: 394.
- Hasegawa, T., Miwa, M., Sakai, Y., Niikura, T., Lee, S. Y., Oe, K., Iwakura, T., Kurosaka, M., Komori, T., 2010. Efficient Cell-seeding into Scaffolds Improves Bone Formation. *Journal of Dental Research*, 89(8), 854–859.
- He, W., Gonsalves, K.E., Batina, N., Poker, D.B., Alexander, E., Hudson, M., 2003. Micro/nanomachining of polymer surface for promoting osteoblast cell adhesion. *Biomedical Microdevices*, 5: 101-108.
- He, Q.J., Huang, Z.L., Cheng, X.K., Yu, J., 2007. Thermal stability of porous A- type carbonated hydroxyapatite spheres. *Materials Letters*, 62: 539-542.
- Healy, K.E., 1998. Dentin and enamel. In: Black J, Hastings G, editors. *Handbook of Biomaterials Properties*. London: Chapman & Hall: 24–39.
- Heath, C.A., 2000. Cell for tissue engineering. *Trends in Biotechnology*, 18: 17-19.
- Hench, L.L., Polak, J.M., 2002. Third-generation biomedical materials. *Science*, 295 (5557): 1014-7.
- Henstock, J.R., Rotherham, M., Rose, J.B. El Haj, A.J., 2013. Cyclic hydrostatic pressure stimulates enhanced bone development in the foetal chick femur in vitro. *Bone*, 53(2): 468–77.
- Higuchi, A., Kurihara, M., Kobayashi, K., Cho, C.S., Akaike, T., Hara, M., 2005. Albumin and urea production by hepatocytes cultured on extracellular matrix proteins-conjugated poly (vinyl alcohol) membranes. *Journal of Biomaterial Science Polymer Edition*, 16(7): 847-860.
- Higuchi, A., Ling, Q.D., Hsu, S.T., Umezawa, M., 2012. Biomimetic Cell Culture Proteins as Extracellular Matrices for Stem Cell Differentiation. *Chemical Review*, 8: 4507-4540.
- Hill, P.A. & Orth, M., 1998. Bone Remodelling. *British Journal of Orthodontics*, 25: 101-107.
- Hillsley, M.V. & Frangos, J.A., 1994. Review: Bone Tissue Engineering: The Role of Interstitial Fluid Flow. *Biotechnology and Bioengineering*, 3: 573-581.
- Hing, K.A., 2004. Bone repair in the twenty-first century: biology, chemistry or engineering? *Philosophical Transactions Series A, Mathematical Physical and Engineering Sciences*, 362(1825): 2821–2850.
- Hing, K.A., 2005. Bioceramic bone graft substitutes: influence of porosity and chemistry. *International Journal of Applied Ceramic Technology*, 2: 184-199.

Hing, K.A., Revell, P.A., Smith, N., Buckland, T., 2006. Effect of silicon level on rate, quality and progression of bone healing within silicate-substituted porous hydroxyapatite scaffolds. *Biomaterials*, 27: 5014–26.

Hollister, S.J., Maddox, R.D., Taboas, J.M., 2002. Optimal design and fabrication of scaffolds to mimic tissue properties and satisfy biological constraints. *Biomaterials*, 23: 4095–103.

Hollister, S.J., 2005. Porous scaffold design for tissue engineering. *Nature materials*, 4(7): 518–24.

Hollinger, J. O., Winn, S., and Bonadio, J. 2000. Options for tissue engineering to address challenges of the ageing skeleton. *Tissue Engineering*, 6(4): 341–350.

Holy, C.E., Shoichet, M.S., Davies, J.E., 2000. Engineering three-dimensional bone tissue in vitro using biodegradable scaffolds: Investigating initial cell-seeding density and culture period. *Journal of Biomedical Materials Research*, 51(3): 376–382.

Horwitz, E.M., Prockop, D.J., Fitzpatrick, L.A., Koo, W.W., Gordon, P.L., Neel, M., Sussman, M., Orchard, P., Marx, J.C., Pyeritz, R.E., Brenner, M.K., 1999. Transplantability and therapeutic effects of bone marrow-derived mesenchymal cells in children with osteogenesis imperfecta. *Nature Medicine*, 5:309-313.

Horwitz, E.M., Gordon, P.L., Koo, W.K.K., Marx, J.C., Neel, M.D, McNall, R.Y., Muul, L., Hofmann, T., 2002. Isolated allogeneic bone marrow-derived mesenchymal cells engraft and stimulate growth in children with osteogenesis imperfecta: Implications for cell therapy of bone. *Proceedings of the National Academy of Sciences of the United States of America*, 99(13): 8932–7.

Hoskins, C., Cuschieri, A., Wang, L., 2012. The cytotoxicity of polycationic iron oxide nanoparticles: Common endpoint assays and alternative approaches for improved understanding of cellular response mechanism. *Journal of Nanobiotechnology*, 10(1): 15.

Hou, X. & Jones, B.T., 2000. Inductively Coupled Plasma–Optical Emission Spectrometry. *Spectroscopy Letters*, 42(1): 58–61.

Huang, R., Li Y., Zhou, X., Zhang, Q., Jin, H., Zhao, J., Pan, S., Deng, H., 2012. LBL fabricated biopolymer-layered silicate based nanofibrous mats and their cell compatibility studies. *Carbohydrate Polymers*, 90: 957–966.

Hull, C., 1990. Method for production of three-dimensional objects by stereolithography. US Patent 4929402.

Hutmacher, D.W., 2000. Scaffolds in tissue engineering bone and cartilage. *Biomaterials*, 21(24): 2529–2543.

Hutmacher D.W., Schantz J.T., Zein I., Ng K.W., Teoh S.H., Tan K.C., 2001. Mechanical properties and cell cultural response of polycaprolactone scaffolds designed and fabricated via fused deposition modelling. *Journal of Biomedical Material Research*, 55:203.

Hutmacher, D.W., Sittinger, M. & Risbud, M. V, 2004. Scaffold-based tissue engineering: rationale for computer-aided design and solid free-form fabrication systems. *Trends in biotechnology*, 22(7): 354–62.

Hutmacher, D.W. & Cool, S., 2007. Concepts of scaffold-based tissue engineering--the rationale to use solid free-form fabrication techniques. *Journal of cellular and molecular medicine*, 11(4): 654–69.

Ibrahim, D., Mostafa, A.A, Korowash, S., 2011. Chemical characterization of some substituted hydroxyapatites. *Chemistry Central Journal*, 5(1), 74.

International Organization for Standardization. ISO 10993-5, 2009. International Standard, Biological evaluation of medical devices-Tests for in vitro cytotoxicity.

Ivanova, T.I., Kamenetskaya, F., Kol'tsov, A.B., Ugolkov, V.L., 2001. Crystal Structure of Calcium-Deficient Carbonated Hydroxyapatite. Thermal Decomposition. *Journal of Solid State Chemistry*, 160(2): 340–349.

Jabbarzadeh, E., Starnes, T., Khan, Y.M., Jiang, T., Wirtel, A.J., Deng, M., Qing, L.V., Nair, L.S., Doty, S.B., Laurencin, C.T., 2008. Induction of angiogenesis in tissue-engineered scaffolds designed for bone repair: a combined gene therapy-cell transplantation approach. *Proceedings of the National Academy of Sciences of the U S A*, 105: 11099–104.

Jahno, V.D., Ribeiro, G.B.M., dos Santos, L.A., Ligabue, R., Einloft ,S., Ferreira, M.R.W., Bombonato-Prado, K.F., 2007. Chemical synthesis and in vitro biocom- patibility tests of poly (L-lactic acid). *Journal of Biomedical Materials Research Part A*, 83: 209–215.

Jain, R.K., 2003. Molecular regulation of vessel maturation. *Nature Medicine*, 9:685–93.

Jayakumar, P. & Di Silvio, L., 2010. Osteoblasts in bone tissue engineering. *Proceeding of the Institution of Mechanical Engineers, Part H*, 224(12): 1415–1440.

Jilka, R.L, Weinstein, R.S., Takahashi, K., Parfitt, A.M., Manolagas, S.C., 1996. Linkage of decreased bone mass with impaired osteoblastogenesis in a murine model of accelerated senescence. *Journal of Clinical Investigation*, 97(7): 1732–1740.

Jin, Q.M., Takita, H., Kohgo, T., Atsumi, K., Itoh, H., Kuboki, Y., 2000. Effects of geometry of hydroxyapatite as a cell substratum in BMP-induced ectopic bone formation. *Journal of Biomedical Materials Research*, 51: 491-499.

Jung, S., Panchalingan, K.M., Rosenberg, L., Behie, L.A., 2012. Ex vivo expansion of human mesenchymal stem cells in defined serum-free media. *Stem Cell International*, 2012: 1-21.

Jukes, J.M., van Blitterswijk, C.A., de Boer, J., 2010. Skeletal tissue engineering using embryonic stem cells. *Journal of Tissue Engineering Regenerative Medicine*, 4(3): 165–180.

Johnson, E.O., Troupis, T., Soucacos, P.N., 2011. Tissue engineered vascularized bone grafts: Basic science and clinical relevance to trauma and reconstructive microsurgery. *Microsurgery*, 31, 176-182.

Jones, J.R., 2006. Observing cell response to biomaterials. *Materials Today*, 9(12): 34-43.

Jones, G.L., Walton, R., Czernuszka, J., Griffiths, S., El Haj, A.J., Cartmell, S.H., 2010. Primary human osteoblast culture on 3D porous collagen-hydroxyapatite scaffolds. *Journal of biomedical materials research. Part A*, 94(4): 1244-50.

Kaiser, L.R., 1992. The future of multihospital systems. *Top Health Care Financial*, 18 (4): 32-45.

Kaigler, D., Krebsbach, P.H., West, E.R., Horger, K., Huang, Y.C., and Mooney, D.J., 2005. Endothelial cell modulation of bone marrow stromal cell osteogenic potential. *FASEB Journal*, 19: 665.

Kaigler, D., Pagni, G., Park, C-H., Tarle, S.A., Bartel, R.L., Giannobile, V.G., 2010. Angiogenic and Osteogenic Potential of Bone Repair Cells for Craniofacial Regeneration. *Tissue Engineering Part A*, 16(9): 2809-2820.

Kanczler, J.M. & Oreffo, R.O.C., 2008. Osteogenesis and angiogenesis: The potential for engineering bone. *European Cells and Materials*, 15: 100-114.

Karageorgiou, V. & Kaplan, D., 2005. Porosity of 3D biomaterial scaffolds and osteogenesis. *Biomaterials*, 26: 5474-5491.

Khademhosseini, A., Suh, K.Y., Yang, J.M., Eng, G., Yeh, J., Levenberg, S., Langer, R., 2004. Layer-by-layer deposition of hyaluronic acid and poly-l-lysine for patterned cell co-cultures. *Biomaterials*, 25(17): 3583-3592.

Kee, C.C., Ismail, H., Mohd Noor, A.F., 2013. Effect of synthesis technique and carbonate content on the crystallinity and morphology of carbonated hydroxyapatite. *Journal of Materials Science & Technology*, 29 (8): 761-764.

Kim, B.S. & Mooney, D.J., 1998. Engineering smooth muscle tissue with a predefined structure. *Journal of Biomedical Materials Research*, 41: 322-332.

Kim, S.S., Utsunomiya, H., Koski, J.A., Wu, B.M., Cima, M.J., Sohn, J., Mukai, K., Griffith, L.G., Vacanti, J.P., 1998. Survival and Function of Hepatocytes on a Novel Three-Dimensional Synthetic Biodegradable Polymer Scaffold With an Intrinsic Network of Channels. *Annals of Surgery*, 228(1): 8-13.

Kim, B. Y. & Bruening, M. L., 2003. pH-dependent growth and morphology of multilayer dendrimer/poly(acrylic acid) films. *Langmuir*, 19: 94-99.

Kim, S.R., Lee, J.H., Kim, Y.T., Riu, D.H., Jung, S.J., Lee, Y.J., Chung, S.C., Kim, Y.H., 2003. Synthesis of Si, Mg substituted hydroxyapatites and their sintering behaviors. *Biomaterials*, 24(8): 1389-98.

- Kim, H-W., Kim, H-E., Salih, V., 2005. Stimulation of osteoblast responses to biomimetic nanocomposites of gelatin-hydroxyapatite for tissue engineering scaffolds. *Biomaterials*, 26: 5221–5230.
- Kim, S-S., Park, M.S., Jeon, O., Choi, C.Y., Kim, B.S., 2006. Poly(lactide-co-glycolide)/hydroxyapatite composite scaffolds for bone tissue engineering. *Scanning*, 27: 1399–1409.
- Kim, T.G., Park, S.H., Chung, H.J., Yang, D.Y., Park, T.G., 2010. Microstructured scaffold coated with hydroxyapatite/collagen nanocomposite multilayer for enhanced osteogenic induction of human mesenchymal stem cells. *Journal of Materials Chemistry*, 20 (40): 8927-8933.
- Kim, N. & Cho, S-G., 2013. Clinical applications of mesenchymal stem cells. *The Korean Journal of Internal Medicine*, 28 (4): 387-402.
- Kini, U. & Nandeesh, B.N., 2012. Physiology of bone formation, remodelling, and metabolism. *Radionuclide and Hybrid Bone Imaging*, 2: 29-57.
- Kirkpatrick, C.J., Bittinger, F., Wagner, M., Köhler, H., van Kooten, T.G., Klein, C.L., Otto, M., 1998. Current trends in biocompatibility testing. *Proceedings of the Institution of Mechanical Engineers Part H*, 212(2): 75-84.
- Klein, C.P.A.T., Driessen, K., De Groot, K., Van der Hooff, A., 1983. Biodegradation behaviour of various calcium phosphate materials in bone tissue. *Journal of Biomedical Materials Research, Part A*, 17(5): 769-784.
- Knothe Tate, M.L., Adamson, J.R., Tami, A.E., Bauer, T.W., 2004. The osteocyte. *The International Journal of Biochemistry & Cell Biology*, 36 (1): 1-8.
- Koutsopoulos, S., 2002. Synthesis and characterization of hydroxyapatite crystals: A review study on the analytical methods. *Journal of Biomedical Materials Research*, 62(4): 600-612.
- Kovaleva, E.S., Shabanov, M.P., Putlayev, V.I., Filippov, Ya. Yu., Tretyakov, Y.D., Ivanov, V.K., 2008. Carbonated hydroxyapatite nanopowders for preparation of bioresorbable materials. *Materials Science & Engineering Technology*, 39, 822-829.
- Krajewski, A., Mazzocchi, M., Buldini, P.L., Ravaglioli, A., Tinti, A., Taddei, P., Fagnano, C., 2005. Synthesis of carbonated hydroxyapatites: efficiency of the substitution and critical evaluation of analytical methods. *Journal of Molecular Structure*, 744-747: 221-228.
- Kretlow, J.D. & Mikos, A.G., 2007. Review: mineralization of synthetic polymer scaffolds for bone tissue engineering. *Tissue Engineering*, 13 (5): 927-38.
- Lafon, J.P., Champion, E., Bernache-Assollant, D., 2008. Processing of AB-type carbonated hydroxyapatite $\text{Ca}_{10-x}(\text{PO}_4)_6-x(\text{CO}_3)_x(\text{OH})_{2-x-2y}(\text{CO}_3)_y$ ceramics with controlled composition. *Journal of the European Ceramic Society*, 28(1): 139–147.

- Lai, L.P. and Mitchell, J., 2005. Indian Hedgehog: Its roles and regulation in endochondral bone development. *Journal of Cellular Biochemistry*, 96 (6): 1163-1173.
- Lam, C.X.F., Mo, X.M., Teoh, S.H., Hutmacher, D.W., 2002. Scaffold development using 3D Printing with a starch-based polymer. *Materials Science and Engineering, C* 20: 49-56.
- Landers, R. & Mulhaupt, R., 2000. Desktop manufacturing of complex objects, prototypes and biomedical scaffolds by means of computer-assisted design combined with computer-guided 3D plotting of polymers and reactive oligomers. *Macromolecular Material Engineering*, 282: 17-21.
- Landers, R., Pfister, A., Hubner, U., John, H., Schmelzeisen, R., Mulhaupt, R., 2002. Fabrication of soft tissue engineering scaffolds by means of rapid prototyping techniques. *Journal of Materials Science*, 37: 3107-3116.
- Landi, E., Celotti, G., Logroscino, G., Tampieri, A., 2003. Carbonated hydroxyapatite as bone substitute. *Journal of the European Ceramic Society*, 23(15): 2931–2937.
- Landi, E., Tampieri, A., Celotti, G., Vichi, L., Sandri, M., 2004. Influence of synthesis and sintering parameters on the characteristics of carbonate apatite. *Biomaterials*, 25: 1763-1770.
- Landi, E., Jacopo, U., Sprio, S., Tampieri, A., Guizzardi, S., 2010. Human osteoblast behavior on as-synthesized SiO(4) and B-CO(3) co-substituted apatite. *Journal of Biomedical Materials Research. Part A*, 94(1): 59–70.
- Langer, R. & Vacanti, J.P., 1993. Tissue Engineering. *Science*, 260: 920-926.
- Langenbach, F. & Handschel, J., 2013. Effects of dexamethasone, ascorbic acid and β -glycerophosphate on the osteogenic differentiation of stem cells in vitro. *Stem cell research & therapy*, 4(5): 117.
- Lanza, R.P., Langer, R. & Vacanti, J., 2000. Principle of Tissue Engineering, Second ed., *Academic Press*, New York: 3-9.
- Laranjeira, M.S., Fernandes, M.H., Monteiro, F.J., 2010. Innovative macroporous granules of nanostructured-hydroxyapatite agglomerates: bioactivity and osteoblast-like cell behaviour. *Journal of Biomedical Materials Research Part A*, 95(3): 891-900.
- Laschke, M.W., Mussawy, H., Schuler, S., Eglin, D., Alini, M., Menger, M.D., 2010. Promoting external inosculation of prevascularised tissue constructs by pre-cultivation in an angiogenic extracellular matrix. *European Cell and Materials*, 20: 356–66.
- Lawrenson, K., Benjamin, E., Turmaine, M., Jacobs, I., Gayther, S., Dafou, D., 2009. In vitro three-dimensional modelling of human ovarian surface epithelial cells. *Cell Proliferation*, 42(3): 385-93.

- Le Blanc, K., Götherström, C., Ringdén, O., Hassan, M., McMahon, R., Horwitz, E., Anneren, G., Axelsson, O., Nunn, J., Ewald, U., Nordén Lindeberg, S., Janson, M., Dalton, A., Aström, E., Westgren, M., 2005. Fetal mesenchymal stem-cell engraftment in bone after in utero transplantation in a patient with severe osteogenesis imperfecta. *Transplantation*, 79:1607-1614.
- Lee, E.J. & Niklason, L.E., 2010. A novel flow bioreactor for in vitro microvascularization. *Tissue Engineering Part C Methods*, 16: 1191–1200.
- Lee, M., Dunn, J.C.Y., Wu, B.M., 2005. Scaffold fabrication by indirect three-dimensional printing. *Biomaterials*, 26(20): 4281–9.
- Lee, Y., Hahm, Y.M., Matsuya, S., Nakagawa, M., Ishikawa, K., 2007. Characterization of macroporous carbonate-substituted hydroxyapatite bodies prepared in different phosphate solutions. *Journal of Materials Science*, 42(18): 7843–7849.
- LeGeros, R.Z., Trautz, O.R., Klein, E., LeGeros, J.P., 1969. Two types of carbonate substitution in the apatite structure. *Experientia*, 25(1955): 5–7.
- LeGeros, R.Z., 1991. Calcium phosphate in oral biology and medicine. *Monographs in Oral Science*, 15: 1-21.
- LeGeros, R.Z., Daculsi, P., LeGeros, J.P., 2006. Bioactive Bioceramic In: Pietzak, W.S. Orthopedics Biology and Medicine: Musculoskeletal Tissue Regeneration, Biological Materials and Methods. *Humana Press*, New Jersey: 17.
- Leite, F.L., Mattoso, L.H.C., Oliveira Jr, O.N., Herrmann Jr, P.S.P., 2007. The Atomic Force Spectroscopy as a Tool to Investigate Surface Forces: Basic Principles and Applications. *Modern Research and Educational Topics in Microscopy*, 22–24.
- Lemaire, V., Tobin, F.L., Greller, L.D., Cho, C.R., Suva, L.J., 2004. Modeling the interactions between osteoblast and osteoclast activities in bone remodeling. *Journal of Theoretical Biology*, 229(3): 293–309.
- Leong, K.F., Cheah, C.M., Chua, C.K., 2003. Solid free form fabrication of three dimensional scaffold for engineering replacement tissues and organs. *Biomaterials*, 24: 3262-3278.
- Leukers, B., Gülkan, H., Irsen, S.H., Milz, S., Tille, C., Schieker, M., Seitz, H., 2005. Hydroxyapatite scaffolds for bone tissue engineering made by 3D printing. *Journal of Materials Science: Materials in Medicine*, 16(12): 1121–1124.
- Li, J., Liu, Y., Hermansson, L., Söremark., R., 1993. Evaluation of Biocompatibility of Various Ceramic Powders with Human Fibroblasts *in vivo*. *Clinical Materials*, 12: 197-201.
- Li, W.J., Jiang, Y.J., Tuan, R.S., 2008. Cell-nanofiber-based cartilage tissue engineering using improved cell seeding, growth factor, and bioreactor technologies. *Tissue Engineering Part A*, 14(5): 69-48.

- Li, J., Yuan, X., He, F., Mak, A.F.T., 2008. Hybrid Coating of Hydroxyapatite and Collagen Within (D, L-lactic-co-glycolic acid) Scaffold. *Journal of Biomedical Materials Research - Part B Applied Biomaterials*, 86 (2): 381-388.
- Li, J., Chen, Y., Maka, A., Tuan, R.S., Li, L., Li, Y., 2010. A one-step method to fabricate PLLA scaffolds with deposition of bioactive hydroxyapatite and collagen using ice-based microporogens. *Acta Biomaterialia*, 6: 2013-2019.
- Li, L., Crosby, K., Sawicki, M., Shaw, L.L., Wang, Y., 2012. Effects of surface roughness of hydroxyapatite on cell attachment and proliferation. *Journal of Biotechnology & Biomaterials*, 2(6): 1-5.
- Liao, S.S., Cui, F.Z., Zhang, W., Feng, L., 2005. Hierarchically biomimetic bone scaffold materials: Nano-HA/collagen/PLA composite. *Journal of Biomedical Material Research Part B Applied Biomaterials* 69: 158-65.
- Lian, J.B. & Stein, G.S., 1995. Development of the osteoblast phenotype: molecular mechanisms mediating osteoblast growth and differentiation. *The Iowa orthopaedic Journal*, 15: 118-40.
- Lin, A.S.P., Barrows, T.H., Cartmell, S.H., Guldberg, R.E., 2003. Microarchitectural and mechanical characterization of orientated porous polymer scaffolds. *Biomaterials*, 24: 481-9.
- Lin, W., Huang, Y.W., Zhou, X.D., Ma, Y., 2006. *In vitro* toxicity of silica nanoparticles in human lung cancer cells. *Toxicology and Applied Pharmacology*, 217: 252-259.
- Lincks, J., Boyan, B.D., Blanchard, C.R., Lohmann, C.H., Liu, Y., Cochran, D.L., Dean, D.D., Schwartz, Z., 1998. Response of MG63 osteoblast-like cells to titanium and titanium alloy is dependent on surface roughness and composition. *Biomaterials*, 19: 2219-2232.
- Liu, C.Z., Xia, Z.D., Han, Z.W., Hulley, P.A., Triffitt, J.T., Czernuszka, J.T., 2007. Novel 3D collagen scaffolds fabricated by indirect printing technique for tissue engineering. *Journal of Biomedical Materials Research Part B: Applied Biomaterials*, 85 (2): 519-28.
- Liu, C., Xia, Z., Czernuszka, J.T., 2007. Design and Development of Three-Dimensional Scaffolds for Tissue Engineering. *Chemical Engineering Research and Design*, 85(7): 1051-1064.
- Liu, Z-M., Lee, S-Y., Sarun, S., Moeller, S., Schnabelrauch, M., Groth, T., 2010. Biocompatibility of poly (L-lactide) films modified with poly(ethylene imine) and polyelectrolyte multilayers. *Journal of Biomaterials Science Polymer Edition*, 21: 893-912.
- Lo, H., Ponticciello, M.S., Leong, K.W., 1995. Fabrication of controlled release biodegradable foams by phase separation. *Tissue Engineering*, 1: 15-28.
- Loeser, R.F., Goldring, S.R., Scanzello, C.R., Goldring, M.B., 2012. Osteoarthritis. *Arthritis & Rheumatism*, 64 (6): 1697-1707.

Lord, C.F., Gebhardt, M.C., Tomford, W.W., Mankin, H.J., 1988. Infection in bone allografts. Incidence, nature and treatment. *The Journal of Bone & Joint Surgery*, 70 (3): 369-376.

Lowman, G.M. & Buratto, S.K., 2002. Nanoscale morphology of polyelectrolyte self-assembled films probed by scanning force and near-field scanning optical microscopy. *Thin Solid Films*, 405: 135–140.

Ma, P.X. & Zhang, R., 2001. Microtubular architecture of biodegradable polymer scaffolds. *Journal of Biomedical Materials Research*, 56: 469–77.

Ma, Z., Gao, C., Gong, Y., Shen, J., 2005. Cartilage tissue engineering PLLA scaffolds with surface immobilized collagen and basic fibroblast growth factor. *Biomaterials*, 26: 1253-1259.

Ma, J., Jeroen J. J. P., van den Beucken, Yang, F., Both, S. K., Cui, F., Pan, J., Jansen, J. A., 2011. Coculture of osteoblasts and endothelial cells: optimization of culture medium and cell ratio. *Tissue Engineering Part C Methods*, 17(3): 349–357.

Mackie, E.J., 2003. Osteoblasts: novel roles in orchestration of skeletal architecture. *The International Journal of Biochemistry and Cell Biology*, 35: 1301-1305.

Macdonald, A.G. & Fraser, P.J., 1999. The transduction of very small hydrostatic pressures. *Comparative Biochemistry and Physiology Part A: Molecular & Integrative Physiology*, 122 (1): 13-36.

Madri, J.A., Pratt, B.M., Tucker, A.M., 1988. Phenotypic modulation of endothelial cells by transforming growth factor- β depends upon the composition and organization of the extracellular matrix. *Journal of Cell Biology*, 106: 1375-1384.

Maes, C., Carmeliet, P., Moermans, K., Stockmans, I., Smets, N., Collen, D., Bouillon, R., Carmeliet, G., 2002. Impaired angiogenesis and endochondral bone formation in mice lacking the vascular endothelial growth factor isoforms VEGF164 and VEGF188. *Mechanisms of Development*, 111: 61-73.

Manolagas, S.C., 2000. Birth and death of bone cells: basic regulatory mechanisms and implications for the pathogenesis and treatment of osteoporosis. *Endocrine Reviews*, 21(2): 115-137.

Marchat, D., Zymelka, M., Coelho, C., Gremillard, L., Joly-pottuz, L., Babonneau, F., esnouf, C., Chevalier, J., Bernache-assolant, D., 2013. Accurate characterization of pure silicon-substituted hydroxyapatite powders synthesized by a new precipitation route. *Acta Biomaterialia*, 9: 6992-7004.

Marks, S.C., Hermey, D.C., 1996. The Structure and Development of Bone. In: Principles of Bone Biology. Bilezikian, J.P., Raisz, L.G., Rodan, G.A. (eds). *Academic Press*, SanDiego, 3-24.

Martin, C., Winet, H., Bao, J.Y., 1996. Acidity near eroding polylactide- polyglycolide in vitro and in vivo in rabbit tibial bone chambers. *Biomaterials*, 17(24): 2373–80.

Martin, I., Wendt, D., Heberer, M., 2004. The role of bioreactors in tissue engineering. *Trends in biotechnology*, 22(2): 80–6.

Masi, L., Franchi, A., Santucchi, M., Danielli, D., Arganini, L., Giannone, V., Formigli, L., Benvenuti, S., Tanini, A., Beghe, F., Mian, M., Brandi, L., 1992. Adhesion, growth and matrix production by osteoblasts on collagen substrata. *Calcified Tissue International*, 51: 202-212.

Mastrogiacomo, M., Scaglione, S., Martinetti, R., Dolcini, L., Beltrame, F., Cancedda, R., Quarto, R., 2006. Role of scaffold internal structure on in vivo bone formation in macroporous calcium phosphate bioceramics. *Biomaterials*, 27: 3230.

Mason, C. & Dunnill, P., 2008. A brief definition of regenerative medicine. *Regenerative Medicine. Future Medicine*, 18(5): 243–245.

Mata, A., Boehm, C., Fleischman, A.J., Muschler, G., Roy, S., 2002. Growth of connective tissue progenitor cells on microtextured polydimethylsiloxane surface. *Journal of Biomedical Materials Research*, 62: 499-506.

Mathews, S., Bhone, R., Gupta, P. K., Totey, S., 2012. Extra- cellular matrix protein mediated regulation of the osteoblast differentiation of bone marrow derived human mesenchymal stem cells. *Differentiation*, 84, 185–192.

McFadden, T. M., Duffy, G. P., Allen, a B., Stevens, H. Y., Schwarzmaier, S. M., Plesnila, N., Murphy, J.M., Barry, F.P., Guldberg, R.R., O'Brien, F. J. (2013). The delayed addition of human mesenchymal stem cells to pre-formed endothelial cell networks results in functional vascularization of a collagen-glycosaminoglycan scaffold in vivo. *Acta Biomaterialia*, 9(12), 9303–16.

Meeder, P.J. & Eggers, C., 1994. The history of Autogenous Bone Grafting. *Injury*, 25: A2-A3.

Meijer, G.J., de Bruijin, J.D., Koole, R., van Blitterswijk, C.A., 2007. Cell-based bone tissue engineering. *PLOS Medicine*, 4 (2): 260-264.

Mekki, A., Holland, D., Zig, Kh., McConville, C.F., 1997. XPS and magnetization studies of cobalt sodium silicate glasses. *Journal of Non-Crystalline Solids*, 220(3): 267–279.

Melchels, F. P. W., Feijen, J. & Grijpma, D. W., 2010. A review on stereolithography and its engineering. *Biomaterials*, 31 (24): 6121-6130.

Melero-Martin, J.M., De Obaldia, M.E., Allen, P., Dudley, A.C., Klagsbrun, M., Bischoff, J., 2010. Host myeloid cells are necessary for creating bioengineered human vascular networks in vivo. *Tissue Engineering Part A*, 16: 2457–66.

Melkounian, Z., Weber, J.L., Weber, D.M., Fadeev, A.G., Zhou, Y., Dolley-Sonneville, P., Yang, J., Oiu, L., Priest, C.A. Shogbon, C., Martin, A.W., Nelson, J., West, P., Beltzer, J.P., Pal, S., Brandenberger, R., 2010. Synthetic peptide-acrylate surfaces for long-term self-renewal and cardiomyocyte differentiation of human embryonic stem cells. *Nature Biotechnology*, 28: 606-610.

- Merfeld-Clauss, S., Gollahalli, N., March, K.L., Traktuev, D.O., 2010. Adipose tissue progenitor cells directly interact with endothelial cells to induce vascular network formation. *Tissue Engineering Part A*, 16: 2953–2966.
- Merry, J. C., Gibson, I., Best, S.M., Bonfield, W., 1999. Synthesis and characterization of carbonate hydroxyapatite. *Journal of Material Science: Materials in Medicine*, 9: 779-783.
- Mhanna, R. F., Vörös, J., Zenobi-Wong, M., 2011. Layer-by-layer films made from extracellular matrix macromolecules on silicone substrates. *Biomacromolecules*, 12: 609–616.
- Mikos, A.G, Bao, Y., Cima, L.G., Ingber, D.E., Vacanti, J.P., Langer, R., 1993. Preparation of poly(glycolic acid) bonded fiber structures for cell attachment and transplantation. *Journal of Biomedical Materials Research*, 27: 183-189.
- Mikos, A.G., Sarakinos, G., Leite, S.M., Vacanti, J.P. and Langer, R., 1993. Laminated three-dimensional biodegradable foams for use in tissue engineering. *Biomaterials*, 14: 323-330.
- Mikos, A.G., Thorsen, A.J., Czerwonka, L.A., Bao, Y., Langer, R., 1994. Preparation and characterization of poly(L-lactic acid) Foams. *Polymer*, 35: 1068-1077.
- Mikos, A. G., Sarakinos, G., Vacanti, J.P., Langer R.S., Cima, L.G., 1996. Biocompatible polymer membranes and methods of preparation of three dimensional membrane structures. U.S. patent 5, 514: 378.
- Mikos, A.G. & Temenoff, J.S., 2000. Formation of highly porous biodegradable scaffolds for tissue engineering. *Electronic Journal of Biotechnology*, 3(2): 114–119.
- Mikos, A. G., Lu, L., Temenoff, J. S., Temmser, J. K., 2004. Synthetic Bioresorbable polymer scaffolds. In: An introduction to material in medicine, Ratner, B.D., Hoffman, A.S., Schoen, F. J., Lemons, J.E., Elsevier Academic Press. USA.
- Mizuno, M. & Kuboki, Y., 2001. Osteoblasts-Related Gene Expression of Bone Marrow Cells during the Osteoblastic Differentiation Induced by Type I Collagen. *Journal of Biochemistry*, 129: 133-138.
- Moon, J.J. & West, J.L., 2008. Vascularization of engineered tissues: approaches to promote angiogenesis in biomaterials. *Current Topics in Medical Chemistry*, 8: 300–310.
- Mooney, D.J., Baldwin, D.F., Suh, N.P., Vacanti, J.P., Langer, R., 1996. Novel approach to fabricate porous sponges of poly (D, L-lactic co-glycolic acid) without the use of organic solvents. *Biomaterials*, 17: 1417-1422.
- Morrison S.J., Shah, N.M., Anderson, D.J., 1997. Regulatory Mechanisms in Stem Cell Biology. *Cell*, 88: 287-298.
- Murugan, R. & Ramakrishna, S., 2006. Production of ultra-fine bioresorbable carbonated hydroxyapatite. *Acta biomaterialia*, 2(2): 201–6.

Nakamura, M., Hentunen, T., Salonen, J., Nagai, A., Yamashita, K., 2013. Characterization of bone mineral-resembling biomaterials for optimizing human osteoclast differentiation and resorption. *Journal of Biomedical Materials Research Part A*, 101A(11): 3141-3151.

National Health Service, Call to Action, Hip fractures are breaking the bank and lives- Are you ready to stop the UK reaching “Breaking Point”?. Available from: http://www.thebms.org.uk/publicdownloads/Call_to_Action_Politicians.PDF. [10 January 2016].

Ni, S., Chang, J., Chou, L., Zhai, W., 2007. Comparison of osteoblast- like cell responses to calcium silicate and tricalcium phosphate ceramics *in vitro*. *Journal of Biomedical Materials Research Part B Applied Biomaterials*, 80:174–183.

Ni, Y., Liu, Z., Gao, W., Qu, S., Weng, J., Feng, B., 2011. Characterization of self-assembled decyl bis phosphonate– collagen layers on titanium by QCM-D and osteoblast-compatibility. *Applied Surface Science*, 257: 9287– 9292.

Nicolaije, C., Koedam, M., van Leeuwen, J.P.T.M., 2012. Decreased oxygen tension lowers reactive oxygen species and apoptosis and inhibits osteoblast matrix mineralization through changes in early osteoblast differentiation. *Journal of Cellular Physiology*, 227(4): 1309–1318.

Novosel, E.C., Kleinhans, C., Kluger, P.J., 2011. Vascularization is the key challenge in tissue engineering. *Advanced Drug Delivery Review*, 63, 300-311.

Noble, B.S. & Reeve, J., 2000. Osteocyte function, osteocyte death and bone fracture resistance. *Molecular and Cellular Endocrinology*, 159 (1-2): 7-13.

Oh, S., Oh, N., Appleford, M., Ong, J.L., 2006. Bioceramics for Tissue Engineering Applications- A Review. *American Journal of Biochemistry and Biotechnology*, 2(2): 49–56.

Okada, T. & Ikada, Y., 1991. Modification of silicone surfaces by graft polymerization of acrylamide with corona discharge. *Macromolecular Chemistry* 192:1705-13.

Osathanon, T., Bessinyowong, K., Arksornnukit, M., Takahashi, H., Pavasant, P., 2011. Human osteoblast-like cell spreading and proliferation on Ti-6Al-7Nb surfaces of varying roughness. *Journal of oral science*, 53(1): 23–30.

Palmoski, M., Perricone, E., Brandt, K.D., 1979. Development and Reversal of a Proteoglycan Aggregation Defect in Normal Canine Knee Cartilage after Immobilization. *Arthritis and Rheumatism*, 22(5): 508-517.

Park, A., Wu, B., Griffith, L.G., 1998. Integration of surface modification and 3D fabrication techniques to prepare patterned poly(L-lactide) substrates allowing regionally selective cell adhesion. *Journal of Biomaterials Science-Polymer E*, 9: 89-110.

- Park, J.H., Park, B.H., Kim, H.K., Park, T.S., Baek, H.S., 2002. Hypoxia decreases Runx2/Cbfa1 expression in human osteoblast-like cells. *Molecular and Cellular Endocrinology*, 192: 197–203.
- Pautke, C., Schieker, M., Tischer, T., Kolk, A., Neth, P., Mutschler, W., Milz, S., 2004. Characterization of Osteosarcoma Cell Lines MG-63, Saos-2 and U-2 OS in Comparison to Human Osteoblasts. *Anticancer Research*, 24: 3743–3748.
- Pelham, R.J. & Wang, Y-L., 1997. Cell locomotion and focal adhesion are regulated by substrate flexibility. *Proceeding National Academy of Sciences USA*, 94: 13661-13665.
- Petrakova, K.V., Tolmacheva, A.A., Friedenstein, A.J., 1963. Bone formation occurring in bone marrow transplantation in diffusion chambers. *Bulletin of Experimental Biology and Medicine*, 56: 87.
- Phinney, D.G. & Prockop, D.J., 2007. Concise review: mesenchymal stem/multipotent stromal cells: the state of transdifferentiation and modes of tissue repair-current views. *Stem cells*, 25(11): 2896–2902.
- Pietak, A.M., Reid, J.W., Stott, M.J., Sayer, M., 2007. Silicon substitution in the calcium phosphate bioceramics. *Biomaterials*, 28(28): 4023–32.
- Pirracò, R.P., Iwata, T., Yoshida, T., Marques, A.P., Yamato, M., Reis, R.L., Okano, T., 2014. Endothelial cells enhance the in vivo bone-forming ability of osteogenic cell sheets. *Laboratory investigation; a journal of technical methods and pathology*, 94(6): 663–73.
- Pittenger, M.F., Mackay, A.M., Beck, S.C., Jaiswal, R.K., Douglas, R., Mosca, J.D., Moorman, M.A., Simonetti, D.W., Craig, S., Marshak, D.R., 1999. Multilineage potential of adult human mesenchymal stem cells. *Science*, 284 (5411): 143-7.
- Plikk, P.; Målberg, S., Albertsson A.C., 2009. Design of resorbable porous tubular copolyester scaffolds for use in nerve regeneration. *Biomacromolecules*, 10(5): 1259-64.
- Plunkett, N. & O'Brien, F.J., 2011. Bioreactors in tissue engineering. *Technology and Health Care*, 19(1): 55–69.
- Porter, A.E., Best, S.M., Bonfield, W., 2003. Ultrastructural comparison of hydroxyapatite and silicon-substituted hydroxyapatite for biomedical applications. *Journal of Biomedical Materials Research Part A*, 68A(1): 133-141.
- Porter, A., Patel, N., Brooks, R., Best, S., Rushton, N., Bonfield, W., 2005. Effect of carbonate substitution on the ultrastructural characteristics of hydroxyapatite implants. *Journal of Materials Science: Materials in Medicine*, 16: 899.
- Pound, J. C., Green, D. W., Chaudhuri, J. B., Roach, H.I., Oreffo, R.O.C., 2006. Bioreactor culture of cartilage from mesenchymal populations. *Journal of Bone & Joint*, 88B: 405.
- Prockop, D.J., 1997. Marrow stromal cells as stem cells for nonhematopoietic tissues. *Science*, 276: 71–74.

Prosecká, E., Buzgo, M., Rampichová, M., Kocourek, T., Kochová, P., Vysloužilová, L., Tvrđík, D., Jelínek, M., Lukáš, D., Amler, E., 2012. Thin-layer hydroxyapatite deposition on a nanofiber surface stimulates mesenchymal stem cell proliferation and their differentiation into osteoblasts. *Journal of biomedicine & biotechnology*, 2012: 428503.

Qing-Qing, Q., Ducheyne, P., Ayyaswamy, P.S., 1999. Fabrication, characterization and evaluation of bioceramic hollow microspheres used as microcarriers for 3-D bone tissue formation in rotating bioreactors. *Biomaterials*, 20: 989–1001.

Qiu, Q., Ducheyne, P., Gao, H., Ayyaswamy, P., 1998. Formation and differentiation of three-dimensional rat marrow stromal cell culture on microcarriers in a rotating-wall vessel. *Tissue Engineering*, 4(1): 19-34.

Quarles, L.D., Yohay, D.A., Lever, L.W., Caton, R., Wenstrup, R.J., 1992. Distinct proliferative and differentiated stages of murine MC3T3-E1 cells in culture: An in vitro model of osteoblast development. *Journal of Bone Mineral Research*, 18: 1842-1853.

Quarto, R., Mastrogiacomo, M., Cancedda, R., Kutepov, S., Mukhachev, S.M., Lavroukov, A., Kon, E., Marcacci, M., 2001. Repair of large bone defects with the use of autologous bone marrow stromal cells. *New England Journal of Medicine*, 344(5): 385–386.

Rao, R.R., Peterson, A.W., Ceccarelli, J., Putnam, A.J., Stegmann, J.P., 2012. Matrix composition regulates three-dimensional network formation by endothelial cells and mesenchymal stem cells in collagen/fibrin materials. *Angiogenesis*, 15(2): 253–64.

Ratner, B.D., Hoffman, A.S., Schoen, F.J., Lemons, J.E., 2013. An introduction to materials in medicine. *Academic Press*, Third edition, United States of America.

Rauh, J., Milan, F., Günther, K-L., Stiehler, M., 2011. Bioreactor systems for bone tissue engineering. *Tissue engineering. Part B, Reviews*, 17(4): 263–280.

Ravichandran, R., Venugopal, J.R., Sundarajan, S., Mukherjee, S., Ramakrishna, S., 2012. Precipitation of nano-hydroxyapatite on PLLA/PBLG/collagen nanofibrous structures for the differentiation of adipose derived stem cells to osteogenic lineage. *Biomaterials*, 33: 846–855.

Reinwald, Y., Leonard, K.H.L., Henstock, J.R., Whiteley, J.P., Osborne, J.M., Waters, S.L., Levesque, P., El Haj, A.J., 2015. Evaluation of the growth environment of a hydrostatic force bioreactor for preconditioning of tissue-engineered constructs. *Tissue engineering. Part C, Methods*, 21(1): 1–14.

Rey, C., Shimizu, M., Collins, B., Glimcher, M.J., 1991. Resolution-enhanced Fourier transform infrared spectroscopy study of the environment of phosphate ion in the early deposits of a solid phase of calcium phosphate in bone and enamel and their evolution with age: 2. Investigations in the $\nu_3\text{PO}_4$ domain. *Calcified Tissue International*, 49(6): 383-388.

Rezwan, K., Chen, Q.Z., Blaker, J.J., Boccaccini, A.R., 2006. Biodegradable and bioactive porous polymer/inorganic composite scaffolds for bone tissue engineering. *Biomaterials*, 27: 3413-3431.

- Ribeiro, N., Sousa, S.R., Monteiro, F.J., 2010. Influence of crystallite size of nanophased hydroxyapatite on fibronectin and osteonectin adsorption and on MC3T3-E1 osteoblast adhesion and morphology. *Journal of Colloid and Interface Science*, 351(2): 398-406.
- Rich, L. & Whittaker, P., 2005. Collagen and Picrosirius Red Staining : a Polarized Light Assessment of Fibrillar Hue and Spatial Distribution. *Brazilian Journal of Morphological Sciences*, 22(2): 97–104.
- Rodan, G.A. & Martin, T.J., 1981. The role of osteoblasts in hormonal control of bone resorption. *Calcified Tissue International*, 33: 349-351.
- Rodan, G.A., 1992. Introduction to bone biology. *Bone*, 13: S3-S6.
- Roveri, N. & Lafisco, M., 2010. Evolving application of biomimetic nanostructured hydroxyapatite. *Nanotechnology, Science and Applications*, 3: 107-125.
- Rodrigues, S.C., Salgado, C.L., Sahu, A., Garcia, M.P., Fernandes, A.H., Monteiro, F.J., 2013. Preparation and characterization of collagen-nanohydroxyapatite biocomposite scaffolds by cryogelation method for bone tissue engineering applications. *Journal of Biomedical Materials Research - Part A*, 101 A (4): 1080–1094.
- Rose, F.R., Cyster, L.A., Grant, D.M., Scotchford, C.A., Howdle, S.M., Shakesheff, K.M., 2004. In vitro assessment of cell penetration into porous hydroxyapatite scaffolds with a central aligned channel. *Biomaterials*, 25(24): 5507–5514.
- Rosenberg, E. & Weis, M., 1983. Chapter 5 Introduction to Electron Microscopy. *Image (Rochester, N.Y.)*: 59–66.
- Rouwkema, J., de Boer, J., Van Blitterswijk, C.A., 2006. Endothelial cells assemble into a 3- dimensional prevascular network in a bone tissue engineering construct. *Tissue Engineering*, 12: 2685–2693.
- Rouwkema, J., Rivron, N.C., van Blitterswijk, C. A., 2008. Vascularization in tissue engineering. *Trends in Biotechnology*, 26(8): 434–441.
- Roux, B.M., Cheng, M.-H, Brey, E.M., 2015. Engineering clinically relevant volumes of vascularized bone. *Journal of Cellular and Molecular Medicine*, 19(5): 903–914.
- Rucci, N., 2008. Molecular biology of bone remodelling. *Clinical cases in mineral and bone metabolism : the official journal of the Italian Society of Osteoporosis, Mineral Metabolism, and Skeletal Diseases*, 5(1): 49–56.
- Rupani, A., Balint, R., Cartmell, S.H., 2012. Osteoblasts and their applications in bone tissue engineering. *Cell Health and Cytoskeleton*, 4: 49–61.
- Sachlos, E. & Czernuszka, J.T., 2003. Making tissue engineering scaffolds work. Review: the application of solid freeform fabrication technology to the production of tissue engineering scaffolds. *European cells & materials*, 5: 29–40.

Salgado, A.J., Coutinho, O.P., Reis, R.L., 2004. Bone Tissue Engineering: State of the Art and Future Trends. *Macromolecular Bioscience*, 4: 743-765.

Schantz, J.T., Hutmacher, D.W., Ng, K.W., Khor, H.L., Lim, M.T., Teoh, S.H., 2002. Evaluation of a tissue-engineered membrane-cell construct for guided bone regeneration. *International Journal of Oral Maxillofacial Implants*, 17(2): 161-74.

Schwarz, K. & Milne, D.B., 1972. Growth-promoting effects of silicon in rats. *Nature*, 239: 333-334.

Schwartz, Z., Raz, P., Zhao, G., Barak, Y., Tauber, M., Yao, H., Boyan, B.D., 2008. Effect of micrometer-scale roughness of the surface of Ti6Al4V pedicle screws in vitro and in vivo. *Journal of Bone Joint Surgery America*, 90: 2485- 2498.

Schmidt, A., Wuest, S.E., Vijverberg, K., Baroux, C., Kleen, D., Grossniklaus, U., 2011. Transcriptome Analysis of the Arabidopsis Megaspore Mother Cell Uncover the Importance of RNA Helicases for Plant Germline Development. *PLoS Biology*, 9(9): e1001155.

Seitz, H., Rieder, W., Irsen, S., Leukers, B., Tille, C., 2005. Three-dimensional printing of porous ceramic scaffolds for bone tissue engineering. *Journal of Biomedical Materials Research. Part B: Applied Biomaterials*, 74(2): 782-788.

Sepulveda, P., Bressiani, A.H., Bressiani, J.C., Meseguer, L., König, B. Jr., 2002. In vivo evaluation of hydroxyapatite foams. *Journal of Biomedical Materials Research*, 62: 587.

Sherwood, J.K., Riley, S. L., Palazzolo, R., Brown, S.C., Monkhouse, D., C., Coates, M., Griffith, L.G., Landeen, L.K., Ratcliffe, A., 2002. A three-dimensional osteochondral composite scaffold for articular cartilage repair. *Biomaterials*, 23: 4739-4751.

Shepherd, J.H., Shepherd, D.V, Best, S.M., 2012. Substituted hydroxyapatites for bone repair. *Journal of materials science. Materials in medicine*, 23(10): 2335-47.

Sheyn, D., Pelled, G., Netanel, D., Domany, E., Gazit, D., 2010. The Effect of Simulated Microgravity on Human Mesenchymal Stem Cells Cultured in an Osteogenic Differentiation System: A Bioinformatics Study. *Tissue Engineering Part A*, 16(11): 3403-3412.

Shin, H.-Y., Jung, J-H., Kim, S-W., Lee, W-K., 2006. XPS Analysis on Chemical Properties of Calcium Phosphate Thin Films and Osteoblastic HOS Cell Responses. *Journal of Industrial and Engineering Chemistry*, 12(3): 476-483.

Siber, J.S. Anderson, D.G., Daffner, S.D., Brislin, B.T., Leland, J.M., Hilibrand, A.S., Vaccaro, A.R., Albert, T.J., 2003. Donor site morbidity after anterior iliac crest bone harvest for single-level anterior cervical discectomy and fusion. *Spine*, 28 (2): 134-139.

Silva, M.M.C.G., Cyster, L.A., Barry, J.J.A., Yang, X.B., Oreffo, R.O.C., Grant, D.M., Scotchford, C.A., Howdle, S.M., Shakesheff, K.M., Roase, F.R.A.J., 2006. The effect of

anisotropic architecture on cell and tissue infiltration into tissue engineering scaffolds. *Biomaterials*, 27(35): 5909–5917.

Sikavitsas, V.I., Temenoff, J.S., Mikos, A.G., 2001. Biomaterials and bone mechanotransduction. *Biomaterials*, 22: 2581-2593.

Ślósarczyk, A., Paszkiewicz, Z., Paluszkiwicz, C., 2005. FTIR and XRD evaluation of carbonated hydroxyapatite powders synthesized by wet methods. *Journal of Molecular Structure*, 744-747: 657–661.

So, P. T. C., 2002. Two-photon Fluorescence Light Microscopy. *Life Sciences*, 1–5.

Sobral, J.M., Caridade, S.G., Sousa, R.A., Mano, J.F., Reis, R.L., 2011. Three-dimensional plotted scaffolds with controlled pore size gradients: Effect of scaffold geometry on mechanical performance and cell seeding efficiency. *Acta Biomaterialia*, 7(3): 1009–1018.

Socol, G., Torricelli, P., Bracci, B., Iliescu, M., Miroiu, F., Bigi, A., Werckmann, J., Mihailescu, I.N., 2004. Biocompatible nanocrystalline octacalcium phosphate thin films obtained by pulsed laser deposition. *Biomaterials*, 25, 2539–2545.

Soldana G., Mercogliano R., 1991. Bioartificial polymeric materials obtained from blends of synthetic polymers with fibrin and collagen. *International Journal of Artificial Organs*, 14(5): 295-303.

Somford, M.P., van den Bekerom, M.P.J., Kloen, P., 2013. Operative treatment for femoral shaft nonunions, a systematic review of the literature. *Strategies in trauma and limb reconstruction*, 8: 77-88.

Sommerfeldt, D.W.& Rubin, C.T., 2001. Biology of bone and how it orchestrates the form and function of the skeleton. *European Spine Journal*, 10: S86-S95.

Song, K., Yang, Z., Liu, T., Zhi, W., Li, X., Deng, L., Cui, Z., Ma, X., 2006. Fabrication and detection of tissue-engineered bones with bio-derived scaffolds in a rotating bioreactor. *Biotechnology and applied biochemistry*, 45 (2): 65–74.

Song, K., Liu, T., Cui, Z., Li, X., Ma, X., 2008. Three-dimensional fabrication of engineered bone with human bio-derived bone scaffolds in a rotating wall vessel bioreactor. *Journal of biomedical materials research. Part A*, 86(2): 323–332.

Sorkin, A.M., Dee, K.C., Knothe Tate, M.L., 2004. “Culture shock” from the bone cell’s perspective: emulating physiological conditions for mechanobiological investigations. *American journal of physiology. Cell physiology*, 287(6): C1527–C1536.

Spence, G., Patel, N., Brooks, R., Rushton, N., 2009. Carbonate substituted hydroxyapatite: resorption by osteoclasts modifies the osteoblastic response. *Journal of Biomedical Materials Research, Part A*, 90A: 217.

Sprio, S., Tampieri, A., Landi, E., Sandri, M., Martorana, S., Celotti, G., Logroscino, G., 2008. Physico-chemical properties and solubility behaviour of multi-substituted

hydroxyapatite powders containing silicon. *Materials Science and Engineering: C*, 28(1): 179–187.

Staton, C.A., Stribbling, S.M., Tazzyman, S., Hughes, R., Brown, N.J. Lewis, C.E., 2004. Current methods for assaying angiogenesis in vitro and in vivo. *International journal of experimental pathology*, 85(5): 233–248.

Stevens, M.M. & George, J.H., 2005. Exploring and Engineering the Cell Surface Interface. *Science*, 310: 1135.

Stevens, M.M., Robert, P.M., Dirk, S., Joshua, A., Robert, L., Prasad Shastri, V., 2005. In vivo engineering of organs: the bone bioreactor. *Proceeding of the National Academy of Science*, 102(32): 11450-11455.

Stevens, M.M., 2008. Biomaterials for bone tissue engineering. *Materials Today*, 11(5): 18–25.

Stock, U.A., Vacanti, J.P., 2001. Tissue Engineering: Current State and Prospects. *Annual Reviews of Medicine*, 52: 443-451.

Subia, B., Kundu, J., Kundu, S., 2010. Biomaterial scaffold fabrication techniques for potential tissue engineering applications. *Tissue engineering*, 3: 141–159.

Suh H., Hwang, Y.S., Lee, J.E., Kim, K.T., Park, J.C., Park, K.D., Kim, Y.H., 1998. Type I atelocollagen grafting on polyurethane tube and its mechanical property. *Biomaterial Research* 2(4): 158-62.

Suh, H., Hwang, Y.S., Lee, J.E., Han, C.D., Park, J.C., 2001. Behavior of osteoblasts on a type I atelocollagen grafted ozone oxidized poly L-lactic acid membrane. *Biomaterials*, 22(3): 219–230.

Swetha, M., Sahithi, K., Moorthi, A., Srinivasan, N., Ramasamy, K., Selvamurugan, N., 2010. Biocomposites containing natural polymers and hydroxyapatite for bone tissue engineering. *International Journal of Biological Macromolecules*, 47(1): 1–4.

Szilagyi, I., Trefalt, G., Tiraferri, A., Maroni, P., Borkovec, M., 2014. Polyelectrolyte adsorption, interparticle forces, and colloidal aggregation. *Soft Matter*, 10: 2479-2502.

Taboas, J.M., Maddox, R.D., Krebsbach, P.H., Hollister, S.J., 2003. Indirect solid free form fabrication of local and global porous, biomimetic and composite 3D polymer-ceramic scaffolds. *Biomaterials*, 24(1): 181–194.

Tada, H., Nemoto, E., Foster, B.L., Somerman, M.J., Shimauchi, H., 2011. Phosphate increases bone morphogenetic protein-2 expression through cAMP-dependent protein kinase and ERK1/2 pathways in human dental pulp cells. *Bone*, 48: 1409–1416.

Tadic, D., Peters, F., Epple, M., 2002. Continuous synthesis of amorphous carbonated apatites. *Biomaterials*, 23(12): 2553–9.

Tan, J.L., Liu, W., Nelson, C.M., Raghavan, S., Chen, C.S., 2004. Simple approach to micropattern cells on common culture substrates by tuning substrate wettability. *Tissue engineering*, 10(5-6): 865–872.

Tancred, D.C., Carr, A.J., McCormack, B.A.O, 1998. Development of a new synthetic bone graft. *Journal of Materials Science: Material in Medicine*, 9: 819-823.

Tang, X. L., Xiao, X.F., Liu, R.F., 2005. Structural characterization of silicon-substituted hydroxyapatite synthesized by a hydrothermal method. *Materials Letters*, 59: 3841-3846.

Taylor, C.R., Shi, S-R., Barr, N.J., 2006. Techniques of Immunohistochemistry: Principles, Pitfalls and Standardization. *Diagnostic Immunohistochemistry: Second ed.*, 1–42.

Temenoff, J.S. & Mikos, A.G., 2000. Review: tissue engineering for regeneration of articular cartilage. *Biomaterials*, 21: 431-440.

Thein-Han, W.W. & Misra, R.D.K., 2009. Biomimetic chitosan–nanohydroxyapatite compositescaffolds for bone tissue engineering. *Acta Biomaterialia*, 5(4): 1182–1197.

Tsai, S.-W., Hsu, F.-Y. & Chen, P.-L., 2008. Beads of collagen-nanohydroxyapatite composites prepared by a biomimetic process and the effects of their surface texture on cellular behavior in MG63 osteoblast-like cells. *Acta biomaterialia*, 4(5): 1332–41.

Tzoneva, R., Seifert, B., Albrecht, W., Richau, K., Groth, T., Lendlein, A., 2008. Hemocompatibility of poly (ether imide) membranes functionalized with carboxylic groups. *Journal of Materials Science: Materials in Medicine*, 19: 3203–3210.

Unger, R.E., Sartoris, A., Peters, K., Motta, A., Migliaresi, C., Kunkel, M., Bulnheim, U., Rychly, J., Kirkpatrick, C.J., 2007. Tissue-like self-assembly in cocultures of endothelial cells and osteoblasts and the formation of microcapillary-like structures on three-dimensional porous biomaterials. *Biomaterials*, 28: 3965–3976.

Unger, R.E., Ghanaati, S., Orth, C., Sartoris, A., Barbeck, M., Halstenberg, S., Motta, A., Migliaresi, C., Kirkpatrick, C.J., 2010. The rapid anastomosis between prevascularized networks on silk fibroin scaffolds generated in vitro with cocultures of human microvascular endothelial and osteoblast cells and the host vasculature. *Biomaterials*, 31(27): 6959–6967.

Vázquez, C.G., Barba, C.P., Munguia, N., 2005. Stoichiometric hydroxyapatite obtained by precipitation and sol gel processes. *Revista Mexicana de Fisica*, 51(3): 284-293.

Vacanti, C.A., Bonassar, L.J., Vacanti, M.P., Shufflebarger, J., 2001. Replacement of an avulsed phalanx with tissue engineered bone. *New England Journal of Medicine*, 344(20): 1511–1514.

Vacanti, C.A., 2006. The history of tissue engineering. *Journal of Cellular and Molecular Medicine*, 10(3): 569-576.

Vagaska, B., Bacakova, L., Filoka, E., Balik, K., 2010. Review: Osteogenic Cells on Bio-Inspired Materials for Bone Tissue Engineering. *Physiology Research*, 59: 309-322.

- Vandrovcová, M., Douglas, T., Hauk, D., Grossner-Schreiber, B., Wiltfang, J., Bacakova, L., Warnke, P.H., 2011. Influence of collagen and chondroitin sulfate (CS) coatings on poly-(Lactide-co-Glycolide) (PLGA) on MG63 osteoblast-like cells. *Physiological Research*, 60(5): 797–813.
- Vater, C., Kasten, P., Stiehler, M., 2011. Culture media for the differentiation of mesenchymal stromal cells. *Acta Biomaterialia*, 7:463–477.
- Vats, A., Tolley, N.S., Polak, J.M., Gough, J.E., 2003. Scaffold and biomaterials for tissue engineering: a review of clinical applications. *Clinical Otolaryngology*, 28: 165-172.
- Velasco, M.A., Narváez-Tovar, C.A., Garzón-Alvarado, D.A., 2015. Design, materials and mechanobiology of biodegradable scaffolds for bone tissue engineering. *BioMed Research International*, 2015: 1-21.
- Voutou, B., Stefanaki, E., Giannakopoulos, K., 2008. Electron Microscopy : The Basics. *Physics of Advanced Materials Winter School*, 1–11.
- Wahl, D.A. & Czernuszka, J.T., 2006. Collagen-Hydroxyapatite composites for Hard Tissue Repair. *European Cells and Materials*, 11: 43-56.
- Wakitani, S., Mitsuoka, T., Nakamura, N., Toritsuka, Y., Nakamura, Y., Horibe, S., 2004. Autologous bone marrow stromal cell transplantation for repair of full-thickness articular cartilage defects in human patellae: two case reports. *Cell Transplant*, 13:595-600.
- Wang, R.Z., Cui, F.Z., Lu, H.B., Wen, H.B., Ma, C.L., Li, H.D., 1995. Synthesis of Nanophase Hydroxyapatite Collagen Composite. *Journal of Materials Science Letter*, 14: 490-492.
- Wang, H-B., Dembo, M., Wang, Y-L., Substrate flexibility regulates growth and apoptosis of normal but not transformed cells. *American Journal of Physiology. Cell Physiology*, 279 (5): C1345-C1350.
- Wang, X., Grogan, S.P., Rieser, F., Winkelmann, V., Maquet, V., Berge, M.L., Mainil-Varlet, P., 2004. Tissue engineering of biphasic cartilage constructs using various biodegradable scaffolds: an in vitro study. *Biomaterials*, 25: 3681-3688.
- Wang, Y.J., Chen, J.D., Wei, K., Zhang, S.H., Wang, X.D., 2006. Surfactants-assisted synthesis of hydroxyapatite crystals. *Materials Letter*, 60: 3227-3231.
- Wang, R-J., Wang, L., Zhao, L., Liu, Z., 2007. Influence of process parameters on part shrinkage in SLS. *International Journal of Advanced Manufacturing Technology*, 33 (5-6): 498-504.
- Wang, P., Zhao, L., Liu, J., Weir, M.D., Zhou, X., Xu, H.H., 2014. Review Article: Bone tissue engineering via nanostructured calcium phosphate biomaterials and stem cells. *Bone Research*, 2: 14017.

Warnke, P.H., Wiltfang, J., Springer, I., Acil, Y., Bolte, H., Kosmahl, M., Russo, P.A., Sherry, E., Lützen, U., Wolfart, S., Terheyden, H., 2006. Man as living bioreactor: fate of an exogenously prepared customized tissue-engineered mandible. *Biomaterials*, 27(17): 3163-7.

Wei, X., Yang, X., Han, Z-p., Qu, F-f., Shao, L., Shi, Y-f., 2013. Mesenchymal stem cells: a new trend for cell therapy. *Acta Pharmacologica Sinica*, 34(6): 747–754.

Weiner, S. & Wagner, H.D., 1998. The material bone: Structure-mechanical function relations. *Annual Review of Material Science*, 28: 271-298.

Williams, J. M., Adewunmi, A., Schek, R. M., Flanagan, C. L., Krebsbach, P. H., Feinberg, S.E., Hollister, S. J. & Das, S., 2005. Bone tissue engineering using polycaprolactone scaffolds fabricated via selective laser sintering. *Biomaterials*, 26 (23): 4817-4827.

Wilson, C.E., de Bruijn, J.D., van Blitterswijk, C.A., Verbout, A.J., Dhert, W.J.A., 2004. Design and fabrication of standardized hydroxyapatite scaffolds with a defined macro-architecture by rapid prototyping for bone-tissue-engineering research. *Journal of biomedical materials research. Part A*, 68: 123–132.

Woodfield, T. B.; Guggenheim, M.; von Rechenberg, B.; Riesle, J.; van Blitterswijk, C. A. Wedler, V., 2009. Rapid prototyping of anatomically shaped, tissue engineered implants for restoring congruent articulating surfaces in small joints. *Cell Proliferation*, 4, 485-97.

Xie, J., Baumann, M.J., McCabe, L.R. 2004. Osteoblasts respond to hydroxyapatite surfaces with immediate changes in gene expression. *Journal of Biomedical Materials Research Part A*, 71(1): 108-117.

Yamauchi, J., Yamaoka, A., Ikemoto, K., Matsui, T., 1991. Graft copolymerization of methyl methacrylate onto polypropylene oxidized with ozone. *Journal of Applied Polymer Science* 43:1197-1203.

Yarlagadda, P.K., 2005. Recent advances and current developments in tissue scaffolding. *Biomedical Materials Engineering*, 15(3): 159-177.

Yaszemski, M.J., Oldham, J.B., Lu, L., Currier, B.L., 1994. Bone engineering, 1st ed., *Em squared*, Toronto: 541.

Yeatts, A.B. & Fisher, J.P., 2011. Bone tissue engineering bioreactors: Dynamic culture and the influence of shear stress. *Bone*, 48(2): 171–181.

Young, B., Lowe, J.S., Stevens, A., Heath, J.W., 2006. Wheater's Functional Histology: A Text and Colour Atlas, 5th ed., *Elsevier*, Philadelphia: Churchill Livingstone.

Yu, X., Botchwey, E.A., Levine, E.M., Pollack, S.R., Laurencin, C.T., 2004. Bioreactor-based bone tissue engineering: the influence of dynamic flow on osteoblast phenotypic expression and matrix mineralization. *Proceedings of the National Academy of Sciences of the United States of America*, 101(31): 11203–11208.

Yu, H.-S., Jin, G.-Z., Won, J.-E., Wall, I., Kim, H.W., 2012. Macrochanneled bioactive ceramic scaffolds in combination with collagen hydrogel: a new tool for bone tissue engineering. *Journal of biomedical materials research. Part A*, 100(9): 2431–2440.

Yuan, H., Kurashina, K., de Bruijn, J.D., Li, Y., de Groot, K., Zhang, X., 1999. A preliminary study on osteoinduction of two kinds of calcium phosphate ceramics. *Biomaterials*, 20: 1799.

Zaidi, M., 2007. Skeletal remodelling in health and disease. *Nature Medicine*, 13 (7): 791-801.

Zein I., Hutmacher D.W., Tan K.C., Teoh S.H., 2002. Fused deposition modelling of novel scaffold architectures for tissue engineering applications. *Biomaterials*, 23: 1169-1185.

Zhang, J., Senger, B., Vautier, D., Picart, C., Schaaf, P., Voegel, J.-C., Lavallo, P., 2005. Natural polyelectrolyte films based on layer-by-layer deposition of collagen and hyaluronic acid. *Biomaterials*, 26(16): 3353–3361.

Zhang, Y., Wang, W.J., Feng, Q.L., Cui, F.Z., Xu, Y.X., 2006. A novel method to immobilize collagen on polypropylene film as substrate for hepatocyte culture. *Materials Science Engineering C*, 26: 657–663.

Zhao, M. Y., Li, L.H., Li, B., Zhou, C.R., 2014. LBL coating of type I collagen and hyaluronic acid on aminolyzed PLLA to enhance the cell-material interaction. *Express Polymer Letters*, 8(5): 322–335.

Zhou, W.Y., Wang, M., Cheung, W.L., Guo, B.C., Jia, D.M., 2008. Synthesis of carbonated hydroxyapatite nanospheres through nanoemulsion. *Journal of materials science. Materials in medicine*, 19(1): 103–110.

Zhu, Y., Gao, C., He, T., Liu, X., Shen, J., 2003. Layer-by-Layer Assembly To Modify Poly (L -lactic acid) Surface toward Improving Its Cytocompatibility to Human Endothelial. *Biomacromolecules*, 4: 446–452.

Appendix

**Characterization of human bone marrow-derived mesenchymal stem cells aspirate
(Cell Source: Lonza, United States; Donor: 24-years old male)**

Based on the guidelines from the International Society of Cellular Therapy, human bone marrow- derived mesenchymal stem cells (hMSCs) can be defined based on the following three criteria:

1. hMSCs must be able to adhere to plastic surface under standard tissue culture conditions
2. hMSCs should be able to differentiate into the tri-lineage of osteogenic, chondrogenic and adipogenic when expanded in their specific culture medium (as shown in Table 2.3)
3. hMSCs must express certain cluster of differentiation surface markers, including CD73, CD90 and CD105, and lack of the expression of markers such as CD14, CD34, CD45, CD19 and HLA-DR.

hMSCs used in this study were adherent to the tissue culture plastic (TCP) as shown in Fig. A1. The cells were also tested for their multilineage potential by culturing them for 21 days in relevant differentiation media followed by histological staining (as described in section 2.2.5.2.). Cells cultured in proliferation media acted as the experimental control. Cells grown in osteogenic media showed positive stain in Alizarin Red for calcium deposition designated by the bright red nodules; cells in chondrogenic media shows the stained for sulphated glycosaminoglycans with Alcian Blue and cells in adipogenic were stained positive by the Oil Red O indicating the lipid droplets formation. Cells cultured in proliferation media demonstrated the absent of stains for all histological staining performed. Results are presented in Fig. A2.

Fluorescent images of hMSCs stained by CD73, CD90, CD105, negative (CD14, CD34, CD45, CD19 and HLA-DR) and isotypes (IgG 1 and IgG 2a) are represented in Fig. A3. The nuclei stained with DAPI (4, 6-Diamidino-2-Phenylindole) appeared blue. Positive stains were only observed for surface markers of CD73, CD90 and CD105, while absent of stains were observed for the hematopoietic markers including CD14, CD34, CD45, CD19 and HLA-DR as well as the isotype control antibodies including IgG 1 and IgG 2a. This was also confirmed by the flow cytometry analysis.

Flow cytometry data showing the intensity of the fluorophore tagged isotypes, positive and negative CD markers are represented in Fig. A4. Isotype controls showed very low intensity of staining (shaded black). Cells stained by CD73, CD90 and CD105 demonstrated strong fluorescence intensity (shaded red) with the entire population was shifted to the higher value, indicating positive staining. On the other hand, negative staining was obtained for CD14, CD34, CD45, CD19 and HLA-DR, which were demonstrated by low fluorescence intensity. From the characterizations performed, it is confirmed that the cells used in this study are bone marrow-derived mesenchymal stem cells and referred as hMSCs throughout the study in this thesis.

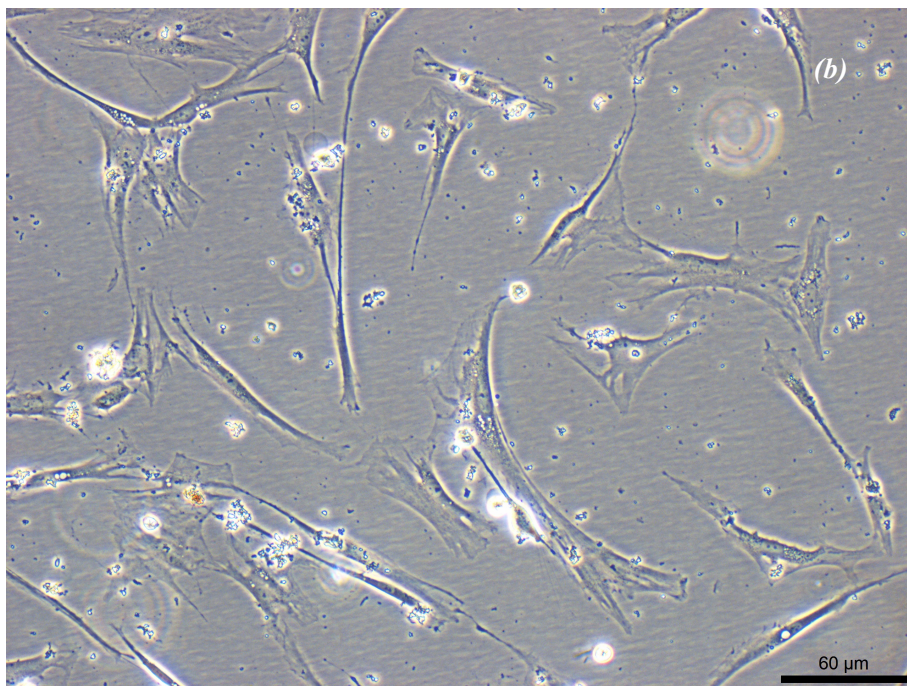
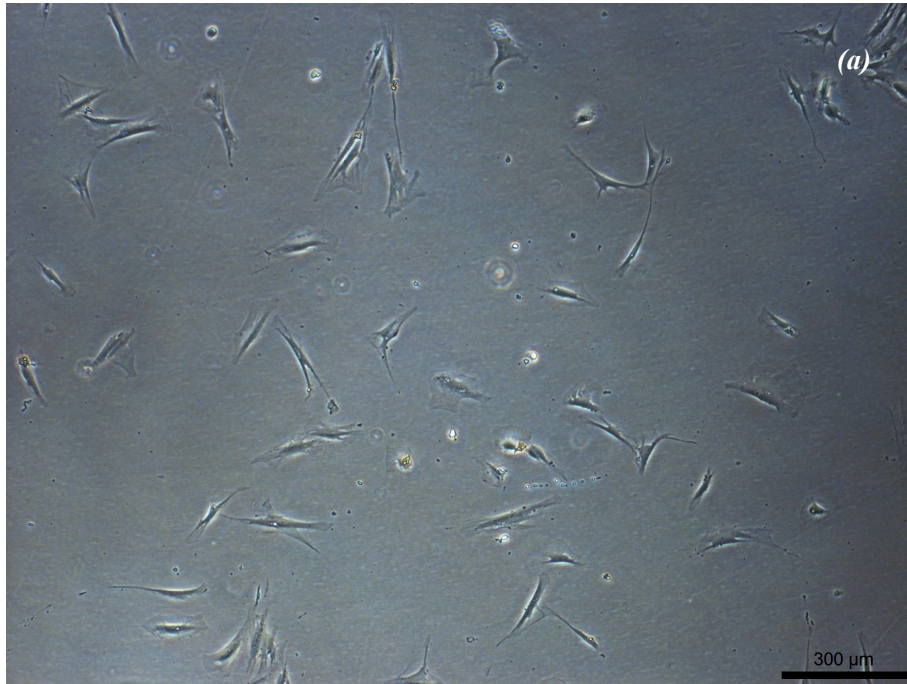


Fig. A1: hMSCs adhere to the tissue culture plastic. Images of hMSCs at (a) lower (4X) and (b) higher (10X) magnification. hMSCs at passage three (P3) remained the spindle fibroblast like appearance after 14 days in culture.

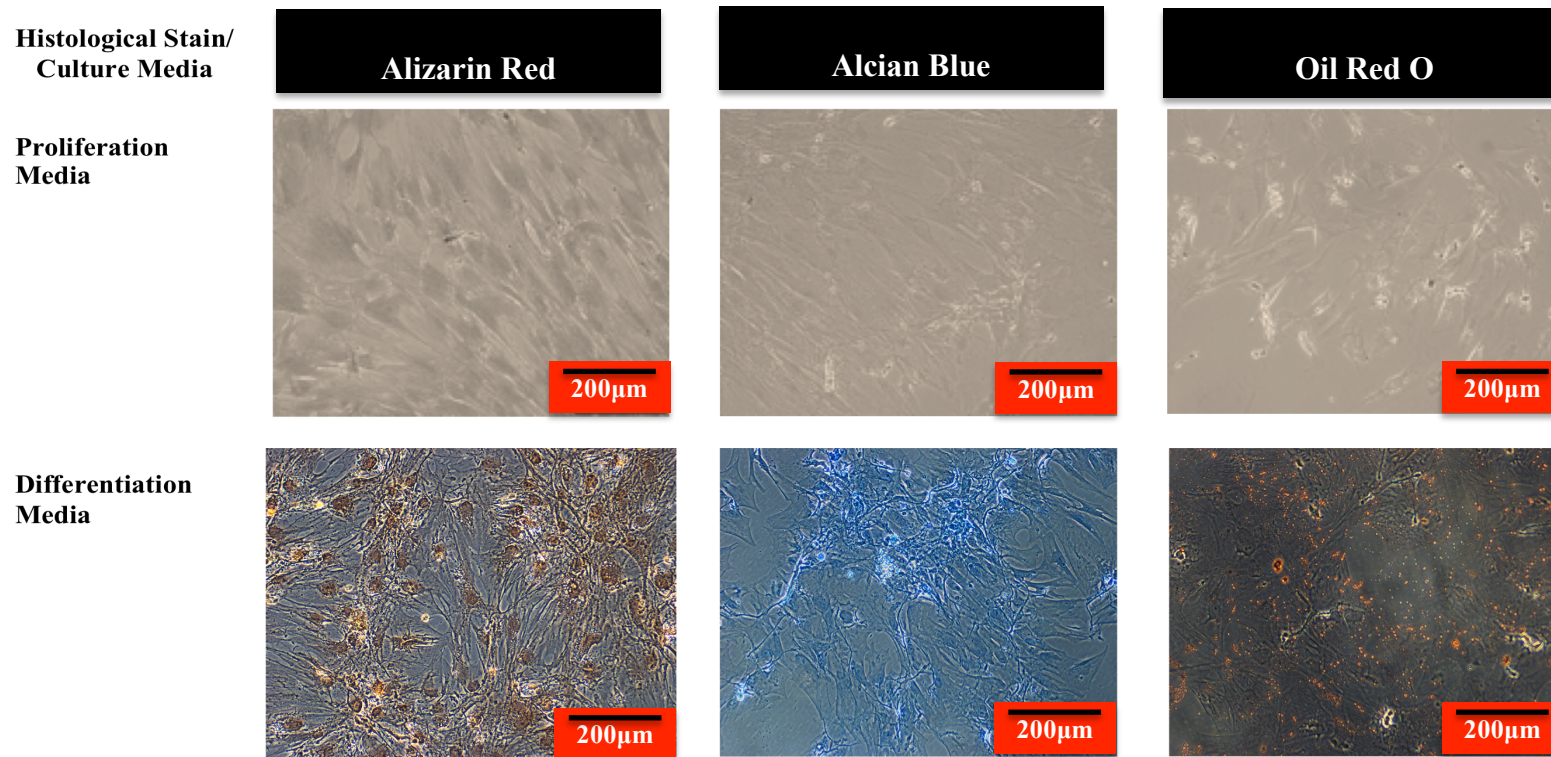


Fig. A2: Multi-lineage differentiation of hMSCs after 21 days in culture. Cells were cultured in proliferation and relevant differentiation media namely, Osteogenic, Chondrogenic and Adipogenic media and were histologically stained with Alizarin Red, Alcian Blue and Oil Red O, respectively. Scale Bar = 200 µm.

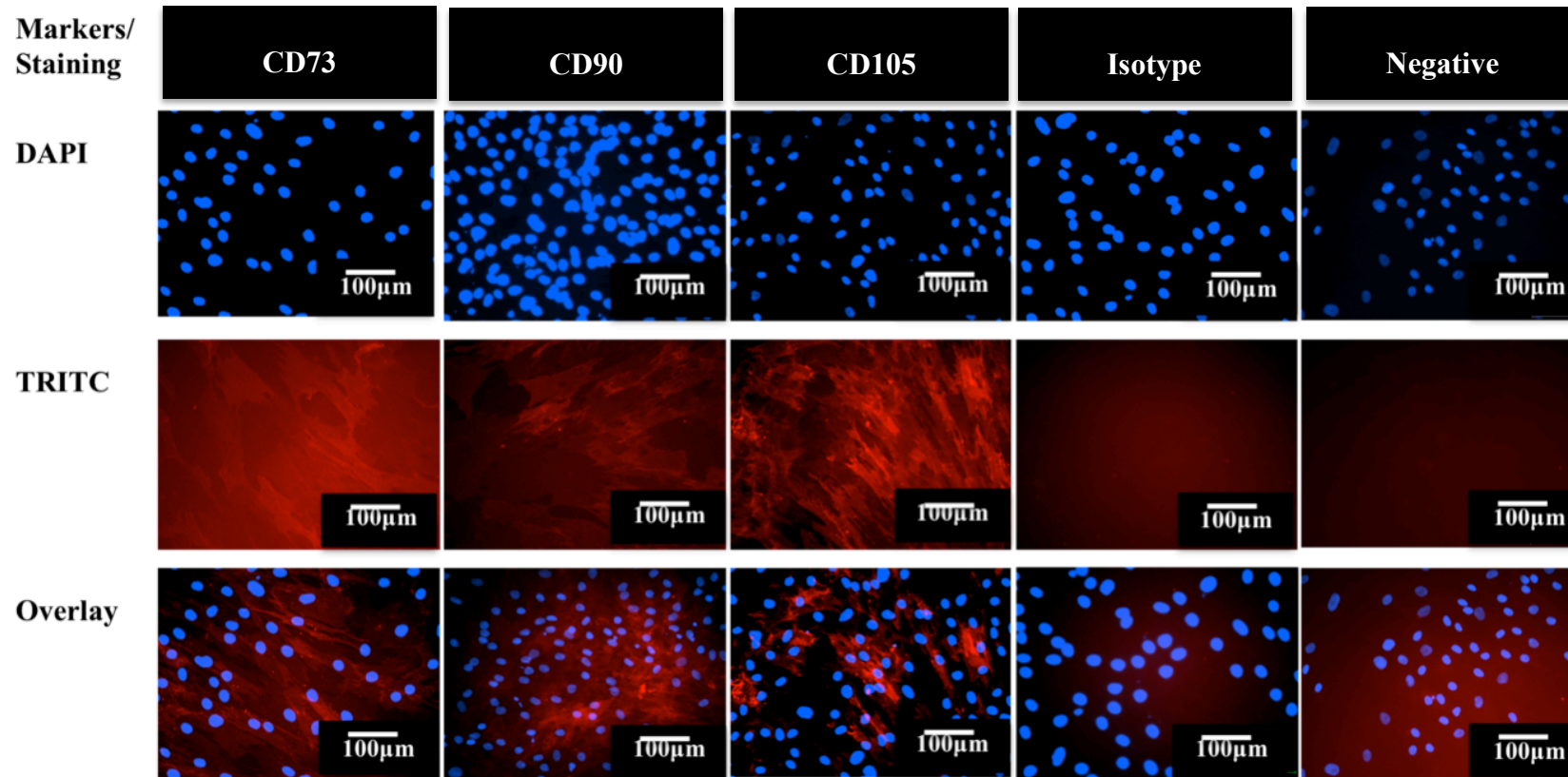


Fig. A3: hMSC staining for CD markers. Immunostaining characterization of the expression profile of typical hMSCs surface markers (CD73, CD90 and CD105) and demonstrating the lack of hematopoietic markers. Isotype represents the IgG 1 and IgG 2a, and negative is the CD14, CD19, CD34 and CD45 and HLA-DR.

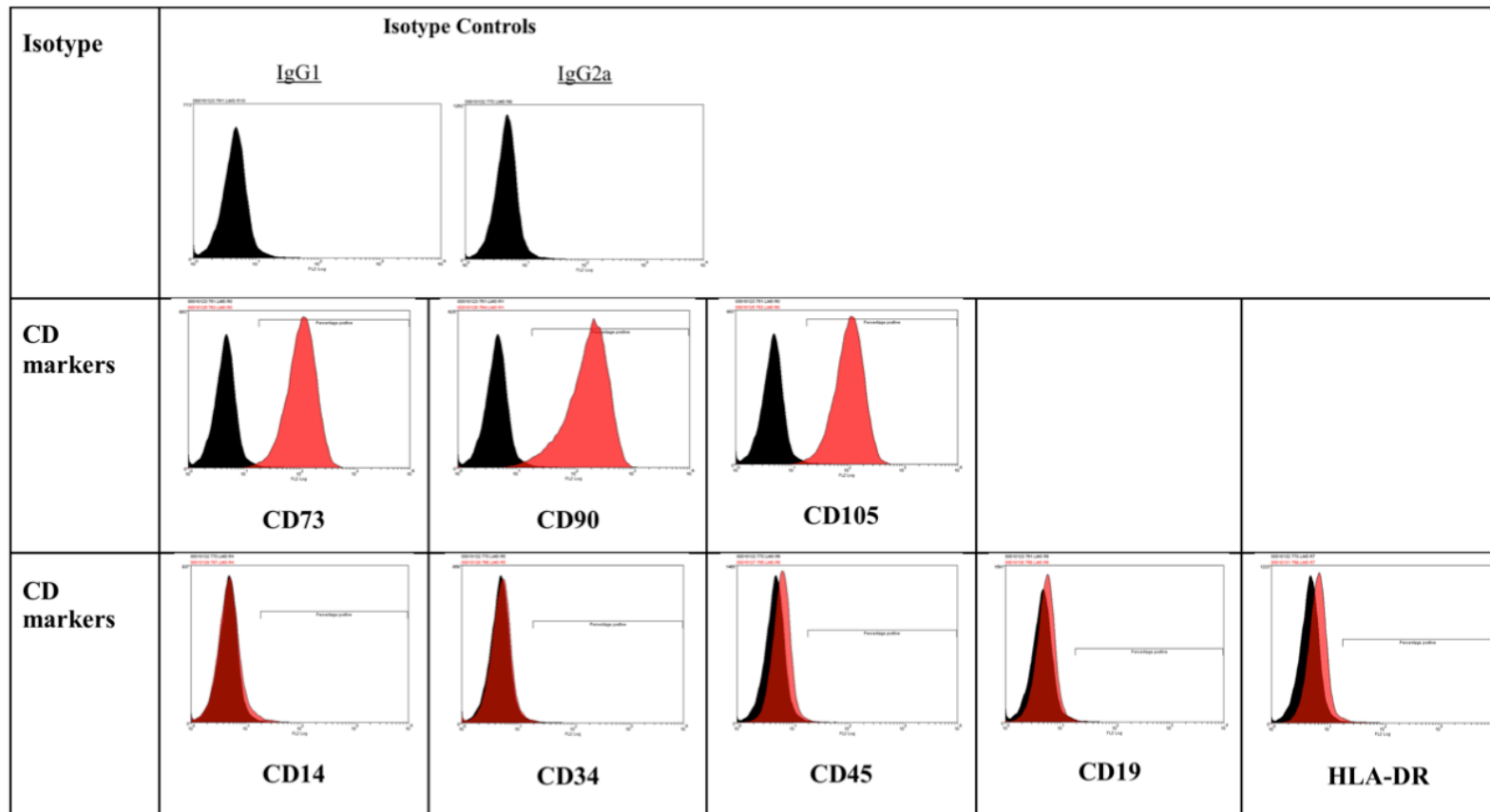


Fig. A4: Quantification of hMSC CD markers. Results demonstrated typical profile of hMSCs surface markers (CD73, CD90 and CD105) and lacking of hematopoietic markers (CD14, CD34, CD45, CD19 and HLA-DR using flow cytometry. (Re-printed with permission from J.C. Price).

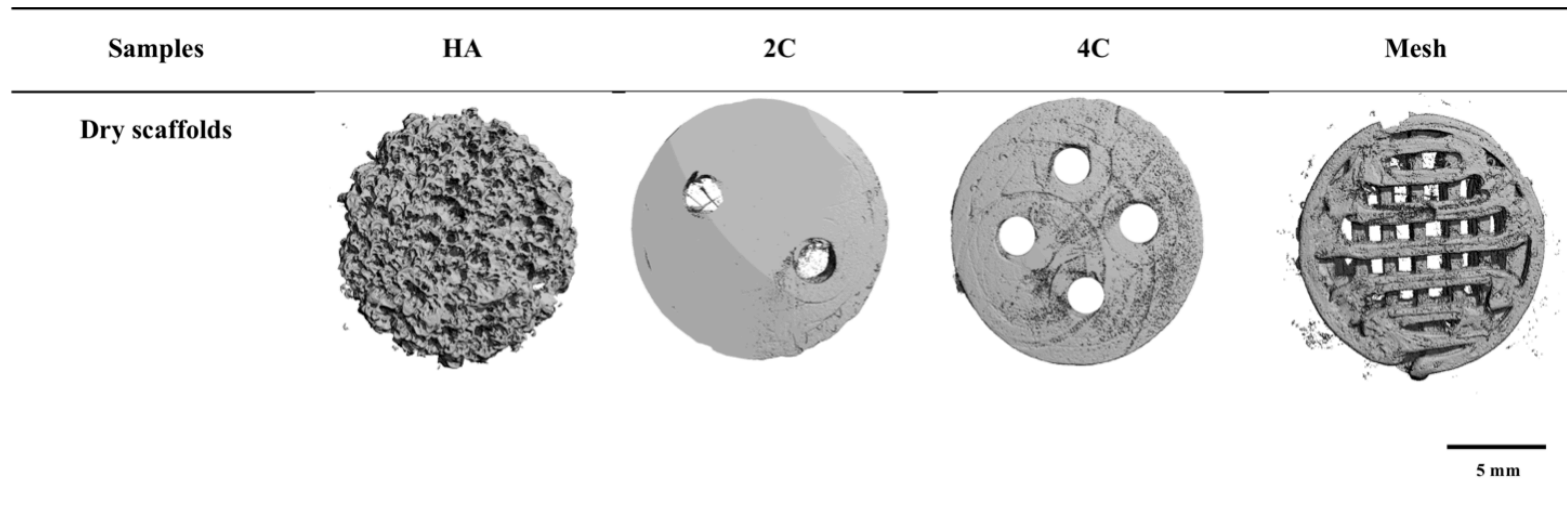


Fig. A5: X-Ray Micro-CT of different structural designs of dry scaffolds (before seeding). HA scaffolds is denser in nature and was scanned at higher density threshold compared to the hybrid scaffolds which was fabricated by Fused Deposition Modelling technique using poly (lactic acid) based scaffolds coated with 5BL of SiCHA in hyaluronan/ SiCHA in Collagen type I and EDC/NHS coupling agent. Dry HA scaffold was scanned at threshold (50/1000), designated as T50. 3DP hybrid scaffolds were scanned at threshold (42/ 1000), designated as T42. Scale bar= 5mm.